Towards a comprehensive, comparative assessment of Climate Engineering schemes
-
Metrics, Indicators and Uncertainties

Dissertation
ZUR ERLANGUNG DES DOKTORGRADES
DER MATHEMATISCH - NATURWISSENSCHAFTLICHEN FAKULTÄT
DER CHRISTIAN-ALBRECHTS-UNIVERSITÄT ZU KIEL

VORGELEGT VON
NADINE MENGIS
KIEL, APRIL 2016

Referent:	Prof. Dr. Andreas Oschlies
Koreferent:	Prof. Dr. Martin Visbeck

Tag der mündlichen Prüfung: 10.06.2016

gez. Prof. Dr. Wolfgang Duschl, Dekan

“Ich mach' mir die Welt - widdewidde wie sie mir gefällt” - Pippi Langstrumpf,

aus der deutschen Übersetzung von
Astrid Lindgren’s Pippi Langstrumpf [Lindgren et al., 1986]

Zusammenfassung

Auf politischer Ebene hat man begonnen über Climate Engineering (CE) als mögliche Option gegen den mensch gemachten Klimawandel zu sprechen. Um gut informierte Entscheidungen zum Thema zukünftiger Forschung oder potentiellen Umsetzung von CE Massnahmen zu treffen, benötigt man eine umfassende und vergleichende Einschätzung der verschiedenen Methoden. In diesem Kontext bestehen grosse Herausforderungen darin, geeignete Indikatoren auszuwählen, die Modellunsicherheiten zu quantifizieren, sowie relevante Metriken für die politische Entscheidungsfindung zu konstruieren.
Diese Arbeit beinhaltet erste, notwendige Schritte, um zu einer umfassenden und vergleichenden Einschätzung verschiedener CE Methoden zu gelangen. Mehr inter- und transdiziplinäre Forschung in diesem Bereich sollte gefördert werden, um eine uninformierte Entscheidungsfindung zu vermeiden.

Im ersten Teil der Arbeit werden Effekte und Nebenwirkungen der CE Methode Ozeanoberflächenaufhellung in der Arktis (AOAM) untersucht. Für alle betrachteten Klimavariablen hat der Einsatz von AOAM den einmaligen Effekt eines zeitlichen Versatzes kurz nach der Umsetzung. Allerdings ermöglicht die Methode keine Umkehrung der Klimatrends solange der atmosphärische CO_2 Gehalt weiter ansteigt. Eine Erweiterung der bisherigen Forschung um eine ozeanographische Perspektive ermöglicht die Untersuchung eines Warmwasser Signals entlang der Arktischen Kontinentalabhänge. Dieses trägt möglicherweise dazu bei, die dort lagernden Methanhydrate zu destabilisieren. Diese Studie verdeutlicht den Mehrwert von multidisziplinärer Arbeit bezüglich der Untersuchung von Potential und Nebenwirkungen von CE Methoden für ein umfassendes Verständins.
Im zweiten Teil der Arbeit wird eine Parameter Studie zur CO_2 Sensitivität von Vegetationstranspiration vorgestellt. Die Studie betont die Bedeutung eines Verbesserten Verständnisses von Umwelteinflüssen auf die Vegetation, um eine bessere Vorhersage von Änderungen im terrestrischen Wasser- und Kohlenstoffkreislaufs zu ermöglichen. Diese Sensitivitätsstudie ist Teil eines Simulationenensembles mit variierten Model-Parametern, welches dazu verwendet wird, die Unsicherheiten verschiedener CE Szenarien im Rahmen eines Methodenvergleichs zu quantifizieren, welches in den nachfolgenden Teilen

der Arbeit verwendet wird.
Ist es ausreichend die Indikatoren für die historische Zeitspanne zu benutzen, um zukünftigen Klimawandel umfassend zu beschreiben? Im dritten Teil der Arbeit wird eine Methodik eingeführt, um systematisch Korrelationsmatrizen auszuwerten. Das ermöglicht die Identifizierung eines Indikatorensets für eine umfassende, naturwissenschaftliche Beurteilung der gegebenen Fragestellung. Wir zeigen, dass es unzureichend wäre, die historischen Indikatoren für eine umfassende Beschreibung sowohl des mittelstarken (RCP4.5) als auch des starken (RCP8.5) Klimawandel-Szenarios zu benutzen, da sich in beiden Szenarien vorherrschenden Korrelationen zwischen Erdsystem-Variablen veränderen.
Im vierten Teil der Arbeit wird diese Methode auf drei CE Szenarien angewendet, wodurch Änderungen in den jeweiligen Korrelationsmustern gegenüber der zwei Klimawandel Szenarien identifiziert werden können. Um einen umfassenden Vergleich der Methoden zu ermöglichen, wird eine zusammengefasste Korrelationsmatrize gebildet und diese, basierend auf Korrelationen, die in allen drei Szenarien signifikant sind, evaluiert. Eine erste Beurteilung der drei exemplarischen CE Methoden, basierend auf den ausgewählten Indikatoren, bleibt zunächst ergebnislos, da es sowohl von den betrachteten Indikatoren als auch von den Sensitivitätsimulationen abhängt, welche der CE Methoden am 'besten' abschneidet. Erst wenn die Indikatoren noch weiter zu einer Metrik zusammen gefasst werden, gelangen wir zu einem klareren Ranking der Szenarien. Unter den gegebenen Annahmen, stellen wir fest, dass das RCP4.5 Szenario am nächsten an dem gewählten Referenzklimazustand bleibt. Das Strahlungsmanagement Szenario ist das 'beste' CE Szenario, gefolgt von der Ozeankalkung und der gross-skaligen Aufforstung. Das letzte Szenario ist in seinem Ranking ähnlich dem RCP8.5. Diese Ergebnisse stimmen mit unseren Erwartungen, basierend auf der Modellimplementierung, überein.

Diese Analysen bringen das naturwissenschaftliche Verständnis von verschiedenen CE Methoden voran, welches massgeblich für eine spätere Entscheidungsfindung ist. Nichtsdestotrotz ist es unvermeidbar, Informationen über das zugrunde liegende Wertesystem der betroffenen Akteure mit einzubeziehen, um relevante Metriken für die politische Entscheidungsfindung zu identifizieren.

Summary

Climate Engineering (CE) as an option to prevent dangerous climate change has reached the political debate. For a well informed decision on CE research and deployment in the future, work towards a comprehensive, comparative assessment is needed. The selection of well suited indicators, the quantification of model uncertainties, as well as the identification of policy-relevant metrics are major challenges for reaching such a CE assessment. In my thesis I present work towards a comprehensive, comparative assessment of CE schemes, although these are inevitable first steps introducing a more systematic approach, more inter- and transdisciplinary research on this topic needs to be encouraged to avoid decision making under ignorance.

In the first part of this thesis, climate impacts and side effects of an artificial Arctic ocean albedo modification (AOAM) scheme are studied. AOAM yields an initial offset during the first years after implementation but no potential for reversing trends, in all assessed Arctic climate indicators under increasing atmospheric CO_2 concentrations. Expanding the previously atmosphere-focused analysis by an oceanic perspective, allowed the investigation of a sub-surface warming signal in the AOAM simulations with the potential to destabilise Arctic marine gas hydrates. This study illustrates the importance of a multidisciplinary investigation of CE impacts and side effects, to obtain a comprehensive assessment.

The second part of this thesis presents a parameter sensitivity study on the uncertainty in the response of transpiration to CO_2 and implications for climate change. This study emphasises the importance of an improved assessment of the dynamics of environmental impact on vegetation to better predict future changes of the terrestrial hydrological and carbon cycles. This parameter sensitivity study is part of a parameter perturbation ensemble used to quantify uncertainties in projections of future CE methods in the context of a comparative CE assessment, which is used in the next parts of this thesis.

Is the application of indicators used for the historical time period valid for an comprehensive assessment of future climate change? In the third part of the thesis we introduce a methodological approach to systematically evaluate correlation matrices, identifying robust indicators from Earth system variables, to be used in a natural-science based as-

sessment. We show that it is not sufficient to apply the indicator set found for the historical period to neither an intermediate-high (RCP4.5) nor a high (RCP8.5) future emission scenario, since prevailing correlations between Earth system variables are changed in a climate change scenario.

In the fourth part of this thesis this method is applied to three exemplary CE scenarios: Large-scale afforestation, ocean alkalinity enhancement and solar radiation management. Changes in correlation patterns induced by the single CE scenarios relative to climate change are identified, providing important information on which variables might become more relevant under CE scenarios. To enable a comprehensive comparison of the thee scenarios, the common correlation matrix of the three methods is systematically evaluated to identify an indicator set. A preliminary evaluation of the three scenarios based on these indicators remains inconclusive, since it depends on the regarded indicator as well as the sensitivity simulation, which scenario performs 'best'. If the indicators are further aggregated into a metric in order to reduce the complexity, a ranking of the different scenarios becomes evident. Given all assumptions, we find that overall the RCP4.5 scenario performs 'best' in staying close to todays climate state. Solar Radiation Management is identified as the 'best' CE scenario, followed by Ocean Alkalinity Enhancement and Large-scale Afforestation. The latter performs comparable to the RCP8.5 scenario. These results agree with our expectations, based on the way the CE methods are implemented in the model.

These analyses advance the natural-science based assessment of CE, which is essential prior to a decision making process. However, for the identification of policy-relevant indicators and the construction of a decision-informing metric, it is unavoidable to include information on the value system of stakeholders.

Contents

1. Introduction

1.1. Motivation

The world has reached a state in which humans manipulate and exploit the environment in an unprecedented global scale to make it more inhabitable, productive and comfortable. Starting with rather small scale agriculture, the exploitation of our planet has speeded up since the industrial revolution, leading to initially unintentional, but nowadays well known pollution of the atmosphere with greenhouse gases [Stocker et al., 2013]. The consequences of this pollution is what we refer to as anthropogenic climate change. During the last decades, the knowledge about possible future consequences from climate change was gained, and society became more aware of the threats we are facing due to changes in Earth's climate system. On a political level, two solutions are discussed: The most intuitive reaction to prevent climate change is to reduce the amount of emitted greenhouse gases (Mitigation), in addition society needs to adjust to expected changes in the climate system (Adaptation).
In the Paris agreement, adopted on December 12^{th} 2015, 195 parties agreed on 'holding the increase in the global average temperature to well below 2 °C above pre-industrial levels and pursuing efforts to limit the temperature increase to 1.5 °C above pre-industrial levels, recognising that this would significantly reduce the risks and impacts of climate change' [UNFCCC, 2015]. This increases the pressure on single countries to reduce their emissions or to find another solution for preventing dangerous climate change. Based on prognoses of future economic growth and the consequent future carbon emissions [e.g. Held et al., 2009; Fyke and Matthews, 2015], reaching the set climate targets very likely depends on the future deployment of negative emissions technologies [Fuss et al., 2014]. This is also represented in the IPCC's scenarios, where 95% of the scenarios with a likely chance (66%) of staying below 2 °C, assume a successful and large-scale implementation of negative emission technologies [Anderson, 2015].
In 2006, Paul Crutzen proposed to manipulate the planetary albedo by injecting sulphur into the stratosphere 'to resolve a policy dilemma' [Crutzen, 2006], and thereby brought the attention of a larger scientific community to another possible solution to the threat of climate change: Climate Engineering. Climate Engineering, Geoengineering, Climate Intervention, Climate Modification are all terms for large-scale deliberate manipulation of the Earth's climate to counteract anthropogenic climate change (hereafter denoted as Climate Engineering (CE)). Principally, Climate Engineering can be separated into carbon dioxide removal (CDR) and radiation management (RM) methods. CDR methods aim at removing CO_2 from the atmosphere to reduce the greenhouse effect, targeting the main cause of anthropogenic climate change. This is often referred to as negative emissions technologies. RM methods aim at manipulating the Earth's radiation budget to reduce

temperatures, targeting the 'symptoms' of climate change (see Section 1.3 for more details).
Due to the perceived political and social inertia in pursuing mitigation and adaption efforts, and in an attempt to expand the portfolio of options for reducing the risk of dangerous climate change, research on this topic started to evolve quickly within the last decade. Open research questions on Climate Engineering emerged in natural science, engineering, legal, economical, ethical, social, and political science fields (Figure 1.1).

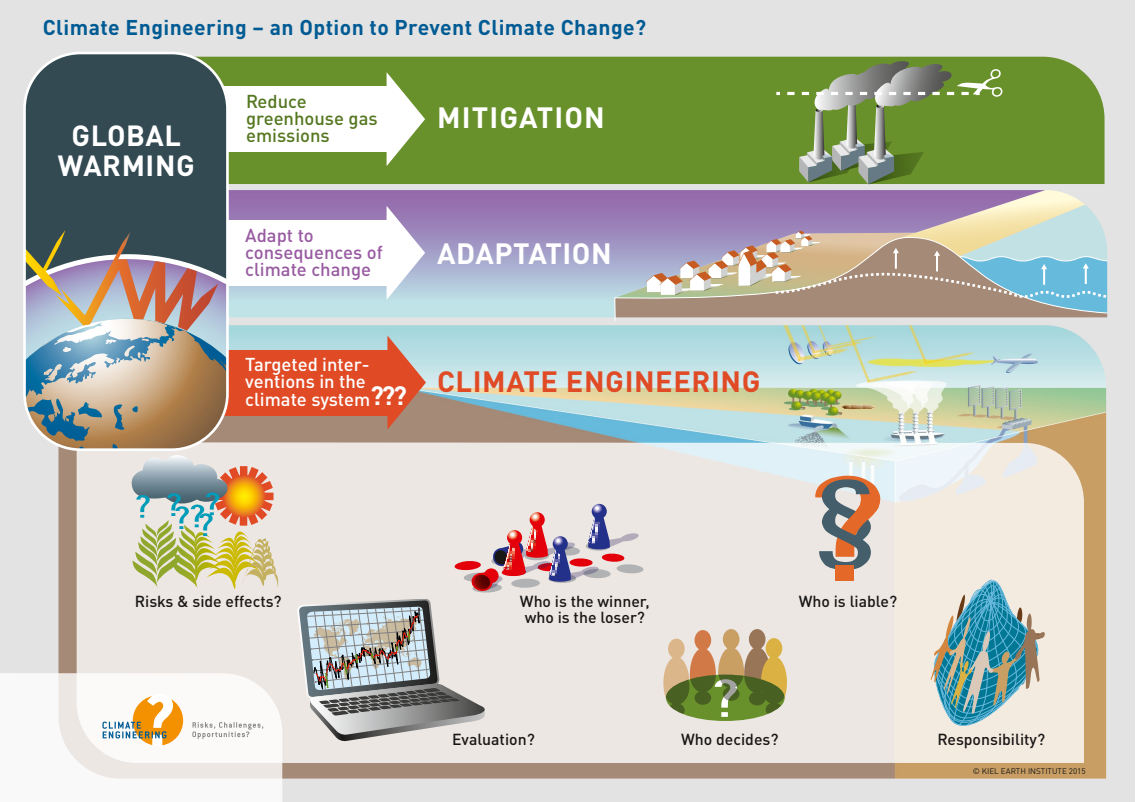

Fig. 1.1.: *Illustration of three proposed solutions to climate change: Mitigation, Adaptation and Climate Engineering. For the latter some research questions from different scientific fields are explicitly shown.*

The aim of this thesis is to advance the progress towards a comprehensive, comparative assessment of different CE methods from a natural science perspective. Note, that here comprehensive is defined in the sense, that all Earth system components should be considered. The selection of well suited indicators, the quantification of model uncertainties, as well as the identification of policy-relevant metrics are major challenges for reaching such a CE assessment. For now the assessment of CE is completely based on models, since field experiments large enough to be detectable given the large natural variability would be too close to an actual deployment (see Section 1.2). The importance of a comprehensive CE assessment, which well suited indicators is illustrated by a case study on an ocean albedo modification scheme, for which a detailed assessment of the oceanic component was missing in the literature [Cvijanovic et al., 2015]. The inclusion of this component

reveals potentially severe side effects (chapter 2 or Mengis et al. [2016]). The parameter sensitivity study on the uncertainty in the response of transpiration to CO_2 (chapter 3) is part of a perturber parameter ensemble, quantifying the uncertainty in future projection of CE. This ensemble of sensitivity simulations is the basis of the investigations on indicator selection in the following parts of the thesis. For both, anthropogenic climate change and Climate Engineering (chapter 4 and 5, respectively) we learn, that the selection of indicators for an comprehensive assessment of future changes needs to be reevaluated, since prevailing correlations between Earth system variables are changed depending on the forcing scenario. With respect to anthropogenic climate change, research on indicator selection has taken place [e.g. Böhringer and Jochem, 2007; Radermacher, 2005; Pintér et al., 2005], but for the CE debate this knowledge is missing. Advancing the Climate Engineering assessment we investigate which indicators have to be considered additionally in an CE assessment, and how they differ from climate change assessment indicators (chapter 5). After relevant indicators are identified for three exemplary CE methods, an evaluation of these methods against two climate change scenarios is carried out and discussed.

1.2. The Role of Models in Climate Engineering Research

Earth system models are an essential tool for understanding the potential, feasibility and possible side effects of different CE methods within the natural system. Since CE is concerned with large-scale future interventions affecting the climate system, the knowledge we obtain by studying small scale (temporal and spacial) natural analogues is limited. However a field test large enough to be detectable, or being able to show the limitations of a CE method would already be close to a deployment, and could have severe natural, but also legal, societal and political consequences [National Academy of Sciences, 2015b]. Therefore, the assessment of the climatic responses from large-scale CE for now is completely based on models.

Since every model is wrong, per definition, as it represents a simplified version of the complex reality, a quantification of structural, process and parameter uncertainties, are of special importance for CE research. The fact that there are no (large-scale) CE observations to evaluate the model performances against, increases the challenge to quantify uncertainties in a CE context.

Furthermore, in a Climate Engineering scenario, relationships between Earth system variables are unnaturally altered, e.g. an implementation of a radiation management scheme would decouple the relationship between temperature and CO_2 [Irvine et al., 2012]. Modellers therefore need to carefully evaluate which processes might become more relevant in a Climate Engineering scenario compared to climate change, and if these processes are (well) represented in the Climate model. Without such careful considerations, CE model results might be interpreted with an unjustified confidence. On the other hand, simulating large perturbation in Climate models, as imposed during CE simulations, creates the chance to learn about the climate system and possible model deficits.

1.3. Overview of currently discussed Climate Engineering methods

This section should provide an overview of the research state of different CE methods. I hereby limit myself to CE methods considered in recent CE model assessment projects, namely the Geoengineering Model Intercomparison Project (GeoMIP) and the Carbon Dioxide Removal Model Intercomparison Project (CDR-MIP). Both these model intercomparison projects aim at quantifying structural uncertainties within different model ensembles, whereby GeoMIP considers radiation management methods and CDR-MIP focuses on terrestrial CDR and marine CDR methods. Future cooperation, to combine the knowledge and assess combinations of CE methods is planned (pers. comm. D.P. Keller).

1.3.1. Radiation management methods and model assessment

Radiation Management describes methods that deliberately manipulate the planetary radiation budget in order to either reduce the incoming solar radiation at the Earth surface (SRM) or to enhance the amount of outgoing long wave radiation into space (LRM). Such methods therefore aim at counteracting global warming, i.e. the symptoms of anthropogenic climate change, rather than treating its causes. Note, that any climate change impacts directly linked to enhanced atmospheric CO_2 concentrations, such as ocean acidification or CO_2 fertilisation, would remain unmitigated. RM methods nevertheless gained much attention, since they promise a faster response time in the climate system compared to any mitigation or CDR scheme.
GeoMIP is the first model intercomparison project (MIP) concerning radiation management research questions[Kravitz et al., 2011]. Starting in 2011, it initially focused on idealized scenarios, in which a reduction of incoming shortwave radiation was simulated, as well as stratospheric aerosol injection (SAI) scenarios, simulating an injection of SO_2 into the stratosphere. In the second phase of GeoMIP, two scenarios on ocean albedo modification and marine cloud brightening were added [Kravitz et al., 2013b]. In the following phase (GeoMIP6, following the CMIP nomenclature) a cirrus cloud thinning scenario was added to the RM methods portfolio, as well as a scenario in which SAI and solar dimming are used to change radiative forcing in a high emission scenario to reach a medium high emission scenario [Kravitz et al., 2015]. These methods were chosen for GeoMIP due to their likely feasibility to have a substantial climate impact [Kravitz et al., 2011]. Hence they gained increasing attention over the last years and will be shortly discussed in the following section.

Stratospheric Aerosol Injection
The CE method of stratospheric aerosol injection (SAI) gained the most attention over the last decade. Following the natural analogue of a plinian volcanic eruption, which was observed to have a cooling effect during the first two years after eruption [Jones, 1994; Robock, 2008], SAI describes a deliberate and continuous injection of sulphate aerosols into the stratosphere, in order to reflect more incoming shortwave radiation and thereby cool the planet [Crutzen, 2006].

Model studies show that this theory proves effective in achieving a global mean cooling effect [e.g. Robock, 2008; Kravitz et al., 2013a], however, there is a natural limit to SAI deployment [Niemeier and Timmreck, 2015]. It was found that in order to achieve a specified global mean temperature target, the tropics would have to be overcooled and high latitude areas would still experience a warming signal [Kravitz et al., 2013a]. Due to local and global temperature changes, precipitation patterns are found to shift during SAI implementation [Tilmes et al., 2013; Robock et al., 2008b; Kravitz et al., 2013a], which would result in a global redistribution of water resources with a high political conflict potential. For both temperature and precipitation patterns, the location as well as the hemispheric balance of the deployment are found to be of importance [Haywood et al., 2016].
Due to atmospheric dynamics in the stratosphere, SAI would be most effective if deployed in low latitudes, since aerosols would quickly spread all around the planet. The same dynamics also define that this method would most likely be deployed on a global scale since even a regional deployment would have global impacts [Robock et al., 2008b]. This fact makes SAI deployment not only a technical challenge [Kuo et al., 2012], but more importantly a deployment under peaceful circumstances would have to be agreed on by all affected countries in the world, which makes SAI deployment foremost a political challenge [Dalby, 2015].
Apart from that, several studies show that the implementation of SAI under increasing atmospheric CO_2 concentrations should not be abruptly discontinued, since model results suggest, that in this case the climate state would rapidly change to match the unmanipulated climate state given the background atmospheric CO_2 concentrations [Matthews and Caldeira, 2007; Jones et al., 2013; Keller et al., 2014]. Thereby the rate of change would be even higher than the rate of change from anthropogenic climate change, and could have dangerous climatic consequences [Keller et al., 2014]. Note that this danger would increase with every emitted ton of CO_2 during an implementation of SAI. This problem, is referred to as 'termination shock' and widely discussed not only in the natural science community [Jones et al., 2013; Keller et al., 2014], but also in the social and ethical science communities [Heutel et al., 2015; Burns and Nicholson, 2016]. The increasing risk in case of SAI deployment under increasing carbon emissions, causes a lock-in situation for future generations to come, i.e. under such circumstances, the choice of discontinuing SAI deployment is taken from these generations, which makes SAI implementation an intergenerational challenge [e.g. Betz and Cacean, 2012].

Marine Cloud Brightening

The concept for Marine cloud brightening (MCB) was introduced by Latham [1990], who combined the theory from Twomey [1974] to propose a brightening of marine clouds by increasing the cloud droplet number in order to cool the planet. This would increase the reflectivity of clouds, as well as their life time by reducing precipitation rates. The theory suggests that seeding stratocumulus clouds in the planetary boundary layer (typically occurring in the lower 1500m of the atmosphere) holds the highest potential. These clouds occur over oceanic upwelling areas, as well as in mid to high latitudes of the respective summer hemisphere [Grosvenor and Wood, 2014]. This implies that MCB would show

high local impacts on albedo and radiative forcing, which vary considerately in space and time [Kravitz et al., 2013b]. An unbalanced implementation and a resulting imbalance of the hemispheric albedo might possibly have severe global impacts [Haywood et al., 2016].
There have been several attempts to assess the potential and side effects of MCB in models, however there are several challenges associated with this method. A good representation of cloud dynamics is still a major challenge in the climate modelling field [Stocker et al., 2013], therefore modelling a well represented implementation of marine cloud brightening in global climate models in order to assess global impacts for longer time scales is still difficult and there is considerable disagreement between the models [Alterskjaer et al., 2013]. Nevertheless, in the context of GeoMIP several studies assessed the potential of a partly idealised implementation of MCB. It was found that MCB has a global cooling potential, with a high local heterogeneity [Kravitz et al., 2013b]. The highest potential was found for clear atmospheric conditions [Latham et al., 2012], and Aswathy et al. [2015] found a small potential in mitigating climate extremes concerning temperature and precipitation. In order to assess the potential of MCB it is important to know the vertical structure of the lower atmosphere. If for example more than one temperature inversion, and therefore two or more cloud layers are present, it is likely, that the lower most layer is affected by the seeding, however the reflectivity of the cloud is most influenced by the top layer clouds [Russell et al., 2013]. In addition, there is considerate uncertainty in the feasibility of MCB deployment. The cost as well as the effectiveness of the technology for a large-scale (spacial and temporal) implementation are highly uncertain [Russell et al., 2013; Leisner and Müller-Kliesner, 2010].

Ocean Albedo Modification
Global or local ocean albedo modification (OAM) theoretically holds a large potential in increasing the planetary albedo, due to the large available areas, and the initial dark colour of the ocean surface. Model studies found some potential of global and local OAM [e.g. Kravitz, 2014; Cvijanovic et al., 2015; Crook et al., 2016], but also found severe side effects, such as circulation changes from changes in land-ocean temperature contrasts [Kravitz, 2014], a southward shift of the inter tropical convergence zone [Kravitz, 2014], as well as compensatory heat fluxes in the Earth system from a local scale implementation [Mengis et al., 2016].
Apart from that, the technological feasibility would still have to be determined. There have been suggestions on how to enhance the ocean surface albedo by for example releasing floating glass spheres [Gordon and Walter, 2011], or injecting microbubbles into the ocean surface layer and making them more stable by adding surfactants [Seitz, 2011; Crook et al., 2016], those methods are however subject to critical debate [e.g. Robock, 2011].

Cirrus Cloud Thinning
Cirrus clouds in the cold, upper half of the troposphere have a net warming effect on the atmosphere, since they absorb and reemit longwave radiation at a higher rate, than they

reflect shortwave radiation. Cirrus cloud thinning (CCT) proposes a seeding of these ice clouds to increase the size of the ice crystals, thereby depleting the atmosphere from water vapour suppressing homogeneous nucleation [Mitchell and Finnegan, 2009]. Thereby, this method would increase the amount of outgoing longwave radiation, and would in contrast to the albedo modification methods also work at night and all year round. Decreasing the amount of 'trapped' longwave radiation more directly counteracts the greenhouse effect of CO_2.
Modelling studies found that CCT has the potential to offset the radiative forcing of a doubling of atmospheric CO_2 [Storelvmo and Herger, 2014]. But changes in the hemispheric balance by CCT implementations would have severe impacts on the atmospheric circulation [Muri et al., 2014]. Kristjánsson et al. [2015] found that CCT counteracts the impacts from climate change concerning the hydrological cycle in an Earth System Model. Similar to the other methods, the technological feasibility as well as the limits of this method is still unclear.

1.3.2. Carbon dioxide removal methods and model assessment

Carbon Dioxide Removal describes methods that aim at removing atmospheric CO_2 by redistributing the carbon into either the marine (mCDR) or the terrestrial (tCDR) carbon reservoir. Such methods correspondingly aim at reducing the atmospheric forcing of CO_2 in the atmosphere, and hence target the main cause of anthropogenic climate change. Compared to RM methods, the time scales on which CDR methods would work are slower.
CDR-MIP started in the beginning of 2016 and first simulations will be performed within the current year [Keller et al., 2016]. The first round of CDR-MIP proposes four experiments: an idealised carbon cycle reversibility experiment, a carbon cycle feedback experiment, an large-scale afforestation (LAF) experiment and an ocean alkalinity enhancement (OAE) experiment. These methods were chosen for CDR-MIP, in order to establish a basic understanding of the reversibility of climate change by CDR methods as simulated in Earths system models, and in order to represent one terrestrial based as well as an ocean based CDR method, both methods will be shortly discussed in the following section.

Large-scale Afforestation
About 32% of cumulated CO_2 emissions since 1750, amounting to 180 ± 79 Pg carbon, arise from deforestation or other land use changes [Stocker et al., 2013]. This amount suggests a upper limit of the potential of unmanaged large-scale afforestation (LAF). However, nowadays afforesting these areas would cause competition with agricultural production areas, which will be of need for society in the near and far future [National Academy of Sciences, 2015a]. The real potential is therefore much lower. Projections of increased agricultural productivity allow scenarios in which these utilised areas can be significantly reduced, freeing areas for afforestation [Taylor et al., 2012]. Due to limits of carbon uptake by naturally growing forests and based on estimates for available

areas, the potential of afforestation was calculated to be about 104 Pg carbon [Nilsson and Schopfhauser, 1995]. Assessing this potential within different Earth system models, as planned for CDR-MIP, will enable a quantification of uncertainties in such estimates, which are expected to be considerably high for terrestrial biosphere models [e.g. Ahlström et al., 2012; Migliavacca et al., 2012; Mengis et al., 2015]. It is noteworthy, that the near term benefits of deforestation reduction are higher compared to reforestation and afforestation [National Academy of Sciences, 2015a].

Ocean Alkalinity Enhancement
About 25% of the anthropogenic carbon emissions are currently taken up by the ocean [Heinze et al., 2015], via either chemical or biological processes. The solution of CO_2 as dissolved inorganic carbon in the surface waters of the ocean, causes ocean acidification. By adding alkalinity this process can be reversed, and the carbon uptake and storage potential is increased. The idea to increase ocean carbon uptake by ocean alkalinity enhancement (OAE) does not directly target the surface ocean pH, but rather a specific amount of carbon [e.g. Ilyina et al., 2013; Lackner, 2002]. Therefor, appropriate minerals would need to be ground up, prepared, transported and released into the ocean [National Academy of Sciences, 2015a]. The release of e.g. calcium carbonate minerals would enhance the capacity of the ocean to take up atmospheric CO_2 [Archer et al., 2009]. Estimates of the carbon sequestration potential of different methods reveal high production and transportation costs, which often strongly reduce the carbon sequestration potential although the material costs for minerals would be small [Kirchofer et al., 2012]. It is noteworthy, that in order for the deployment to be at scale, substantial masses of mineral (in the order of 100 Pg/yr) would be needed to offset current CO_2 emissions [National Academy of Sciences, 2015a] (for comparison the world production of coal amounts to 8 Pg/yr [National Academy of Sciences, 2015a]). The precise amount of any particular alkalising agent that could be mined, processed, transported, and delivered to the ocean in a form that would easily dissolve and enhance alkalinity is still poorly constrained [Ilyina et al., 2013; Köhler et al., 2013].

1.4. Comparative assessment of Climate Engineering

A conclusive environmental, political and ethical assessment, characterised by the appropriate disciplinary breadth and depth, of Climate Engineering (CE) is lacking so far. Assessing potential efficacy as well as possible side effects of individual CE methods is essential prior to any decisions about possible large-scale field experiments or eventual deployment of any CE scheme. This implies that the assessment has to be performed in the absence of directly relevant observations. For some CE schemes natural analogs have been referred to, such as explosive volcanic eruptions for solar radiation management or natural iron fertilization by sediments around Southern Ocean islands for artificial iron fertilization. However, it is uncertain to what extent such analogies are valid [e.g. Trenberth and Dai, 2007; Pollard et al., 2009]. Hence, a CE assessment during the next decade will probably be based on model simulations (see Section 1.2 for more details).

A number of model-based CE assessments have been included in recent national and international scoping studies reporting on the current state of the CE debate [Rickels et al., 2010; Schäfer et al., 2015; National Academy of Sciences, 2015b,a]. However, all reports so far had to rely on studies on individual CE techniques, making a direct comparison of different techniques difficult. The National Academy of Science report for example was split into two volumes, one focusing on Carbon Dioxide Removal (CDR) and the other one on Solar Radiation Management (SRM). This was motivated by the 'very different posture concerning the currently known risks' [National Academy of Sciences, 2015a,b] of the two categories. Results from a first comparison of various idealized CE deployments within a single intermediate complexity Earth System model, however, showed that risks associated with SRM and CDR, when employed intensively at large-scale, may not be so different [Keller et al., 2014]. Hence a careful and unbiased comparison of very different CE techniques in a unified model framework is necessary.
The choice of comprehensive indicators is central in the context of comparing and evaluating different CE methods within a single, or between different models. A first attempt was to use indicators typical for climate change studies. The formulation of these indicators was guided by their suitability to describe the state of the Earth system in a way assumed relevant for society (e.g., global mean temperature, terrestrial precipitation) [Stocker et al., 2013]. However, in an engineered climate the prevailing relationships between Earth system properties may no longer persist [Klepper and Rickels, 2014], and the understanding of these effects from a natural science perspective is essential for the consideration of these processes later on. The most prominent example is the impact on the transient climate response to cumulative CO_2 emissions [e.g. Irvine et al., 2012]: In a natural climate system temperature tends to rise when CO_2 increases, whereas under SRM deployment temperatures may decrease while atmospheric CO_2 increases. Furthermore, by affecting the climate state and in addition the uncertainties, any CE application is expected to affect probability distributions on uncertain outcomes. This implies that previously applied aggregations of metrics for assessment might no longer be valid [Klepper and Rickels, 2014]. Accordingly, the selection of relevant and possibly new indicators and metrics is essential for obtaining a comprehensive assessment framework of CE. Inter- and transdisciplinary exchange between researchers in this field is an important step in achieving such an assessment framework, which will eventually require the consideration of further (non-academic) actors to deal with the diverging goals of statistical measurability, scientific consistency, and political relevance [Radermacher, 2005]. Deriving and agreeing on appropriate indicators and metrics for CE assessment is probably one of the major challenges in the CE debate.

1.5. Chapter synopsis and author contribution

The aim of this thesis is to advance the knowledge of CE, to enable a comprehensive, comparative assessment of different CE methods on a natural science basis. In this section the contribution of the different chapters in reaching this goal is summarised.

Chapter 2 is a contribution to the research on Arctic Ocean albedo modification (AOAM), a local shortwave radiation management scheme introduced by Cvijanovic et al. [2015]. Our analyses reveal that this method has no potential for reversing trends in any of the assessed Arctic climate indicators under increasing atmospheric CO_2 concentrations. It rather has a one-time offsetting effect. Considering longer time scales, emission reduction is more effective in staying close to today's climate state compared to a high emissions AOAM scenario. Adding an oceanic perspective to the analyses to advance the understanding of AOAM, we investigated consequences for ocean circulation, water masses and heat transport and found a sub-surface warming signal in the Arctic Ocean, which could potentially act to destabilise marine gas hydrates.
Our study stresses the necessity for a multidisciplinary assessment in the Climate Engineering research. The study by Cvijanovic et al. [2015], as most of the Arctic radiation management studies, focused on atmospheric Earth system indicators, and mainly discusses the potential of the CE methods concerning these (targeted) indicators. If other components of the Earth System are neglected in the assessment, we risk a biased evaluation of CE methods.
This chapter is based on the paper: Mengis, N., T. Martin, D. P. Keller and A. Oschlies, (2016), *Assessing climate impacts and risks of ocean albedo modification in the Arctic*, accepted for publication in Journal of Geophysical Research: Oceans. N.M., A.O. and D.P.K. conceived and designed the experiments. N.M. implemented and performed the experiments and analysed the data. N.M. wrote the manuscript with contributions from D.P.K., T.M. and A.O..

Chapter 3 is a parameter sensitivity study on the uncertainty in the response of transpiration to atmospheric CO_2 concentrations and implications for climate change. While terrestrial precipitation is a societally highly relevant climate variable, there is little consensus among climate models about its projected 21^{st} century changes. An important source of precipitable water over land is plant transpiration. Plants control transpiration by opening and closing their stomata. The sensitivity of this process to increasing CO_2 concentrations and its impact are assessed by varying the strength of CO_2-sensitivity in the model. Changing the sensitivity of transpiration to CO_2 causes simulated terrestrial precipitation to change by -10 % to +27 % by the year 2100 under a high emission scenario. This study emphasises the importance of an improved assessment of the dynamics of environmental impact on vegetation to better predict future changes of terrestrial hydrological and carbon cycles.
This parameter sensitivity study is also part of a parameter perturbation ensemble used to assess uncertainties in projections of the future Climate Engineering methods that are used in chapter 4 and 5.
This chapter is based on the paper: Mengis N., D. P. Keller, M. Eby and A. Oschlies, (2015), *Uncertainty in the response of transpiration to CO_2 and implications for climate change*, Environ. Res. Lett., doi:10.1088/1748-9326/10/9/094001. A.O., M.E. and D.P.K. conceived and designed the experiments. N.M. implemented and performed the experiments and analysed the data. N.M. wrote the manuscript with contributions from D.P.K., M.E. and A.O..

Chapter 4 introduces a methodological approach for a systematic correlation matrix evaluation for indicator selection from Earth system model output variables. This method can be applied to different scientific questions in order to increase the objectivity in evaluating model output. In this study we focus on the question: Is the application of the indicators identified for the historical time period valid for an assessment of future time periods?
Our analyses concerning three different time periods and forcing scenarios, highlight the necessity of a re-evaluation of the selected indicator sets with time. We show that it is not appropriate to apply the indicator set found for the historical period to an intermediate-high or a high future emission scenario. By combining the three time periods, we found a common indicator set, which has a higher number of indicators compared to each of the single indicator sets. This enables us to identify robust correlations between Earth system variables across the three periods, and points out the Earth system variables that are uncorrelated, if all three periods are considered.
This chapter is a manuscript in preparation by Mengis N., D. P. Keller, and A. Oschlies (2016), to be submitted to Earth System Dynamics Discussions. N.M., A.O., and D.P.K. conceived the experiment. N.M. and D.K. implemented and performed the simulations. N.M. analysed the data, designed the methodology, and wrote the manuscript with contributions from D.P.K., and A.O..

In **chapter 5**, the methodology introduced in chapter 4 is applied to find indicators for three idealised Climate Engineering (CE) methods: Large-scale Afforestation, Ocean Alkalinity Enhancement and Solar Radiation Management. First we investigate how the chosen CE methods alter prevailing correlations between Earths system variables compared to one intermediate-high (RCP4.5) and one high (RCP8.5) future emission scenario. To enable a comprehensive comparison of the thee scenarios, the common correlation matrix of the three methods is systematically evaluated to identify an indicator set. A preliminary evaluation of the three scenarios based on these indicators remains inconclusive, since it depends on the regarded indicator as well as the sensitivity simulation, which scenario performs 'best' in staying close to the 2005–2010 reference climate state. If the indicators are further aggregated into a metric in order to reduce the complexity, a ranking of the different scenarios becomes evident. Given all assumptions, we find that overall the RCP4.5 scenario performs 'best' in staying close to the reference climate state. Solar Radiation Management is identified as the 'best' CE scenario, followed by Ocean Alkalinity Enhancement and Large-scale Afforestation. The latter performs comparable to the RCP8.5 scenario.
This chapter is a manuscript in preparation by Mengis N., W. Rickels, D. P. Keller, M. Quaas and A. Oschlies (2016). N.M., A.O. and D.P.K. conceived the experiment. N.M. and D.K. implemented and performed the simulations. N.M. and W.R. analysed the data, and wrote the manuscript with contributions from D.P.K., M.Q. and A.O..

2. Assessing Climate Impacts and Risks of Ocean Albedo Modification in the Arctic

This chapter is based on the paper 'Assessing climate impacts and risks of ocean albedo modification in the Arctic' accepted in the Journal of Geophysical Research: Oceans. Citation: Mengis, N., Martin, T., Keller, D.P. and Oschlies, A. (2016), Assessing climate impacts and risks of ocean albedo modification in the Arctic. J. Geophys. Res. Oceans. Accepted Author Manuscript. doi:10.1002/2015JC011433

Abstract The ice albedo feedback is one of the key factors of accelerated temperature increase in the high northern latitudes under global warming. This study assesses climate impacts and risks of idealized Arctic Ocean albedo modification (AOAM), a proposed climate engineering method, during transient climate change simulations with varying representative concentration pathway (RCP) scenarios. We find no potential for reversing trends in all assessed Arctic climate metrics under increasing atmospheric CO_2 concentrations. AOAM only yields an initial offset during the first years after implementation. Nevertheless, sea ice loss can be delayed by 25(60) years in the RCP8.5(RCP4.5) scenario and the delayed thawing of permafrost soils in the AOAM simulations prevents up to 40(32) Pg of carbon from being released by 2100. AOAM initially dampens the decline of the Atlantic Meridional Overturning and delays the onset of open ocean deep convection in the Nordic Seas under the RCP scenarios. Both these processes cause a sub-surface warming signal in the AOAM simulations relative to the default RCP simulations with the potential to destabilize Arctic marine gas hydrates. Furthermore, in 2100, the RCP8.5 AOAM simulation diverts more from the 2005-2015 reference state in many climate metrics than the RCP4.5 run without AOAM. Considering the demonstrated risks, we conclude that concerning longer time scales, reductions in emissions remain the safest and most effective way to prevent severe changes in the Arctic.

2.1. Introduction

Over the last decades air temperatures have been rising much faster in the Arctic than in other regions of the planet [Screen and Simmonds, 2010]. This Arctic amplification of global warming is strongly connected to positive feedback mechanisms [Stocker et al., 2013; Serreze and Francis, 2006], with the ice albedo feedback being of special importance [Holland and Bitz, 2003]. Positive feedbacks can amplify the consequences and spatial impact of an initially local perturbation. While our scientific understanding of feedback processes of the Earth system is still far from complete, currently the Arctic is

perceived as a system that holds tipping points of relevance for the global climate [Lenton et al., 2008; Lenton, 2012]. However, the existence of such tipping points especially concerning Arctic sea ice has been challenged and is under debate [e.g. Tietsche et al., 2011; Wadhams, 2012]. Six of 15 policy-relevant potential future tipping elements discussed by Lenton et al. [2008] are located in the high northern latitudes: (i) the risk of Arctic summer sea ice loss, (ii) the break down of Atlantic deep water formation and an associated slowing down of the meridional overturning circulation (MOC), (iii) permafrost thawing and consequently a release of carbon and methane from the soils, (iv) a destabilisation of marine methane hydrates, (v) the melt and collapse of the Greenland ice sheet, and (vi) the development of an Arctic ozone hole.

With global CO_2 emissions still increasing and climate change progressing [Stocker et al., 2013], there is more and more interest in technological approaches that would counteract climate change. A number of so-called Climate Engineering (CE) methods have been suggested [Crutzen, 2006]. They can be partitioned into carbon dioxide removal methods, aimed at reducing atmospheric CO_2 concentrations, and solar radiation management (SRM) methods, aimed at manipulating the Earth's radiation budget without addressing atmospheric CO_2 concentrations. For both CE methods implementation and governance concepts are discussed widely, e.g. Robock et al. [2008a]; Blackstock et al. [2009]; Feichter and Leisner [2009]; Keith [2000]; Hulme [2014].

Because of the already progressing large anthropogenic warming signal in the Arctic, the expected future warming threats, and the regionally relatively confined atmospheric and oceanographic circulation features, the Arctic is of particular interest when it comes to debating regional-scale interventions in the climate system. Most of the previous studies on the impact of Arctic CE investigate atmospheric SRM by either dimming the incoming short wave radiation [Caldeira and Wood, 2008; MacCracken et al., 2013; Tilmes et al., 2014] or by explicitly modelling the implementation of sulphate aerosols in the high northern latitudes [Robock et al., 2008b]. The focus of these studies was set predominately on CE impacts on atmospheric metrics, such as surface temperature and precipitation [Caldeira and Wood, 2008; Robock et al., 2008b]. Tilmes et al. [2014] additionally investigated changes in atmospheric as well as oceanic heat transports. Recently Cvijanovic et al. [2015] investigated the potential of ocean albedo modification on Arctic sea ice restoration and climate in a model set up of an abrupt quadrupling of CO_2. They found that a constant albedo of 0.9 applied to the area north of 70 °N or 75 °N was most effective in restoring Arctic sea ice, with September sea ice area stabilizing at about 40% of preindustrial sea ice coverage in both idealized scenarios. They did not investigate possible impacts on ocean heat content or ocean circulation however. In the current study, we investigate modifications of the ocean surface albedo at high northern latitudes during transient climate change under 21^{st} century Coupled Model Intercomparison Project 5 (CMIP5) [Taylor et al., 2012] emission scenarios, with special emphasis of changes in ocean heat content and meridional overturning circulation.

Holland and Bitz [2003] state that the ice albedo feedback is one of the key factors of the positive feedback mechanisms, which amplify climate change in the high northern latitudes. Open water has an albedo of 0.03-0.4 [Jin, 2004], whereas the albedo of sea ice ranges between 0.6-0.7 for bare ice and 0.8-0.9 for snow-covered ice [Perovich et al.,

2002]. The CE approach studied here aims to exploit this feedback by implementing an albedo modification on ice-free ocean areas in summer. Arctic amplification of global warming is strongest in autumn and winter [Serreze and Barry, 2011], which is the season when the ocean releases the heat absorbed over summer to the atmosphere. Larger ice-free areas in summer enable more oceanic heat storage and a larger heat release to the atmosphere in autumn and winter. Therefore, the objective of this CE approach is to increase ocean surface albedo, reducing energy absorption by the ocean, and thus limiting the heat exchange with the atmosphere during summer and fall. This approach is expected to limit the sea ice loss in summer and foster the formation and maintenance of a multi-year ice cover in the long term.
Suggestion on possible implementation schemes for an artificial surface albedo modification include the use of oceanic foams [Evans et al., 2010], microbubbles [Seitz, 2011] in combination with surfactants [Crook et al., 2016], or floating glass spheres [Gordon and Walter, 2011]. However, a detailed discussion of the technical aspects of deployment is beyond the scope of this paper. We focus on modelling potential consequences of an assumed successful implementation, using an ocean-sea ice model coupled to a simple atmospheric model and a global carbon cycle model, in order to investigate an idealized albedo modification over the Arctic Ocean surface.
This study is organized as follows: Section 2 describes the model implementation of the CE approach. In section 3 we present the results of our study, whereby the above mentioned potential tipping elements in the Earth system of Lenton et al. [2008] are used as a guideline for the analysis. Section 4 includes a general discussion and the conclusion is presented in section 5.

2.2. Methods

2.2.1. Model description

The model employed is the University of Victoria Earth System Climate Model (UVic ESCM) version 2.9, an Earth system model of intermediate complexity [Weaver et al., 2001; Eby et al., 2013]. It includes schemes for ocean physics based on the Modular Ocean Model Version 2 (MOM2) [Pacanowski, 1995], ocean biogeochemistry [Keller et al., 2012], and a terrestrial component including soil and vegetation dynamics [Meissner et al., 2003]. It is coupled to a dynamic-thermodynamic sea ice model with several ice thickness categories [Bitz et al., 2001] and elastic visco-plastic rheology [Hunke and Dukowicz, 1997]. The atmosphere is represented by a two dimensional atmospheric energy moisture balance model [Fanning and Weaver, 1996]. Note, that Skvortsov et al. [2009] positively evaluated the UVic ESCM for surface air temperature as well as snow cover in the Arctic. All model components have a common horizontal resolution of 3.6° longitude and 1.8° latitude and the oceanic component has a vertical resolution of 19 levels, with vertical thickness varying between 50 m near the surface to 500 m in the deep ocean.
Wind velocities used to calculate advection of atmospheric heat and moisture as well as

the air-sea ice exchange of surface momentum, is prescribed as monthly climatological wind fields from NCAR/NCEP reanalysis data [Keller et al., 2014]. The planetary albedo varies as a function of latitude and time of year to account for changes in solar zenith angle. Atmospheric albedo, representing clouds and aerosols, are prescribed monthly fields held constant throughout the simulations. The surface albedo in the model depends on the vegetation and snow coverage over land areas and on the sea ice coverage over the ocean, where the default sea ice albedo has a value of 0.8 (see Figure A.1 for the reference model surface albedo distribution in 2005).

2.2.2. Experimental Set Up and Forcing

The UVic ESCM was spun up with pre-industrial (year 1800) seasonally varying forcing for over ten thousand years. All simulations were integrated from 1765 until 2005 using historical fossil-fuel and land-use carbon emissions, as well as radiative forcing from solar variability and volcanic activity. Historical land use changes were implemented following the protocols of the CMIP5. Following Keller et al. [2014], continental ice sheets were held constant to facilitate the experimental setting and analyses. Branching off from the control simulation in 2005, three default experiments running until 2100 were conducted. Two follow the CO_2 emission scenarios of the Representative Concentration Pathways (RCPs) 8.5 and 4.5 from Meinshausen et al. [2011] and one features no CO_2 emission from 2005 onward (noEmit). The latter represents an idealized maximum mitigation scenario (disregarding the possibility of negative emissions). Note, that there is a concomitant warming and associated further reduction in sea ice even in this simulation due to the CO_2 that is already emitted until 2005, a large portion of which remains in the atmosphere until the end of the simulation.
For each of these three scenarios we ran an additional simulation with Arctic Ocean Albedo Modification (AOAM) starting in 2020. AOAM is implemented by prescribing a surface albedo of 0.8, i.e. the model's default value for sea ice, whenever the sea ice concentration drops below 50 % in grid cells north of 70 °N (Figure 2.1). This is done for every model time step from 2020 to 2100. Note, that AOAM only affects the incoming shortwave fluxes directly. Atmosphere-ocean heat fluxes, longwave fluxes and evaporative fluxes may change due to interactive physical processes. If a specific implementation method were to be tested, the model implementation would need to be adjusted. For example, if we considered the implementation of microbubbles, this would in addition to surface albedo also affect evaporative fluxes. For diagnostic purposes, a virtual tracer that is analogous to adding an inert dye to water was implemented in the whole Arctic basin north of 70 °N over all depth levels, where it was set to the value 1, at the beginning of the experiment in 2020. The tracer allowed us to track the pathways of the water masses entering and leaving the Arctic Ocean (for more details on the tracer evaluation, see section A in the Supplemental Material).
For all emission scenarios, the annual maximum area over which AOAM is applied in 2020 is about 5.1 million km^2 (Figure 2.1). By the end of the century, for simulations with increasing CO_2 emissions, the maximum AOAM area increased to 7.8 (5.8) million km^2 for the RCP8.5 (RCP4.5) simulation during summer times. These areas account for

77 (58) % of the oceanic Arctic area north of 70°N. For the noEmit simulation, the maximum AOAM area in the summers of 2090–2100 has slightly decreased to 4.3 million km^2, which amounts to 42% of the Arctic Ocean area. The fact that the area of implementation is increasing with time for the two scenarios with increasing atmospheric CO_2 concentrations already indicates a loss in summer Arctic sea ice, regardless of the implemented albedo modification, and hints at the enormous technical challenge of maintaining AOAM over time in reality.

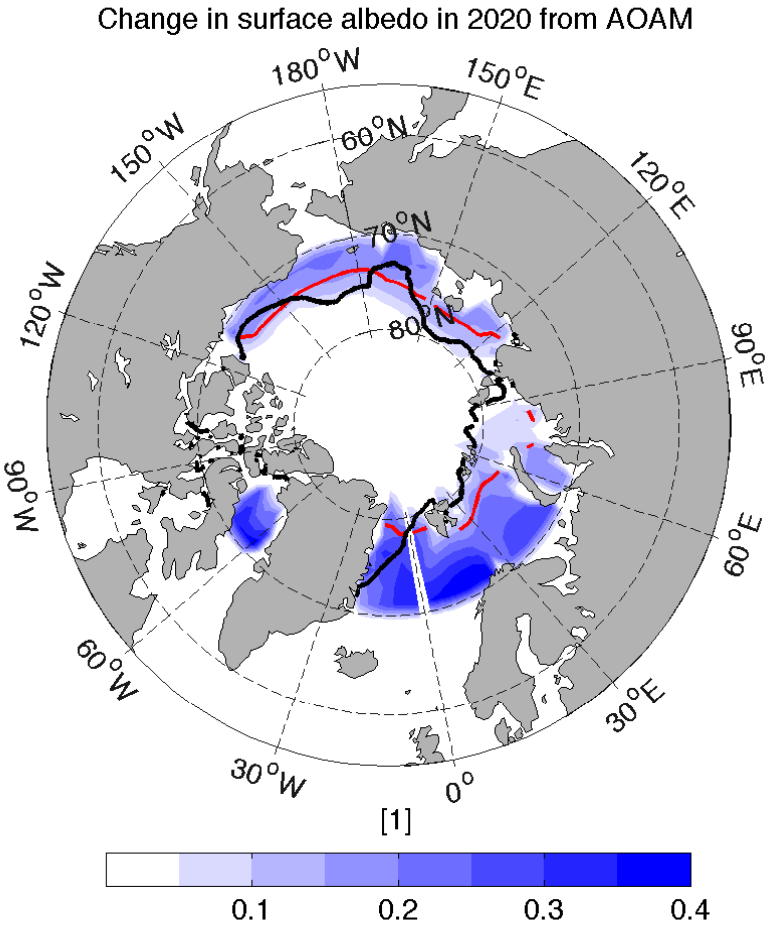

Fig. 2.1.: *Annual mean changes in surface albedo in the Arctic due to the AOAM implementation in 2020 exemplarily in the RCP8.5 scenarios, i.e. RCP8.5 AOAM minus RCP8.5. As a reference the mean september sea ice edge defined as the 15% sea ice concentration contour line from observations (black line) and the UVic ESCM (red line) for the period of 2005 to 2014 is shown, where observations are taken from Meier et al. [2013].*

The objective of AOAM is to alter the radiation budget at the Arctic Ocean surface by mimicking an initiation of the ice-albedo effect, one of the key factors for Arctic amplification of climate change [Holland and Bitz, 2003]. Other feedbacks, such as the cloud-albedo feedback [Serreze and Barry, 2011] are not included in the simulations, since the UVic ESCM simulates no change of cloud albedo with time. This neglected cloud response might lead to a bias in the effect from the AOAM.

2.3. Results

For both, the RCP8.5 and RCP4.5, emission scenarios, the global impact of simulated AOAM is small compared to the reference global annual mean surface air temperature changes of 2.9 °C and 1.4 °C in 2090–2100, respectively. Global mean surface air temperatures are reduced by only 0.2 °C in 2090–2100 in both scenarios when AOAM is implemented. Accordingly there is little potential for this method as a global CE measure, consistent with the previous results by Cvijanovic et al. [2015]. Therefore in the following, we focus on the Arctic defined as the region north of 70 °N and all numbers given are averages over this region if not mentioned otherwise. The implementation of AOAM will be analysed with respect to its potential to reduce Arctic warming and its impact on potential tipping elements discussed by Lenton et al. [2008] relative to the reference state in 2005–2015.

2.3.1. Arctic Radiation Balance and Temperature Changes

The albedo increase associated with the AOAM reduces the amount of shortwave radiation absorbed by the Arctic Ocean areas in summer. In the RCP8.5 (RCP4.5) AOAM simulations surface net downward shortwave radiation is reduced by maximum values of 82 (65) W m^{-2} in boreal summer by the end of the century relative to the default simulations without AOAM. This causes a cooling of the surface and consequently a decrease in the surface outgoing longwave radiation in the subsequent autumn of up to 16 (15) W m^{-2} compared to the default simulations. These changes in surface radiation fluxes cause a strong increase in upward net radiation at the top of the atmosphere (TOA). The two default RCP simulations show a negative 21^{st} century trend in the upward TOA net radiation in the Arctic (Table 2.1), which is reversed if AOAM is implemented. The strongest effect is found for RCP8.5 simulations with an increase of net upward radiation at TOA by 62 W m^{-2} in the summers 2090–2100 upon the simulated deployment of AOAM. In the noEmit simulation no significant trend in TOA net radiation is evident. If AOAM is implemented in noEmit, radiative losses to space increase and temperatures decline. In 2005–2015 the simulated annual mean Arctic surface air temperature is -13.3 °C (Table 2.1), followed by a positive annual mean temperature change until 2090–2100, which ranges between 4.4 °C in the RCP8.5 simulation and 0.0 °C in the noEmit simulation. With the exception of the noEmit simulations, for which the Arctic surface air temperature is reduced by 0.6 °C in 2090–2100 relative to 2005–2015 under the deployment of AOAM, the warming trend in the Arctic can only partly be offset by AOAM. Within the first five years of AOAM deployment there is an initial decrease of Arctic surface air temperatures of 0.5 °C, but thereafter Arctic temperatures start to increase again and follow the same trends as in the corresponding default simulations. The difference between the RCP8.5 and the RCP8.5 AOAM simulation at the end of the century is largest in autumn with lower temperatures of up to 4 °C (and 3 °C for RCP4.5) in the AOAM simulation.
Higher surface air temperatures cause an earlier spring melt of snow on land and a prolonged summer season, with a consequently higher rate of exposure to dark snow-free

Tab. 2.1.: *Arctic climate system changes for the different forcing scenarios and experiments. The given differences are calculated from annual mean values between 2090–2100 and 2005–2015. The considered area is 70–90°N for all properties but for permafrost area and land albedo, where we consider the area of 50-90°N.*

Property	total value in 2005	RCP8.5	RCP8.5 AOAM	RCP4.5	RCP4.5 AOAM	noEmit	noEmit AOAM
TOA net upward radiation [W m^{-2}]	121	-3.3	4.5	-1.2	3.9	0.4	3.8
Surface temperature [$°C$]	-13.3	4.4	3.2	2.2	1.2	-0.0	-0.6
Ocean ice volume [$10^3 km^3$]	14.2	-7.7	-5.2	-4.2	-1.2	-0.5	1.6
Permafrost area [$10^6 km^2$]	17.3	-8.1	-6.6	-4.0	-2.8	-0.1	0.7
Ocean albedo [1]	0.548	-0.104	0.065	-0.054	0.063	-0.005	0.070
Land albedo [1]	0.46	-0.048	-0.043	-0.029	-0.024	-0.004	-0.001

areas in summer [Serreze and Barry, 2011]. The annual mean land surface albedo in the 2005–2015 reference state north of 50 °N is 0.46 (Table 2.1). In all six experiments this value decreases, meaning that more of the incoming shortwave radiation is absorbed. Hence the soils warm and emit more longwave radiation, further warming the atmosphere above. The AOAM simulations show lower land albedo decreases relative to their respective default simulations without AOAM (Table 1), because the lower temperatures in the AOAM simulations partly prevent the reduction of snow cover and changes in vegetation cover. Over the ocean, albedo changes are strongly related to sea ice. In the AOAM simulations, the annual mean albedo over the Arctic Ocean is forced to increase with respect to year 2005, in contrast to an oceanic albedo reduction in the default simulations (Table 2.1).

2.3.2. Arctic Sea Ice

The reduction of the Arctic surface temperatures achieved by AOAM is evaluated for its potential to reduce Arctic summer sea ice loss and to allow for the formation of thicker and therefore more robust winter sea ice. The simulated Northern Hemisphere annual minimum sea ice extent in the UVic ESCM amounts to 4.3 million km^2 in the summers of 2005–2015 (Figure 2.2a). This value is within the range of the summer sea ice extent simulated in the same time period by the CMIP5 models' of about 3 to 10 million km^2 [Stroeve et al., 2012], but lower than the observed minimum sea ice extent of about 5.5 million km^2 in 2005–2012 [Stocker et al., 2013]. The modelled mean September sea ice extent averaged over 2005–2014 is close to the observed sea ice extent in the same period

(Figure 2.1, contour lines), although the simulated ice edge position differs slightly.

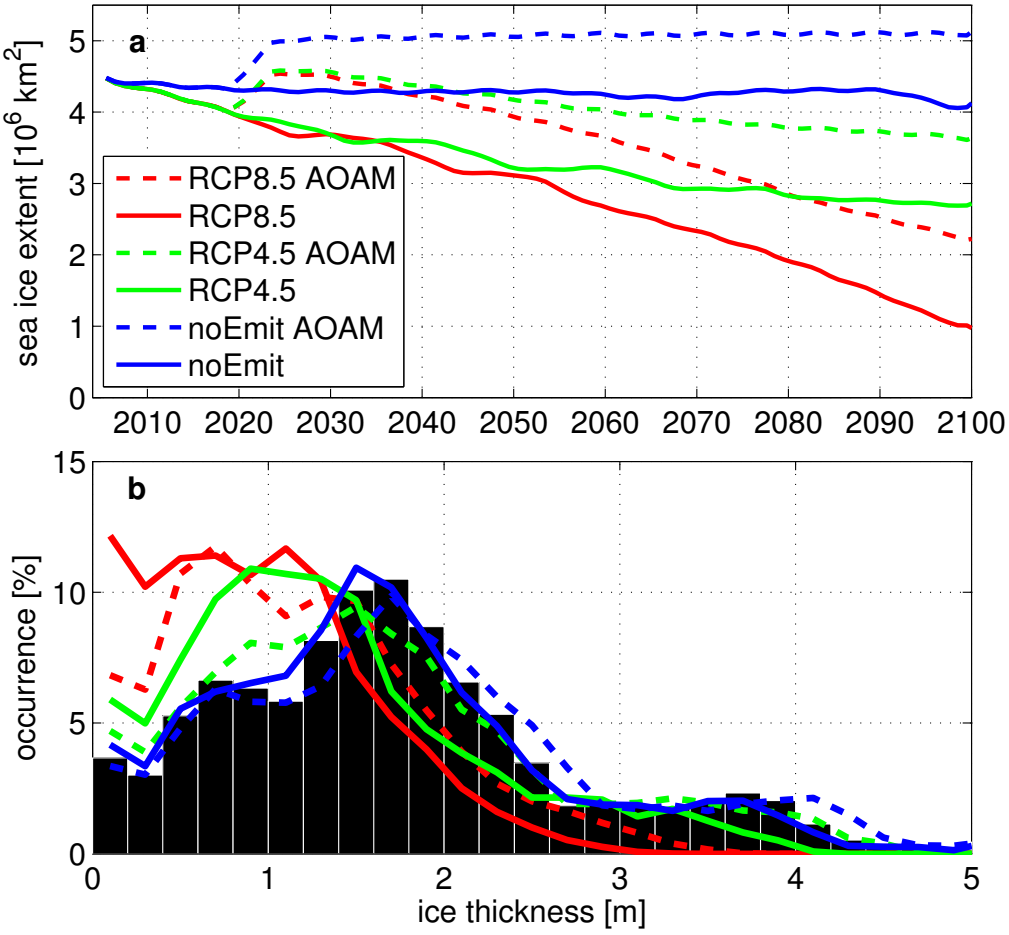

Fig. 2.2.: *a) Northern Hemisphere annual minimum sea ice extent for the different forcing scenarios, see legend, calculated as the yearly minimum of Arctic sea ice extent with a temporal resolution of 15 days; b) Areal sea ice thickness distribution in the Arctic Ocean from 15 day mean value occurrences relative to total non-zero value occurrences in the year 2005 (black bars) and in the years 2090–2100 for the different forcing scenarios, color coding is the same as for a).*

In all three simulations without AOAM, the warming causes a decrease in the minimum sea ice extent until 2100. In the high emission RCP8.5 simulation only 1 million km^2 of the Arctic Ocean are still ice covered in summer, which is comparable to the CMIP5 mean of 0.5 million km^2 [Stocker et al., 2013]. The AOAM deployment causes a sea ice extent increase by about 0.75 million km^2 within the first 5 years after implementation, regardless of the emission scenario (Figure 2.2a). Thereafter the development of the minimum sea ice extent in the AOAM simulations follows very similar negative trends as the respective simulation without AOAM, i.e. a negative trend of 0.40 (0.12) million km^2 per decade for the RCP8.5 (RCP4.5) scenario and almost no trend in the noEmit simulations.

This indicates that, after some positive effects in the first few years of implementation, AOAM is not able to prevent sea ice from decreasing in the longer term, as long as CO_2 continues to accumulate in the atmosphere. Nevertheless, the decline in Arctic sea ice cover is delayed in the simulations with AOAM: In the RCP8.5 (RCP4.5) case the implementation of AOAM causes the sea ice extent of 2100 to resemble the state of the default simulation of 2075 (2040). That is, AOAM may help to delay the effects of global warming by 25 (60) years with respect to Arctic sea ice decline under the RCP8.5 (RCP4.5) scenario.
In addition to sea ice extent, which is important for the radiation budget, sea ice thickness provides information about the robustness of the ice cover concerning short term temperature changes or weather fluctuations. The simulated annual modal ice thickness in the reference state of 2005 is 1.7 m, which agrees well with observed basin mean ice thicknesses of about 1.1 to 1.8 m for the same decade [Lindsay and Schweiger, 2015]. To get a better understanding of the development of the sea ice thickness distribution, we regard the initial sea ice thickness distribution of the Arctic Ocean in 2005 and its mean distribution for 2090–2100 for the six different experiments (Figure 2.2b). In 2005 the modal ice thickness is 1.7 m, with local maximum ice thicknesses reaching 5.1 m. As expected there is a shift towards thinner ice in the RCP8.5 simulation without AOAM, strongly reducing the amount of ice thicknesses larger than 1.5 m. The thickest ice toward the end of the 21^{st} century is only 3 m thick. In the RCP4.5 simulation without AOAM, the shift in sea ice thickness toward lower values is also evident. The area with sea ice thicker than 1.7 m is strongly reduced and the maximum thickness is 3.9 m. Sea ice in the noEmit simulation without AOAM follows the distribution of the reference state in 2005 very closely.
AOAM causes the distribution to shift towards higher values. There is a more frequent occurrence of sea ice thicknesses larger than 1.5m in the RCP8.5 AOAM simulation. For the RCP4.5 AOAM simulation the sea ice thickness distribution is very close to the 2005 distribution. An implementation of AOAM in the noEmit case accordingly causes the sea ice thickness distribution to shift to slightly higher values compared to the reference state. In addition, in the high emission simulations without AOAM, the total Northern Hemisphere ice volume is strongly reduced by the end of the century. In the RCP8.5 (RCP4.5) simulation over 54 (30) % of the ice volume is lost (Table 2.1). This negative trend is only weakened and not reversed by the implementation of AOAM despite its positive effect on the ice thickness distribution. If we compare the ice volume in 2090–2100 to the reference state in 2005–2015, we see a larger decrease in the RCP8.5 AOAM simulation of 37 %, compared to the default RCP4.5 simulation.

2.3.3. Meridional Overturning Circulation and Ocean Bottom Temperatures

The effects of AOAM on the radiation budget and sea ice coverage are generally consistent with findings of earlier studies [Cvijanovic et al., 2015]. In the following, we thus focus on remote consequences of AOAM for the three-dimensional ocean circulation, water masses and heat transport. Generally, the Earth System regulates the meridional imbalance of the net radiation via meridional heat transports in the atmosphere and ocean. Climate model experiments suggest a weakening of the Atlantic Meridional Overturn-

ing Circulation (AMOC) under global warming conditions in response to a reduction in meridional temperature gradients resulting from Arctic amplification of global warming [Stocker et al., 2013].

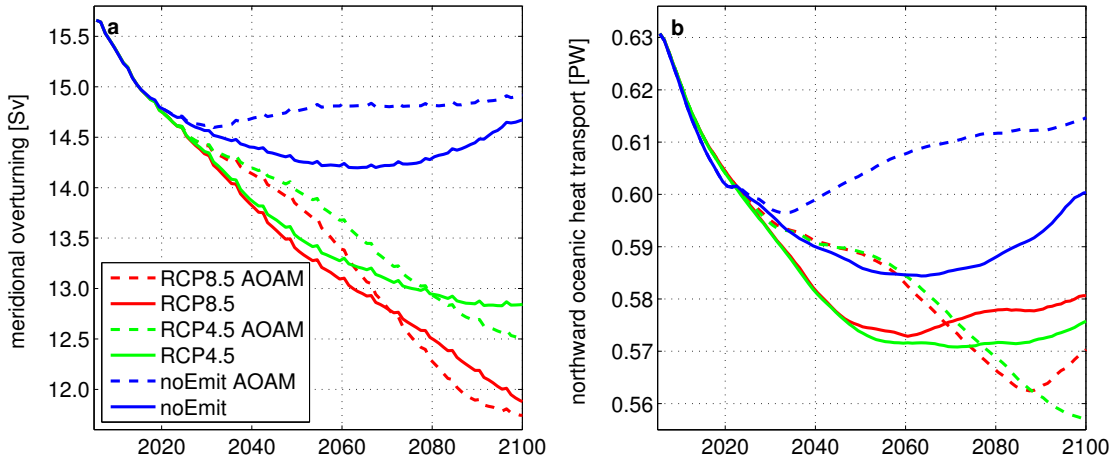

Fig. 2.3.: *a) Annual mean maximum North Atlantic meridional overturning and b) annual mean northward oceanic heat transport in the Atlantic at 26° N for the different forcing scenarios and experiments, see legend.*

This negative trend is evident in the evolution of the AMOC in all three simulations without AOAM until 2050 (Figure 2.3a). A recovery of the AMOC is seen for the noEmit default simulation after 2070 and the decline has stopped in the RCP4.5 default simulation by 2100. In contrast, the AMOC strength keeps declining in the RCP8.5 simulation until 2100 because in this scenario atmospheric CO_2 concentrations still increase at the end of the century.

The reduction in high-latitude surface temperatures in the AOAM simulations causes the sea ice extent in the high northern latitudes to increase during the first 5 years of AOAM implementation (Figure 2.2a). The associated sea ice formation results in a salt flux into the ocean increasing the density of water exported from the Arctic ocean. This causes more intense deep convection in the subpolar North Atlantic between 50 °N and 70 °N, which is not temperature but salinity driven (Figure A.2). As a consequence, a slower reduction of the AMOC is found in the experiments with AOAM between 2020 and about 2060 (Fig. 2.3a). In the RCP8.5 and RCP4.5 AOAM simulations, the AMOC shows a stronger decrease after 2050, even stronger than in the default simulations without AOAM, which can again be attributed to changes in the freshwater budget in the North Atlantic deep convection areas. There is continued sea ice melt while regional precipitation does not change during this time period (Figure A.2d). As a result, sea surface salinity in the North Atlantic area between 50-70 °N is reduced between 2040 and 2080 (Figure A.2c). As a result, the AMOC in the AOAM emission simulations show weaker overturning strengths compared to the respective default simulations in year 2100.

The initial delay in the AMOC reduction in the AOAM simulations causes a higher rate of

northward heat transport from 2020 until 2060 compared to the default simulations (Figure 2.3b). For the period from 2005 to 2100 the accumulated northward heat transport in the AOAM simulation is higher by 0.021 PW for the RCP8.5 scenarios, whereas the increase is 0.228 PW for RCP4.5 and as high as 1.265 PW in the noEmit simulations.

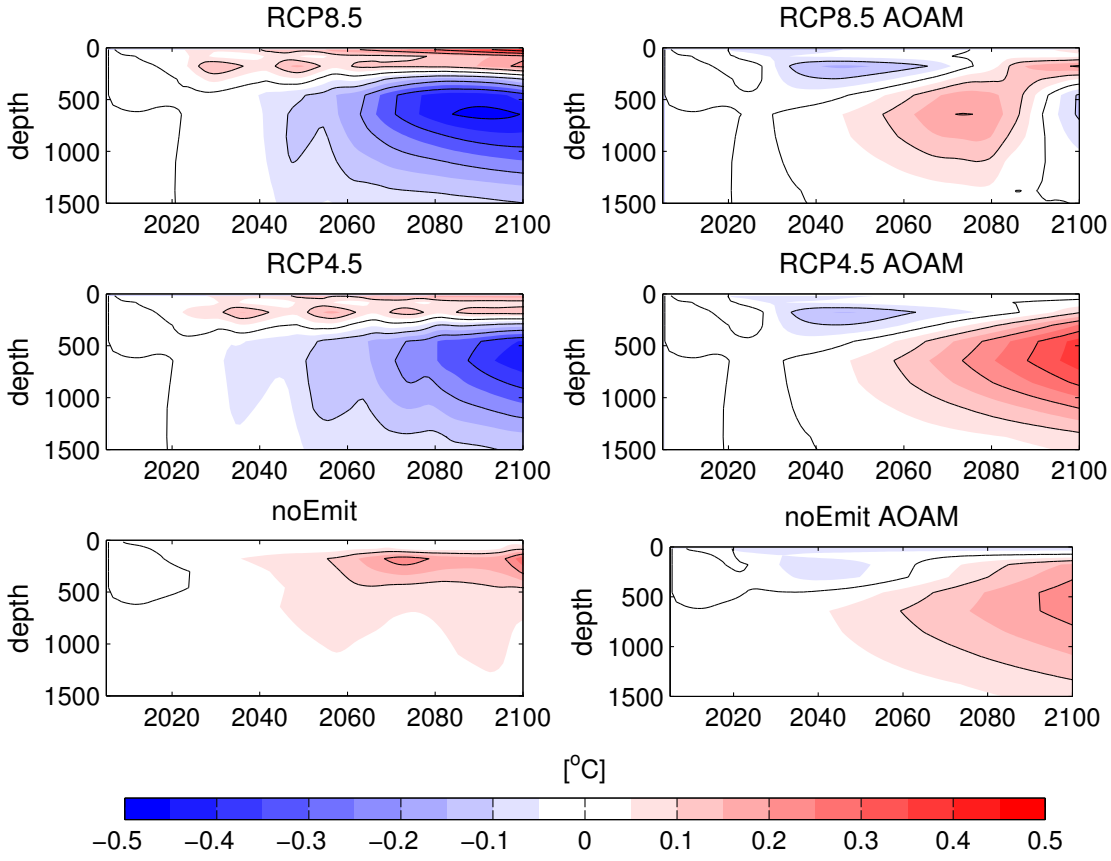

Fig. 2.4.: *Hovmöller diagrams of mean Arctic vertical temperature profile changes relative to 2005 between 70 and 90 °N for the six different forcing scenarios (left) and AOAM experiments (right). Black contours mark 0.1 °C temperature intervals.*

The increased oceanic northward heat transport causes an unexpected sub-surface warming in the AOAM simulations (Figure 2.4). In both RCP default simulations a surface warming, due to local heat exchange with the warming atmosphere in summer, and sub-surface cooling are evident. The latter is associated with oceanic heat loss to the atmosphere during deep convection events in the Nordic Seas in winter and spring (Figure 2.5a). Note, in our model these convection sites extend to north of 70 °N (Figure A.3), and occur in addition to the main North Atlantic deep convection south of Iceland. Retreat of the winter sea ice edge due to progressing warming in the default emission scenarios enables open ocean deep convection in this buoyantly unstable ocean area, which otherwise is prevented by a solid sea ice cover inhibiting direct exchange with the atmosphere. These events are much more unlikely to occur in the noEmit simulation, in which the ice

cover does not retreat but nonetheless experiences natural variability.

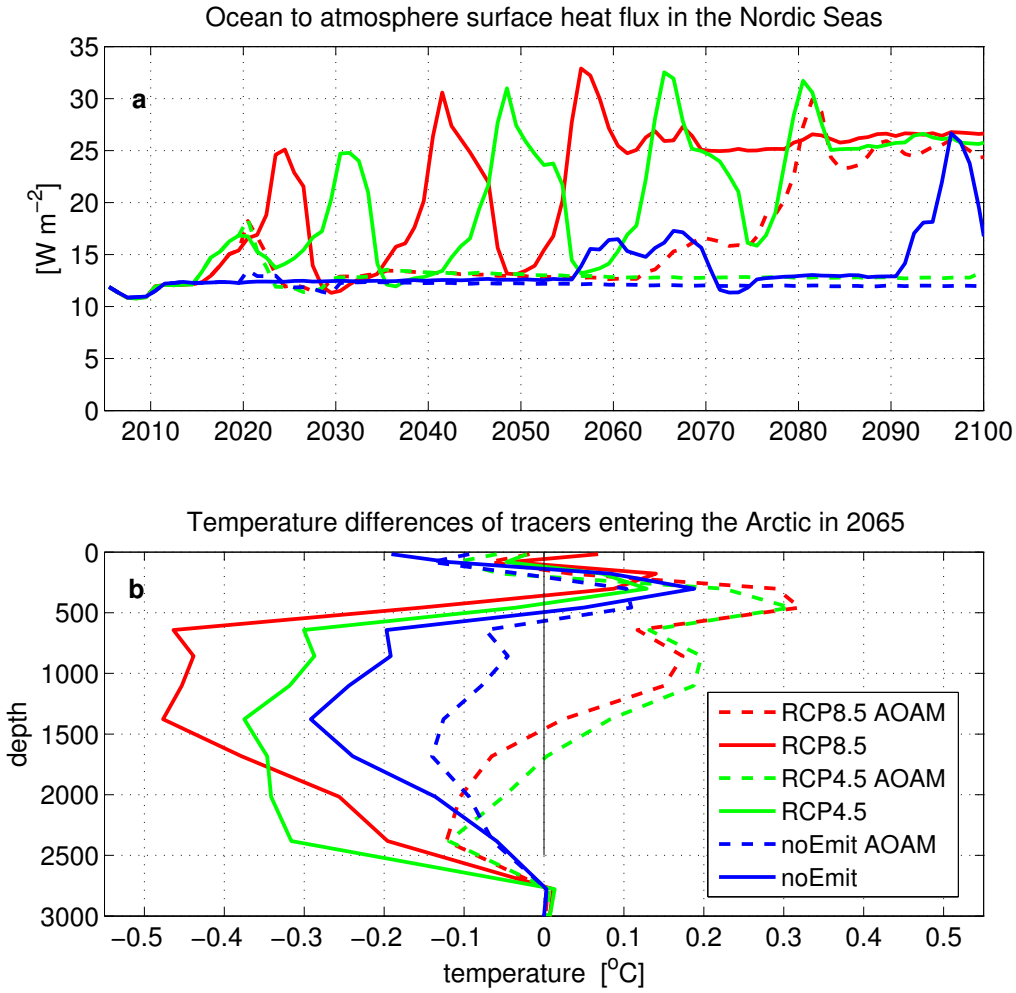

Fig. 2.5.: *a) Mean ocean to atmosphere surface heat flux in the Nordic Seas (defined as the area 65 to 80 °N and 30 °W to 30 °E); b) Temperature differences in traced water masses entering the Arctic for the different forcing scenarios and experiments, exemplarily for the period 2060-2070 relative to 2020–2025, i.e. the beginning of the tracer experiment.*

In contrast, a sub-surface warming signal is emerging at depths of 400 to 1200 m in the AOAM simulations, which is caused by two accompanying features. First, the lack of deep convection events in the AOAM simulations (Figure 2.5a), due to a winter sea ice cover which is forced to extent to 70 °N, i.e. the location of the newly formed convection sites, prevents the deeper ocean from cooling. The RCP8.5 AOAM simulation is an exception, where deep convection occurs from 2080 onward, resulting in a cooling signal at the end of the century similar to the default runs. And second, water mass transport into the Arctic increases, which is evident from enhanced dilution of the implemented

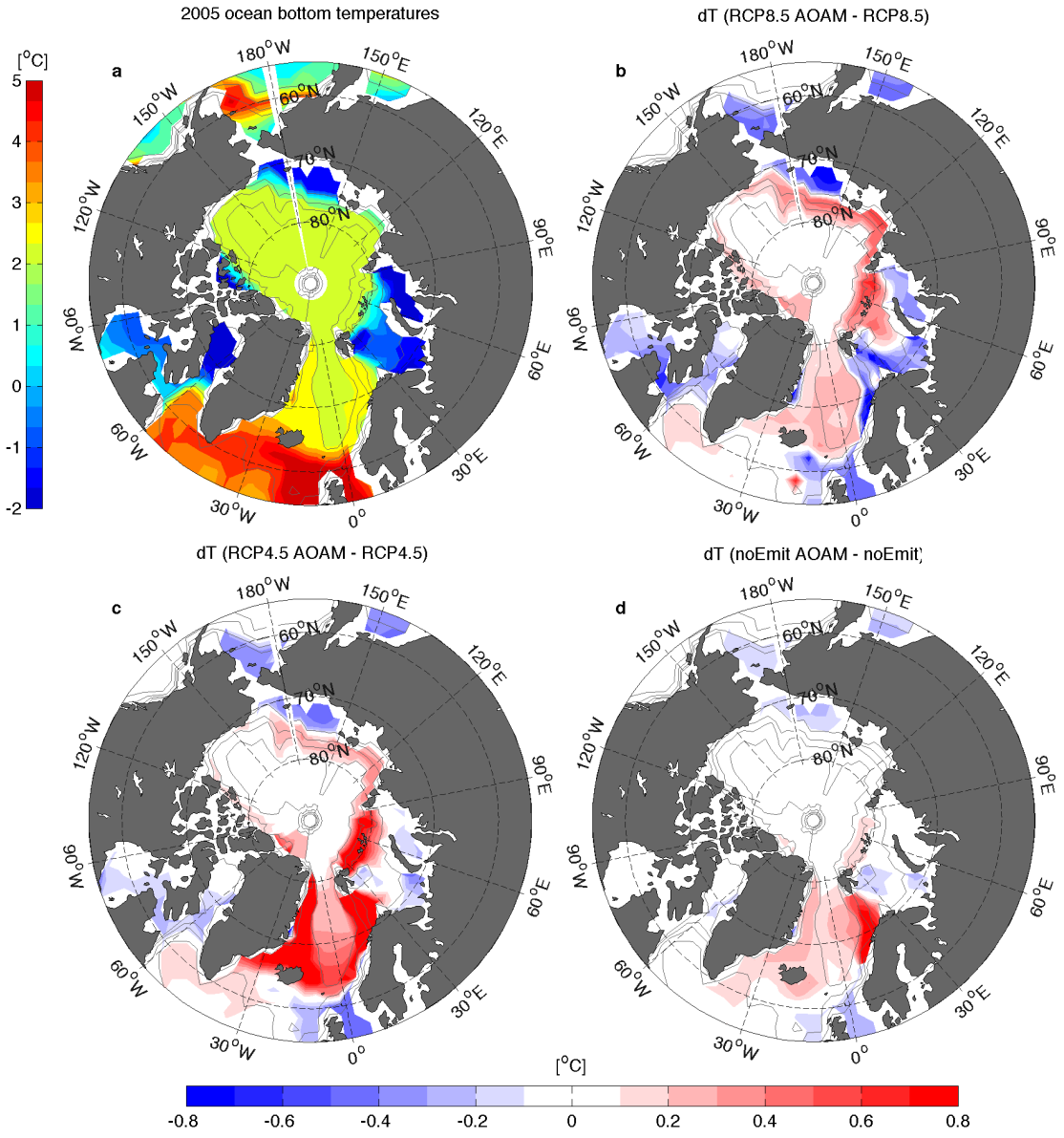

Fig. 2.6.: *a) Annual mean Arctic Ocean bottom temperatures simulated for 2005–2010; Annual mean changes in Arctic Ocean bottom temperatures in 2090–2100 due to the implementation of the AOAM in the RCP8.5 simulation b), in the RCP4.5 simulation c), and in the noEmit simulation d). Contour lines are model topography of 750m, 1500m and 2500m depth.*

Arctic dye tracer (Figure A.4 and A.7). The dilution coincides with an increase in water temperatures, most notably at depths of 400 to 1200 m (Figure 2.5b and Figure A.5). Note, that the entering water masses are again influenced by the heat exchange with the atmosphere (Figure A.3), which explains the deep reaching negative temperature changes in the RCP8.5, RCP4.5 and NoEmit simulations. However, in the RCP8.5 AOAM and the RCP4.5 AOAM simulations, a warming signal in the entering water masses is evident, indicating a warming from entering water masses, uninfluenced by the deep convection. Increasing inflow to the Arctic always means warming as the entering water mass is always warmer, especially when there is no deep convection in the Nordic Seas. In addition the inflow water warms in the emission scenarios due to global warming.
Both the prevented deep convection and the increasing inflow lead to the sub-surface warming signal located along the continental slope in the Arctic Ocean (Figure 2.6), where the effect of both features can be regarded separately. In the two RCP8.5 runs with and without AOAM, deep convection occurs continuously after 2080. Therefore, the warming signal along the continental shelf slope (Figure 2.6b) can be related to the temperature increase of the inflow from global warming. In contrast, the two RCP4.5 runs have opposing deep convection states and we see en enhanced warming signal from accumulated heat due to the lack of deep convection in RCP4.5 with AOAM (Figure 2.6c). It is noteworthy that most of the Arctic marine methane hydrates are located along the slope of the continental margin [Kvenvolden et al., 1993; Biastoch et al., 2011]. A cooling trend as found in the default simulations would act to stabilize the hydrates. Our simulations indicate that introducing AOAM yields warming instead. We thus conclude that AOAM could increase the risk of melting methane hydrates, which could lead to a further increase in atmospheric greenhouse gas concentrations.

2.3.4. Permafrost thawing

Increasing terrestrial temperatures in the Arctic can impact permafrost. The active layer in the upper meters of the soil is controlled by the annual mean air temperature and the amplitude of the seasonal cycle, while the actual temperature of the permafrost layer below is very close to the annual mean temperature [Koven et al., 2013]. In an attempt to assess the future development of permafrost, we take annual mean soil temperatures at 1m depth below zero degrees Celsius as a simple indicator for the presence of permafrost. This estimate yields a simulated permafrost area of 17.6 million km^2 in 2005–2015 (Table 2.1 and Figure 2.7a). This is similar, though slightly lower, than the observational estimate by Tarnocai et al. [2009] with a permafrost area of 18.8 million km^2. In the UVic ESCM, the simulated soil temperature in the permafrost area of 2005–2015 increases by 1.2 °C in the period from 1985-2015, which is in line with the observed trends of Romanovsky et al. [2011], who report that the permafrost temperature in Northern Russia has increased by 1-2 °C over the last 30-35 years.
Permafrost soil temperatures increase at 0.5 (0.2) °C per decade from 2020 to 2100 in the RCP8.5 (RCP4.5) scenario (Figure 2.7a). In the noEmit simulation temperatures in the permafrost soils start to stabilize at mean temperatures of about −5.6 °C. As a consequence of increasing temperatures the permafrost area decreases in the two reference RCP

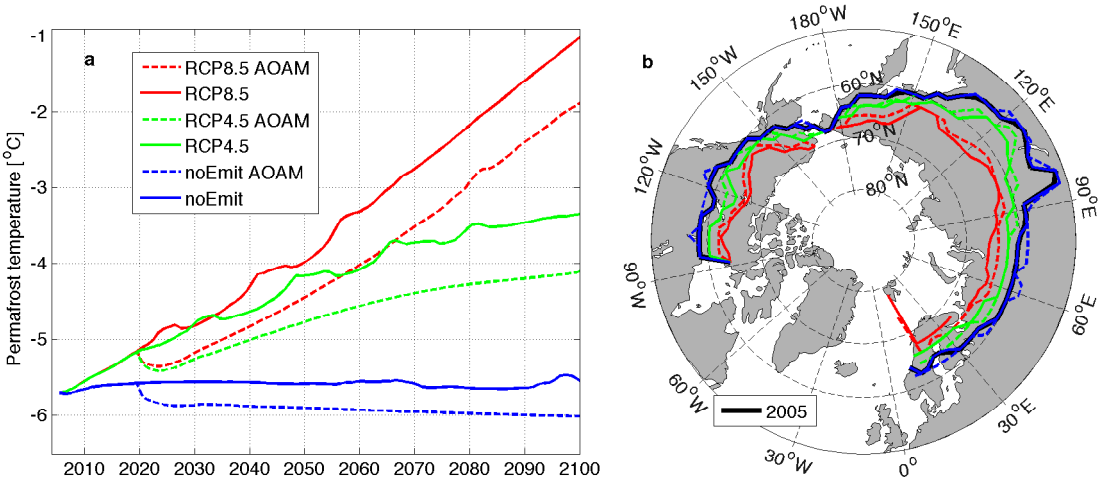

Fig. 2.7.: *a) Temporal development of the annual mean soil temperature in the uppermost meter in the area defined as permafrost in 2005-2015, see black border in b) for the different forcing scenarios; b) Map of annual mean permafrost boundaries in the years 2005–2015 (black) and in 2090–2100 for the different forcing scenarios and experiments, color coding is the same as for a)*

simulations and the annual mean permafrost boundaries migrate northward (Figure 2.7b). In the default simulations under RCP8.5 (RCP4.5) the annual mean surface permafrost area is reduced by 8.9 (4.3) million km^2 by the end of the century. This is a reduction of 50.6 (24.4) % compared to the permafrost area in 2005–2015. For the noEmit simulation without AOAM the decrease by 2090–2100 is 1.1 % of the 2005–2015 permafrost area. AOAM delays the shrinking of the permafrost area. Since the positive temperature trends can not be reversed but only offset in the first few years of AOAM implementation, there is still an increasing soil temperature trend in the permafrost soils in the RCP8.5 (RCP4.5) AOAM simulations of 0.5 (0.1) °C per decade. This initial offset in soil temperature trends relative to the default simulations, is reflected in larger surface area of annual mean permafrost in the AOAM simulations. For the noEmit AOAM simulation, the soil temperature trend is slightly negative, leading to a simulated expansion of permafrost area under AOAM.

Similar to surface air temperature and sea ice extent, soil temperatures highlight that AOAM only yields an initial onetime offset. Would this delay in surface warming still make a difference in terms of carbon release to the atmosphere? Tarnocai et al. [2009] provide estimates of soil carbon pools in the circumpolar permafrost area. Using their estimate of carbon content in the first meter of the soil of 26.4 kg m^{-2}, a prevented permafrost soil loss of about 1.7 (1.2) million km^2 until 2100 would amount to a prevented carbon release of 44.9 (31.7) Pg of carbon by 2100. These amounts correspond to about 3 to 4 years of todays annual carbon emissions and are small compared to the amount that would be released due to the permafrost area reduction in the reference RCP8.5 (RCP4.5) simulation of 235 (114) Pg C by 2100. Note, that these estimates are very simplistic and do not include feedbacks from the released carbon of the permafrost soils.

2.4. Discussion

2.4.1. Limitations of this study

Some climatically important limitations of this study arise from the chosen model set up. With respect to the tipping elements of Lenton et al. [2008] and the Arctic radiation budget the most important ones are the treatment of the Greenland ice sheet, atmospheric chemistry and cloud processes. For the simulations in this study continental ice sheets were held constant to facilitate the interpretation of the results. While variations in ice sheet dynamics only play a marginal role during the 100-year period studied, the lack of simulated melting from the Greenland ice sheet will cause a bias in the simulated freshwater input to the North Atlantic Ocean. The melt water would likely cause a reduction in deep water formation due to increased vertical stratification and thus could potentially interfere with a recovery of the AMOC as initially seen upon implementation of AOAM in the model. On the other hand, AOAM causes a reduction in surface air temperatures as well as ocean surface temperatures around Greenland, and could therefore possibly reduce Greenland ice melt. It is beyond the scope of this study to investigate, which of these processes is dominant on different time scales.
The UVic ESCM does not include atmospheric chemistry. Thus we cannot investigate whether or not a cooling of the ocean surface would favour, for example, ozone depletion in the stratosphere and potentially impact the Arctic ozone hole. We can only speculate, that the changes in meridional temperature gradients due to the implementation of AOAM might influence atmospheric circulation patterns and thereby might affect ozone depletion. However, AOAM is implemented mostly during summer, and chemical ozone depletion takes place in winter/spring. We therefore expect no strong interference between these two processes.
Further limitations of our study include the coarse resolution of our model, the simplistic representation of the atmosphere and the lack of a more sophisticated permafrost model. Due to the coarse resolution grid, our model simulates North Atlantic deep convection not at the observed location in the Labrador Sea, but further east, south of Iceland. This bias does not have a strong impact on the results of this study concerning the changes in the deep convection, since these are forced by changes in sea surface salinity, which occur everywhere in the Atlantic between 50 and 70 °N. However, it is noteworthy that salinity in the western part of the North Atlantic in our model are in general lower, and might therefore be more sensitive to changes in sea surface salinity. The UVic ESCM lacks a vertical representation of atmospheric dynamics and does not simulate a dynamic cloud response. Therefore, the model misses part of the changes in meridional heat and moisture transports [Graversen et al., 2008] and lacks the cloud-albedo feedback as described by Serreze and Barry [2011]. Other atmospheric feedbacks such as the response of sensible and latent heat fluxes as well as the longwave radiation response are however implemented. Furthermore, our estimate of soil permafrost is a simple calculation lacking the dynamical representation of vertical soil temperature profiles as used by e.g. Avis et al. [2011]; MacDougall et al. [2012].

2.4.2. Assessment of AOAM

We assess the potential of AOAM in light of the Arctic tipping elements described by Lenton et al. [2008] under varying CO_2 emission scenarios: In line with Cvijanovic et al. [2015] we find a limited potential in global temperature reduction. However, Arctic surface air temperatures in 2090–2100 can be reduced by 1.2 °C in the RCP8.5 AOAM simulation relative to the default emission simulation, which is comparable to the regional 1.6 °C temperature reduction found by Cvijanovic et al. [2015] in an experiment with an albedo modification of 0.8 over the area north of 70 °N, i.e. the same AOAM implementation, but with different CO_2 forcing.
In all AOAM simulations, Arctic summer sea ice area can initially be increased by 0.75 million km^2, but then continues to follow the negative trend of the respective default simulation. In 2090–2100, 53 % of the 2005–2015 summer sea ice area remains in the RCP8.5 AOAM simulation, compared to 27 % of the ice area remaining in the RCP8.5 simulation. Our values are higher compared to the 29 % remaining summer sea ice cover from the study of Cvijanovic et al. [2015, their experiment: albedo of 0.8 north of 70 °N], since we use different reference states, namely 2005–2015 in our study, compared to a preindustrial $1xCO_2$ atmosphere reference in the study by Cvijanovic et al. [2015], as well as different averaging areas.
In contrast to the study by Cvijanovic et al. [2015] focusing on atmospheric variables, we here focus on oceanic and terrestrial processes. All AOAM simulations reveal a potential to initially increase the strength of the AMOC relative to the default simulations. A side effect of the associated initial higher northward oceanic heat transport in the AOAM simulations compared to the default simulations is a sub-surface warming located along the continental slope. This is the region where most of the Arctic marine methane hydrates are located [Kvenvolden et al., 1993; Biastoch et al., 2011]. Our results indicate that the partial recovery of the AMOC, which is one of the potential tipping elements from Lenton et al. [2008], as well as the inhibited deep convection is favouring a destabilisation of the marine methane hydrates in the Arctic, another listed potential tipping element discussed by Lenton et al. [2008]. This trade off illustrates that it might not be possible to simultaneously address all Arctic tipping elements with such a local CE measure. Nevertheless, an initial offset of the positive temperature trends yields some potential in reducing the risk of releasing additional greenhouse gases to the atmosphere. Until 2100 this offset leads to a prevented carbon release from melting permafrost soils of 19 (28) % in the RCP8.5 (RCP4.5) AOAM simulation relative to the default simulations without AOAM. Cvijanovic et al. [2015] show that about 40 % of the preindustrial permafrost area remains in their model simulations. In our RCP8.5 AOAM simulation 59 % of the 2005–2015 permafrost area remains frozen. Furthermore, we find that with progressing climate change, deep convection events start to occur in the Nordic Seas in the default emission simulations, and act to cool the deep ocean. These convection events are initially prohibited by the implementation of AOAM. Since the newly formed deep convection areas are located right at the edge of the 70 °N border, i.e. the AOAM implementation border in the Nordic seas, where with progressing climate change the sea ice starts to retreat if AOAM is not implemented. This hints to the fact that the Arctic climate system reacts sensitive to the

location of the AOAM implementation.
In contrast to the study by Cvijanovic et al. [2015], our transient climate change setting enables us to look at changes in simulated trends of the various metrics. It is found that, AOAM has no potential to reverse trends in Arctic surface air temperature, sea ice and soil temperatures, but rather holds some potential to temporarily offset these trends. This holds true for all simulations, including a high emission scenario as well as a very idealized maximum mitigation scenario (excluding negative emissions). In line with the fact that a local cooling at high northern latitudes causes compensatory heat fluxes in the atmosphere and the ocean [Tilmes et al., 2014], the regulation of internal heat budgets in the climate system limits the potential of AOAM to counteract Arctic amplification of global warming. Moreover, we find that no matter when the deployment of AOAM is terminated even under the intermediate emission scenario RCP4.5, the sea ice extent quickly reverses to match the sea ice extent of the default simulation (Figure A.6). This demonstrates how AOAM must be maintained over decades to keep up its initial effect of delaying global warming consequences in the Arctic.

2.5. Conclusion

The self-regulating nature of the climate system prevents regional, high latitude CE methods from having global and sustainable effects. In line with Tilmes et al. [2014] we find that the Arctic cooling introduced by AOAM causes compensatory meridional heat transports, limiting the effect of AOAM to a single, non-repeatable delay of the warming, sea ice loss and permafrost retreat if greenhouse gas emissions continue to rise. Moreover, undesirable side effects arise from the potential of enhanced warm water inflow into the Arctic Ocean to destabilize methane hydrates. In this respect AOAM could even increase the risk of releasing additional, natural greenhouse gases to the atmosphere.
At the end of the 21^{st} century the state of the intermediate emission simulation (RCP4.5) without AOAM is closer to the 2005–2015 reference state than the state of the high emission scenario (RCP8.5) with AOAM applied, for all metrics considered. This demonstrates that AOAM only delays impacts of ongoing CO_2 emissions. Thus on longer time scales a reduction in emissions still appears to be the safest way to prevent severe climate change in the Arctic.

Acknowledgments The model data used to generate the table and the figures will be made available at http://thredds.geomar.de. We thank Christina Roth, Julia Getzlaff and Heiner Dietze for helpful discussions. This work was funded by the German DFG in the context of the Priority Program 'Climate Engineering: Risks, Challenges, Opportunities?' (SPP 1689). The authors declare that they have no competing financial interests. N.M., A.O. and D.P.K. conceived and designed the experiments. N.M. implemented and performed the experiments and analysed the data. N.M. wrote the manuscript with contributions from D.P.K., T.M. and A.O.. The authors would like to thank Ivana Cvijanovic, an anonymous reviewer, and the associate editor for their helpful and constructive comments, and the editorial staff for their efforts.

3. Uncertainty in the response of transpiration to CO_2 and implications for climate change - A sensitivity study

This chapter is based on the paper 'Uncertainty in the response of transpiration to CO_2 and implications for climate change' published in the journal Environmental Research Letters. Citation: Mengis N., D. P. Keller, M. Eby and A. Oschlies, (2015), Uncertainty in the response of transpiration to CO2 and implications for climate change, Environ. Res. Lett., 10 094001, doi:10.1088/1748-9326/10/9/094001.

Abstract While terrestrial precipitation is a societally highly relevant climate variable, there is little consensus among climate models about its projected 21^{st} century changes. An important source of precipitable water over land is plant transpiration. Plants control transpiration by opening and closing their stomata. The sensitivity of this process to increasing CO_2 concentrations is uncertain. To assess the impact of this uncertainty on future climate, we perform experiments with an intermediate complexity Earth System Climate Model (UVic ESCM) for a range of model-imposed transpiration-sensitivities to CO_2. Changing the sensitivity of transpiration to CO_2 causes simulated terrestrial precipitation to change by -10 % to +27 % by 2100 under a high emission scenario. This study emphasises the importance of an improved assessment of the dynamics of environmental impact on vegetation to better predict future changes of the terrestrial hydrological and carbon cycles.

3.1. Introduction

Terrestrial evapotranspiration is the transfer of water from the land surface to the atmosphere. It is the sum of evaporation from soils and vegetation, and plant transpiration [Wang and Dickinson, 2012]. The partitioning of evapotranspiration into its three components is not accurately know [Lawrence et al., 2007]. In the Second Global Soil Wetness Project [Dirmeyer et al., 2006] 13 land models were forced by reanalyses data and direct measurements and it was found that the multi-model mean estimate of plant transpiration amounts to 48 % of global evapotranspiration [Lawrence et al., 2007]. Transpiration describes the evaporation of water from the vascular system of plants through leaf pores, or stomata. It couples the biochemical process of leaf carbon uptake through photosynthesis with the biophysical process of moisture exchange [Niyogi et al., 2009]. Both processes depend on the opening of stomata, defining the strength of stomatal conductance [Keenan et al., 2013].
Stomatal conductance is sensitive to atmospheric CO_2 concentrations, since the rate of

photosynthesis that can be performed by the plant, depends on how much carbon and moisture is available. Opening the stomata allows plants to take up more CO_2 through diffusive fluxes from the ambient air, simultaneously they will lose more water through the opened stomata. Thus, there is a trade off between CO_2 uptake and the associated water loss, which defines the water-use efficiency (WUE) of the plant.
With increasing atmospheric CO_2 concentrations, the diffusive flux of CO_2 will increase and the stomata can take up the same amount of carbon, while opening their stomata less often [Ball et al., 1987]. However, it is currently under debate if plants will take up more carbon and grow more biomass by optimising their WUE or if they will reduce their water loss and grow the same biomass. A recent study in which WUE was derived from satellite-based remote sensing data suggest that land-cover and land-use changes in recent years caused an small decline in the global WUE [Tang et al., 2014], with a lot of internal variability. In contrast to this, in various CO_2 enrichment experiments a decrease in stomatal conductance was evident. However, even under experimental conditions, there is a large uncertainty in the CO_2 induced change in stomatal conductance [Kruijt et al., 2008]. In open-top chamber experiments, the relative decrease in stomatal conductance varied between 8.3 to 59 %, with CO_2 concentrations increased to between 550 and 900 ppm. Likewise an overall decrease in evapotranspiration and an increase in the plants' WUE with higher levels of CO_2, were observed during open field and forest, free-air concentration enrichment (FACE) experiments [Keenan et al., 2013]. The observed changes in these terrestrial ecosystems are larger in magnitude than predicted by 13 terrestrial biosphere models and suggest a partial closure of stomata [Keenan et al., 2013]. Closing stomata will reduce the water exchange between vegetation and atmosphere [Wang and Dickinson, 2012], which is likely to feed back on the amount of water vapour in the atmosphere available for precipitation.
Although a positive trend in precipitation under CO_2 induced global warming is expected from the Clausius-Clapeyron equation [Allan et al., 2013; Wentz et al., 2007], it is not yet evident over land. For the recent historical period, between 1951 and 2005, in which atmospheric CO_2 concentrations have increased by about 70ppm, observed terrestrial precipitation shows changes between -7 to +2 mm per decade, with error bars ranging from 3-5 mm per decade [Solomon et al., 2007]. In comparison, the models of the Coupled Model Intercomparison Project 5 (CMIP5) simulate terrestrial precipitation changes for the period of 1930-2004 with values ranging between -4.2 and +1.2 mm per decade [Kumar et al., 2013]. Due to the large uncertainty in the observations and the large inter-model range, it is difficult to make out a clear trend in terrestrial precipitation.
For projections under the Representative Concentration Pathway 8.5 (RCP8.5) emission scenario, the CMIP5 models simulate global precipitation increases of 5-11 %, relative to present day, by 2100 [Allan et al., 2013]. The sign of this response is consistent with the predicted physically driven increase in atmospheric water vapour [Wentz et al., 2007]. In contrast to the positive precipitation trends of all CMIP5 models, the University of Victoria Earth System Climate Model (UVic ESCM) in its standard configuration used by the Kiel group [Keller et al., 2012], simulates a negative global trend in future precipitation of -0.3 % during this period if forced with the same CO_2 emission scenario, but no other forcing [Keller et al., 2014] (see Experimental Set Up and Forcing). The negative trend

can be traced back to the high CO_2-sensitivity of plants in the UVic ESCM. In a 4xCO_2, biogeochemically uncoupled, experiment (in which CO_2 changes only affect the radiative forcing) the UVic ESCM shows a positive precipitation trend of roughly 2 % K^{-1}. However, the model reacts differently if the physiological response to CO_2 is included. Under the RCP8.5 emissions scenario the model simulates a reduction of precipitation over land by 3.4 % per K of global warming, which is only partly compensated by the physically driven increase of precipitation of 1.3 % K^{-1} over the ocean [Keller et al., 2014].
The objective of the following analysis is to investigate how uncertainties in the CO_2-sensitivity of transpiration affect simulations of a future climate. Transpiration contributes to three fundamental equations of state in the Earth system. The water mass transfer contributes to the hydrological cycle and the mass balance, the latent heat flux from transpiration is part of the energy budget, and due to the relationship to the carbon uptake of the terrestrial biosphere, transpiration indirectly influences the carbon cycle as well. In this study we want to assess how the uncertainty in the dynamical response of transpiration to increasing CO_2 concentrations impacts these three components. Since terrestrial precipitation is an important climate variable and commonly used in other model intercomparisons, the emphasis of our sensitivity study lies in the evolution of simulated precipitation over land under simulated global warming. We will, in addition, investigate the consequences for simulated terrestrial transpirational cooling, water availability, and carbon exchange and storage.

3.2. Methods

3.2.1. General Model Set Up

The model used in the following analysis is version 2.9 of the University of Victoria Earth System Climate Model (UVic ESCM), a climate model of intermediate complexity, with a horizontal resolution of 3.6^o longitude x 1.8^o latitude. It includes schemes for ocean physics based on the Modular Ocean Model Version 2 (MOM2) [Pacanowski, 1995], ocean biogeochemistry [Keller et al., 2012], and a two dimensional atmospheric energy moisture balance model including a thermodynamic sea ice model [Bitz et al., 2001; Fanning and Weaver, 1996]. The terrestrial component consists of simplified versions of the Met Office Surface Exchange Scheme (MOSES) and the Top-down Representation of Interactive Foliage and Flora Including Dynamics (TRIFFID) vegetation model [Cox, 2001; Cox et al., 1999]. The land surface scheme calculates surface albedo, runoff and evapotranspiration, which is a function of canopy resistance and based on the Penman-Monteith equation [Monteith, 1981]. The vegetation scheme calculates the state of the terrestrial biosphere in terms of soil carbon, and the structure and coverage of bare soil or five plant functional types [Cox et al., 1999; Meissner et al., 2003]. Changes in vegetation biomass and distribution are driven by net carbon fluxes, which are derived for each vegetation type using the coupled photosynthesis stomatal conductance model [Cox et al., 1998].

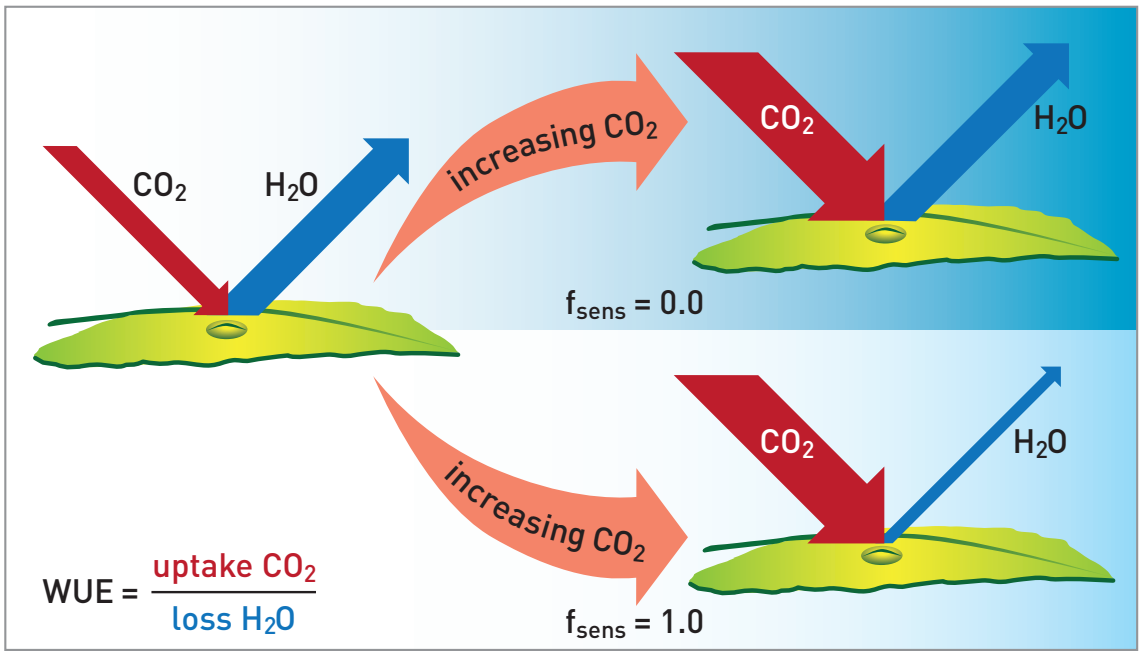

Fig. 3.1.: *Illustration of the effect of different applied scaling factors for the cases of* $f_{sens} = 0.0$ *(top) and* $f_{sens} = 1.0$ *(bottom).*

3.2.2. Scaling Methodology

In the UVic ESCM the leaf conductance of H_2O (g_w) is directly proportional to the leaf conductance of CO_2 (g_c) via their molecular diffusivities:

$$g_w = \beta * g_c \tag{3.1}$$

β accounts for different molecular diffusivities of water vapour and CO_2. As in numerous other models [Damour et al., 2010], g_c is directly proportional to the amount of carbon uptake by photosynthesis (P) and the gradient between the internal (C_I) and ambient (C_A) CO_2 concentration.

$$g_c = (P * \alpha)/(C_A - C_I) \tag{3.2}$$

α is a unit conversion factor.
Since transpiration is an important parameter connecting the energy balance, water mass balance and the carbon cycle, the objective of the applied scaling was to investigate the relevance of changes in the CO_2-sensitivity of transpiration to future climate projections. The scaling could have been applied to both, the stomatal conductance of carbon and water vapour, which would have kept the molecular diffusivities consistent.
In models, the effect of CO_2 on photosynthesis and transpiration are highly parameterized and not well constrained by observations. The UVic ESCM underestimates the fertilization effect on photosynthesis over the historical period [Eby et al., 2013] and the transpiration response to CO_2 appears to be larger compared to other models. Therefore,

we decided to scale only the strength of g_w relative to its preindustrial value, undoing the direct proportionality of CO_2 and H_2O stomatal conductance. Since we do not change the effect of CO_2 on photosynthesis we keep the model's photosynthesis response closer to observations. Simultaneously, we manipulate the CO_2-sensitivity of transpiration, in order to cover the wide range simulated by other models. While modifying only the transpiration response to CO_2 may seem to make the model inconsistent in terms of stomatal conductance, it is a simple and clean way to separate the two different effects and allows us to manipulate plant water use efficiency.
In order to vary the sensitivity of transpiration to increasing atmospheric CO_2 concentrations, a scaling is applied to the ambient CO_2 concentration, C_A, used in calculating the stomatal conductance of water vapour. $C_{A,scaled}$ can be scaled up or down, relative to preindustrial concentrations of 280 ppm ($CO_{2,preind}$), using a sensitivity factor, f_{sens}:

$$C_{A,scaled} = CO_{2,preind} + (C_A - CO_{2,preind}) * f_{sens} \tag{3.3}$$

This scaling is only applied to ambient CO_2 used in calculating the leaf's conductivity to water vapour. The other equations used in the model, including those for photosynthesis continue to use the unaltered ambient CO_2 concentration for all calculations.
For consistency, in the calculations for g_w, a scaled version of the internal CO_2 concentration ($C_{I,scaled}$) is calculated by replacing the C_A with $C_{A,scaled}$.) Note that the calculation itself was not altered.

$$C_{I,scaled} = (C_{A,scaled} - C_*) * F_0(m) * (1 - Q/Q_{crit}(m)) + C_* \tag{3.4}$$

Here C_* is the canopy-level photorespiration compensatory point and F_0 is the ratio of the internal to the ambient CO_2 concentration for plants that are not water stressed. Plants are not water stressed if the canopy-level specific humidity deficit, Q, equals zero. The critical humidity deficit Q_{crit} and F_0 are constant values depending on the plant functional type, m, their values are given in Table 3.1. Both scaled CO_2 concentrations, $C_{A,scaled}$ and $C_{I,scaled}$, are used to calculate the leaf's conductivity with respect to water vapour:

$$g_w = \beta * (P * \alpha)/(C_{A,scaled} - C_{I,scaled}). \tag{3.5}$$

In case C_A is scaled down, plants will only feel a reduced increase in ambient CO_2 and the difference between C_A and C_I would be reduced, causing the leaf conductivity for water vapour, and consequently transpiration, to increase. Note, that the scaling only affects the leaf conductance of H_2O and not the leaf conductance of CO_2 (Figure 3.1). Consequently, the scaling alters the amount of transpirational water lost by the plant per unit of carbon uptake, so effectively the WUE.

3.2.3. Experimental Set Up and Forcing

The UVic ESCM was spun up with seasonal, year 1800 forcing for over ten thousand years. Since the scaling is only applied to CO_2 concentrations deviating from preindustrial, all sensitivity simulations started from the same initial preindustrial spin-up. All

Tab. 3.1.: *List of parameters used in the calculations for the internal CO_2 concentration, the leaf conductance of CO_2 and water vapour. Given are descriptions or values of the parameter and their units.*

Parameter	Description/Value	Units
C_A	Ambient canopy CO_2 pressure	[Pa]
C_I	Leafs internal CO_2 pressure	[Pa]
f_{sens}	{0.0; 0.2; 0.4; 0.6; 0.8; 1.0}	[1]
C_*	Canopy-level photo-respiratory compensatory point	[mol/m^3]
m	Plant Functional Types: Broad Leaf Tree (BT); Needle Leaf Tree (NT); C3 grass (C3); C4 grass (C4); Shrub (S)	
$F_0(BT,NT,C3,C4,S)$	(0.875, 0.875, 0.900, 0.800, 0.900)	[1]
Q	Canopy level specific humidity deficit	[kg H_2O/kg air]
$Q_{crit}(BT,NT,C3,C4,S)$	(0.090, 0.060, 0.100, 0.075, 0.100)	[kg H_2O/kg air]
g_c	Leaf conductance for CO_2	[m/s]
g_w	Leaf conductance for H_2O	[m/s]
P	Net leaf photosynthesis	[mol CO_2/m^2/s]
α	Factor for converting mol/m^3 into Pa	[J/mol]
β	1.6	[1]

simulations were integrated for 500 years until 2300, using historical emissions followed by RCP8.5 and the Extended Concentration Pathway 8.5 emissions scenario until 2250 [Meinshausen et al., 2011]. Thereafter the atmospheric CO_2 concentrations were held constant until 2300. For the following analyses yearly output was used. Continental ice sheets, volcanic forcing and astronomical boundary conditions were held constant to facilitate the experimental setting and analyses [Keller et al., 2012]. There was no land use forcing or burning applied, in order to investigate the systems' sensitivity in an unperturbed state.

Realising that the UVic ESCM's sensitivity of transpiration to ambient CO_2 is at the high end of current models [Keller et al., 2014] we decided to scale down its sensitivity. Hence, we implemented the scaling factor with values of $f_{sens} = \{0.0; 0.2; 0.4; 0.6; 0.8; 1.0\}$, allowing us to scale down the sensitivity of transpiration to increasing CO_2 concentrations. This is expected to cause a relative increase in terrestrial evapotranspiration and precipitation compared to the default setting ($f_{sens} = 1.0$). In addition, for the comparison with the CMIP5 models three simulations following the CMIP5 forcing protocols were performed with values for $f_{sens} = \{0.0; 0.5; 1.0\}$. In the default simulations following the CMIP5 forcing protocols, terrestrial precipitation trends between 1961-1990 and 2071-2100 are higher by 20 mm yr^{-1} compared to the runs forced by CO_2 only. This increase results in an overall positive global precipitation trend, and can be explained by the reduction in vegetation cover due to the implementation of land use changes.

3.3. Results

3.3.1. Simulated Future Precipitation Patterns

The applied scaling has a strong impact on the spatial patterns of simulated future precipitation changes (Figure 3.2). The default model ($f_{sens} = 1.0$) simulates an increase in precipitation at higher latitudes between 50-80 °S and 50-80 °N, of about 50-200 mm yr^{-1} by the end of the century (Figure 3.2a). At high latitudes, spatial patterns are relatively independent of the land-ocean distribution and hence zonally coherent. For the mid and low latitudes a distinction can be drawn between areas over land and ocean. Regions of strongly reduFced future precipitation in the default simulation lie mainly over continental areas. The strongest simulated decrease occurs over Australia with end-of-the-century precipitation decreasing by up to 270 mm yr^{-1}. In contrast, simulated precipitation increases by approximately 220 mm yr^{-1} over adjacent oceanic regions. Reducing the sensitivity of transpiration of plants towards higher CO_2 concentration by applying lower scaling factors, f_{sens}, this pattern shifts to an increasing trend for precipitation values over tropical land areas, while oceanic and desert areas remain largely unchanged.
At high latitudes simulated future precipitation is independent of the applied scaling factor f_{sens}, indicating that these areas are less sensitive to variability in transpiration. In mid to low latitudes, the $f_{sens} = 0.0$ model simulates increased future precipitation over all vegetated land areas relative to the default simulation. The largest increase in terrestrial precipitation of up to 500 mm yr^{-1} (increase by 60 % relative to the $f_{sens} = 1.0$ simulation) is seen over the northern part of South America, Central Africa and Southeastern Asia. These areas are mainly covered by broad leaf trees in the UVic ESCM, corresponding to tropical rain forest or savannah.

3.3.2. Latitudinal and Absolute Trends of Terrestrial Future Precipitation

When the scaled model simulations of the UVic ESCM are compared to the range of the CMIP5 simulations (Figure 3.3a, model details in supplementary table B.1), the general shape of the latitudinal changes in simulated precipitation is similar among the three sensitivity simulations in the extra-tropical regions. There is an increase of precipitation in the high latitudes and a decrease in the mid latitudes of both hemispheres. The latitude of transition between these two trends, however, depends on the applied scaling and varies between 45° N for a scaling of $f_{sens} = 0.0$ and 60° N for the default simulation. The tropical latitudes reveal large differences between the differently scaled model simulations. Precipitation between 10° N and 10° S either increases by 400 mm yr^{-1} for the scenario, where transpiration is calculated with preindustrial CO_2 levels, or it decreases by 90 mm yr^{-1} for the default sensitivity of transpiration to CO_2 implemented in the UVic ESCM. Similar to the UVic ESCM, the CMIP5 models show consistent terrestrial precipitation trends in the extra-tropical latitudes, with a slightly more positive trend compared to the default UVic ESCM simulation. In the tropics, however, the different CMIP5 model results show an even wider range from -290 mm yr^{-1} to 450 mm yr^{-1}. This range of

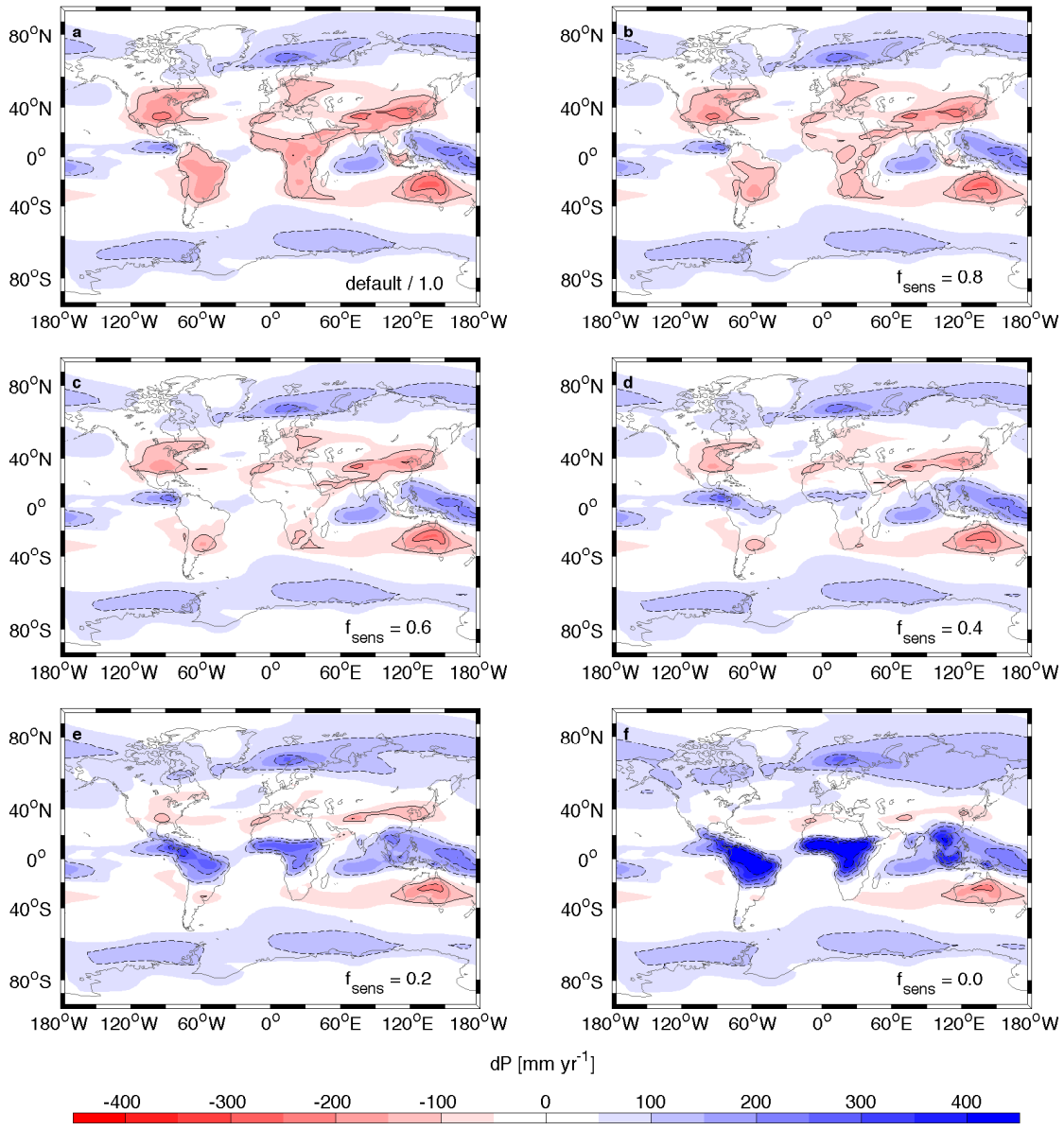

Fig. 3.2.: *Maps of mean future precipitation changes.*
Changes in mm yr^{-1} are shown for the six scaling factors applied and were calculated between 1961-1990 and 2071-2100.

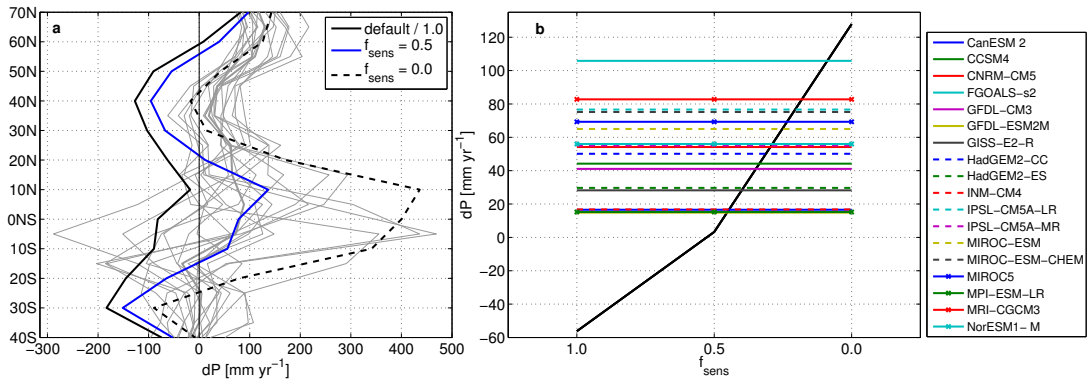

Fig. 3.3.: *Comparison of precipitation trends to CMIP5.*
a) Latitudinal dependency of mean annual accumulated terrestrial precipitation changes in mm yr^{-1} between 1961-1990 and 2071-2100 for three scaling factors implemented in the UVic ESCM (see legend). As a reference the grey lines show the results of the analyses from 18 CMIP5 models [Ahlström et al., 2012], the thick grey line gives the multi model mean (the same figure, but for the only CO_2 forced simulations can be found in Figure B.2);
b) Change in mean annual precipitation sums over land in mm yr^{-1} between 1961-1990 and 2071-2100 for the UVic ESCM depending on the different scaling factors applied (thick black line) and the 18 CMIP5 simulations (vertical lines, see legend and for details Table 3.1) in [Ahlström et al., 2012].

terrestrial tropical precipitation changes in the CMIP5 global warming simulations indicates the large uncertainty associated with this climate variable. It is remarkable that the range within the three scaled UVic ESCM model simulations covers almost the complete range of future tropical precipitation changes simulated by the CMIP5 models.
For the global mean terrestrial precipitation changes (Figure 3.3b) the UVic ESCM covers the complete range of the CMIP5 models by implementing different CO_2-sensitivities of transpiration. Simulated changes in terrestrial precipitation range from -55 mm yr^{-1} for the default simulation to $+128$ mm yr^{-1} when the plants' transpiration is insensitive to increasing CO_2 concentrations. In comparison all CMIP5 models show a positive trend in simulated terrestrial precipitation with a mean annual increase from 15 to 105 mm yr^{-1}. The UVic ESCM's terrestrial precipitation trends seem to be more consistent with the CMIP5 models for the model configuration with applied low CO_2-sensitivities of transpiration.

3.3.3. Transpirational Cooling, Terrestrial Water Availability, and Carbon Exchange

Latent heat flux is the flux of heat from the Earth's surface to the atmosphere, that is associated with evapotranspiration of water at the surface. An increase in transpiration, therefore would cool the land surface. Globally the land surface temperature is reduced by 0.3 K in 2100 in case of a higher transpiration in the $f_{sens} = 0.0$ simulation relative to the $f_{sens} = 1.0$ simulation. This amounts to local cooling of the soil temperature in the tropical regions of up to 1.3 K (Figure B.1).

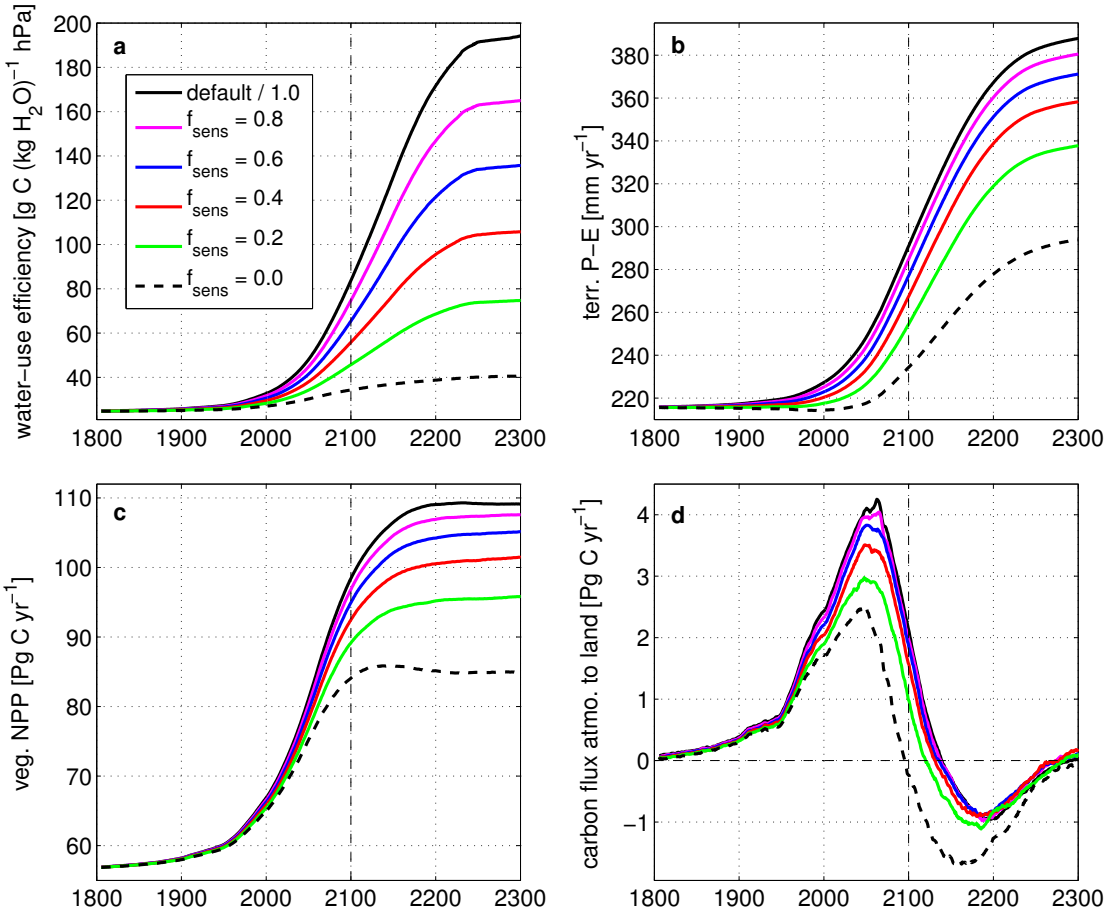

Fig. 3.4.: *Temporal development of parameters relevant to the vegetation system. Time series of water-use efficiency a), terrestrial precipitation minus evapotranspiration b), vegetation net primary production c), and carbon flux from atmosphere to land d), for the default simulation and the scaling factors applied.*

The scaling of the CO_2-sensitivity of transpiration also influences the simulated vegetation and the corresponding carbon fluxes. The carbon response is driven by the photosynthetic response and the transpiration response. As plants become more water stressed, due to a higher rate of transpiration, they open their stomata less often. This affects how much carbon can be taken up. More carbon is taken up in simulations with less transpiration, because stomata can stay open longer, allowing for more photosynthesis for the same amount of water loss. This reduces the plants WUE (Figure 3.4a, calculation of the WUE in supplementary material B.1). In our analysis there is an increase of the WUE for all simulations, with the strongest increase evident for the default simulation, in which transpiration is strongly reduced and the NPP has the largest increase. However, as expected, the increase in the WUE for the $f_{sens} = 0.0$ simulation is much lower compared to the default model and is mainly driven by increased carbon uptake, rather than by reduced transpiration.

A lower WUE, as for the $f_{sens} = 0.0$ simulation, makes it more likely for the plant to

become water stressed. The reduced evapotranspiration also influences the terrestrial water availability, the residual of precipitation and evapotranspiration on land, P-E, (Figure 3.4b). Under a high emission scenario, the default UVic ESCM simulates a decrease in terrestrial evapotranspiration of 8.7 % K^{-1}, which is higher than the rate of decrease in precipitation over land, resulting in an overall increase in the terrestrial water availability. For all scaling factors the global average terrestrial water availability still increases with time. However for the simulation, in which transpiration is insensitive to CO_2, P-E is reduced by 20 % relative to the default simulation in 2100. This reduction in terrestrial water availability relative to the default simulation leads to a relatively higher plants' water stress level for the $f_{sens} = 0.0$ simulation. Correspondingly, the expected future increase in terrestrial net primary productivity, and hence total vegetation carbon, is reduced if transpiration is less sensitive to CO_2 (Figure 3.4c). The total terrestrial carbon pool consists of vegetation and soil carbon. An increase in net biological primary production causes an increase in the terrestrial pool, while an increase in soil respiration causes a decrease in terrestrial carbon storage. On longer time scales, soil respiration mainly depends on the soil carbon pool, which is decreased by the scaling relative to the default simulation.
The resulting carbon fluxes between atmosphere and land show that the terrestrial system remains a sink for atmospheric carbon until 2100 for all applied scaling factors (Figure 3.4d). The simulated transition from a land carbon sink to a source, happens earlier for lower CO_2 sensitivities than for higher ones. Simulated future carbon uptake by the terrestrial system varies from 1.68 to 3.44 Pg C yr^{-1} over this century, depending on the applied CO_2-sensitivities, with a reduced uptake for lower CO_2-sensitivities of transpiration.

3.4. Discussion and Conclusion

In a series of sensitivity experiments, we scaled the CO_2-sensitivity of transpiration under the RCP8.5 emission scenario in an Earth System Model, in order to investigate the relevance of dynamical changes in this process for climate change predictions. We found that, varying the strength of the CO_2-sensitivity of transpiration caused simulated terrestrial precipitation to range from a decrease of 10 % to an increase of 27 % by the end of the century, compared to today's simulated precipitation. The scaling enables the UVic ESCM to cover the full range of CMIP5 models' precipitation changes over land. The range of global precipitation changes of the UVic ESCM with different scaling factors applied and following the CMIP5 RCP8.5 forcing varies from 0.6 to 7.4 % increase in precipitation relative to 1988-2005, which is at the lower end of the CMIP5 models range of 5 to 11.5 % [Allan et al., 2013].
Locally, precipitation in the UVic ESCM in the tropics is more sensitive to differences in CO_2-driven transpiration compared to higher latitudes. Observations of tropical tree growth rings suggest no growth stimulation from an increasing atmospheric CO_2 concentration, but an increase in the ecosystem WUE by 30-35% in the last 150 years [Sleen et al., 2014], indicating a reduction in transpiration and an associated reduced recycling of precipitation. In the UVic ESCM the local differences amount to decreased global ter-

restrial precipitation by up to 60 % in the $f_{sens} = 1.0$ relative to the $f_{sens} = 0.0$ simulation in 2100. This is in line with a study investigating the strength of the CO_2-physiological effect, i.e. the effect of stomata closing, with the National Centre for Atmospheric Research Community Model [Cao et al., 2010]. Under high atmospheric CO_2 concentrations, they found that the CO_2-physiological effect reduced the precipitable water by 40 % compared to the amount that would be available without this effect. The CMIP5 models display a larger inter-model variance in simulated future precipitation changes in the tropics [Ahlström et al., 2012]. Assessing the uncertainty in the transpiration fluxes might improve the models agreement and the overall performance in this region.

A reduction in transpiration due to an increase in WUE would act to warm the land surface due to a reduced evaporative cooling. In our simulations local temperature differences between the $f_{sens} = 0.0$ and the default simulation, are as high as 1.3 K in the year 2100, where the default simulation has higher temperatures, due to reduced transpiration. A similar result was found in the study investigating the strength of the CO_2-physiological effect with the National Centre for Atmospheric Research Community Model [Cao et al., 2010], where 11% of the simulated land surface warming was caused by closing stomata.

Transpiration couples the hydrological cycle with the carbon cycle. An increase in transpiration relative to the default simulation is likely to cause a higher water stress level, reducing terrestrial net primary production and hence terrestrial carbon uptake. Changes in the terrestrial carbon pool of the UVic ESCM with different scalings applied and following the CMIP5 forcing protocols, range between -86 and +43 Pg C until 2100, with the largest uptake found in the default simulation. The total change in the terrestrial carbon pool for 9 CMIP5 Earth system models until 2100 varies between -120 and +500 Pg C [Ahlström et al., 2012]. These uncertainties in terrestrial carbon uptake influences predictions about atmospheric carbon content and hence climate forecasts.

Transpiration is not only sensitive to atmospheric CO_2, but is also influenced by other environmental factors that were not specifically addressed in this study. To correctly model transpiration any vegetation model needs to be forced with either real data or realistically simulated factors such as the amount of incoming solar radiation at the leaf level, soil and air temperatures, relative humidity, water vapour deficit, soil moisture, nutrients, root extent, leaf area index, and other environmental factors such as weather fluctuations and extremes [Wang and Dickinson, 2012]. Factors such as the plants life history and health may also be important. Which of these factors is most important in determining the amount of transpiration, strongly depends on the environmental conditions. For example, a good representation of roots and soil moisture is important in tropical rain forests as well as in arid and semiarid regions, where the amount of transpiration at a forested site during a drought year has been found to be higher than the water available from precipitation because trees were able to access ground water reservoirs [Leuning et al., 2005]. Also of importance in these regions are the frequency and strength of rain events, because they determine the water availability in the soils. In contrast to this, a good representation of roots and soil moisture becomes less important in wetlands or peatlands, where evapotranspiration is closely related to the potential evaporation estimate from the Penman equation [Wang and Dickinson, 2012]. Here factors such as the water vapour pressure deficit, incoming solar radiation, and temperature become more important in determining

the transpiration rates.
The UVic ESCM has simplified representations of both the atmosphere and land surface. These simplifications affect transpiration rate estimates, due to the lack of weather fluctuations and corresponding dry or wet spells. The idealised prescribed seasonal cloud coverage in the UVic ESCM also prevents cloud feedbacks, which would affect the amount of incoming solar radiation, to occur during wet or dry events. The lack of weather fluctuations likely has a strong influence on terrestrial productivity. In addition, the UVic ESCM land surface scheme is a one-layer soil model, which integrates the energy and moisture balance at the surface. The lack of a vertical soil moisture profile, could lead to an over- or under-estimation of the surface water availability and thus also effect transpiration. Despite these simplifications the model does a reasonable job of simulating annual present-day vegetation distributions, surface temperatures, and precipitation and evapotranspiration [Meissner et al., 2003].
Our results illustrate the substantial sensitivity of one intermediate-complexity Earth System Model, the UVic ESCM, towards the CO_2-sensitivity of the plants' leaf conductance of water vapour. While there is disagreement on the future development of the terrestrial system among different CMIP5 models [Ahlström et al., 2012; Arora et al., 2013], it is currently unknown how much of this disagreement arises from the uncertainty in stomatal behaviour.
As a previous model study pointed out [Cao et al., 2010], the strength of the stomata closing with increasing atmospheric CO_2 will strongly influence the water available for precipitation in simulated future climates. An observation-based study [Keenan et al., 2013] identified the need for a better understanding of the role of stomata in regulating land atmosphere interactions. These findings are in line with our model results showing that the future development of the simulated atmosphere-to-land carbon fluxes and the terrestrial part of the hydrological cycle are uncertain, even within the context of a single model, as long as the stomatal conductivity's CO_2-sensitivity cannot be better constrained by observations. An assessment of the dynamical response of transpiration is needed, since it is an relevant process and needs to be considered in projections of future climate.

Acknowledgements We thank A. Ahlström for providing the CMIP5 model output used in Figure 3.3, and our graphic designer Rita Erven for designing Figure 3.1 from the draft of the authors. his work was funded by the DFG in the context of the Priority Program 1689: Climate Engineering: Risks, Challenges, Opportunities?. The authors declare that they have no competing financial interests. A.O., M.E. and D.P.K. conceived and designed the experiments. N.M. implemented and performed the experiments and analysed the data. N.M. wrote the manuscript with contributions from D.P.K., M.E. and A.O..

4. Systematic Correlation Matrix Evaluation (SCoMaE) - A methodological approach to find Indicators from Earth System variables

This chapter is a manuscript in preparation by Mengis N., D. P. Keller, and A. Oschlies (2016).

Abstract We present a methodological approach to select indicators from Earth system models with the aim of making climate system evaluation and reporting less subjective. Therefore we use an Earth system model of intermediate complexity to test i) if it is a valid approach to apply the same indicators as found for the historical scenario also for an assessment of future scenarios, ii) how this depends on the future forcing scenario, and iii) if we have to reevaluate the chosen indicators over time. We find that there is a necessity of reevaluating the historical indicators for an accurate assessment of future scenarios, since some of the prevailing relationships in the Earth system as represented by our model change due to the different forcing in future scenarios. We show that it is not sufficient to apply the indicator set found for the historical scenario to either an intermediate-high or a high future emission scenario. Furthermore we show that including expert judgement in the indicator selection, simplifies the interpretation of the clusters, however the total number of indicators needed for a thorough assessment increases. By combining the three scenarios, we found a common indicator set, which enables us to identified robust correlations between Earth system variables across the three considered scenarios, and points out the Earth system variables which are uncorrelated, if all three scenarios are to be considered. Although it is beyond the scope of this study to provide a normative framework for indicator selection, we here provide scientific-based information on the robustness of the indicator selection.

4.1. Introduction

An indicator is a quantitative value, measured or calculated, that allows one to obtain insight into the state of a defined system. Indicators have gone through a selection and or aggregation process [Ebert and Welsch, 2004]. In this study we focus on indicators describing the Earth's climate state and changes, which are also referred to as environmental indicators. Environmental indicators are developed based on quantitative measurements or statistics of environmental conditions in order to allow a comparison of states of the environment across time or space [Ebert and Welsch, 2004].

How to select indicators for climate change? A useful indicator should fulfil certain characteristics, which depend on the purpose of the indicator [Gallopín, 1996]. Radermacher [2005] defined statistical measurability, scientific consistency, and political relevance as three main characteristics for (environmental) indicator selection, whereby the consideration of all three of these characteristics is important for an indicator selection process.
Due to the historical development of climate science and Earth system models, global mean temperature evolved as the most important indicator for assessing climate change. This example allows us to discuss the above mentioned characteristics: Firstly, several long term temperature records as well as proxies for assessing air temperature exist, which makes this indicator well measured (Statistical measurability). Furthermore its environmental relevance is emphasised by many other climate variables that are closely linked to temperature, e.g. evaporation, sea level rise, or biological productivity. So although global mean surface air temperature might not be the most important variable for society, using this indicator as a proxy for the climate impacts is scientifically consistent. Its political, economical and ethical relevance is seen in the discussions which are concerned with e.g. global warming [Ott et al., 2004] or the 2-degree temperature increase target [Held et al., 2009].
Assessments reports, which aim to inform policy and public, as published by the Intergovernmental Panel on Climate Change (IPCC) have to deal with the question of indicator selection before they are able to assess changes in the climate system, represented by the chosen indicators. Depending on the objective, nowadays global mean precipitation, or precipitation extremes, as well as the Arctic summer sea ice or the rate of ocean acidification are considered as climate metrics, to name only some examples of indicators discussed in e.g. the summary for policy makers of the recent assessment report of climate change [Stocker et al., 2013]. These indicators are meant to provide simple information to policy-makers and society about the state of the climate system. However, such selections are usually influenced by expert judgement of the scientist and to a lesser extent by objective indicator selection criteria.
Earth system models are essential for assessing climate change because the inertia of the climate system to carbon perturbations requires projections of future climate states. While early climate models applied simple zero to two dimensional calculations to assess the effect of CO_2 in the atmosphere on the climate and assessed global mean temperature as an indicator [e.g., Arrhenius, 1896; Callendar, 1938; Sellers, 1969], the continuously increasing complexity of Earth system models through time required selection of climate variables as indicators for the state of the climate system. Starting with a broad set of model output variables and consecutively selecting more appropriate ones, is a common approach for measuring complex systems (e.g. Pintér et al. [2005]; Kopfmüller et al. [2012]). However, already the initial selection of a possible (socially relevant) indicator is a normative choice and there exist no unambiguous rules for the selection process (Krellenberg et al. [2010] and Böhringer and Jochem [2007], respectively). Any selection of indicators from climate variables implies a value and implicit weighting decision, requiring therefore a well-informed and broad participation in the selection process. While the latter usually requires ideally the inclusion stakeholders, the former requires the contribution from science [Radermacher, 2005]. This study adds to this requirement by providing

scientific-based information on the robustness of the indicator selection.
Here, we present a methodological approach to systematically select indicators from Earth system variables for an comprehensive description of the climate system, with the aim to make climate system evaluation and reporting less subjective. As an example, we use an Earth system model of intermediate complexity to test i) if it is a valid approach to apply the same indicators as found for the historical scenario also for an assessment of future scenarios, ii) how this depends on the future forcing scenario, and iii) if we have to reevaluate the chosen indicators over time. In order to account for uncertainties in model parameterizations, we perform several parameter perturbations concerning physical and biogeochemical model parameters, and assess the models sensitivity towards them. By correlating temporal changes of different model output variables from the parameter perturbation simulations, we learn which climate variables show the same behaviour to the imposed parameter perturbation, making them robust indicators for climate change assessment.

4.2. Methods

4.2.1. Systematic Correlation Matrix Evaluation (SCoMaE)

4.2.1.1. Step 1: Building the Correlation matrices

To obtain a set of indicators in form of Earth system variables, to describe changes in the climate system, we first need to construct a correlation matrix, i.e. a matrix including the correlation information on all the Earth system variables towards each other (see Figure 4.3a as an example). The construction of the correlation matrix strongly depends on the regarded question and needs to be adjusted accordingly. If enough data were available, correlations between time series of observations could be regarded systematically evaluated. To evaluate the correlation matrix, a significance test of the correlations based on the test statistic $t = |r| * (1 - r^2)^{-1} * (N-2)^{1/2}$ following the t-distribution is performed. We performed a two sided test on a 5% significance level, with $N = 16$ and accordingly $t_{crit} = 2.145$. The information on the significance of the correlation for all Earth system variables is then transferred into a matrix.
In our example we correlate temporal changes of the single model output variables from parameter perturbation simulations, with each other, in order to understand if the output variables show the same behaviour to the respective parameter perturbation. As an example of these analysis, we show the correlations of three different model output variables towards global mean surface air temperature (A_sat) under the RCP8.5 emission scenario (Figure 4.1) (see Table C.1 for a list with explanations on the variable abbreviations). There is a significant positive/negative correlation evident between temporal changes in surface air temperature (A_sat) and global mean ocean temperature (O_temp)/northern hemisphere sea ice area (O_iceareaN). This illustrates that these model output variables show similar reactions towards a parameter perturbation. For example, surface air temperature (A_sat) shows a higher increase in case of the simulation with no CO_2 fertilisation

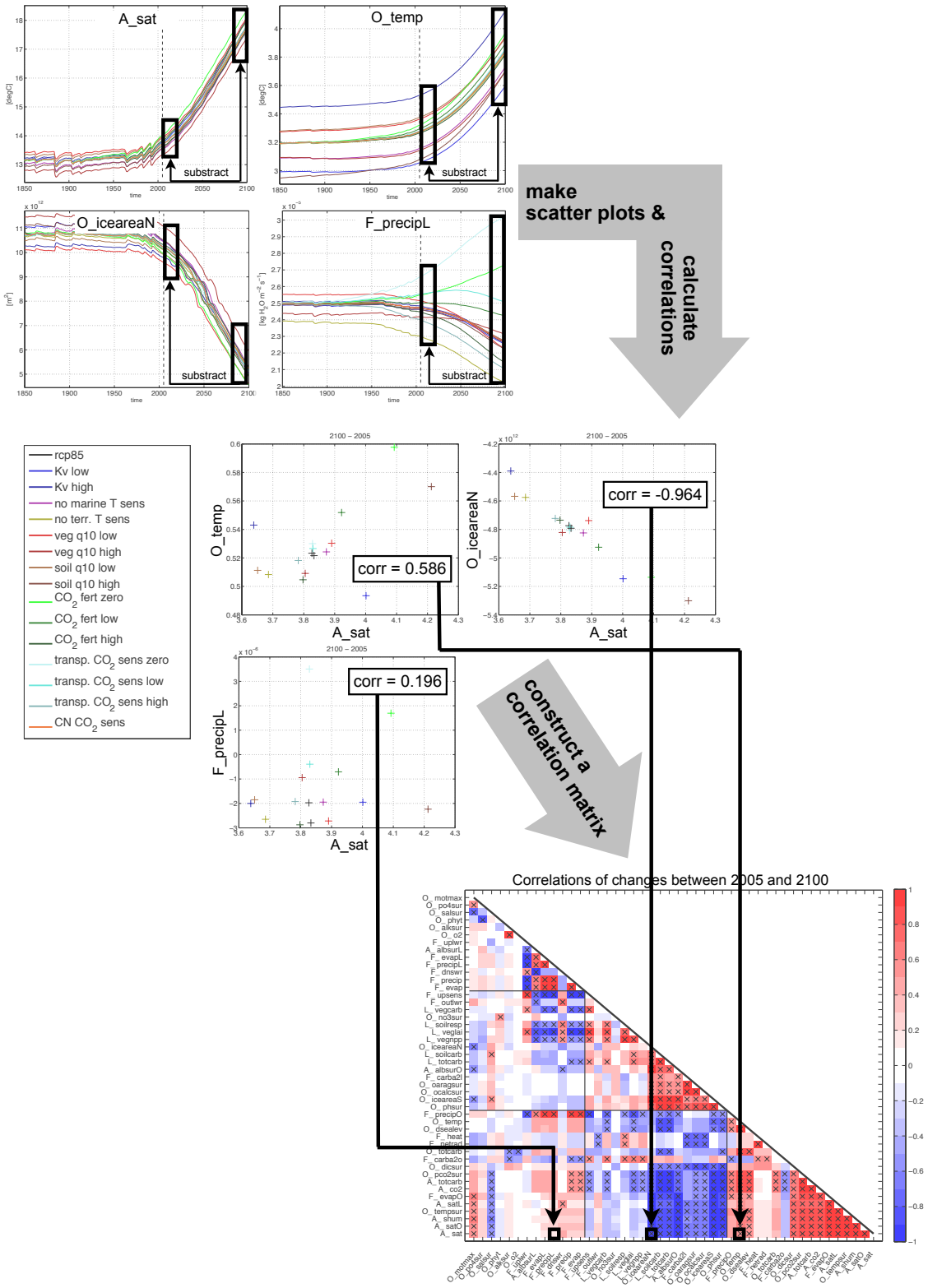

Fig. 4.1.: *Illustration of the Correlation Matrix Construction on the examples of mean ocean temperature (O_temp), northern hemisphere sea ice area (O_icareaN) and precipitation over land (F_precipL) to be correlated against surface air temperature (A_sat).*

(CO_2 fert zero) compared to the simulation with a high CO_2 fertilisation (CO_2 fert high), and the same is true for the mean ocean temperature (O_temp). Note, that the sign of correlation shows the relative temporal changes of the output variables, e.g. if surface air temperature (A_sat) increases over time, also global mean ocean temperature (O_temp) increases, therefore the correlation is positive. The correlation between changes in precipitation over land (F_precipL) and surface air temperature (A_sat) is not significant. During our example, to simplify the visual analysis we sort the variables in the matrices according to their strength in correlation towards surface air temperature (A_sat) in the historical scenario.

4.2.1.2. Step 2: Systematic Correlation Matrix Evaluation (SCoMaE)

We need to systematically evaluate the correlation matrix, to obtain a set of indicators for the assessment of changes in the regarded system. The first indicator is chosen to be the model output variable with the highest number of significant correlations towards all the other variables. All output variables that are significantly correlated to this one are excluded from the further selection process, since they are now clustered under this indicator. Then again the output variable with the highest number of significant correlations from all the remaining output variables is chosen. This procedure is performed until all output variables are clustered under an indicator. If an output variable is not significantly correlated to any other variables, this output variable is considered to be a single indicator, since it is needed for a fully comprehensive assessment (see Figure 4.2 for an illustration of this procedure).

4.2.2. Model description

The model employed is version 2.9 of the University of Victoria Earth System Climate Model (UVic ESCM), an Earth system model of intermediate complexity [Eby et al., 2013]. It includes schemes for ocean physics based on the Modular Ocean Model Version 2 (MOM2) [Pacanowski, 1995], ocean biogeochemistry [Keller et al., 2012], and a terrestrial component including soil and vegetation dynamics [Meissner et al., 2003]. It is coupled to a thermodynamic sea-ice model [Bitz et al., 2001] with elastic viscoplastic rheology [Hunke and Dukowicz, 1997]. The atmosphere is represented by a two dimensional atmospheric energy moisture balance model [Fanning and Weaver, 1996]. All model components have a common horizontal resolution of 3.6 $^\circ$ longitude and 1.8 $^\circ$ latitude and the oceanic component has a vertical resolution of 19 levels, with vertical thickness varying between 50 m near the surface to 500 m in the deep ocean. Wind velocities used to calculate advection of atmospheric heat and moisture as well as the air-sea-ice fluxes of surface momentum, heat and water fluxes, are prescribed as monthly climatological wind fields from NCAR/NCEP reanalysis data [Keller et al., 2014]. Wind anomalies, which are determined from surface pressure anomalies with respect to pre-industrial surface air temperature, are added to the prescribed wind fields.

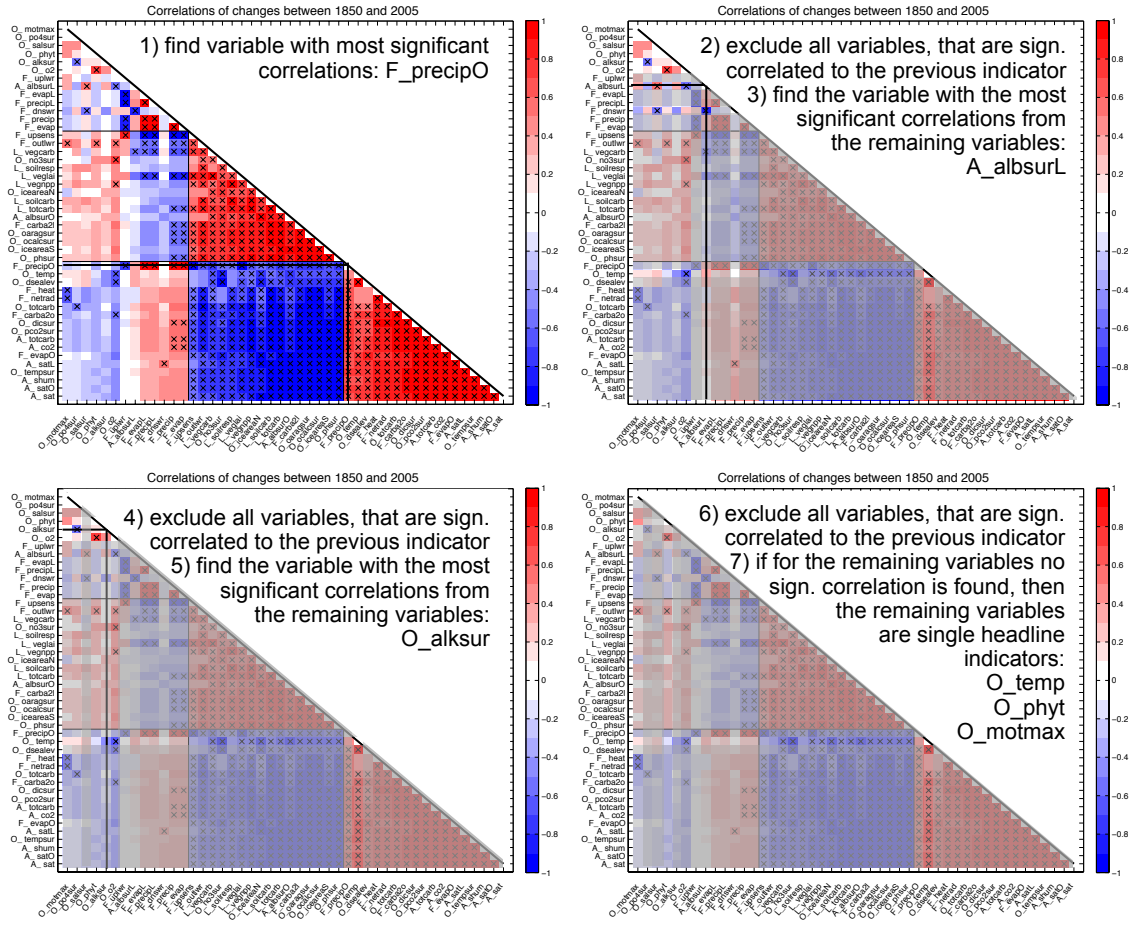

Fig. 4.2.: *Illustration of the indicator selection process on the example of the correlation matrix for the historical scenario.*

4.2.3. Spin-up and Forcing

For the default model simulation, the UVic ESCM was spun up with pre-industrial (year 1800) seasonal forcing for over ten thousand years. All simulations were integrated from 1765 until 2005 using historical fossil-fuel and land-use carbon emissions, as well as radiative forcing from solar variability and volcanic activity. Historical land use changes were implemented following the protocols of the Coupled Model Intercomparison Project 5 (CMIP5) [Taylor et al., 2012]. Following Keller et al. [2014], continental ice sheets were held constant to facilitate the experimental setting and analyses. Warming from black carbon, indirect ozone effects, and cooling from indirect sulphate aerosol effects were not included. From 2005 onward until 2100 the Representative Concentration Pathway (RCP) 4.5 and 8.5 from Meinshausen et al. [2011] were implemented as a intermediate and high CO_2 emission scenario.
For the sensitivity analysis performed with the UVic ESCM different parameters of the model were perturbed, and for some of them it was necessary to do a new model spin-up, apart from that the forcing was the same for all simulations. For our analysis we will consider two scenarios namely the historical scenario, i.e. 1850 to 2005, and two RCP scenarios, i.e. 2005 to 2100, for both the RCP4.5 and the RCP8.5 future forcing scenario. We consider 10-years averaged values of the variables, from which we construct correlation matrixes for all three scenarios.

4.2.4. Parameter Perturbations

In the following the single parameter perturbation experiments are explained in detail. We chose these parameters to explore the sensitivity of the UVic-ESCM to uncertainties in terrestrial and marine biological productivity with respect to temperature and CO_2, since these processes will influence the future carbon cycle. In addition, we added vertical diffusivity, since this is a physical process influencing marine carbon uptake. All parameters were perturbed within physically meaningful ranges, which was evaluated based on their agreement with the time series of historical global mean air temperature (manuscript in preparation by D. P. Keller).

Vertical Ocean Diffusivity
Small-scale physical mixing (vertical diffusivity or diapycnal mixing) in the ocean is parameterized in all global models because of their resolution. Thus, this important process, which plays a key role in determining ocean circulation and biogeochemical cycles as well as ocean to atmosphere heat and carbon fluxes, is set by necessity as a single global, or several regional, values that falls within the range of observational estimates of vertical diffusivity. To test how this affects all model results we are varying this parameterization by increasing and decreasing it by 50% (Kv low and Kv high), which is within the range of observational estimates Duteil and Oschlies [2011]. For these sensitivity analysis the model was spun-up with the corresponding setting for 10000 years, until a new equilibrium climate state was reached.

Biological Temperature Sensitivity

Although biological processes are known to be sensitive to temperature, there is a significant amount of uncertainty in how biology will respond to warming caused by climate change [Friedlingstein et al., 2006; Taucher and Oschlies, 2011]. Furthermore, there are many different ways to model the effects of temperature on biology and it is unknown which is best for Earth system model applications. To investigate the sensitivity of biological processes to direct temperature effects we conduct simulations where direct temperature effects on biology are not included. In order to ensure that global biogeochemical fluxes are as close to present-day ones as possible, flux-weighted global averages for temperature-dependent rates are set for all temperature-dependent functions (see Taucher and Oschlies [2011] for details).

a) No marine biological sensitivity to temperature: The results of this analysis can be used to estimate a lower boundary for how marine plankton and their effect on biogeochemical cycles will respond directly to global warming (no marine T sens). For this sensitivity analysis the model was spun-up with the corresponding setting for 10000 years, until a new equilibrium climate state was reached.

b) No terrestrial vegetation sensitivity to temperature: The results of this analysis can be used to estimate a lower boundary for how terrestrial vegetation and its effect on the carbon cycle will respond directly to global warming (no terr. T sens). For this sensitivity analysis the model was spun-up with the corresponding setting for 10000 years, until a new equilibrium climate state was reached.

Vegetation and Soil Sensitivity to Temperature

To further investigate the sensitivity of terrestrial biology to temperature we vary the vegetation and soil Q10 values, which are observationally-derived coefficients that are used to model the biological system rate of change in response to a 10 °C temperature increase. Low and high Q10 values of 1.5 and 3.0 (model default is 2.0), which are within the range of observational estimates [Lloyd and Taylor, 1994], were set to investigate how different terrestrial biological sensitivities to temperature affects the model results (veg q10 low/high and soil q10 low/high). For this sensitivity analysis the model was spun-up with the corresponding setting for 10000 years, until a new equilibrium climate state was reached.

CO_2 Fertilization of Vegetation

Increasing atmospheric CO_2 is thought to stimulate terrestrial carbon uptake, through the process of CO_2 fertilization [Matthews, 2007]. This negative carbon cycle feedback results in reduced atmospheric CO_2 concentrations, and has likely accounted for a substantial portion of the historical terrestrial carbon sink [Friedlingstein et al., 2006]. However, the future strength of CO_2 fertilization in response to continued carbon emissions is highly uncertain. In order to test the impact of this uncertainty for future climate change simulations, we followed the approach of Matthews [2007]. We scaled the CO_2 sensitivity of the terrestrial photosynthesis model, where we performed a simulation with no

CO_2 fertilisation effect (CO_2 fert zero), as well as two simulations where we varied the strength of the CO_2 fertilisation effect by increasing and decreasing it by 50% (CO_2 fert high/low) relative to the default model. No additional model spin-up was needed, since the CO_2 fertilization effect only happens when the atmospheric CO_2 concentration begins to increase, e.g., from the preindustrial period onward.

CO_2 Sensitivity of Transpiration
Transpiration by plants is highly sensitive to increases in atmospheric CO_2, since plants tend to open their stomata less often in a higher CO_2 environment, in order to reduce the water loss to the atmosphere. Several studies, both observation and model based, attempted to assess the importance of this process [Keenan et al., 2013; Sleen et al., 2014]. To test how strongly this affects simulations of future climate, the amount of transpiration for all plant functional types was scaled after Mengis et al. [2015]. This way the CO_2 fertilization effect is not changed. Three simulations are performed: For the first simulation, transpiration did not change compared to preindustrial levels (transp. CO_2 sens zero). For the other two simulations, the scaled transpiration was increased and decreased by 50% of the amount that the model would simulate in the default setting (transp. CO_2 sens high/low). No additional model spin-up was needed, since the effect of changing CO_2 on transpiration only becomes evident when the atmospheric CO_2 concentration begins to increase, e.g., from the preindustrial period onward.

Stoichiometric Changes in Response to Changing Ocean Carbonate Chemistry
Mesocosm studies that artificially increase the amount of CO_2 in seawater (e.g., climate change experiments) have suggested that the C:N content of marine plankton is sensitive to the amount of carbon in seawater (sort of a fertilisation effect). The mesocosm study of [Riebesell et al., 2007] indicated that as CO_2 increases the C:N content of phytoplankton increases, which is a change that would affect the amount of carbon exported to the deep ocean by biological processes and have an effect on other marine biogeochemical cycles. To test how this affects all model results we are implementing the mesocosm-derived relationship between the atmospheric CO_2 concentration and the C:N content of plankton as in [Oschlies et al., 2008] (CN CO_2 sens). No additional model spin-up was needed, since the effect of changing CO_2 on plankton stoichiometry only becomes evident when the atmospheric CO_2 concentration begins to increase, e.g., from the preindustrial period onward.

4.3. Results

4.3.1. Indicators for the historical scenario

From the evaluation of the correlation matrix for the historical scenario as described in section 4.2.1.2, we find that the first indicator is precipitation over ocean areas (F_precipO) (Figure 4.3). In the correlation matrix it is evident that this model output variable is

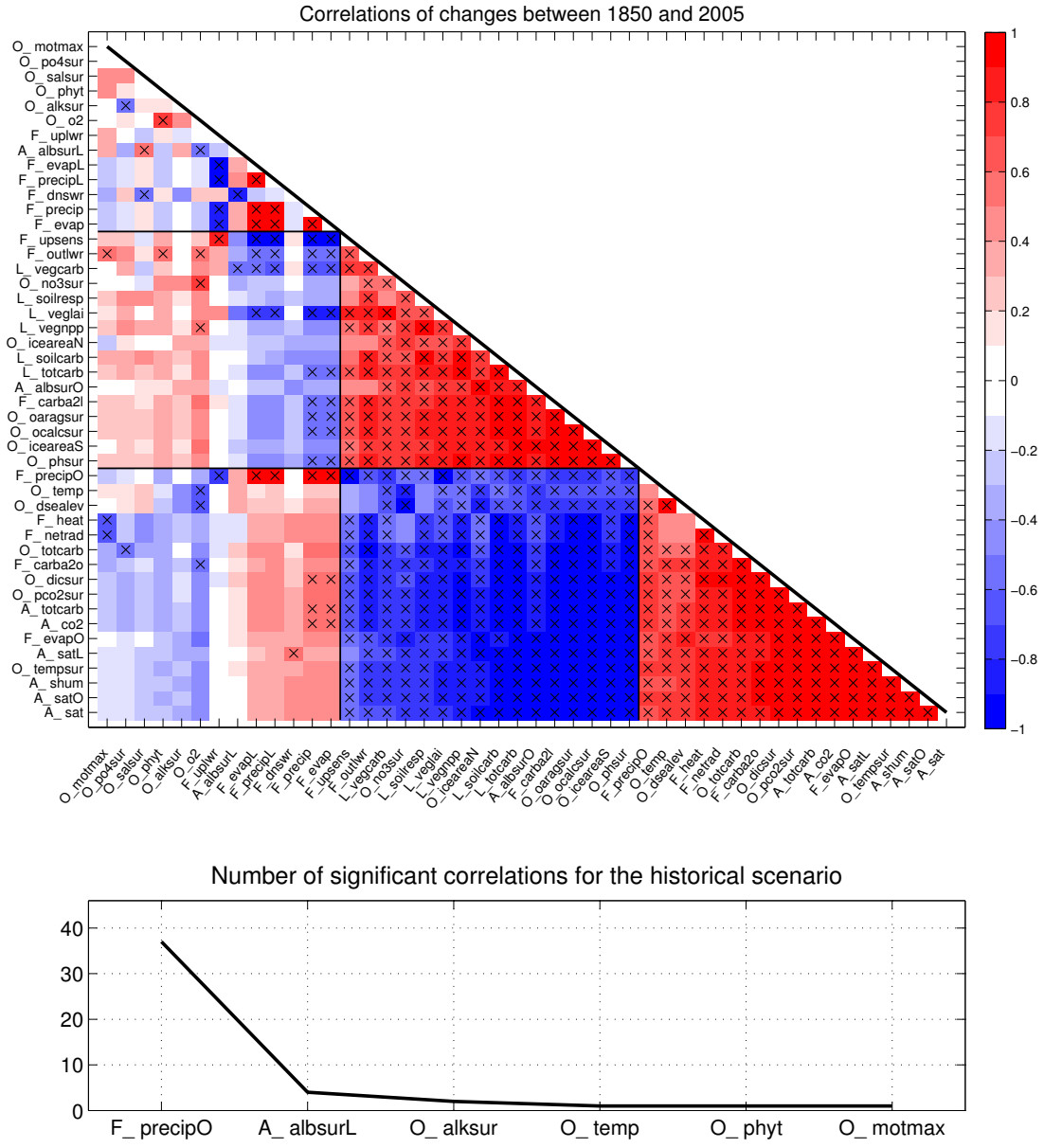

Fig. 4.3.: *a) Correlation matrix for the historical scenario. The correlations are calculated after the example from Figure 4.1 for each of the 46 model output variables, respectively. The 'x's mark the significant correlations on a 5% significance level. The order of the variable was determined based on their correlation strength to surface air temperature (A_sat) in the historical scenario. For details on the regarded model output variables see Table C.1.*
b) indicators as found from our analysis based on the correlation matrix above as illustrated in Figure 4.2, against the number of significant correlations.

significantly correlated to all variables that are significantly correlated to the surface air temperature (A_sat), with the exception of mean ocean temperature (O_temp), but in addition also links global and terrestrial precipitation and evapotranspiration (F_precip/L and F_evap/L) as well as the surface net upward longwave radiation (F_uplwr), which are not significantly correlated to surface air temperature (A_sat). Correspondingly it has the highest number of significant correlations.
Surface albedo on land (A_albsurL) was identified as the second indicator. It is, after excluding all variables correlated to precipitation over ocean (F_precipO), significantly correlated to net surface downward shortwave radiation (F_dnswr), ocean oxygen (O_o2) and sea surface salinity (O_salsur). The third indicator is ocean surface alkalinity (O_alksur), which shows the same response for the parameter perturbations as ocean surface phosphate concentrations (O_po4sur). When excluding all variables that are correlated to either one of the three above mentioned indicators (precipitation over ocean (F_precipO), surface albedo on land (A_albsurL) or ocean surface alkalinity (O_alksur)) three variables remain unclustered: Mean ocean temperature (O_temp), maximum meridional overturning (O_motmax), and ocean phytoplankton (O_phyt). Those themselves are hence single indicators, which are needed for a fully comprehensive assessment of the regarded system.

4.3.2. Indicators for the RCP4.5 and RCP8.5 scenarios

Are these indicators found for the historical scenario sufficient for a comprehensive assessment of future climate change?
If we would prescribe the indicators from the historical scenario, for the assessment of the two RCP scenarios, we would not be able to comprehensively assess the entire system as represented by our model (Figure 4.4). For the RCP4.5 scenario, we would miss information about the variables net top of atmosphere radiation (F_netrad), ocean surface heat flux (F_heat), net upward longwave radiation (F_uplwr) and ocean surface salinity (O_salsur). Since net top of atmosphere radiation (F_netrad) and ocean surface heat flux (F_heat) are significantly correlated these two are clustered under the indicator net top of atmosphere radiation (F_netrad), and the same thing is true for the last two remaining variables, which are clustered under the indicator net upward longwave radiation (F_uplwr), in order to obtain a comprehensive assessment. Note, that also the variables clustered under the single indicators differ (Figure C.1). For the historical scenario the indicator precipitation over ocean (F_precipO) includes the output variables net top of atmosphere radiation (F_netrad), ocean surface heat flux (F_heat), ocean surface nitrate (O_no3sur), top of atmosphere outgoing longwave radiation (F_outlwr), and net upward longwave radiation (F_uplwr), all of which are not included in the precipitation over ocean (F_precipO) indicator for the RCP4.5 scenario. The other way around, the indicators precipitation over ocean (F_precipO) for the RCP4.5 scenario includes mean ocean temperature (O_temp), which is not included for the historical scenario.

For the RCP8.5 scenario, the differences between the correlation matrices compared to historical scenario are even higher (compare Figure 4.3 and 4.6). The previous analysis already indicated that it is insufficient to use only the indicators from the historical sce-

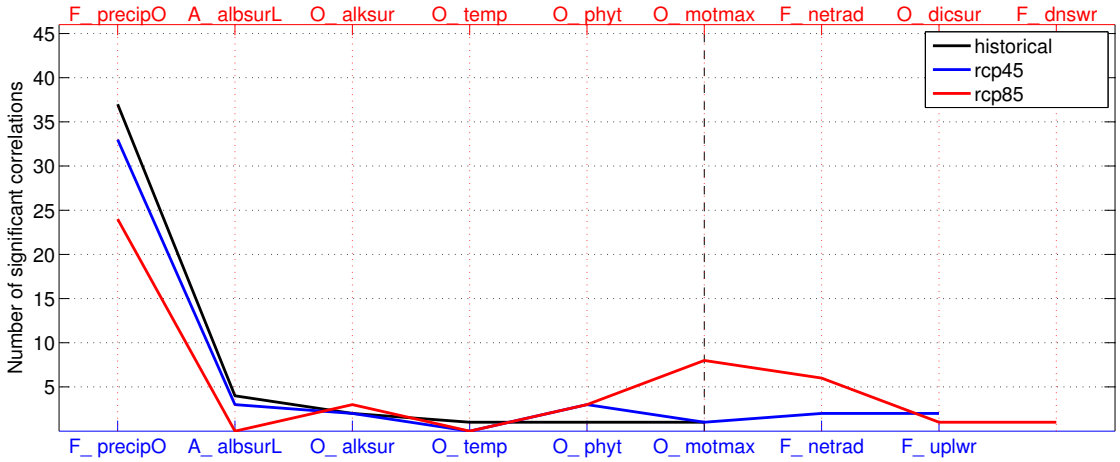

Fig. 4.4.: *Indicators identified from the analysis of the RCP4.5 (blue) and RCP8.5 (red) correlation matrices with the precondition to use the historical indicators first.*

nario, this becomes even more obvious under the high emission scenario. Eight out of 46 considered variables would not be eincluded by the indicators of the historical scenario. We need three additional indicators for a comprehensive assessment of the entire system under consideration, namely net top of atmosphere radiation (F_netrad), ocean surface dissolved inorganic carbon (O_dicsur), and net surface downward shortwave radiation (F_dnswr) (Figure 4.4). Note that six of the eight remaining variables were initially included by the first indicator in the historical scenario (precipitation over ocean (F_precipO)), but are no longer significantly correlated to it in the RCP8.5 scenario. This suggests that correlations valid for the historical scenario are no longer significant in under future climate change.

Which indicators would be selected if we performed the same analysis for the RCP4.5 and RCP8.5 scenarios?

For the two future scenarios, RCP4.5 and RCP8.5 we impose higher CO_2 and green house base forcing, as well as different land use forcing compared to the historical scenario. In the RCP4.5 scenario, carbon emissions continue to rise in an intermediate high emission scenario. In addition, the area of historical land use changes is reduced and forrest is grown on the newly freed areas. Some of imposed parameter perturbations are designed to scale the sensitivity of vegetation and soil to temperature and carbon, we therefore expect these to react sensitive to this scenario. For the RCP8.5 scenario we impose a high CO_2 emission scenario (RCP8.5) and further increasing land use changes. Some of the perturbed parameters react directly sensitive to CO_2 or are temperature sensitive, and therefore will show a strong reaction to the additional forcing. These additional forcings are expected to change the selection of indicators.

The evaluation of the correlation matrix for the RCP4.5 scenario (Figure 4.5), resulted in oceanic evaporation (F_evapO) as the first indicator, which is significantly correlated

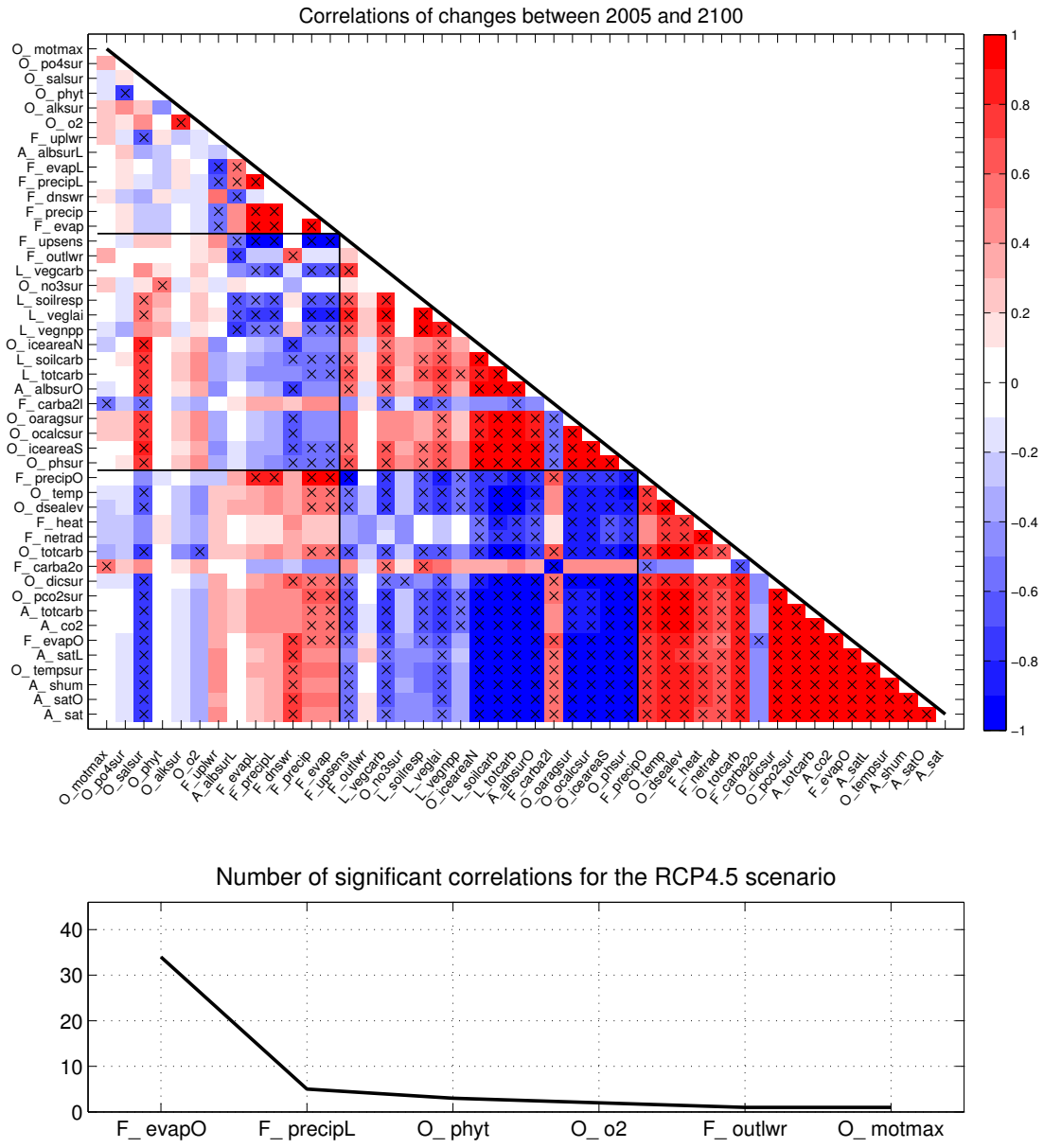

Fig. 4.5.: *Same as Figure 4.3, for the RCP4.5 scenario.*

with 34 other variables. The second indicator for the RCP4.5 scenario is precipitation over land (F_precipL), which is in addition to all variables correlated to evaporation over ocean (F_evapO) significantly correlated to vegetation net primary productivity (L_vegnpp), terrestrial evapotranspiration (F_evapL), surface albedo on land (A_albsurL) and net upward longwave radiation (F_uplwr) (Figure C.2). The next indicators are ocean phytoplankton (O_phyt), which is clustered with ocean surface nitrate (O_no3sur) and ocean surface phosphate (O_po4sur), and ocean oxygen (O_o2), which is clustered with ocean surface alkalinity (O_alksur). The last two indicators, top of atmosphere outgoing longwave radiation (F_outlwr) and maximum meridional overturning (O_motmax), are needed to assess the entire system, but are not significantly correlated to any remaining variables.
These changes in the selected indicators, can be explained when visually comparing the correlation matrices of the historical and the RCP4.5 scenarios (Figures 4.3 and 4.5). It is most obvious for two variables, namely air to sea carbon flux (F_carba2o) and the air to land carbon flux (F_carba2l), which stand out in particular, because they change the sign of correlation towards their indicator, and correspondingly to other related variables. These changes are driven by the land forcing of the different scenarios as well as the carbon storage capacities of the reservoirs. In the historical scenario the land use changes, which are prescribed from the CMIP5 forcing and based on historical data, prohibits the land to store carbon regardless of the e.g. increasing atmospheric CO_2 concentrations, which naturally would act to fertilise the plants and increase the carbon uptake on land. For this scenario the ocean is a carbon sink, taking up the carbon emissions from fossil fuel combustion as well as from anthropogenic land use changes. Now in the RCP4.5 scenario, anthropogenic land use is prescribed to be strongly reduced, due to an increase in the efficiency of crop production. Hence the area of naturally occurring forest and grass lands increase, and a higher amount of carbon is taken up by the land due to the CO_2 fertilisation effect. Later in the simulations between 2050 and 2100, the land as well as the upper ocean carbon uptake potential are saturated, the land reservoir turns into a carbon source for the atmosphere and the ocean carbon uptake starts to decrease from about 2050 onward. This changes in behaviour, from forced to more natural behaviour in the terrestrial carbon reservoir, and the transition from sink to source in the oceanic reservoir, cause the correlations to change their signs.

The first indicator for the RCP8.5 scenario is the atmospheric CO_2 concentration (A_co2) (Figure 4.6), which is significantly correlated to most other model output variables. In addition to the variables that are also significantly correlated to surface air temperature (A_sat) [with the exception of maximum meridional overturning (O_motmax), and air to land carbon flux (F_carba2l), which are both significantly correlated to surface air temperature (A_sat) but not to atmospheric CO_2 (A_co2)], changes in atmospheric CO_2 (A_co2) are correlated to the changes in air to sea carbon flux (F_carba2o), total ocean carbon (O_totcarb), precipitation over ocean (F_precipO), vegetation net primary productivity (L_vegnpp), leaf area index (L_veglai), vegetation carbon (L_vegcarb), the surface upward sensible heat flux (F_upsens), global precipitation (F_precip) and global evaporation (F_evap). Soil respiration (L_soilresp) is found to be the second indicator for the RCP8.5 scenario, and is in addition to all variables correlated to atmospheric CO_2 (A_co2) significantly correlated to surface albedo on land (A_albsurL), terrestrial evapo-

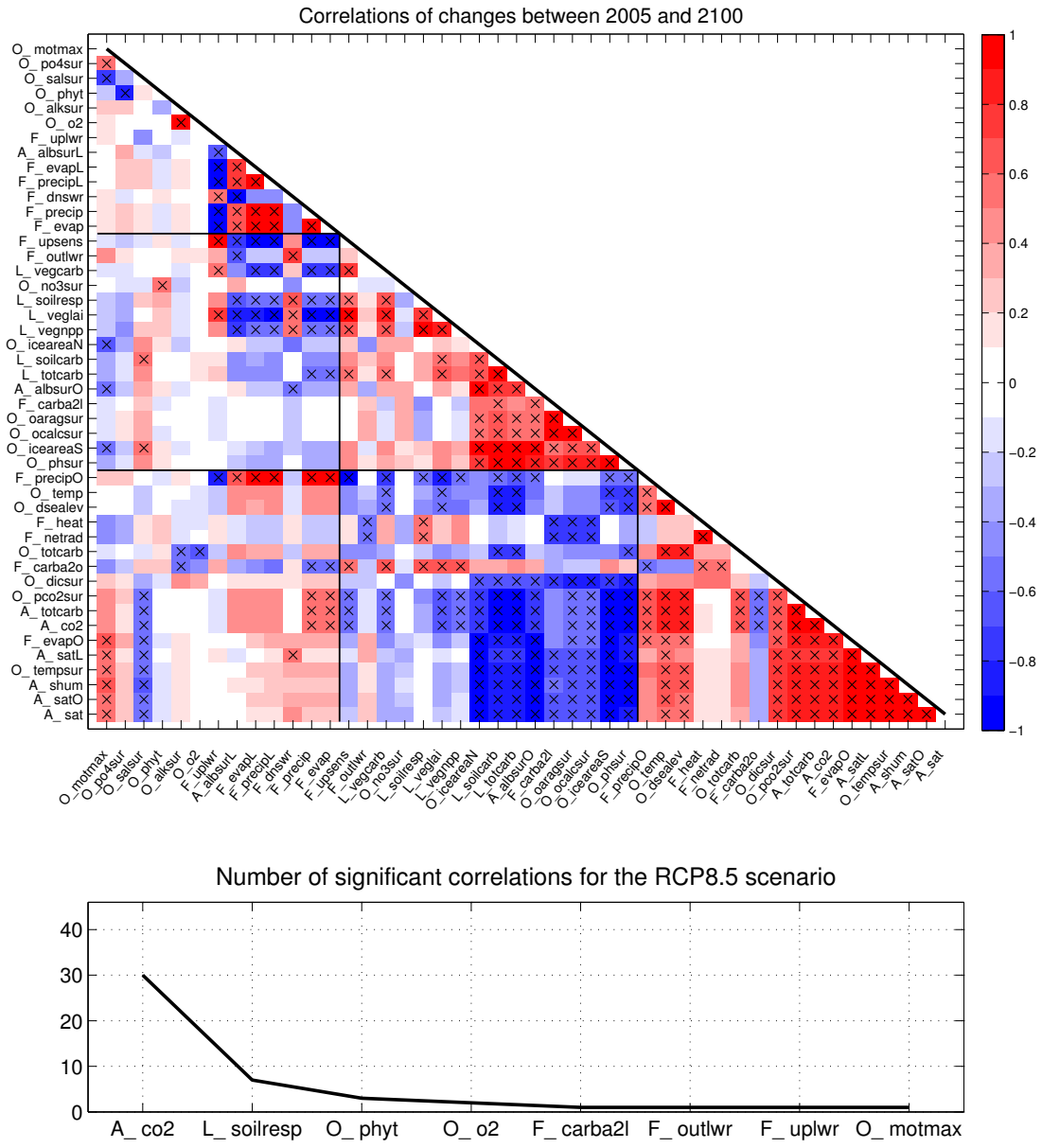

Fig. 4.6.: *Same as Figure 4.3, for the RCP8.5 scenario.*

transpiration (F_evapL), precipitation over land (F_precipL), net surface downward shortwave radiation (F_dnswr), ocean surface heat flux (F_heat), and net top of atmosphere radiation (F_netrad) (Figuer S3). Ocean phytoplankton (O_phyt) was identified as the third indicator for this scenario, it is significantly correlated with ocean ocean surface nitrate (O_no3sur) and ocean surface phosphate (O_po4sur), this is the same cluster as for the RCP4.5 scenario. The fourth indicator is ocean oxygen (O_o2), which explains the variability in ocean surface alkalinity (O_alksur), again the same cluster is found in the RCP4.5 scenario. As before, there are variable left, which are needed fro a comprehensive assessment, but are uncorrelated to any other leftover variable for the RCP8.5 scenario, which then in turn become single indicators: air to land carbon flux (F_carba2l), top of atmosphere outgoing longwave radiation (F_outlwr), net upward longwave radiation (F_uplwr), and maximum meridional overturning (O_motmax).

4.3.3. Indicators from common correlation matrix of the historical, RCP4.5 and RCP8.5 scenarios

Is it possible to find a general indicator set, valid for all three scenarios?

Considering only correlations, that are significant in all three scenarios, makes it possible to find an indicator set, that comprehensively assesses all three scenarios and clusters the same variables under one indicator. The resulting indicator set looks very different from the sets found for the single scenarios. Most obvious is the fact, that it has a larger number of indicators needed (Figure 4.7), due to the lower number of significant correlations. The first indicator is atmospheric CO_2 (A_co2), the same first indicator as for the RCP8.5 scenario. It is significantly correlated to 27 other output variables for all the regarded scenarios, i.e. independent of strength of the CO_2 forcing. Note that only two variables which were correlated to atmospheric CO_2 (A_co2) in the RCP8.5 scenario are now uncorrelated: air to sea carbon flux (F_carba2o) and sea surface salinity (O_salsur). The fact that atmospheric CO_2 (A_co2) is the first indicator hints to the importance of the atmospheric CO_2 content for determining the reaction of other variables that describe e.g. changes in temperatures, carbon fluxes and moisture fluxes over the ocean. The next indicator is precipitation over land (F_precipL), which is clustered with terrestrial evapotranspiration (F_evapL) and net upward longwave radiation (F_uplwr) (Figure C.4). This cluster would accordingly represent changes in terrestrial moisture fluxes and the resulting surface upward longwave radiation. The surface net upward longwave radiation relates to the surface air temperature, which is strongly influenced by the amount of evapotranspiration, and the resulting evaporative cooling. Note, that the fact that terrestrial moisture fluxes are clustered under a different indicator, hints to a different sensitivity of this variable to climate change and the perturbed parameters. Since these three variables show significant correlations to each other in all three scenarios, one could use all of them as the indicator for this cluster interchangeably. The same is true for the next indicators and their clusters, which are air to sea carbon flux (F_carba2o) and soil respiration (L_soilresp), net top of atmosphere radiation (F_netrad) and ocean surface heat flux (F_heat), and net surface downward shortwave radiation (F_dnswr) and surface albedo on land (A_albsurL). In addition, remaining indicators needed for a comprehensive as-

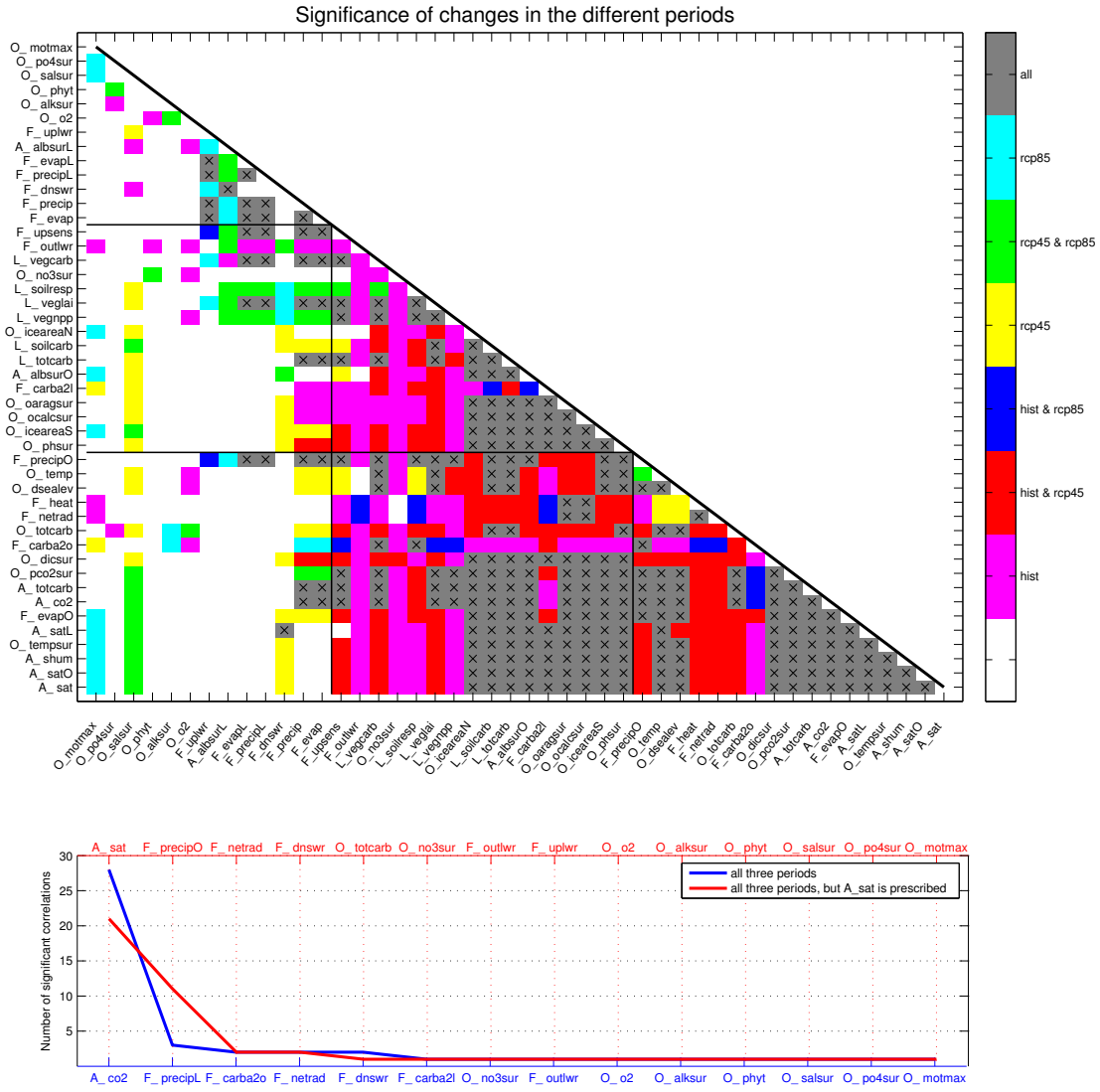

Fig. 4.7.: *a) Correlation matrix for all three scenarios, the colors indicate in which scenarios the corresponding variables show a significant correlation, see colorbar for explanation. The 'x's mark variable combinations, where the correlation is significant on a 5% significance level in all three scenarios. For details on the regarded model output variables see Table C.1.*
b) indicators as found from the analysis based on the correlation matrix above against the number of significant correlations (blue) and with the condition, that surface air temperature (A_sat) is prescribed as the first indicator (red).

sessment are air to land carbon flux (F_carba2l), ocean surface nitrate (O_no3sur), top of atmosphere outgoing longwave radiation (F_outlwr), ocean oxygen (O_o2), ocean surface alkalinity (O_alksur), ocean phytoplankton (O_phyt), sea surface salinity (O_salsur), ocean surface phosphate (O_po4sur) and maximum meridional overturning (O_motmax). The comparison of the correlations in the different scenarios shows, that there are more similar correlation patterns for the historical and RCP4.5 scenarios, than for the historical and RCP8.5 scenarios (Figure 4.7), i.e. more reddish shading than bluish. Indicating that for a lower future emission scenario, the indicators from the historical scenario are more suitable than for a higher future emission scenario, with the exception of the terrestrial and oceanic carbon fluxes as discussed before. Furthermore, greenish shading indicated that the correlations are valid in both RCP scenarios, indicating that those correlations depend on a higher atmospheric carbon content in order to become valid.

What happens if we decide to prescribe that surface air temperature (A_sat) should be the first indicator?

Prescribing the variables surface air temperature (A_sat) as the first indicator, due to its political societal, ethical and economical, importance, leads to a different indicator set (Figure 4.7, Bottom). Of course the indicators, that are not significantly correlated to any other variable remain, i.e. the last eight indicators as mentioned above. However, three of the first 5 indicators also changed, namely surface air temperature (A_sat), precipitation over ocean (F_precipO) and total ocean carbon (O_totcarb) replaced atmospheric CO_2 (A_co2), precipitation over land (F_precipL) and air to sea carbon flux (F_carba2o) (Figure C.5). Net top of atmosphere radiation (F_netrad) and net surface downward shortwave radiation (F_dnswr) remain as indicators with the same underlying clusters. Almost all of the variables which are initially clustered under atmospheric CO_2 (A_co2), but are not significantly correlated to surface air temperature (A_sat), are now clustered under precipitation over ocean (F_precipO), with the exception of total ocean carbon (O_totcarb), which becomes a single indicator in that case. These are variables (precipitation over ocean (F_precipO), global evaporation (F_evap), global precipitation (F_precip), vegetation net primary productivity (L_vegnpp), leaf area index (L_veglai), vegetation carbon (L_vegcarb) and surface upward sensible heat flux (F_upsens)) are mainly describing global and oceanic moisture fluxes, as well as carbon fluxes or reservoirs on land. In addition to those variables, precipitation over ocean (F_precipO) incorporates air to sea carbon flux (F_carba2o) and soil respiration (L_soilresp), both of which are clustered under the air to sea carbon flux (F_carba2o) indicator in the initial analysis, and precipitation over land (F_precipL) and terrestrial evapotranspiration (F_evapL), which where both clustered under precipitation over land (F_precipL) indicator before. net upward longwave radiation (F_uplwr), which was also clustered under precipitation over land (F_precipL) becomes a single indicator, remaining unclustered in the case that surface air temperature (A_sat) as first indicator is prescribed. Air to land carbon flux (F_carba2l), which was a single indicator in the initial analysis, now is clustered under surface air temperature (A_sat).

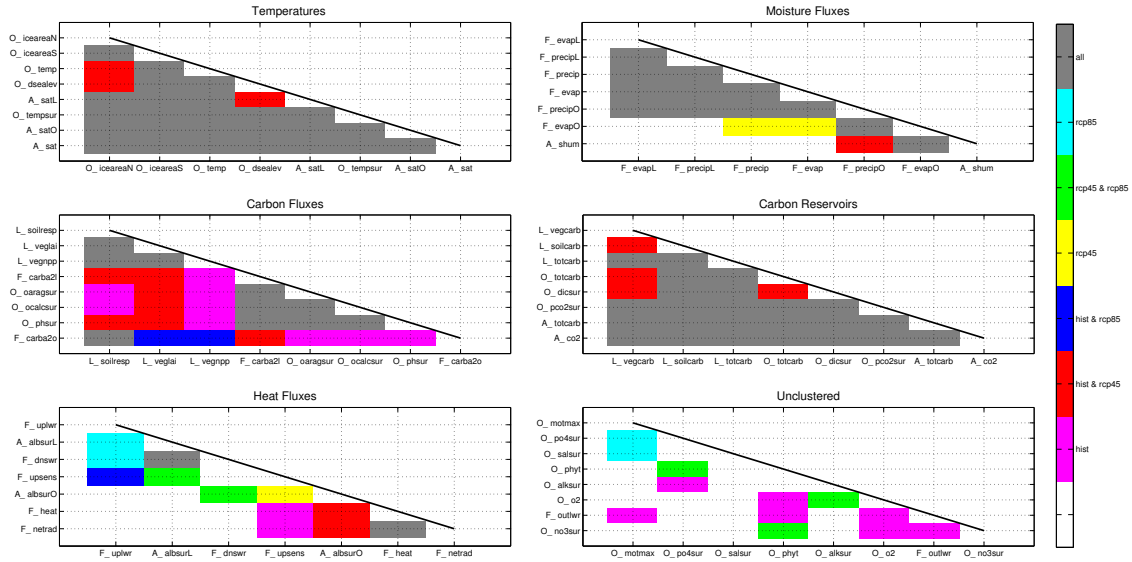

Fig. 4.8.: *Clusters of the common indicator that are scientifically meaningful to identify indicators from them.*

What if we prescribe the clusters by scientific meaningful categories?

To test if we can use knowledge of the Earth system to find meaningful clusters and reduce the amount of needed indicators, we clustered the model output variables into five categories describing temperatures, moisture fluxes, carbon fluxes, carbon reservoirs, and heat fluxes. The eight unclustered variables as found in the previous analysis will of course remain.

After clustering the variables following these categories (Figure 4.8), we can see very different behaviours in the single clusters. For the temperatures cluster we find that almost all the variables are significantly correlated in all the three scenarios. A similar result is found for the carbon reservoirs cluster. Both of these clusters can be represented by choosing one indicator for the clusters, e.g. for the temperatures we surface air temperature (A_sat), surface air temperature over ocean (A_satO) or sea surface temperature (O_tempsur) could be used. For the the clusters describing fluxes in the Earth system model, the selection of one indicator is more difficult, since often the forcing in one of the scenarios changes the correlation between the variables. For the moisture fluxes, we would need to chose two indicators, namely precipitation over ocean (F_precipO) or global evaporation (F_evap) and surface specific humidity (A_shum). The carbon fluxes cluster also needs two indicators to represent the whole cluster, soil respiration (L_soilresp) and sea surface pH (O_phsur). For both these clusters it is mainly the RCP8.5 scenario that changes the significance of the correlations, with only two exceptions (the correlation of air to sea carbon flux (F_carba2o) to leaf area index (L_veglai) and vegetation net primary productivity (L_vegnpp), which is changes if the land use forcing is reduced). This again indicates that with increasing atmospheric carbon concentrations some prevailing relationships in the Earth system might be changed.

The heat fluxes cluster has the most complicated outcome. All combinations of signifi-

cant correlations between the three scenarios are represented, hinting to the fact that heat fluxes might be very sensitive to changes in the imposed forcing. This results in two indicator that can be found due to clusters of robust correlations across all scenarios, namely net top of atmosphere radiation (F_netrad) and net surface downward shortwave radiation (F_dnswr). But the three remaining heat fluxes are unclustered and would be needed as single indicators. Adding up all the newly found indicators we would end up with 19 indicators, which would be needed for a comprehensive assessment of the system as clustered by the inclusion of expert judgement. Although this is a higher number of indicators than what was found, under the systematic correlation matrix evaluation, but it is noteworthy, that these indicators now would already include some kind of meaningful information about the system.
It could be argued that the expert judgement was made imperfectly, and with better understanding of the Earth system fewer indicators could be selected. This is undoubtably true, however this clusters were defined without regarding the correlation matrix in the first place, so to be uninfluenced by the results. This would reflect an expert judgement excluding the learning process from looking at the outcome, i.e. testing if the hypothesis is true without adjusting it to the outcome. It is noteworthy, that by defining clusters we lose the opportunity to find previously unknown relationships or correlations between variables.

4.4. Discussion

4.4.1. Limitations of this study

One limitation of the presented case study, is that the results are strongly dependent on the model used, as well as on the chosen perturbed model parameters. The selected parameters in this study mainly represent temperature and CO_2 sensitivities of the model. This biases the correlation analysis of the model output variables towards their sensitivity to the selected perturbations (for a detailed discussion see section C.1 and Figure C.6 in the supplemental information). For out case study, we wanted to assess the uncertainty of the biological system towards increasing temperatures and CO_2 levels as well as some parameters that might influence these factor due to uncertainty in physical parameterisations. Therefore we chose to implement these parameter perturbations, since these sensitivities will become important under future high CO_2 and temperature forcing. For other experiments, one might be more interested in different uncertainties in the simulated Earth system, such as clouds or climate sensitivity, then these parameter perturbations ought to be considered, which will change the patterns of the correlation matrix.
It is important to stress the fact, that the regarded Earth system variables are global aggregates and miss information on regional changes. Again for our case study it might be sufficient to initially regard global aggregates, but it is important to mention, that the global aggregate is not always positively correlated to the regional changes (for more details see section C.2 and Figure C.7 of the supplemental information), and therefore misrepresents these regions. It is therefore insufficient to only regard the global aggre-

gates for a thorough assessment of the climate change impacts.
Furthermore, we restrict our case study to regard temporal changes between two time scenarios, and thereby miss information about the temporal development of the model variables. This approach was chosen, since the UVic ESCM is a model with low internal variability, which would hence not show interesting information in case of temporal correlations. Investigating the model's sensitivity to the parameter perturbations was therefore the more interesting choice of experiment.
These discussion points from our case study already illustrate the sensitivity of the correlation matrix towards the way it is constructed. Starting with the question to use global vs. regional aggregates, which model to use, parameter sensitivity analysis vs. temporal correlations, choice of significance level, and so on. These questions have to be answered depending on the research hypothesis, as is the case before every scientific experiment. Thereafter, the correlation matrix and SCoMaE can be used as a tool for a thorough assessment of the experiment. All these choices on the construction of the correlation matrix make the assessment partly subjective again.
It needs to be mentioned, that this assessment, if based on an Earth system model, represents the natural science perspective on the indicator selection. Important characteristics as discussed by [Radermacher, 2005], are not necessarily included in this evaluation. The selection process of the indicators misses political, ethical and economical considerations and therefore is not suited to identify, policy-relevant indicators on its own. Nevertheless, if political, ethical and economical considerations were to be included in this analysis, and e.g. it was decided to use surface air temperature (A_sat) as the first indicator this can be implemented and the remaining indicators needed to assess the entire system can be identified using this approach. In addition, we are regarding the Earth system as represented in a model, hence we do not include information about measurability in this analysis. The selected indicators are reasonable in our model domain, but hold problems in their application, since the measurability may not be given. This would be the case for e.g. precipitation over ocean (F_precipO), the indicator for the historical scenario. Although this variable might be correlated to a lot of other relevant variables, there is a lack of long term historical precipitation measurements over the ocean [New et al., 2001]. Accordingly it would be difficult to obtain longterm time series for this variable and is therefore limited in the assessment of trends and variability.

4.4.2. Discussion of results from the case study

Our analyses showed, that an assessment of the Earth system depends on the considered time scenario, or maybe more accurately the imposed forcing scenario. For future scenarios with different forcings (e.g. higher CO_2 forcing during the RCP8.5 scenario, or reduced anthropogenic land use forcing during RCP4.5 scenario compared to the historical scenario) it is insufficient to apply the historical indicator set. We find that different indicators sets are needed in order to account for climatic changes in the future forcing scenarios.
Nevertheless, there is some overlap between the clusters of the different scenarios. Two clusters are repeated for both future emission scenarios, namely ocean phytoplankton

(O_phyt), clustered with ocean surface phosphate (O_po4sur) and ocean surface nitrate (O_no3sur); and ocean oxygen (O_o2) clustered with ocean surface alkalinity (O_alksur). These two clusters seem to be consistent, if the atmospheric CO_2 concentration is increased, but do not hold for the historical scenario. As a result, all these variables are unclustered in case of a common indicator selection, causing the number of selected indicators for a common indicator set to increase.

For the common indicator selection (as well as the assessment of the RCP8.5 scenario) atmospheric CO_2 (A_co2) is the first indicator, being significantly correlated to most of the other model output variables parameter sensitivities. In addition, we find four smaller clusters with interchangeable indicators, which show robust correlations between variables for all three scenarios. Lastly there are eight unclustered variables.

For the clusters of the common indicator set, the correlations remain significant even under different atmospheric carbon contents or land use forcings. Are these correlations scientifically sound? Atmospheric CO_2 (A_co2) as the first indicator clusters changes in carbon fluxes, temperatures, and moisture fluxes over the ocean. The second indicator represents the variability of moisture fluxes on land and the associated cooling effect. This is different from the global and oceanic moisture fluxes, due to the sensitivity of transpiration to CO_2 [Mengis et al., 2015], which is represented in the parameter perturbations. Two other clusters are net top of atmosphere radiation (F_netrad) and ocean surface heat flux (F_heat), which are intuitively connected, and net surface downward shortwave radiation (F_dnswr) and surface albedo on land (A_albsurL), which are connected, since changes in vegetation on land due to the parameter perturbations influence both the surface albedo on land and the incoming shortwave radiation at the surface.

Air to sea carbon flux (F_carba2o) and soil respiration (L_soilresp) are also clustered for all the scenarios, but shows a negative correlation in the historical scenario and positive correlations in the two RCP scenarios, indicating that they are dependent on the carbon concentrations in the atmosphere. The predominant parameter perturbation for those correlations is the CO_2 fertilisation sensitivity. For the historical scenario, with higher CO_2 fertilisation the soil respiration increases due to an increase in the soil carbon pool, while the carbon fluxes from atmosphere to ocean slightly decrease with increasing fertilisation effect, due to the reduced atmospheric carbon concentration. Now in the future scenarios, both carbon fluxes are increased with higher CO_2 fertilisation strength, for soil respiration (L_soilresp) the underlying process is still the same. For the air to sea carbon flux (F_carba2o) flux the correlation to atmospheric CO_2 (A_co2) however turns negative for the future scenarios and the high CO_2 fertilisation scenario. With higher CO_2 fertilisation, the atmospheric carbon content still decreases, however the atmosphere to ocean carbon fluxes are increasing with higher CO_2 fertilisation strength, since the terrestrial and oceanic carbon reservoir reach saturation during this scenario. Now with higher CO_2 fertilisation, the rate of carbon uptake on land is higher causing the land to reach its saturation state earlier, but the ocean to reach its later. This results in a higher flux of carbon to the ocean for higher CO_2 fertilisation simulations. Although the clusters of significant correlations all are reasonable (scientific sound), some connections are more straightforward, than others.

This is different than when we prescribe the clusters by scientific meaningful categories.

In this case the interpretation of the results is straight forward, however we rid ourselves of the possibility finding correlations that are meaningful, but were not considered before, i.e. the possibility to learn something from this method.

4.5. Conclusions

In this study we introduce a method to systematically identify indicators from Earth system variables, and we show an example of how the method could be applied by using an intermediate-complex Earth system model. Our analyses concerning three different scenarios, highlighted the necessity of a re-evaluation of the selected indicator sets with time. We show that it is not sufficient to apply the indicator set found for the historical scenario to neither an intermediate-high nor a high future emission scenario. Different indicator sets are needed for the assessment of these three scenarios.
Furthermore, we show that including expert judgement in the indicator selection, simplifies the interpretation of the clusters. However, the total number of indicators needed for a thorough assessment increases. Since some correlations between Earth system variables might not be considered, due to the lack of knowledge/expertise, they cannot be taken into account for process of finding clusters.
By combining the three scenarios, we found a common indicator set, which had a higher number of indicators compared to each of the single indicator sets. It enables us to identified robust correlations between Earth system variables across the three scenarios, and points out the Earth system variables which are uncorrelated, if all three scenarios are to be considered.
Although it is beyond the scope of this study to provide a normative framework for indicator selection, which would require the inclusion of stakeholders, we here provide scientific-based information on the robustness of the indicator selection. If however the decision was made to use surface air temperature (A_sat) as the first indicator this can simply be implemented in this methodology and the remaining indicators needed to assess the entire system can be identified using this approach.

Acknowledgements The authors thank Christian Baatz and Wilfried Rickels for their helpful comments, as well as the participants of the Metrics Workshop of the SPP 1689 in March 2015, Hamburg, for their thoughts on metrics and indicators. The model data used to generate the figures will be made available at http://thredds.geomar.de. This work was funded by the German DFG in the context of the Priority Program: Climate Engineering: Risks, Challenges, Opportunities? (SPP 1689). The authors declare that they have no competing financial interests. N.M., A.O. and D.P.K. conceived and designed the experiments. D.P.K. and N.M. implemented and performed the experiments. N.M analysed the data and wrote the manuscript with contributions from D.P.K., and A.O..

5. Selecting Indicators from Earth system variables to assess Climate Engineering

This chapter is a manuscript in preparation by Mengis N., W. Rickels, D. P. Keller, M. Quaas and A. Oschlies (2016).

Abstract This is the first study to systematically identify changes in correlation patterns introduced by three idealised Climate Engineering (CE) scenarios: Large-scale Afforestation, Ocean Alkalinity Enhancement and Solar Radiation Management. First we investigate how the chosen CE methods alter prevailing correlations between Earths system variables compared to one intermediate-high (RCP4.5) and one high (RCP8.5) future emission scenario. To enable a comprehensive comparison of the thee scenarios, the common correlation matrix of the three methods is systematically evaluated to identify an indicator set. A preliminary evaluation of the three scenarios based on these indicators remains inconclusive, since it depends on the regarded indicator as well as the sensitivity simulation, which scenario performs 'best' in staying close to the 2005–2010 reference climate state. If the indicators are further aggregated into a metric in order to reduce the complexity, a ranking of the different scenarios becomes evident. Given all assumptions, we find that overall the RCP4.5 scenario performs 'best' in staying close to the reference climate state. Solar Radiation Management is identified as the 'best' CE scenario, followed by Ocean Alkalinity Enhancement and Large-scale Afforestation. The latter performs comparable to the RCP8.5 scenario. This study is an important first step towards a more systematic assessment of CE methods, however side-effects of the different CE methods will require a more detailed assessment, particularly, an extensive risk analysis on regional scales is necessary for a thorough evaluation.

5.1. Introduction

Measured, calculated, and forecasted quantitative variables are used to assess the complex reality by indicating the state of a specific matter. For the specific matter of current climate change, most attention is usually devoted to global mean temperature, making it the most commonly used indicator among the various Earth system variables for climate change assessment. This indicator on the state of the climate system can then be combined with other indicators (for example reflecting information about socio-economic states) for the assessment of mitigation and adaptation policies. Besides practical and social aspects for selecting global mean temperature over other possible indicators, its selection can be (scientifically) justified by the aspect that other Earth system variables are often correlated with global mean temperature. However, in an engineered climate resulting from the ap-

plication of radiation management (RM), terrestrial or marine carbon dioxide removal (t- and mCDR, respectively), prevailing relationships between Earth system variables may no longer remain valid. Consequently, a comparative assessment of climate engineering requires a comprehensive discussion of the indicator selection process from Earth system variables. Deriving and agreeing on appropriate indicators for Climate Engineering (CE) assessment is probably one of the major challenges in the CE debate.

In the following we shortly discuss typical indicators used in the assessment of the two major CE categories. RM methods are supposed to change the Earth's radiation budget by, e.g. increasing the reflectivity of the Earths surface and thereby reducing the amount of incoming solar radiation, or by making the atmosphere more transparent for outgoing long-wave radiation emitted from the Earth's surface. In studies on the topic, authors have stressed that applications of SRM cannot exactly compensate for the greenhouse gas (GHG)-induced temperature increase and therefore will have different impacts on climate than application of emission control [Kravitz et al., 2013a]. Since the early studies, precipitation in addition to temperature and atmospheric circulation changes has been in the focus of the debate, both on a global and regional scale [Tilmes et al., 2013]. Generally, the assessment of RM methods is focused on atmospheric variables. Less attention has been devoted to variables like sea ice coverage, vegetation net primary production or sea level rise [e.g., Berdahl et al., 2014; Pongratz et al., 2012; Keller et al., 2014] (See Table D for an overview on assessed indicators of the different CE methods).

CDR methods generally aim at reducing the anthropogenic carbon content in the atmosphere, by sequestering carbon in reservoirs with long term storage capacities, this is apart from the possibility of reducing the emissions in the first place. For tCDR methods large areas of forest or grassland are managed in order to remove carbon from the atmospheric and sequester it in the terrestrial carbon reservoir, or to use the products as a substitute for fossil fuels and sequester the emitted carbon [Stavi and Lal, 2012; Azar et al., 2013]. The literature on the assessment of LAF concentrates on terrestrial impacts, such as vegetation carbon content, terrestrial respiration or soil moisture, as well as on atmospheric consequences, like the atmospheric carbon content, precipitation or land surface albedo [e.g. Pongratz et al., 2011; Ridgwell et al., 2009]. For mCDR the carbon storage capacity of the marine system ought to be enhanced, by either enhancing the biological productivity and the carbon sequestration via the biological pump, or by enhancing the physical storage capacity of seawater by adding alkaline substances to the ocean's surface waters. Comparable little literature on mCDR exists and it mainly focuses of oceanic Earth system indicators for circulation changes and ocean biogeochemistry, as well as atmospheric temperature (see Table D).

The (implicit) selection of additional indicators for the assessment of CE is not based on any set of agreed guidelines or a comprehensive discussion and is therefore, even though in a kind of scientific consensus, a normative choice in the assessment of CE. However, there exist no unambiguous rules for selecting indicators [Böhringer and Jochem, 2007]. Thus, we propose that indicators should be selected in a more systematic and transparent manner. There is a wide agreement that a broad set of variables and therefore possible indicators should be considered at the initial level from which one selects then appropriate ones according to some transparently explained method [e.g., Pintér et al., 2005;

Kopfmüller et al., 2012]. In general, the selection and construction of indicators has to deal with the conflicting goals of statistical measurability, scientific consistency, and political relevance [Radermacher, 2005].
In this study, we provide a comprehensible method to determine robust indicators for a systematic CE assessment. In section 5.4, we investigate how the simulation of three idealised CE methods changes prevailing relationships as represented in the model. By constructing a common correlation matrix, in section 5.5, indicators needed for a comprehensive, comparative assessment of these CE methods are identified. Finally, in section 5.6 we attempt to evaluate the three CE methods based on the identified indicators as well as based on an aggregated metric.

5.2. Earth system indicators and reference points in the CE literature

5.2.1. Earth system indicators

Available published climate engineering research articles were examined to see which indicators are evaluated in figures, tables, and main sections of the text. The utilised indicators were then classified according to the assessed spatial and temporal scales (Table D).
The overview of indicators from the literature review added information to the list of Earth system variables, which was initially constructed based on expert judgement. Finally, we obtained a list of 46 Earth system variables, which was uses as a basis for the assessment of CE. Note that for this study as a first attempt globally aggregated Earth system variables will be considered.

5.2.2. Choice of Reference Points

For an evaluation of different climate engineering methods, we need to define a reference point in time at which we want to compare the climate states of the different scenarios. Most model assessment approaches chose the climate state in 2100. Now for a climate change assessment naturally one would consider changes from present day or pre-industrial to 2100. Already this choice implicitly includes some kind of judgement: If the future climate change is to be compared to pre-industrial conditions, this will look more drastic, than a comparison against present day climate. On the other hand, this choice might be reasonable, because changes are put into more perspective and show deviations from the natural unperturbed climate system. Does this already imply, that such a climate state might be the desirable goal for the future climate state? One might argue that the comparison to present day conditions will illustrated more practically what changes we are to expect compared to our todays climate, accepting the changes of the system that have occurred so far.
In the CE literature as well as in the results of the Geoengineering Model Intercomparison Project (GeoMIP), there is not a common reference point against which CE methods are evaluated. Some use preindustrial, some the Representative Concentration Pathway

(RCP) 4.5, or the RCP8.5 climate state in 2100 as the reference, this also depends on the chosen reference emissions scenario. Note, that within the progress of GeoMIP even the reference climate change scenario changed. While in the first two phases of GeoMIP, the RCP4.5 emission scenario was used as the underlying climate change scenario and Climate Engineering experiments were imposed on this reference scenario, realising that with our current emissions we are more likely to follow a high emissions scenario, in the next round of GeoMIP the high forcing (likely similar to RCP8.5) will be used as the underlying emission scenario. The medium high forcing scenario (likely similar to RCP4.5) is then used as a target to be reached by Climate Engineering in the two new GeoMIP experiments.
It makes sense to compare the 2100 climate states of the reference scenario and the experiment in order to assess which impact the methods would have. However, this does not give information of the changes that we would have to expect compared to nowadays climate. If for example future precipitation is decreased by a CE method relative to the RCP8.5 scenario, in which precipitation might increase, the important question is how much does it change relative to today's precipitation. Again the choice of reference scenario for the evaluation of CE methods holds a value judgment. If results are shown with respect to RCP8.5 in 2100, we will most likely see e.g. a cooling of surface temperatures, however compared to nowadays the climate system might still be warming, indicating that the choice of reference point defines the sign of the presented changes.

5.3. Methods

5.3.1. Model Description

The model employed is version 2.9 of the University of Victoria Earth System Climate Model (UVic ESCM), an Earth system model of intermediate complexity [Eby et al., 2013]. It includes schemes for ocean physics based on the Modular Ocean Model Version 2 (MOM2) [Pacanowski, 1995], ocean biogeochemistry [Keller et al., 2012], and a terrestrial component including soil and vegetation dynamics [Meissner et al., 2003]. The ocean biogeochemistry is based on a simple NPZD model [Keller et al., 2012]. The terrestrial component consists of simplified versions of the Met Office Surface Exchange Scheme (MOSES) and the Top- down Representation of Interactive Foliage and Flora Including Dynamics (TRIFFID) vegetation model [Cox et al., 1998; Cox, 2001]. The vegetation scheme calculates the state of the terrestrial biosphere in terms of soil carbon, and the structure and coverage of bare soil or five plant functional types [Meissner et al., 2003]. The ocean models is coupled to a thermodynamic sea-ice model [Bitz and Lipscomb, 1999] with elastic visco-plastic rheology [Hunke and Dukowicz, 1997]. The atmosphere is represented by a two dimensional atmospheric energy moisture balance model [Fanning and Weaver, 1996].
All model components have a common horizontal resolution of 3.6 $^\circ$ longitude and 1.8 $^\circ$ latitude and the oceanic component has a vertical resolution of 19 levels, with vertical thickness varying between 50 m near the surface to 500 m in the deep ocean. Wind veloci-

ties used to calculate advection of atmospheric heat and moisture as well as the air-sea-ice fluxes of surface momentum, heat and water fluxes, are prescribed as monthly climatological wind fields from NCAR/NCEP reanalysis data [Keller et al., 2014]. Wind anomalies, which are determined from surface pressure anomalies with respect to pre-industrial surface air temperature, are added to the prescribed wind fields.

5.3.2. Implemented Climate Engineering Methods

For our experiments we implemented three exemplary Climate Engineering methods, each of which concerns one of the three main components of the Earth system: Solar radiation management (SRM) directly affects the radiation balance of the atmosphere, large-scale afforestation (LAF) influences primary production on land, and ocean alkalinity enhancement (OAE) directly affects biogeochemistry in the ocean. All CE schemes are implemented under a high emission scenario (RCP8.5) and aim at reaching an intermediate high emission scenario (RCP4.5) concerning varying components of the Earth system.
For the implemented SRM scheme, a dimming of the sun by e.g. successful deployed sunshades, is implemented in the model, reducing the amount of top of the atmosphere incoming shortwave radiation. This climate engineering method was designed to reach the top of the atmosphere radiative forcing of the RCP4.5.
The LAF scenario reduces the area of land used for agriculture, following the RCP4.5 land use changes. For the UVic ESCM this means that areas prescribed as grasslands, representing agricultural areas, are reduced and allowed to develop naturally. This unmanaged afforestation scheme assumes that the naturally occurring vegetation has a higher carbon storage capacity compared to the vegetation that is planted if the land is used for agriculture. In our model the main transition occurs in the tropical areas, where the C3 grass lands, representing agriculture lands, are reduced in favour of broadleaf trees, which indeed have a higher carbon content per square meter.
For the OAE scenario, the ocean surface alkalinity is enhances so that the ocean takes up enough carbon for the atmospheric CO_2 content to matches RCP4.5 CO_2 concentrations. Note, that for this approach, the surface alkalinity of each grid cell is multiplied by a factor larger one, if the simulated atmospheric CO_2 concentration deviates by more than 1% from the target RCP4.5 CO_2 concentration, so that the surface ocean can take up more CO_2. This leads to local high surface alkalinity values.
All three CE methods start in 2005 so that they smoothly follow the RCP4.5 forcing. It is however noteworthy, that since the RCP4.5 and RCP8.5 scenarios start to deviate (concerning CO_2 and radiative forcing) only from about 2020 onward, the SRM and OAE methods start gradually to show effects only then. However the LAF scenario continually changes the land surface forcing starting from 2005 onward, which reflects the reality.

5.3.3. Indicator Selection and Metric Construction

Systematic Correlation Matrix Evaluation (SCoMAE)

For the evaluation of the model results we applied the method described in Chapter 4 using the same sensitivity simulations as described in Section 4.2.4, with the exception of the zero CO_2 fertilisation simulation. This simulation forces a unrealistically strong ocean alkalinity enhancement, due to its rather large atmospheric CO_2 content, resulting from the lack of carbon uptake by land. This make a total of 15 parameter perturbation simulations. The correlation matrices were constructed to find a common indicator for the single CE methods and the two underlying forcing scenarios (RCP8.5 and RCP4.5), as well as to find a common indicator for the assessment of the three CE methods.
The indicator identified for the three CE methods, are the used for a preliminary evaluation of the CE methods. Two reference points are chosen. First all five scenarios, Climate Engineering and climate change, are evaluated against their closeness to the 2005–2010 reference state. The closer the scenarios are to this reference state is defined the 'better'. This implies the normative statement, that it is desirable to stay close to todays climate conditions. The second reference point is the state of the RCP4.5 simulation in 2090–2100. Here we evaluate the three CE scenarios based on their ability to reach the defined target.

Metric Construction from Earth system variables

In order to construct a metric from the selected Earth system indicators, we need to transform the Earth system variables so that the averaging process is not influenced by the measurement units in which the indicators are expressed [e.g. Ebert and Welsch, 2004]. We therefore apply a min-max scaling to the absolute differences of all simulations of all scenarios in 2090–2100 relative to the chosen reference point of 2005–2010, and subtract them from 1.

$$I_{norm} = 1 - [(I - I_{min})/(I_{max} - I_{min})] \tag{5.1}$$

Where I_{norm} is the normalised Earth system variable with $0 \leq I_{norm} \leq 1$ and a value of 1 indicates a good performance. I is the absolute difference of the specific simulation of the scenario in 2090–2100 relative to 2005–2010, whereby deviations in both direction lead to a bad performance, and I_{min} and I_{max} are the respective minimum and maximum values of all the simulations and scenarios.
Thereafter, generalised means of (i) the selected indicators from the SCoMaE and (ii) all 46 Earth system variables are calculated, following:

$$X(\alpha_i, I_i, \sigma) = [\sum_{i=1}^{N} \alpha_i * I_i^{(\sigma-1)/\sigma}]^{\sigma/(\sigma-1)} \tag{5.2}$$

Where $\alpha_i > 0$ are the weights of the indicators, and $0 \leq \sigma \leq \infty$, it the elasticity of substitution between the different indicators [Solow, 1956; Arrow et al., 1961].
For the metric constructed from the identified Earth system indicators from the SCoMaE analysis we apply weights α_i based on the number of correlated relative to the total

number of variables. Here we explicitly weight all non-selected variables with a weight of zero. For the metric constructed from all 46 Earth system variables we apply equal weights. Following Sterner and Persson [2008], we take $\sigma = 0.5$.
The metric is lastly averaged over the sensitivity simulations to obtain one number for each scenario, based on which we can identify the scenario with the 'best' outcome.

5.4. Earth system indicators for CE schemes compared to the default RCP scenarios

Based on the approach described in Chapter 4, the correlation matrices for the different climate engineering as well as for the climate change and mitigation scenario are compared. The aim is to find common features between the scenarios to understand the forcing effect from the imposed climate engineering methods.

5.4.1. Solar Radiation Management

In the SRM scenario, the radiative forcing targets the RCP4.5 scenario, and atmospheric CO_2 is close (but not equal, due to carbon cycle feedbacks) to the RCP8.5 scenario. Comparing patterns of significant correlations for the different scenarios (Figure 5.1, Top), illustrates how the implementation of SRM changes prevailing relationships in the Earth system, as represented by the UVic ESCM. The SRM implementation allows the distinction of temperature/radiative forcing dependent correlations and atmospheric CO_2 dependent correlations. From the evaluation of the common correlation matrix, we identify six clusters in the SRM scenarios (Figure 5.2). The first indicator is evaporation over ocean (F_evapO) and represents mainly changes in temperatures and therefore associated in sea ice, but also sea surface partial CO_2 pressure (O_pco2sur), total land carbon (L_totcarb), and soil carbon (L_soilcarb), i.e., three carbon based Earth system variables are clustered under this indicator. The second indicator is leaf area index (L_veglai), representing land based Earth system variables concerning carbon, moisture and heat fluxes. The third indicator is total ocean carbon (O_totcarb), representing changes in ocean temperatures, carbon and partly also in biogeochemistry. Some of these changes are however also clustered in the fifth indicator ocean phytoplankton (O_phyt), which in addition also represents changes in ocean surface nitrate and phosphate (O_no3sur and O_po4sur, respectively). The fourth indicators is atmospheric CO_2 concentration (A_co2) and represents variables, which are directly linked to atmospheric CO_2, namely total atmospheric carbon (A_totcarb), sea surface dissolved inorganic carbon (O_dicsur), and sea surface pH (O_phsur). The last cluster represents radiative heat fluxes, i.e., net top of atmosphere radiation (F_netrad) and ocean heat flux (F_heat). Five of the Earth system variables remain unclustered: ocean maximum meridional overturning (O_motmax), ocean surface salinity (O_salsur), top of atmosphere outgoing longwave radiation (F_outlwr) and the atmosphere to land and ocean carbon fluxes (F_carba2l and F_carba2o, respectively).

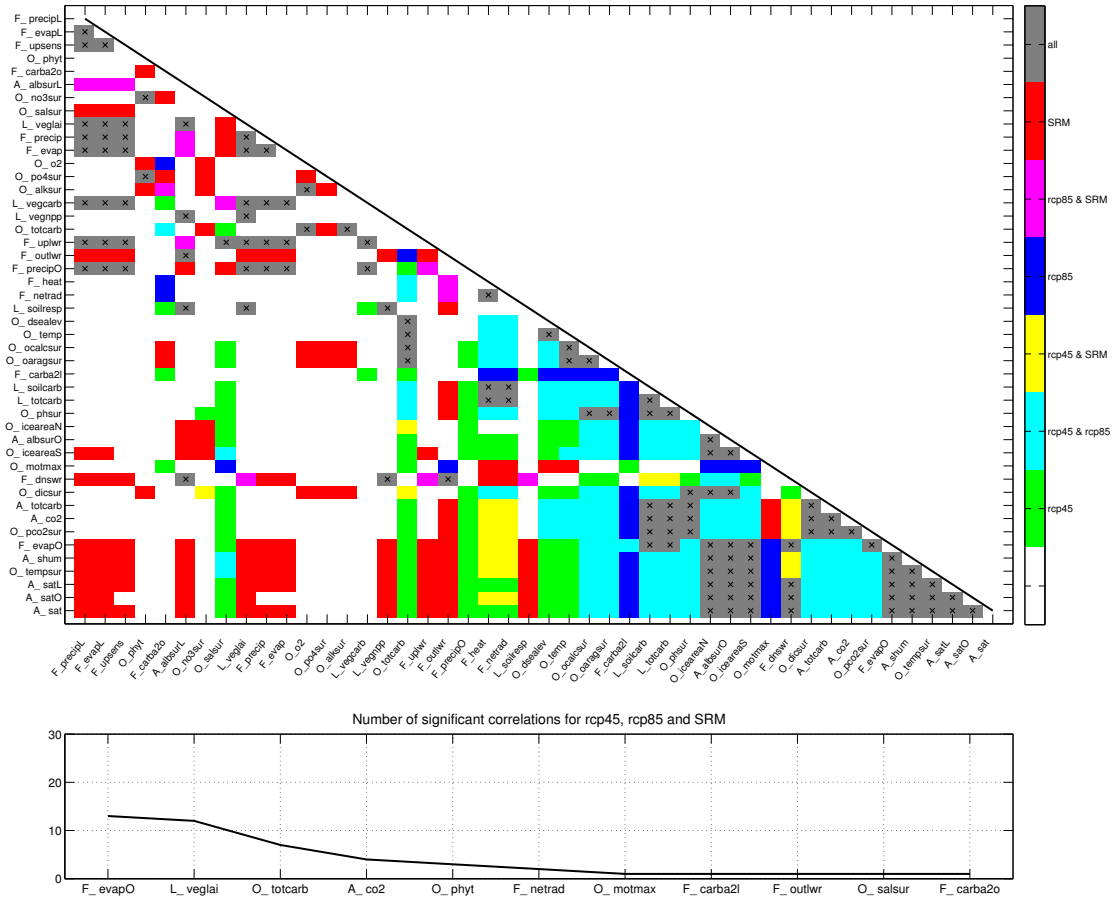

Fig. 5.1.: *Top: Common correlation matrix for the SRM, RCP4.5 and RCP8.5 scenarios. The shading indicates in which scenarios correlations between Earth system variables are significant, crosses indicate where they are significant in all three scenarios. Bottom: Headline indicators resulting from the systematic evaluation of the correlation matrix.*

Light blue shading in Figure 5.1 illustrates significant correlations in both default RCP scenarios, but no significant correlation in the SRM scenario, indicating that the SRM implementation changed the relationships between these variables to be insignificant, and often to even change the sign of correlation to e.g. surface air temperature (A_sat). Many of these correlations are associated with the carbon reservoirs in the model, namely the atmospheric carbon concentration (A_co2), total atmospheric carbon (A_totcarb), total oceanic carbon (O_totcarb), sea surface partial CO_2 pressure (O_pco2sur), sea surface dissolved inorganic carbon (O_dicsur), total land carbon (L_totcarb), and soil carbon (L_soilcarb). This arises from the decoupling of the relationship between temperature and CO_2 in case of SRM implementation, and implies that these variables would need to be specially considered if SRM were to be implemented. Note that all these variables are represented in clusters other than the first cluster, which represents temperature changes. Red shading illustrate correlations, which are significant only if SRM is implemented, i.e., under low temperature high CO_2 concentrations.

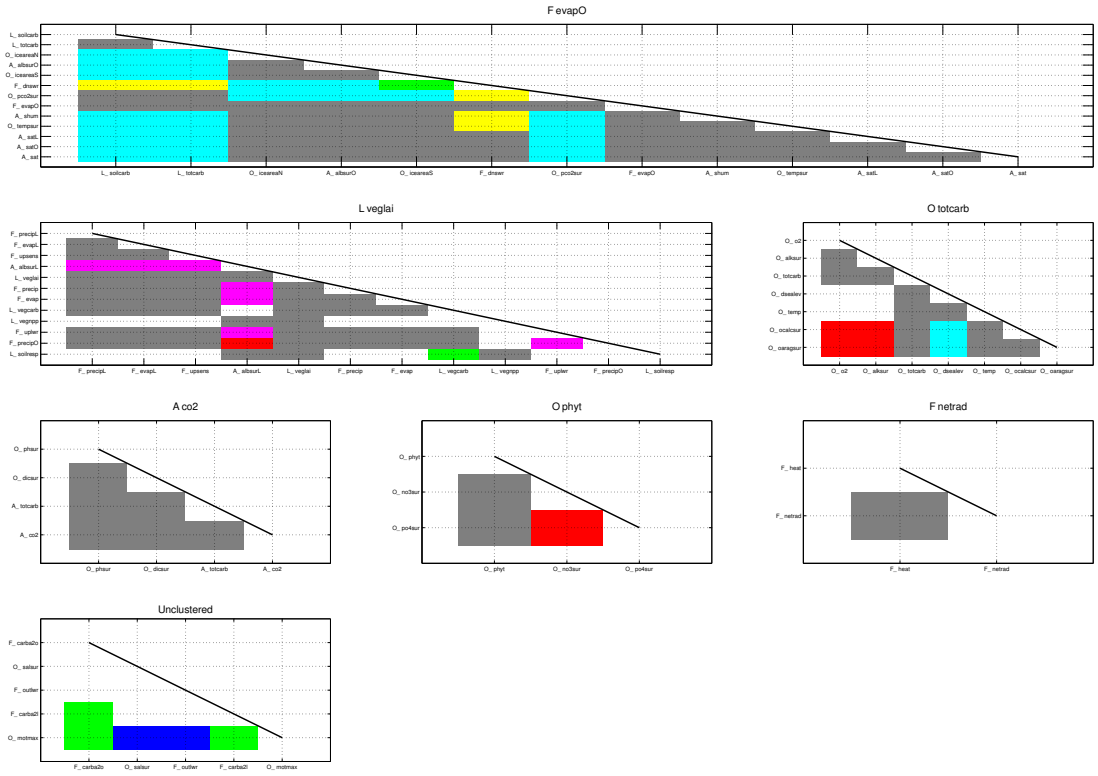

Fig. 5.2.: *Clusters identified in the common correlation matrix for the SRM, RCP4.5 and RCP8.5 scenarios. Color coding is the same as for figure 5.1*

These correlations would not occur in a natural/un-engineered climate state. This is the case for many correlations between temperature related Earth system variables and land associated carbon, moisture and heat fluxes, which are clustered under the second indicator. Yellow shading illustrates the correlations that are significant under both the RCP4.5 and the SRM scenario, i.e., under low radiative forcing and regardless of the background atmospheric carbon content. These correlations are mainly found for radiation and heat fluxes (net surface downward shortwave radiation (F_dnswr), net top of atmosphere radiation (F_netrad) and ocean heat flux (F_heat)) with respect to temperature related (sea surface temperature (O_tempsur) and surface specific humidity (A_shum)) and atmospheric carbon related (atmospheric carbon concentration (A_co2), total atmospheric carbon (A_totcarb), total oceanic carbon (O_totcarb), and sea surface partial CO_2 pressure (O_pco2sur)) variables.
In contrast to this purple shading illustrates correlations between Earth system variables that are valid for the RCP8.5 and the SRM scenarios, i.e., under high atmospheric CO_2 concentrations, and regardless of the radiative forcing. This is the case for correlations between the land surface albedo (A_albsurL) and heat fluxes, as well as terrestrial and correspondingly also global moisture fluxes. In addition net surface downward shortwave radiation (F_netrad) shows significant correlations towards the leaf area index (L_veglai) and the soil respiration (L_soilresp).

5.4.2. Large-scale Afforestation

For the LAF scenario the land use changes follow the RCP4.5 scenario, and the remaining atmospheric forcing follows the RCP8.5 scenario. This means that we can distinguish which correlations depend on the imposed land use forcing, or which are robust under varying CO_2 scenarios. Note that although LAF is a CDR method, the impact on atmospheric carbon is comparably low. Following the RCP4.5 land use changes yields the potential to reduce atmospheric CO_2 by about 30ppm relative to the RCP8.5 scenario in the default simulation.

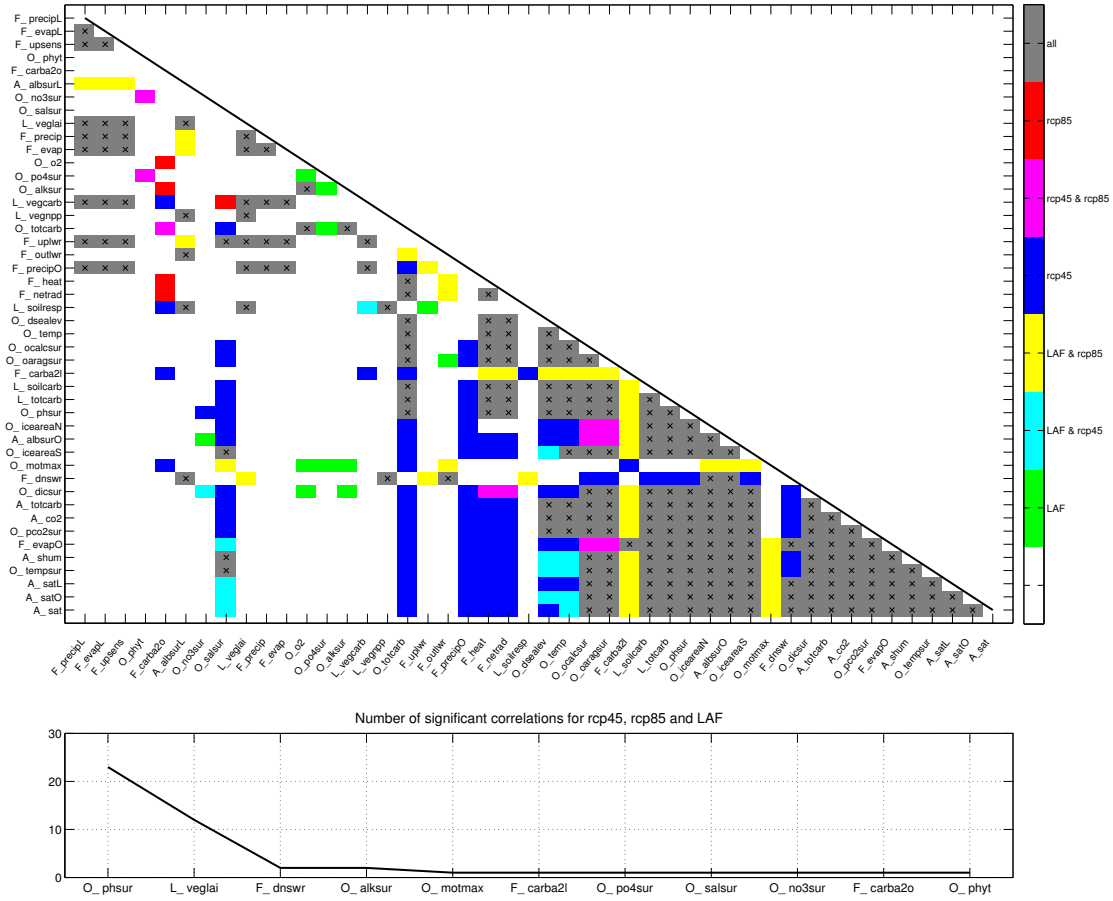

Fig. 5.3.: *Top: Common correlation Matrix for the LAF and the RCP4.5 and RCP8.5 scenarios. The shading indicates in which scenarios correlations between Earth system variables are significant, crosses indicate where they are significant in all three scenarios. Bottom: Headline indicators resulting from the systematic evaluation of the correlation matrix.*

From the evaluation of the common correlation matrix (Figure 5.3, Top), we identify four clusters in the LAF scenarios (Figure 5.3, Bottom and 5.4). The first indicator is ocean surface pH (O_phsur) and represents changes in temperature related and atmospheric carbon related variables as well as some radiative fluxes.

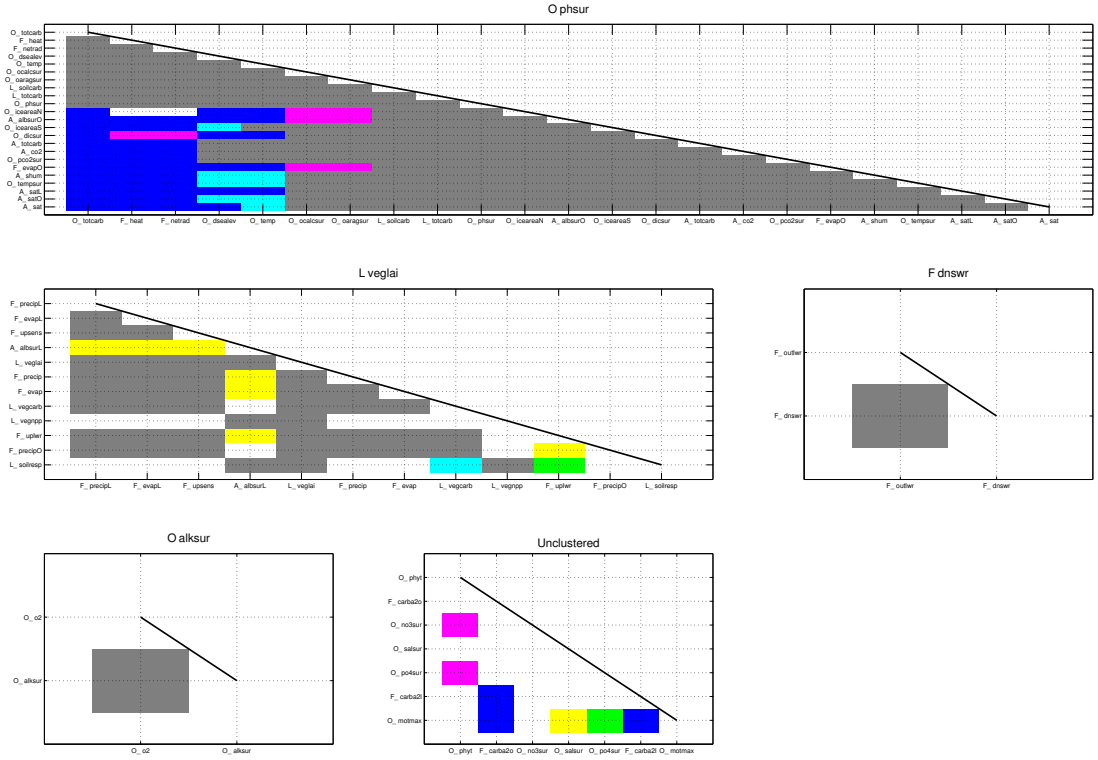

Fig. 5.4.: *Clusters identified in the common correlation matrix for the LAF, RCP4.5 and RCP8.5 scenarios. Color coding is the same as for figure 5.3*

Interestingly, the second cluster for the common LAF and climate change matrix is the same as for the common SRM and climate change matrix. The indicator is leaf area index (L_veglai) and it represents the land based Earth system variables concerning carbon, moisture and heat fluxes. The third indicator is net surface downward shortwave radiation (F_dnswr) and represents the correlation between two radiative fluxes. The last cluster represents the correlation between ocean oxygen (O_o2) and ocean surface alkalinity (O_alksur), i.e., biochemical processes. Seven variables remain unclustered: ocean maximum meridional overturning (O_motmax), ocean surface salinity (O_salsur), ocean phytoplankton (O_phyt), ocean surface phosphate and nitrate (O_ph4sur and O_no3sur, respectively) and the atmosphere to land and ocean carbon fluxes (F_carba2l and F_carba2o, respectively).

Dark blue shading in Figure 5.3 indicates correlations valid under the RCP4.5 scenario, but not under the two scenarios with high atmospheric carbon concentrations. However, the more interesting shading is purple, which indicates that these correlations are significant under the default RCP scenarios, but are changed by the implementation of LAF. These are correlations between sea surface omega aragonite and calcite (O_oaragsur and O_ocalcsur, respectively) and the northern hemisphere sea ice area (O_icareaN) and correspondingly sea surface albedo (A_albsurO), and between sea surface dissolved inorganic carbon (O_dicsur) and net top of atmosphere radiation (F_netrad) as well as ocean heat flux (F_heat). All of these variables are clustered under the first indicator ocean sur-

face pH (O_phsur). Other purple shaded correlations occur between ocean phytoplankton (O_phyt) and sea surface nitrate and phosphate (O_no3sur and O_po4sur, respectively). These three Earth system variables are clustered under one indicator in the correlation matrix evaluation of the common SRM matrix, but are all unclustered variables for the LAF scenario.
Green shading indicates correlations which are valid for the case of the LAF implementation and not in the case of the two reference climate change scenarios, i.e., under conditions with high atmospheric CO_2 concentrations and reduced anthropogenic land use changes. These correlations would need to be specially considered if LAF were implemented. Interestingly, these correlations are mainly associated with oceanic variables, e.g. ocean surface phosphate (O_po4sur) correlation to maximum meridional overturning (O_motmax), ocean oxygen (O_o2) and ocean surface alkalinity (O_alksur). In addition correlations between the latter two and sea surface dissolved inorganic carbon (O_dicsur) and maximum meridional overturning (O_motmax) is also significant under LAF implementation. In addition correlations between other biochemical variables towards some heat flux related variables become significant.
Yellow shading in Figure 5.3 indicates correlations valid for the RCP8.5 and the LAF scenarios, but not for the RCP4.5 scenario, i.e., under situations with high atmospheric carbon content and regardless of the implemented land use change scenario. This is the case for air to land carbon flux (F_carba2l) towards all temperature and carbon related variables, and also for maximum meridional overturning (O_motmax) towards many temperature related variables. Both Earth system variables are unclustered, when evaluating the correlation matrix. Furthermore, the correlations between land surface albedo (A_albsurL) and the terrestrial and correspondingly global moisture fluxes are only valid under high atmospheric CO_2 concentrations. Further more, several heat/radiation fluxes and their correlation towards other radiation fluxes or vegetation related variables are valid under high atmospheric carbon contents, regardless of the implemented land use changes.
Light blue shading indicates correlations valid if the same land use changes are implemented, regardless of the atmospheric carbon contents. This is true mainly for correlations between temperature related variables towards mean ocean temperature (O_temp), change in sea level (O_dsealev) and sea surface salinity (O_salsur).

5.4.3. Ocean Alkalinity Enhancement

For the OAE scenario the atmospheric CO_2 concentration is forced to follow the RCP4.5 scenario. Note that due to the reduced carbon content in the atmosphere also the net radiative forcing is close to the RCP4.5 scenarios, however this is at the expense of large biogeochemical changes in the ocean.
From the evaluation of the common correlation matrix (Figure 5.5, Top), we find seven clusters (Figure 5.5, Bottom and 5.6). The first indicator is atmospheric CO_2 and represents temperature and carbon related Earth system variables.

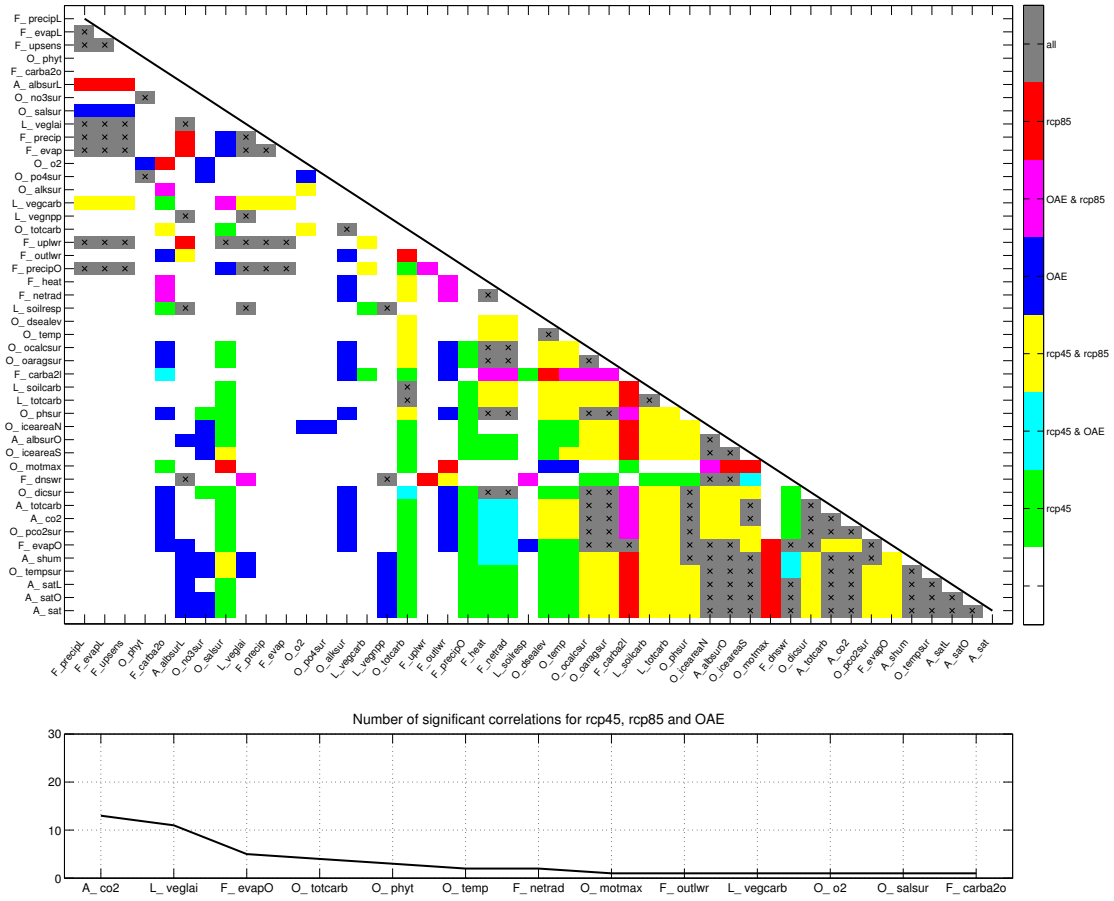

Fig. 5.5.: *Top: Common correlation Matrix for the OAE, RCP4.5 and RCP8.5 scenarios. The shading indicates in which scenarios correlations between Earth system variables are significant, crosses indicate where they are significant in all three scenarios. Bottom: Headline indicators resulting from the systematic evaluation of the correlation matrix.*

The second cluster is represented by the indicator leaf area index (L_veglai) and is almost the same cluster as found for the common climate change and SRM and LAF scenarios, with the only exemption of the Earth system variable vegetation carbon (L_vegcarb), that is unclustered in the OAE case.The indicator for the third cluster is evaporation over ocean (F_evapO), and it represents net surface downward shortwave radiation (F_dnswr), air to land carbon fluxes (F_carba2l), northern hemisphere sea ice area (O_iceareaN) and correspondingly sea surface albedo (A_albsurO). The fourth cluster represents changes in carbon reservoirs, with the indicator total ocean carbon (O_totcarb), and the fifth cluster has the indicator ocean phytoplankton and represents changes in the ocean biogeochemistry. The next cluster represents the ocean temperature and sea level changes, with the indicator mean ocean temperature (O_temp). It is noteworthy, that the in the OAE scenario an additional cluster is needed to represent all both physical and biogeochemical processes, adding to the total amount of indicators.

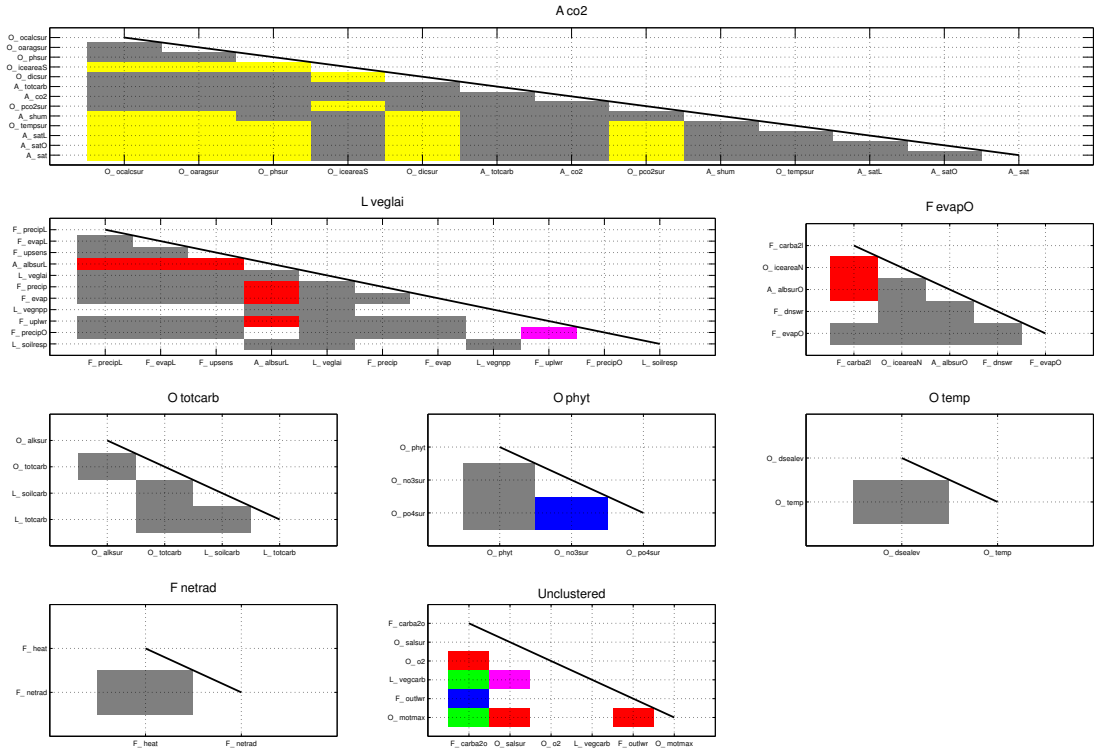

Fig. 5.6.: *Clusters identified in the common correlation matrix for the OAE, RCP4.5 and RCP8.5 scenarios. Color coding is the same as for figure 5.5*

Lastly, the seventh indicator is net top of atmosphere radiation (F_netrad), representing ocean heat fluxes (F_heat), the same indicator was found in the SRM case. There are six Earth system variables that remain unclustered, namely ocean maximum meridional overturning (O_motmax), ocean surface salinity (O_salsur), top of atmosphere outgoing longwave radiation (F_outlwr), ocean oxygen (O_o2), air to sea carbon flux (F_carba2o), and as mention before vegetation carbon (L_vegcarb).

Similar to the SRM correlation matrix, many correlations in the OAE correlation matrix are shaded yellow (Figure 5.5), indicating significant correlations for the two default RCP scenarios, but insignificant in the OAE scenario, indicating that the implementation of OAE changed the strength and also partly the sign of the correlations. This is especially the case for many ocean carbon variables, but also partly for land based ones (total land carbon (L_totcarb) and soil carbon (L_soilcarb)) towards temperature and atmospheric carbon related variables. In addition there is a lot of green shading, indicating that the correlations are only valid under the low emission scenario RCP4.5.

The dark blue shading indicates correlations which are valid for the case of the OAE implementation and not in the case of the two default RCP scenarios. Most of these correlations are directly linked with ocean surface alkalinity (O_alksur) and concern the relationships towards carbon fluxes and reservoirs or radiation fluxes, which are changed due to the implementation of OAE. The same is true for air to ocean carbon fluxes (F_carba2o) and the top of atmosphere outgoing longwave radiation (F_outlwr). In addition to that

there are correlations between temperature related Earth system variables and land net primary production (L_vegnpp), land surface albedo (A_albsurL) and ocean surface nitrate (O_no3sur), that are only significant in case of OAE implementation.
Light blue shading in Figure 5.5, indicates correlations valid in both the RCP4.5 and the OAE scenarios, i.e., under low atmospheric carbon concentrations and regardless of changes in ocean biogeochemistry. These correlations occur mostly between heat and radiation fluxes and atmospheric carbon related variables, namely between ocean heat flux (F_heat) and net top of atmosphere radiation (F_netrad) towards atmospheric CO_2 (A_co2), total atmospheric carbon (A_totcarb), sea surface partial CO_2 pressure (O_pco2sur) and in addition surface specific humidity (A_shum) and evaporation over ocean (F_evapO), two variables which are closely linked to temperature. Furthermore, net surface downward shortwave radiation (F_dnswr) shows significant correlations towards ocean surface temperature (O_tempsur), surface specific humidity (A_shum) and southern hemisphere sea ice area (O_iceareaS), as well as the air to land carbon flux (F_carba2l) to the air to ocean carbon flux (F_carba2o), and the total ocean carbon (O_totcarb) to the sea surface dissolved inorganic carbon (O_dicsur).
Purple shading on the other hand indicates, that the correlations are valid under the OAE and the RCP8.5 scenarios, but not for the RCP4.5 scenario, i.e., under condition in which the ocean takes up a lot of carbon. This is the case for correlations between the air to land carbon flux (F_carba2l) towards many carbon and some temperature related variables, such as mean ocean temperature (O_temp), ocean heat flux (F_heat) and net top of atmosphere radiation (F_netrad). The latter two variables in addition show purple shaded correlations towards air to ocean carbon fluxes (F_carba2o), and top of atmosphere outgoing longwave radiation (F_outlwr). Apart from that there are some sporadic correlations between e.g. radiation fluxes and land bases variables, carbon fluxes or ocean based variables.

5.5. Common indicators for the three CE schemes

Combining all three CE schemes into one correlation matrix allows us to separate effects within the three Earth system components, atmosphere, land and ocean. From the evaluation of the common correlation matrix of the SRM, LAF, and OAE scenarios (Figure 5.7, Top) we can identify eight clusters (Figure 5.7, Bottom and 5.8). The first cluster is very similar to the land sensitivity clusters from the previous analysis (except for the fact that net surface downward shortwave radiation is added) again with the indicator vegetation leaf area index (L_veglai). The fact that this cluster reappears in the common CE indicators is not surprising, since this cluster was found for all three common correlation matrices for the single CE methods. Remember, that this cluster represents land based Earth system variables concerning carbon, moisture and heat fluxes. The second indicator, ocean surface albedo (A_albsurO), represents atmospheric temperature related variables. Note that the Earth system variable mean ocean temperature (O_temp) is represented in a separate cluster together with sea level change (O_dsealev). The third indicator, ocean surface pH (O_phsur), represents all atmospheric carbon re-

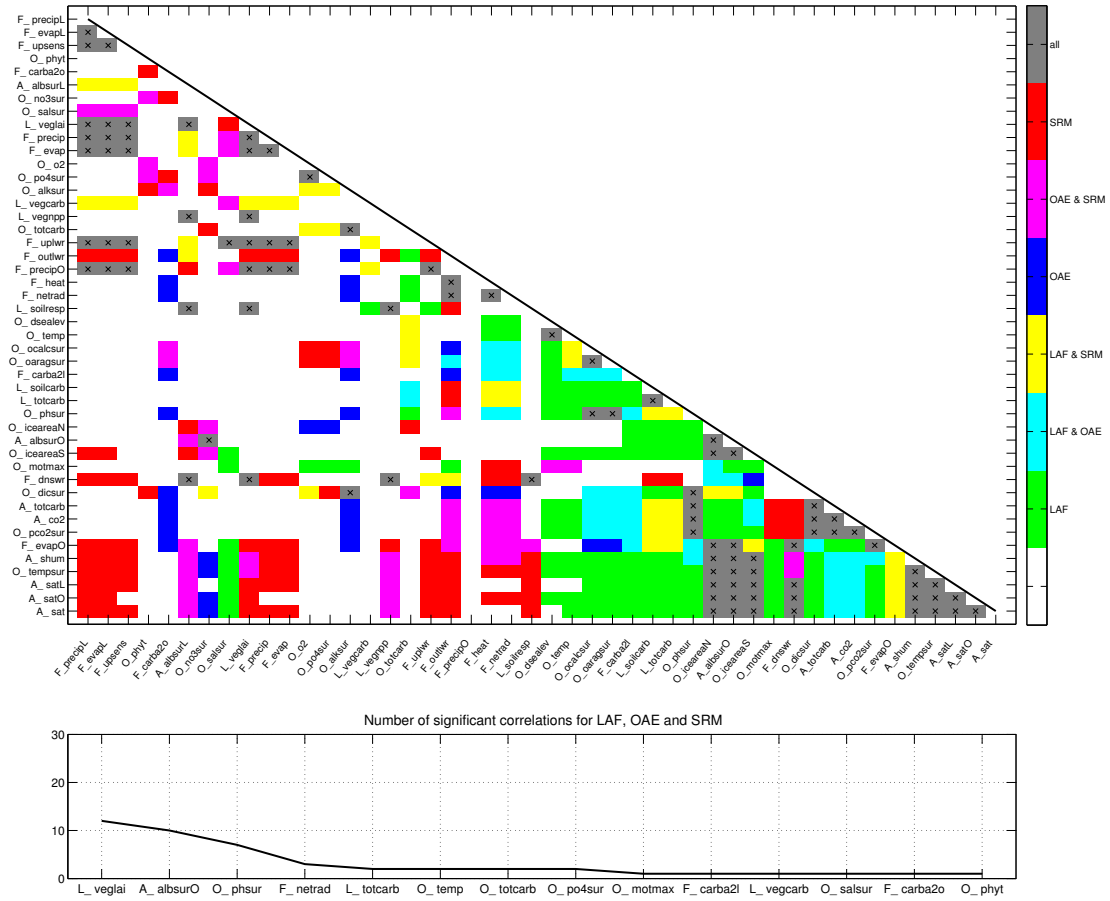

Fig. 5.7.: *Top: Common correlation Matrix for the LAF, OAE and SRM scenarios. The shading indicates in which scenarios correlations between Earth system variables are significant, crosses indicate where they are significant in all three scenarios. Bottom: Headline indicators resulting from the systematic evaluation of the correlation matrix.*

lated variables. In addition there is a land carbon cluster, with the indicator total land carbon (L_totcarb), and an ocean carbon cluster with the indicator total ocean carbon (O_totcarb). The fourth cluster represents the radiation fluxes, with the indicator net top of atmosphere radiation (F_netrad), and the last cluster represents ocean biogeochemistry with ocean surface phosphate (O_po4sur), which can be used as indicator interchangeably with ocean oxygen (O_o2). Six Earth system variables remain unclustered in the common CE correlation matrix: ocean maximum meridional overturning (O_motmax), ocean surface salinity (O_salsur), ocean phytoplankton (O_phyt), vegetation carbon (L_vegcarb), and atmosphere to land and ocean carbon fluxes (F_carba2l and F_carba2o, respectively).

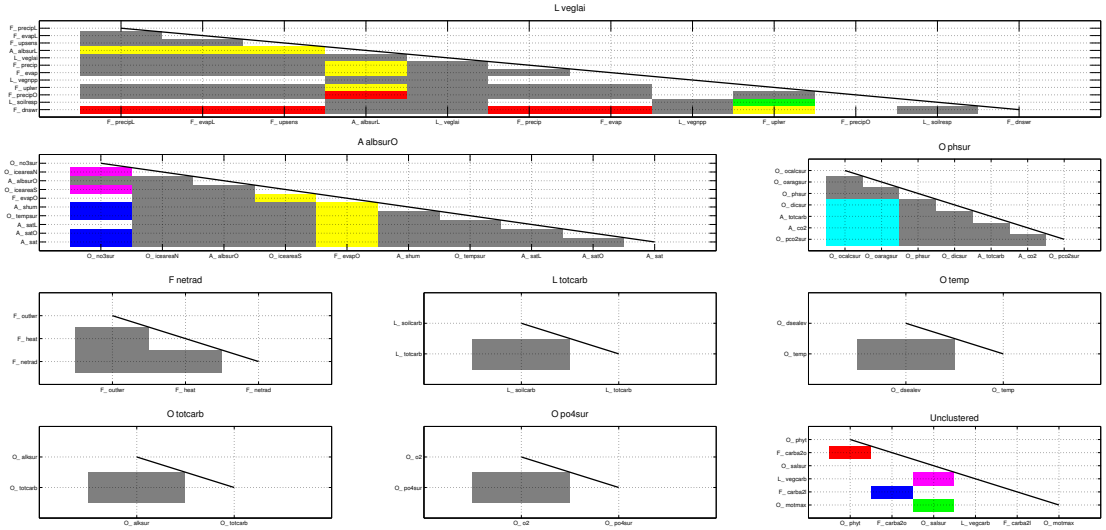

Fig. 5.8.: *Clusters identified in the common correlation matrix for the LAF, OAE and SRM scenarios. Color coding is the same as for figure 5.7*

5.6. Preliminary Evaluation of the CE methods

5.6.1. Based on selected indicators from the SCoMaE for two reference points

From each of the 14 indicators identified by the SCoMaE analysis of the common CE correlation matrix, we calculate deviations from a defined reference state. Initially we chose 2005–2010, which is meant to represent nowadays climate conditions and we define any deviation from this reference point as bad. Note that, this selection of reference point is a normative statement, which includes the value judgment, that we want to stay close to todays climate state. This most likely represents the position of people or countries, which are well adapted to todays climate and will not profit from climate change. However it is also possible to argue for other reference points, in case of different values and objectives.

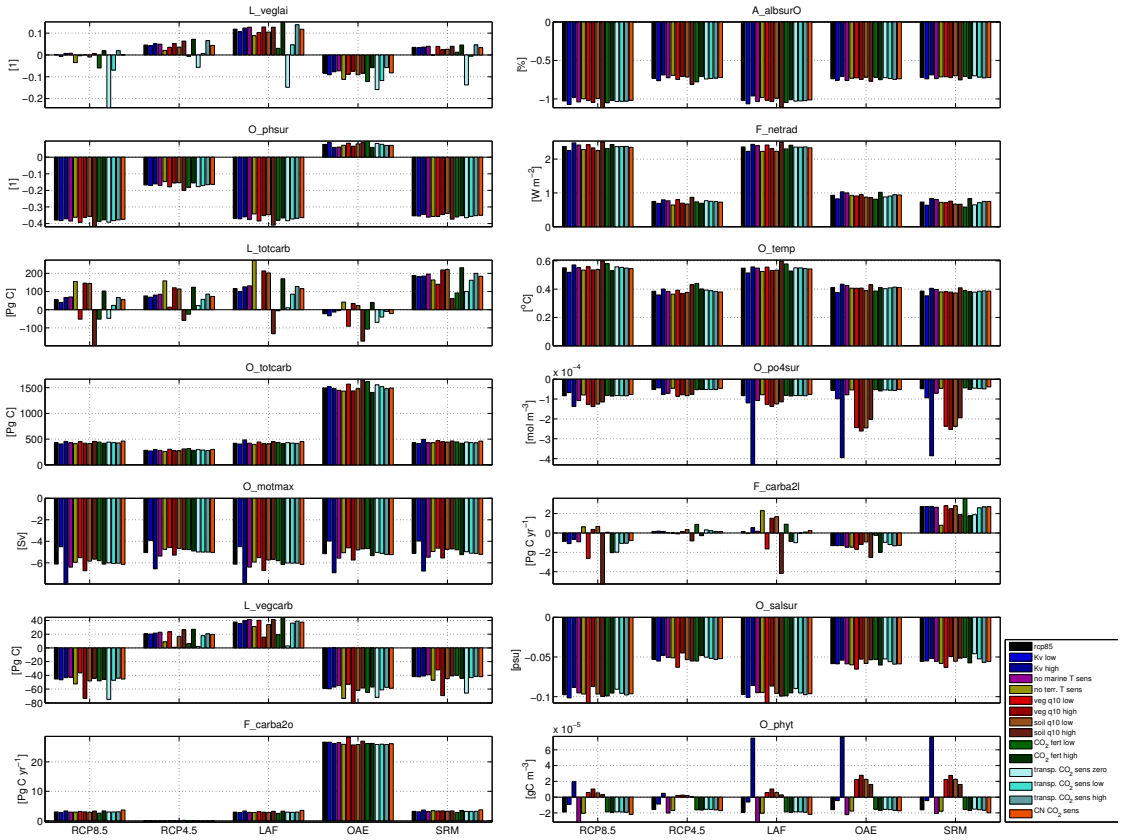

Fig. 5.9.: *Shown are deviations from the 2005–2010 reference state for the single parameter perturbation simulations for each of the three CE methods (LAF, OAE, SRM) and the two reference scenarios (RCP4.5, RCP8.5). Each panel shows the results for one of the selected indicators. Colour coding represents the single sensitivity simulations, see legend.*

Although the number of indicators is already reduced by the selection process it is still difficult to directly identify which scenario is 'better' compared to the others (Figure 5.9). In case of the control simulations and the first indicator leaf area index (L_veglai), which represents the land sensitivities in the model, we find that the RCP8.5 scenario is the 'best' future scenario, since it is closest to the references state. If it was however true, that under climate change there is no CO_2 sensitivity of transpiration (co2t0) as represented by many models, the RCP8.5 suddenly has the 'worst' outcome of the five scenarios. Due to a high variability in the different parameter simulations it is not possible to define the 'best' scenario for the indicator leaf area index (L_veglai). The same conclusion has to be drawn for the cluster represented by total land carbon (L_totcarb), and ocean surface phosphate (O_po4sur), as well as for the single indicators air to land carbon flux (F_carba2l), vegetation carbon (L_vegcarb), and ocean phytoplankton (O_phyt). For all these indicators, there is no robust pattern throughout the parameter perturbations, indicating that there is no robust answer to which scenario is the 'best'.

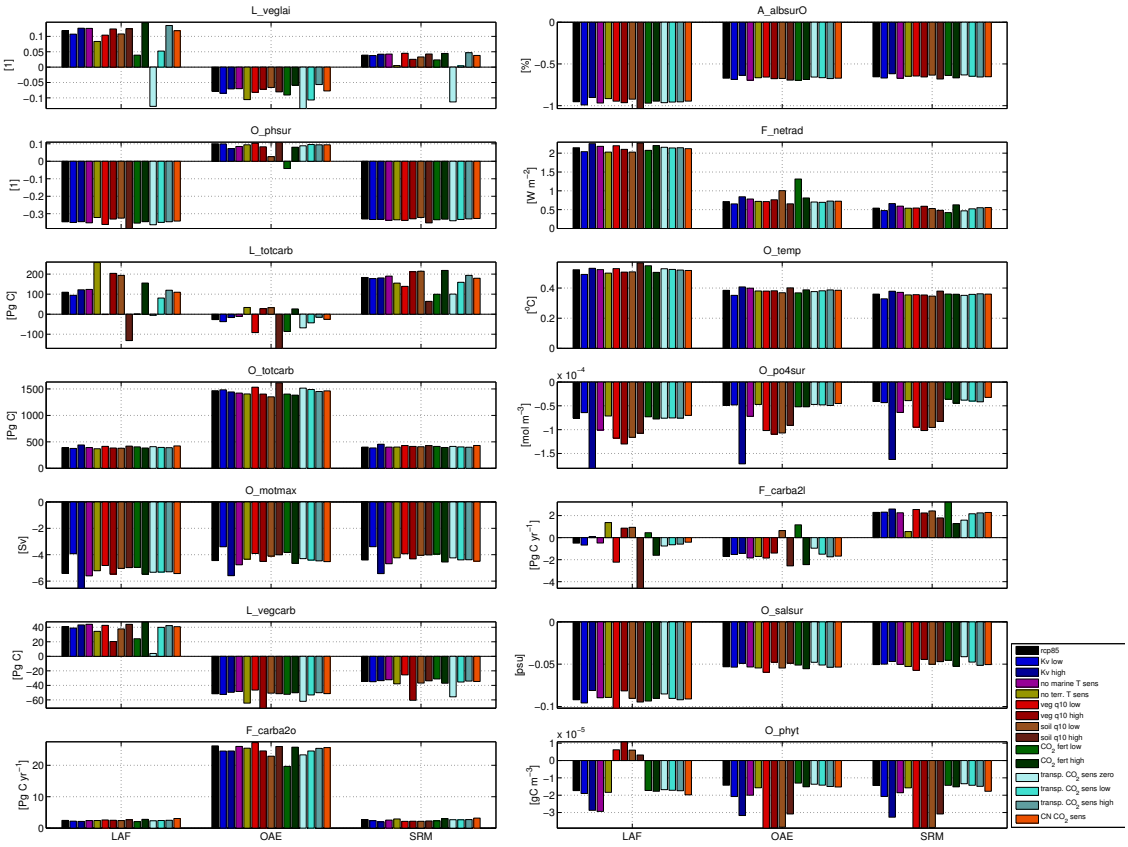

Fig. 5.10.: *Same as Figure 5.9, but with the reference climate state of the RCP4.5 scenario in 2100.*

This is true but for two exceptions, ocean surface phosphate (O_po4sur) and vegetation carbon (L_vegcarb), for which we can at least conclude, that the RCP4.5 scenario is closest to the reference state for all parameter perturbation simulations.

For the remaining indicators, the relative differences between the scenarios are more robust throughout the sensitivity simulations. For the second indicator, surface albedo over ocean (A_albsurO), representing atmospheric temperature related variables, the fourth indicator, net top of atmosphere radiation (F_netrad), representing radiation fluxes, the sixth indicator mean ocean temperature (O_temp) and the single indicator sea surface salinity (O_salsur), we find that the SRM, the OAE and the RCP4.5 scenario are all performing 'better' than the RCP8.5 and LAF scenario. However it is still difficult to say, which of the three performs better.

For the third indicator, ocean surface pH (O_phsur), representing all atmospheric carbon related variables, the OAE scenario performs 'best', compared to the other scenarios. For all the remaining indicators, namely ocean total carbon (O_totcarb), ocean overturning (O_motmax) and air to ocean carbon flux (F_carba2o), we find that the RCP4.5 scenario is closer to the 2005 reference state than any of the implemented CE schemes or the high emission scenario.

It is noteworthy, that for many land and ocean carbon based indicators the OAE scenario lies outside the range of changes as imposed by the RCP4.5 and RCP8.5 scenarios (Figure 5.9), i.e., the OAE scenario is not within the range of the two reference scenarios. The same is true for the LAF scenario concerning land carbon related indicators, and the SRM scenario concerning air to land carbon fluxes and the resulting land carbon. These indicators hint towards the Earth system components, which are altered to behave unnaturally due to the implementation of CE.
When we change the reference point to be the climate state of the RCP4.5 scenario (the target of all the CE methods) in 2100 as a reference state, this allows us to evaluate the different CE methods against each other, concerning their skill to reach the given target.
For the first indicator, leaf area index (L_veglai), OAE shows an opposite reaction compared to LAF and SRM, namely an decrease in leaf area index, compared to an increase in the other two scenarios. This can be explained by the CO_2 fertilisation effect that is still present in the SRM scenario, and the explicit afforestation scheme in addition to high CO_2 concentration for the LAF scenario. Nevertheless, across all parameter sensitivity studies the SRM scenario stays closest to the reference state, and is therefore the 'best' CE method. The same conclusion is also true for net top of atmosphere radiation (F_netrad).
For the indicator ocean surface pH (O_phsur) the OAE scenario is the 'best', but also shows the opposite sign of reaction compared to the other scenarios. For the indicator surface albedo over ocean (A_albsurO), mean ocean temperature (O_temp), ocean surface phosphate (O_po4sur), sea surface salinity (O_salsur) and for the indicator maximum meridional overturning (O_motmax), it depends on the parameter perturbation, if either the OAE or SRM scenario is 'better', in any case the LAF scenario shows the largest deviations from the reference state. For the indicators total ocean carbon (O_totcarb), vegetation carbon (L_vegcarb), and air to sea carbon flux (F_carba2o), the LAF and SRM scenarios are closest to the reference state, here the OAE scenario shows the highest deviations.
For the indicator ocean phytoplankton (O_phyt) all three CE scenarios show a strong reaction in the simulation with high vertical diffusivity (Kv+), and in addition for the OAE and SRM scenarios there is a large deviation in the simulations with changes in soil or vegetation q10 (sq10, and vq10, respectively). Similarly the variability in the sensitivity simulations is too high for the indicator air to land carbon flux (F_carba2l) and total land carbon (L_totcarb). For these indicators it is not possible to say which CE method is the 'best', since the parameter uncertainty is too high.

5.6.2. Based on two different metrics for the 2005–2010 reference point

Combining all the indicators found for the common correlation matrix of the LAF, OAE, and SRM scenarios into one aggregated metric, using the information on the number of correlated variables as weights, should simplify the assessment of which CE method performs 'best'. Note, that since the weights from the number of significant correlations are applied the indicators leaf area index (L_veglai), surface albedo over ocean areas (O_albsurO) and ocean surface pH (O_phsur), have the strongest influence on this metric, with weights of 0.37, 0.21, and 0.15, respectively.

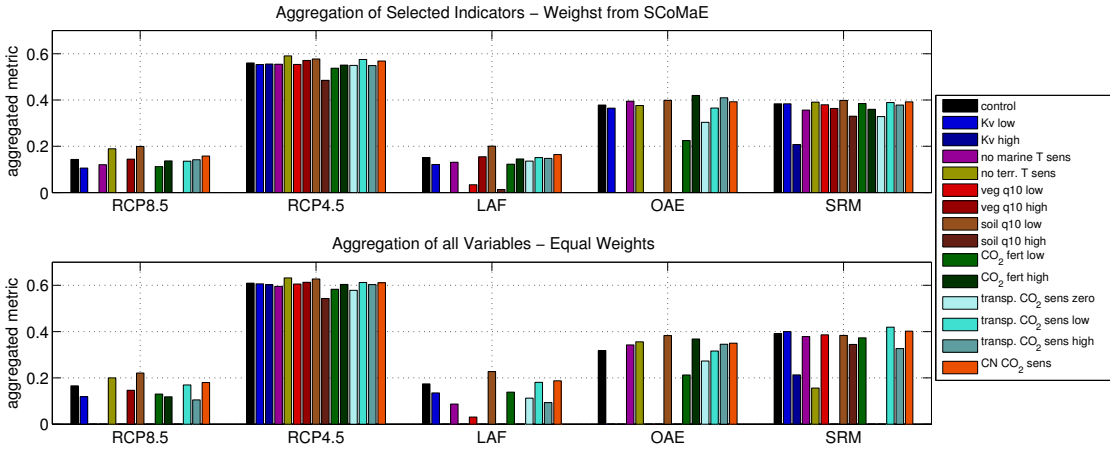

Fig. 5.11.: *Evaluation of the CE methods based on two metrics, values close to one indicates a good performance in staying close to the 2005–2010 reference climate state.*
Top: Metric constructed as generalised means of the identified Earth system indicators from section 5.5 and their weights depending on the number of correlated variables.
Bottom: Metric constructed from all 46 Earth system variables using equal weights.

It is obvious, that the RCP4.5 scenario overall performs 'best' in staying close to the 2005–2010 reference state, since for all simulations the metric is closest to one (Figure 5.11, Top). In contrast for four of the sensitivity simulations in the RCP8.5 scenario, as well as the OAE scenario, the metric drops to zero, indicating that the deviation from the 'desired' climate state is large. This is also the case for the high vertical diffusivity simulation (Kv high) and the simulation without terrestrial temperature sensitivity (no terr. T sens) in the LAF scenario, which generally shows no good performance based on this metric. In that sense the SRM scenario is 'better' than the other two, since no simulation actually drops to zero. Based on this metric, for many sensitivity simulations the SRM scenario performs 'better' than the LAF or the OAE scenario. This is true but for the exceptions of the simulations with no marine temperature sensitivity (no marine T sens), a high CO_2 fertilisation effect (CO_2 fert high) and a high sensitivity of transpiration to CO_2, in which OAE performs 'better'. Considering the metric, in which we include all 46 Earth system variables with equal weights, i.e., a metric considering more Earth system variables and hence including more information (Figure 5.11, Bottom), we arrive at the same overall conclusion, namely the RCP4.5 scenario shows the 'best' overall performance, and considering the three CE methods SRM shows the 'best' score for most of the simulations. Nevertheless, a more detailed analysis shows that the metric in all high emissions driven scenarios drops to zero at least for three sensitivity simulations. Note, that for all scenarios different simulations drop to zero. Again we find simulations (no terrestrial temperature sensitivity (no terr T sens), high CO_2 fertilisation effect (CO_2 fert high), and no or high transpiration sensitivity to CO_2 (transp. CO_2 sens zero and high, respectively)) for which the OAE scenario performs 'better' than the SRM scenario.
The comparison of the two differently derived metics for the single scenarios, reveals that

single simulations seem to be sensitive to the inclusion of further information in the case of the second metric. For example, in the LAF scenario the simulations with a high vegetation q10 value (veg q10 high) and a high CO_2 fertilisation effect (CO_2 fert high) drop to zero for the second metric. For the OAE scenario the simulation with low vertical diffusivity (Kv low) drops to zero for the second metric, the response of the other simulations seems to be rather robust for the two metrics. In case of the SRM scenario the simulations with high vegetation q10 (veg q10 high), a high CO_2 fertilisation effect (CO_2 fert high) and zero sensitivity of transpiration to CO_2 (transp. CO_2 sens zero) drop to zero in case of the second metric. In addition, the simulation with no terrestrial temperature sensitivity (no terr T sens) shows a considerable drop for the second metric in the SRM scenario. All these simulations have a high vegetation productivity in common.

5.7. Discussion

From the comparison of correlation matrices of single CE scenarios to the two reference RCP scenarios, we find two types of correlations which would have to be considered additionally in an comprehensive assessment, if the respective CE method were to be implemented. First, correlations valid for the two climate change scenarios, but not for the implemented CE scenario, indicating that this prevailing correlation is no longer valid in an manipulated climate state. And second, correlations valid only in the climate engineering scenario, indication that in an manipulated climate state, this correlation becomes significant.

As expected, for the SRM scenario correlations between carbon reservoirs and temperature related model variables, become insignificant compared to the two reference RCP scenarios. This arises from the decoupling of the relationship between temperature and CO_2 in case of SRM implementation [Irvine et al., 2012].

Many correlations between temperature related variables and land associated carbon, moisture and heat fluxes become only significant under the manipulated climate state, if SRM is implemented. This indicates that in case of SRM implementation the relationship between temperature and land processes become predominant, compared to the un-manipulated climate state, in which land processes might be predominantly influenced by atmospheric carbon content and land use changes.

For the LAF scenario, we find that correlations between ocean surface biogeochemistry and sea ice and correspondingly ocean albedo become insignificant compared to the two RCP scenarios. This can be explained by the manipulation of the vegetation and the resulting higher rate of soil runoff, which alters mainly the dilution rate of the surface ocean, and therefore the biogeochemistry. In an un-engineered climate the surface water dilution is often correlated with the fresh water input from melting ice, this is no longer the case if the soil runoff becomes predominant. The same argument explains, why mean ocean phytoplankton is no longer correlated to surface properties of nitrate and phosphate. The higher rate of fresh water input disconnects the relationship to the global phytoplankton growth.

Apart from this, we found that mainly correlations associated with oceanic variables are

only significant if the climate state is manipulated in the LAF scenario. This is again connected to the increase in surface runoff and the associated freshening of the surface ocean. Ocean surface phosphate and alkalinity are now correlated with ocean oxygen and maximum meridional overturning, which are all influenced by the enhanced stratification of the surface ocean. Under un-manipulated climate change these processes are predominantly influenced by biological processes in the ocean, or in case of the maximum meridional overturning, more by changes in sea ice.
For the OAE scenario, correlations become invalid, for many ocean and land based carbon reservoir variables towards temperature and atmospheric carbon related variables. The implementation of OAE disrupts the relation between these carbon reservoirs. Under un-manipulated conditions atmosphere, ocean and land carbon are connected to each other, but if we force the ocean to take up an disproportional amount of the atmospheric carbon, this changes the relationship between oceanic to land carbon reservoirs.
Correlations valid in the manipulated climate state of the OAE scenario, are mainly connected directly to the ocean surface alkalinity or air to sea carbon flux, and mostly concern relationships towards other carbon fluxes and the atmospheric reservoirs or radiation fluxes. This hints to the predominance of the oceanic carbon uptake though the OAE scenario, relating these variables, which would otherwise be influence by different factors, such as ocean biology.
The systematic evaluation of the common correlation matrix from the three climate engineering scenarios, identified eight scientifically meaningful clusters of Earth system variables, representing atmospheric and oceanic temperature depended variables, land process variables, ocean biogeochemical variables, radiation variables, as well as the single carbon reservoirs, each category separated in a different cluster. The identified clusters are all represented by one indicator. It is remarkable that the evaluation of these three CE methods, each targeting a different Earth system component, reveals such a meaningful separation between the different Earth system variables.
For a comprehensive evaluation of the three CE methods against the two RCP scenarios, the previously identified indicators are applied. We chose two reference points in time, namely 2005–2010 representing nowadays conditions and the 2100 climate state of the RCP4.5 scenario, which was defined as the climate state target of the CE scenarios, against which the CE scenarios are evaluated. If the nowadays climate state is chosen as a desirable target, the evaluation reveals that for most indicators the RCP4.5 scenario is found to be the 'best' scenario. This is partly explained by the way the three CE methods were implemented. Since the RCP4.5 scenario was used as a target for the CE implementation, it is unlikely that the CE scenarios will perform 'better' than the target. This is at least true for the Earth system component that was used as a target. Some variables, however, lie outside the range of both reference climate change scenarios, or show opposite signs, indicating that these Earth system variables were manipulated on the expenses of meeting a specific target, e.g. in case of the OAE scenario, total ocean carbon lies outside the range of the two reference scenarios, since the target was atmospheric carbon. Note, that for most of the indicators the (parameter) uncertainty was too high to make a robust statement about the 'best' CE scenario.
For evaluating which CE method was most effective in reaching the RCP4.5 scenario,

which was defined as the target for the different CE methods, we chose the 2100 state of the RCP4.5 scenario as a second reference point. Identifying which CE method performs best across all identified indicators is impossible. The SRM scenario is often closest to the RCP4.5 reference state, however for five (three) out of 10 indicators it depends on the sensitivity simulation whether SRM or OAE (LAF) performs 'best' in reaching the target. For temperature related indicators, the SRM and OAE scenarios are closer to the reference level, than the LAF, indicating a higher skill in reducing temperatures, which agrees with the specific targets of the single CE methods, and the effectiveness of the scenarios. Remember the limited potential of the implemented LAF scenario in reducing atmospheric CO_2 concentrations. For the ocean carbon reservoir, land and ocean carbon fluxes, the SRM and LAF scenario show the 'best' performance in staying close to the RCP4.5 scenario. For these variables the OAE scenario shows very strong deviations from the reference state, due to the manipulation of the air to sea carbon fluxes. In agreement with the target of the CE method, the OAE scenario shows the best performance for the indicator ocean surface pH. The parameter uncertainty concerning the indicators total land carbon, ocean surface phosphate and mean ocean phytoplankton is too large to find robust results on the 'best' CE scenario.

If we construct metrics to further simplify the comparison between the three CE and the two climate change scenarios, we find that the RCP4.5 scenario performs 'best' in staying close to the 2005–2010 reference climate state. For the three CE scenarios we can find a clear ranking, namely the SRM scenario performs 'best' considered most of the sensitivity simulations, for few however the OAE scenario performs 'best' and the LAF scenario, which is only slightly 'better' than the RCP8.5 scenario, shows the least skill in staying close to todays climate state. This result is robust for both constructed metrics, encouraging the results from the SCoMaE analysis.

The ranking agrees with the expectations based on the way the CE methods are implemented in the model. The fact that the LAF scenario performs 'badly' and stays so close to the RCP8.5 scenario can be explained by the comparably small effect of the RCP4.5 afforestation scheme on atmospheric CO_2 concentrations (reduction by 30ppm). This is in agreement with findings of previous analysis [e.g. House et al., 2002; Arora and Montenegro, 2011] indicating that a naturally regrown, unmanaged forest only has a limited CDR potential.

The OAE scenario is forced to match RCP4.5 atmospheric CO_2 levels, therefore many atmospheric CO_2 related climate variables, i.e., terrestrial productivity, temperatures and sea ice, should be close to the RCP4.5 climate state. However, this is at the expense of air to ocean carbon fluxes and ocean biogeochemical Earth system variables, which are forced to cope with unnaturally high alkalinity concentrations.

The SRM scenario matches the TOA radiative forcing of the RCP4.5 scenario, an thereby targets all temperature related Earth system variables. In addition, Keller et al. [2014] found that a similar SRM scenario implemented in the same model, showed a considerable potential in mitigating atmospheric CO_2 concentrations. This was mainly caused by the cooling of the surface ocean and the soil temperatures, causing an increase in the carbon uptake potential of both the terrestrial and oceanic reservoirs. In case of our default model simulation the implemented SRM scenario reduces the atmospheric CO_2 concen-

tration by about 70 ppm relative to the RCP8.5 scenario. Note, that this about three times higher than the reduction in atmospheric carbon content in the LAF scenario, which is an explicit CDR scheme.
The analyses presented in this study are based on simplified implementations of Climate Engineering schemes in an intermediate complex Earth system model. A refined implementation of plausible CE scenarios would enable a more detailed analysis of the changes in correlation patterns. This could be done in the context of a more complex Earth system model, with a better representation of e.g. atmospheric processes. Such an analysis would certainly add value to the CE assessment. In addition the results of this study are biased by the selection of the parameter perturbations. We concentrated on temperature and CO_2 sensitivities of terrestrial and marine primary production. Adding further parameter perturbations of processes that are relevant in Climate Engineering scenarios, would improve the robustness of the analysis.
By evaluating the CE methods based on changes at one point in time (2005 and 2100), we assume that this is a relevant time frame and discount any changes in-between as well as for future time periods. For an evaluation of climate engineering it is important to separately discuss the time frame we are interested in, since we might be delaying possible risks to future periods and generations. Furthermore, the chosen reference points include a value judgement, which is fair if made transparent, but it needs to be kept in mind that other societies/countries might have different targets of desirable climate states, this includes the view, that a little bit of more climate change would not be too bad, i.e., nowadays is not the optimum, as well as the view, that we need to get back to conditions well before we started the manipulation of the Earth climate all together, which would imply a target closer to a preindustrial climate state.
The evaluation presented here is based on indicators selected for a natural-science based assessment. Considering the three goals from Radermacher [2005], statistical measurability, scientific consistency and political relevance, the indicator selection is unbalanced towards the scientific consistency. Nevertheless, it presents the first systematic evaluation of changes in correlation patters between Earth system variables as introduced by climate engineering and enables scientists to inform the necessary future debate. Note that the SCoMaE analysis allows to prescribe pre-selected indicators, which might be chosen due to their political relevance.

5.8. Summary and Conclusion

The aim of this study was to advance the assessment of CE, by reducing the amount of complexity by indicator selection and metric construction, in order to enable a natural science based, comprehensive comparison of three exemplary CE scenarios. This is the first study to systematically identify changes in correlation patterns introduced by three exemplary CE scenarios in comparison to two climate change scenarios. In line with the findings from Klepper and Rickels [e.g. 2014]; Irvine et al. [e.g. 2012], our analyse show, that the implementation of SRM would change prevailing relationships in the Earth system, concerning temperature and CO_2. Based on our analysis, we can conclude that this

effect is not limited to radiation management schemes. We find that adding large amounts of alkalinity would change prevailing correlations between biogeochemical and physical ocean properties. In the same way an increase in soil runoff from afforestation would change correlations between ocean surface nutrient concentrations and evaporation and sea ice. This information is important to be considered in the selection of appropriate indicators for a comprehensive assessment of stand alone climate engineering schemes.
To enable a comprehensive, comparative assessment of all three CE scenarios, we systematically evaluated the common correlation matrix of the three scenarios. We thereby could identify eight scientifically meaningful clusters, in addition to six single indicators, which are needed for a fully comprehensive assessment.
An evaluation of the CE scenarios based on these 14 indicators was inconclusive. It depends on the selected indicator as well as the sensitivity simulation, which CE scenario performs 'best'. This is true for both chosen reference points.
If the indicators are further aggregated into a metric in order to reduce the complexity, we find that the RCP4.5 scenario is the 'best' scenario for the target of staying close to todays climate state. With this simplification also the three exemplary CE scenarios can be ranked according to their ability to force the Earth system as close as possible to today's climate, despite continued high CO_2 emissions. We find that the SRM scenario performs 'best', followed by the OAE scenario and lastly the LAF scenario, which is close to the RCP8.5 ranking.
It is important to keep in mind that after this first assessment step, side-effects of the different CE methods require a more detailed assessment, particularly, an extensive risk analysis on regional scales. Also, it is important to note, that at present state of knowledge the model outputs contain a considerable degree of uncertainty and our results are influenced by many assumptions, e.g., the chosen model, the chosen parameter perturbations, the specific CE implementation, and the choice of reference point.

Acknowledgements The authors thank Ulrike Loeptien for helpful comments and discussion, as well as the participants of the Metrics Workshop of the SPP 1689 in March 2015, Hamburg,and in April 2016 in Kiel, for their thoughts on metrics and indicators.
The data used to generate the figures will be made available at http://thredds.geomar.de.
This work was funded by the German DFG in the context of the Priority Program: Climate Engineering: Risks, Challenges, Opportunities? (SPP 1689). The authors declare that they have no competing financial interests.
N.M., D.P.K., W.R. M.Q. and A.O. conceived the experiment. N.M. and D.K. implemented and performed the simulations. N.M. and W.R. analysed the data, and wrote the manuscript with contributions from D.P.K. and A.O..

6. Conclusion and Outlook

6.1. Summary and Conclusion

Climate Engineering as an option to prevent dangerous climate change has reached the political debate [UNFCCC, 2015]. For a well informed decision on CE research and potential future deployment, work towards a comprehensive, comparative assessment is needed. The selection of well suited indicators, the quantification of model uncertainties, as well as the identification of policy-relevant metrics are some of the major challenges for reaching such a Climate Engineering assessment.

In this thesis, we advanced the understanding of Arctic Ocean albedo modification (AOAM), a proposed local scale CE method, by adding an oceanic perspective to the previous assessment (chapter 2). We investigated consequences for ocean circulation, water masses and heat transport and found a sub-surface warming signal in the Arctic Ocean, which could potentially act to destabilise marine gas hydrates. Considering longer time scales, emission reduction is more effective in staying close to today's climate state when compared to a high emissions AOAM scenario. Our study stresses the necessity for a multidisciplinary assessment in the Climate Engineering research, since a disregard of Earth System components in an comprehensive assessment yields the risk of an biased evaluation of CE methods.
Studies on single methods, as presented in chapter 2, are important to advance the understanding of proposed methods and need to be carried out for a comprehensive CE assessment of single methods. However, the study also points to the fact that often CE research is too limited to the corresponding discipline, e.g., radiation management research is mostly carried out by atmospheric scientists, terrestrial CDR and marine CDR mostly by terrestrial and oceanic scientists, respectively.

The parameter sensitivity analysis in chapter 3, assessed the implications for climate change from uncertainty in the response of transpiration to atmospheric CO_2 concentrations. While terrestrial precipitation is a societally highly relevant climate variable, there is little consensus among climate models about its projected 21^{st} century changes. We found that varying the strength of the CO_2-sensitivity of transpiration caused simulated terrestrial precipitation to range from a decrease of 10 % to an increase of 27 % by the end of the century, compared to today's simulated precipitation. The applied parameter variations enable the UVic ESCM to cover the full range of CMIP5 models' precipitation changes over land. The considerable climate impacts from the CO_2-sensitivity of the plants' leaf conductance of water vapour in our model indicates, that the future development of the simulated atmosphere-to-land carbon fluxes and the terrestrial part of the

hydrological cycle are uncertain, even within the context of a single model, as long as the CO_2-sensitivity of stomatal conductance cannot be better constrained by observations.
The perturbed parameter ensemble applied in the context of a comparative CE assessment (based on chapter 3 and used in chapter 4 and 5), was an important first step to quantify uncertainties in an intermediate complex Earth system model.

The method, systematic correlation matrix evaluation (SCoMaE) (chapter 4), enables natural scientists to identify correlations in the simulated Earth system, which are altered due to a given forcing. By applying this method to a intermediate-high (RCP4.5) and high (RCP8.5) climate change scenario (chapter 4) we learn that these scenarios alter correlations relative to the historical time period. The selection of a comprehensive indicator set for future climate change hence needs to be a dynamic process.
The methodology introduced in chapter 4 allows us to systematically investigate changes in correlation patterns between Earth system variables. This information can be used to identify sets of indicators, which are independent and do not provide redundant information, for use in a natural science based assessment.

The application of this method to three climate engineering and two climate change scenarios (chapter 5), enables us to identify which correlations are changed under Climate Engineering (as implemented in the model) with respect to climate change, and which sets of indicators are needed for a comprehensive, comparative assessment. A preliminary evaluation of the three scenarios based on these indicators remains inconclusive du to the too high (parameter) uncertainties. It depends on the regarded indicator as well as the sensitivity simulation, for evaluating which scenario performs 'best' in staying close to the 2005–2010 reference climate state. If the indicators are further aggregated into a metric in order to reduce the complexity, a ranking of the different scenarios becomes evident. Given all assumptions, we find that overall the RCP4.5 scenario performs 'best' in staying close to the reference climate state. Solar Radiation Management is identified as the 'best' CE scenario, followed by Ocean Alkalinity Enhancement and Large-scale Afforestation. The latter performs comparable to the RCP8.5 scenario.
This study is an important first step towards a more systematic assessment of CE methods, however side-effects of the different CE methods will require a more detailed assessment, particularly, an extensive risk analysis on regional scales is necessary for a thorough evaluation.

6.2. Outlook

The field of research on climate engineering is young compared to that of climate change research. In order to enable a well informed decision under uncertainty about a possible future deployment of Climate Engineering many unresolved questions still need to be addressed.

More inter- (and also trans-) disciplinary cooperations would help to identify processes

that might become more relevant in a Climate Engineering scenario, and thereby inform the research community about further relevant indicators. Only the inclusion of more natural science disciplines will enable the research community to deal with the challenge of a comprehensive comparison of different CE methods, as well as the challenge of investigating combinations of CE methods.

Furthermore, an improved, more systematic uncertainty quantification is needed to inform the decision making process. For an improved uncertainty quantification further parameter sensitivity simulations should be included. The application of latin hypercube sampling would allow for analysis of parametric uncertainty within a multi-dimensional parameter space [e.g. Fyke et al., 2014]. Bayesian calibration of simple climate models with observations to estimate parametric and predictive uncertainties [e.g. Ricciuto et al., 2008], would enable discussion about changes in probability density functions introduced by CE methods and thereby inform about impacts on climate extremes. These techniques are all well developed for climate change assessment, and should now be applied for climate engineering assessment.

For the identification of policy-relevant indicators and the construction of a decision-informing metrics, including information on the value system of stakeholders is unavoidable. Therefore, a decision-making loop [Argyris, 1976; Ylhäisi et al., 2015] could be entered, which would promote an iterative learning process through the exchange between scientific experts and stakeholders. This could start with a refinement of possible future CE implementation scenarios, allowing for a more focused discussion on the specific CE scenario. Thereafter, an exchange between scientific advisors and stakeholders would point to the societally relevant indicators, e.g., amount of precipitation, or cleanness of the local lake, what ever is important to the stakeholder. For these indicators a quantification of uncertainties is desirable to inform the stakeholders about the robustness of the presented results. Finally, based on the underlying value system of the considered stakeholders, decision-informative metrics could be constructed and used for an comprehensive, comparative assessment of different CE proposals.

A. Supporting Information for 'Assessing Climate Impacts and Risks of Ocean Albedo Modification in the Arctic'

A.1. Tracer Analysis

A virtual dye tracer was implemented in the whole Arctic basin north of 70°N over all depth levels, where it was set to the value 1, at the beginning of the experiment in 2020. To calculate the mean temperature of the water masses that enter the Arctic Ocean, defined as the ocean area north of 70°N, we started by tracking the dilution of the dye tracer. In order to being able to use this information we subtracted 1 from the tracer field and take the absolute value. This enables us to investigate where water masses entered the Arctic Ocean. The mean temperature of the water masses entering the Arctic Ocean, was then calculated as a weighted mean of all temperatures in the Arctic Ocean marked by the tracer with respect to the grid box volume and the dye tracer concentration.

$$T_{mean,entering}(x,y,z,t) = mean_{x,y,z}[T(x,y,z,t) * t_{inv}(x,y,z,t) * V(x,y,z)]/ \quad \text{(A.1)}$$

$$mean_{x,y,z}[t(x,y,z,t) * V(x,y,z)] \quad \text{(A.2)}$$

T is the ocean temperature, t_{inv} is the inverted tracer concentration with values in $[0,1]$, and V is the volume of the grid box. Figure A.5, shows the mean temperature of entering water masses in the Arctic Ocean over time. Note, that the deep convection events in the default RCP4.5 and RCP8.5 simulations are also detectable in this time series, since these events act to cool the entering water masses.
For the calculation of the vertical temperature profiles as shown in Figure 2.5b, we did not integrate over z.

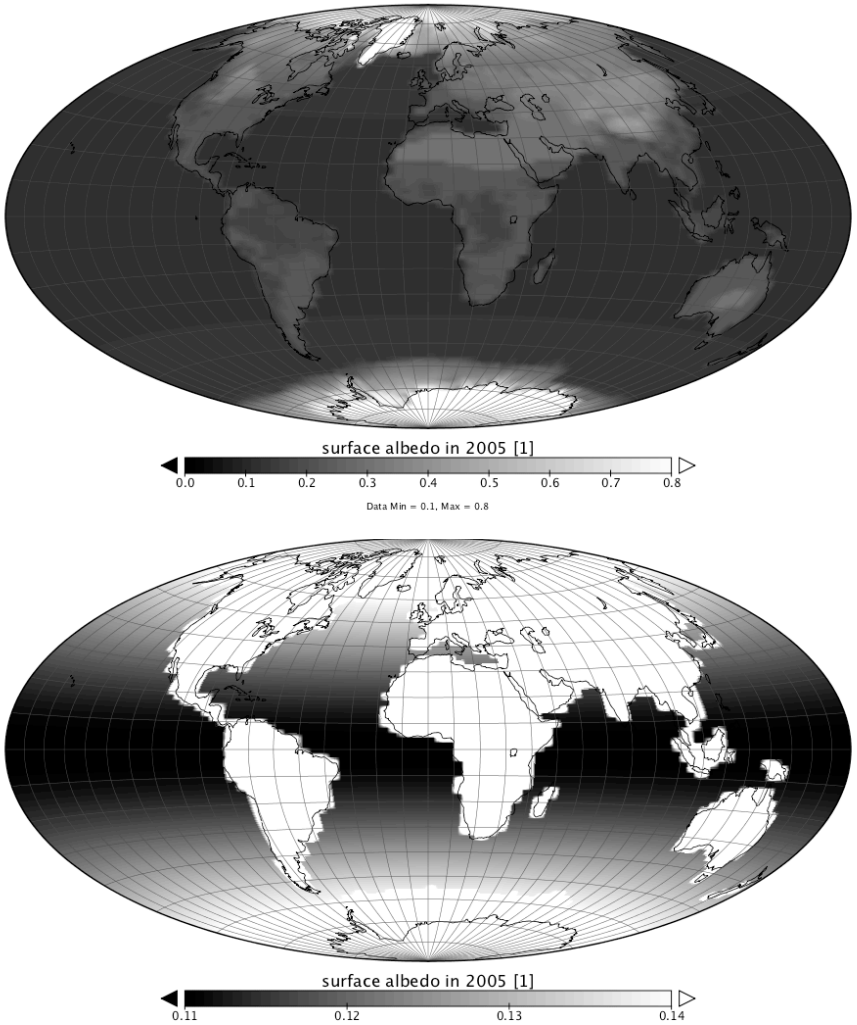

Fig. A.1.: *Regional distribution of the surface albedo in UVic ESCM in 2005. top: For a global perspective with colour axis from 0 to 0.8; bottom: For an oceanic perspective with colour axis from 0.11 to 0.14.*

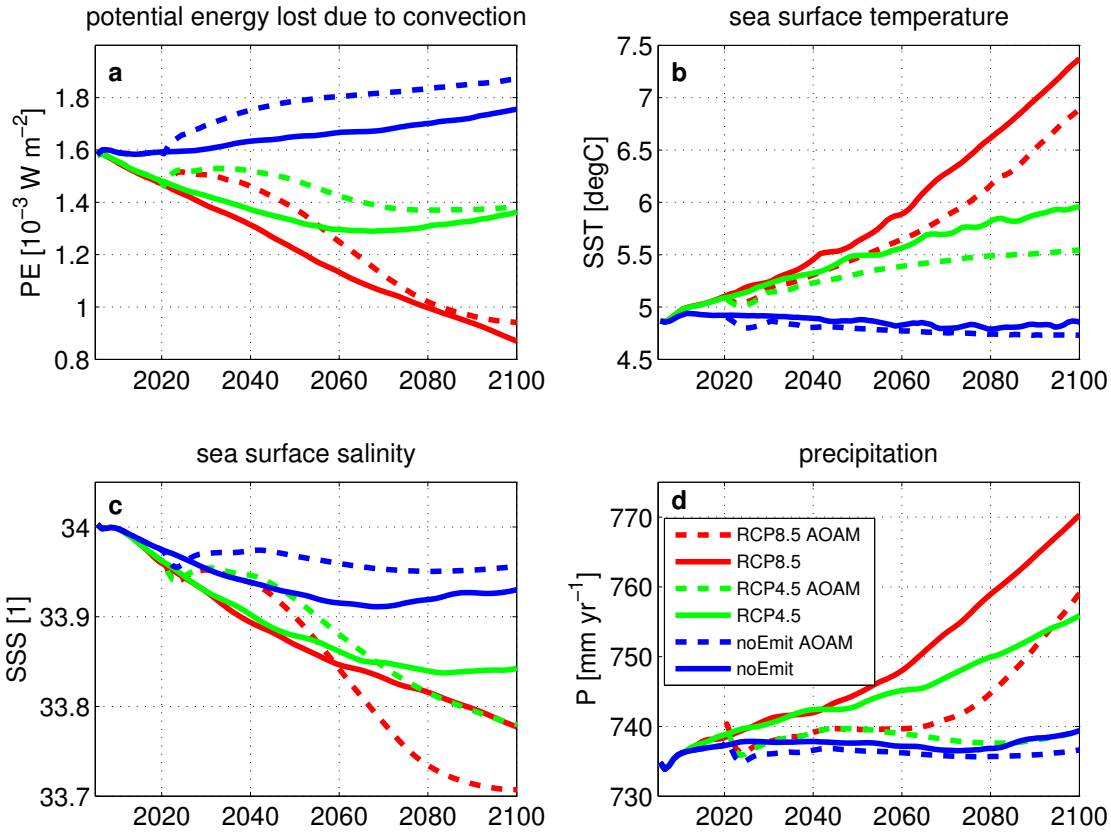

Fig. A.2.: *Annual average properties of the Atlantic ocean surface between 50 to 70° N. a) Potential energy lost to convection; b) sea surface temperature; c) sea surface salinity; and d) precipitation.*

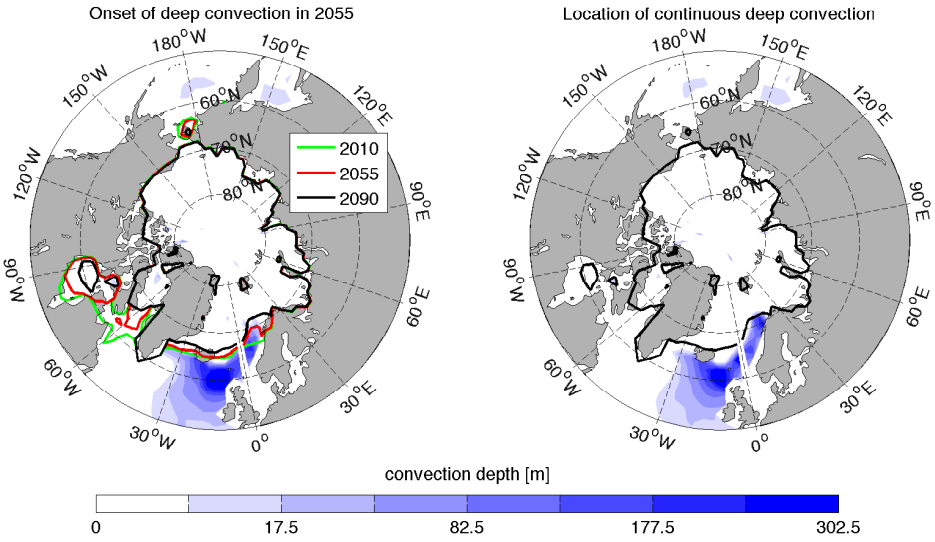

Fig. A.3.: *left: Location of deep convection areas in 2055, when deep conception is starting to emerge north of 65° N in the RCP8.5 experiment, as an exemplary temporal snap shots. Shown are annual mean sea ice edges for 2010 (green), 2055 (red) and 2090 (black), to show the ice edge location before and with fully developed deep convection.*
right: The location of the newly formed continuous deep convection sites in the Nordic seas in the RCP8.5 simulation averaged over 2090-2100. Shading indicates the average number of convected levels and the black contour is the mean ice edge.

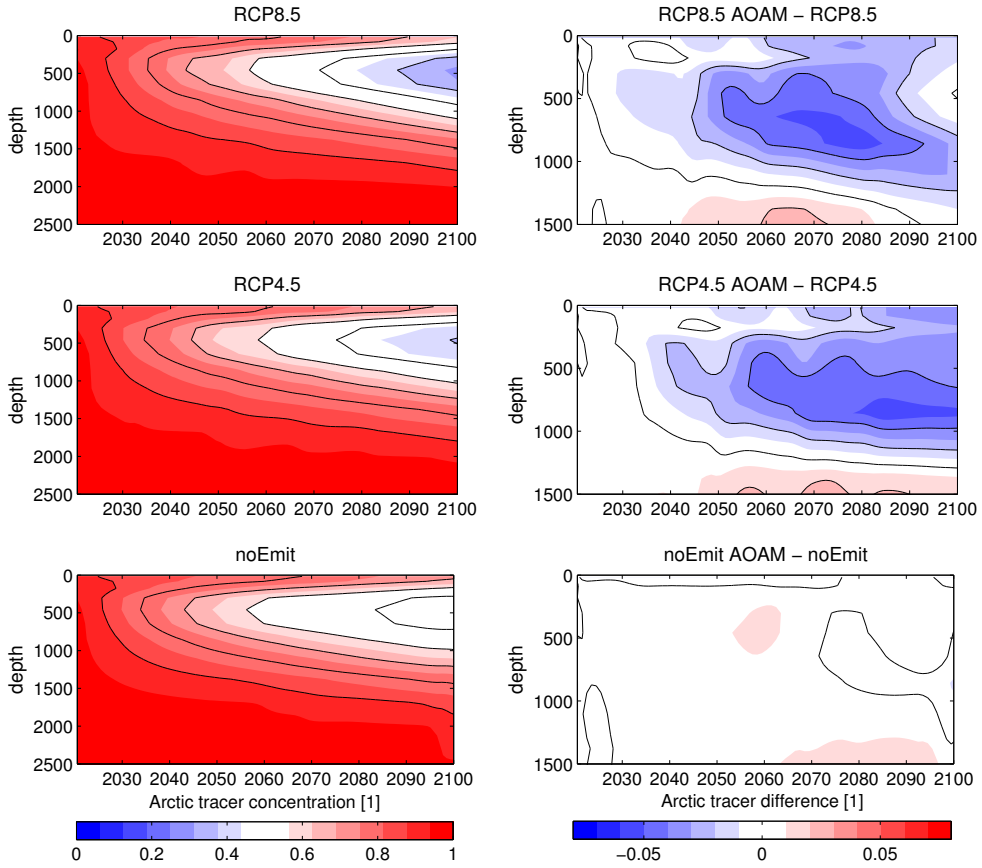

Fig. A.4.: *left: Hovmöller diagrams of the Arctic tracer for the three default scenarios; right: Hovmöller diagrams of the impact of the AOAM implementation on the mean Arctic vertical tracer concentration.*

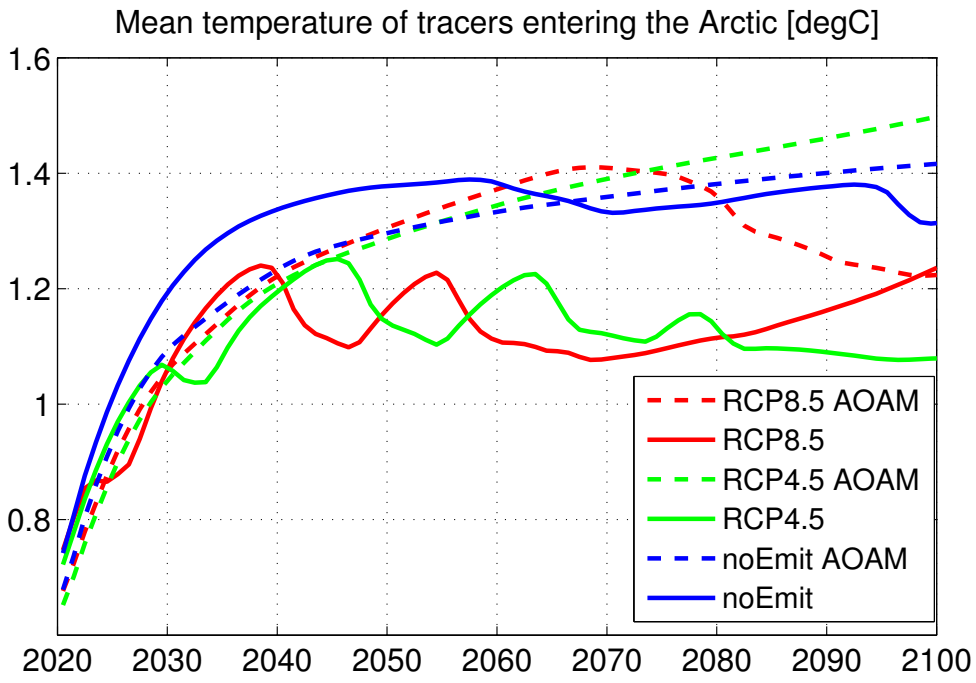

Fig. A.5.: *Time series of mean temperature of traced water masses entering the Arctic Ocean, calculated as described in Appendix A. Note, that this display includes both, changes in the dye tracer volume as well as changes in the temperature of the traced water masses.*

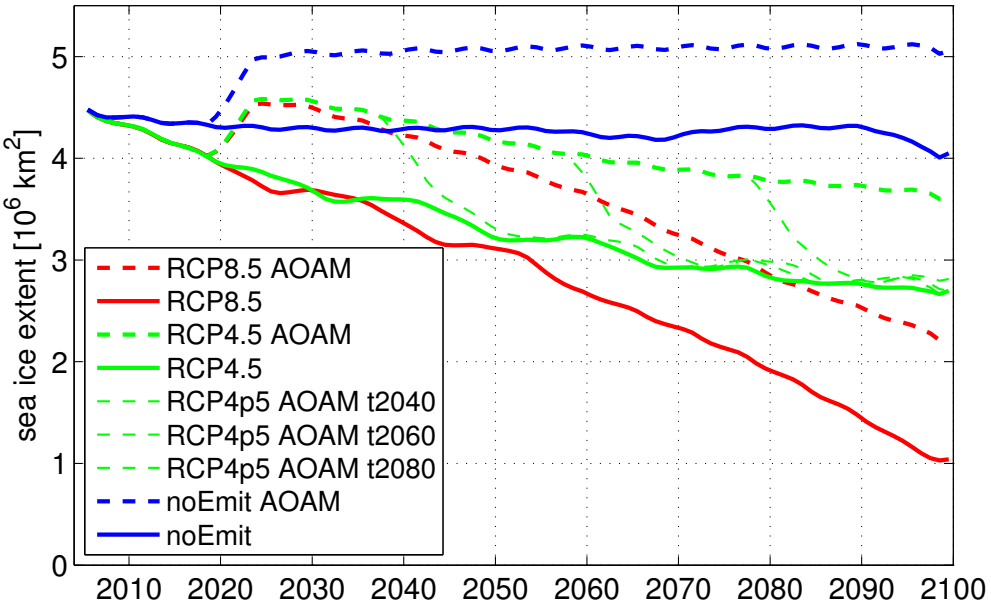

Fig. A.6.: *Northern Hemisphere annual minimum sea ice extent for the different forcing scenarios, see legend. Same as Figure 2.2a of the main article, with the addition of three termination experiments in the RCP4.5 AOAM simulation starting in 2040 (RCP4p5 AOAM t2040), 2060 (RCP4p5 AOAM t2060) and 2080 (RCP4p5 AOAM t2080).*

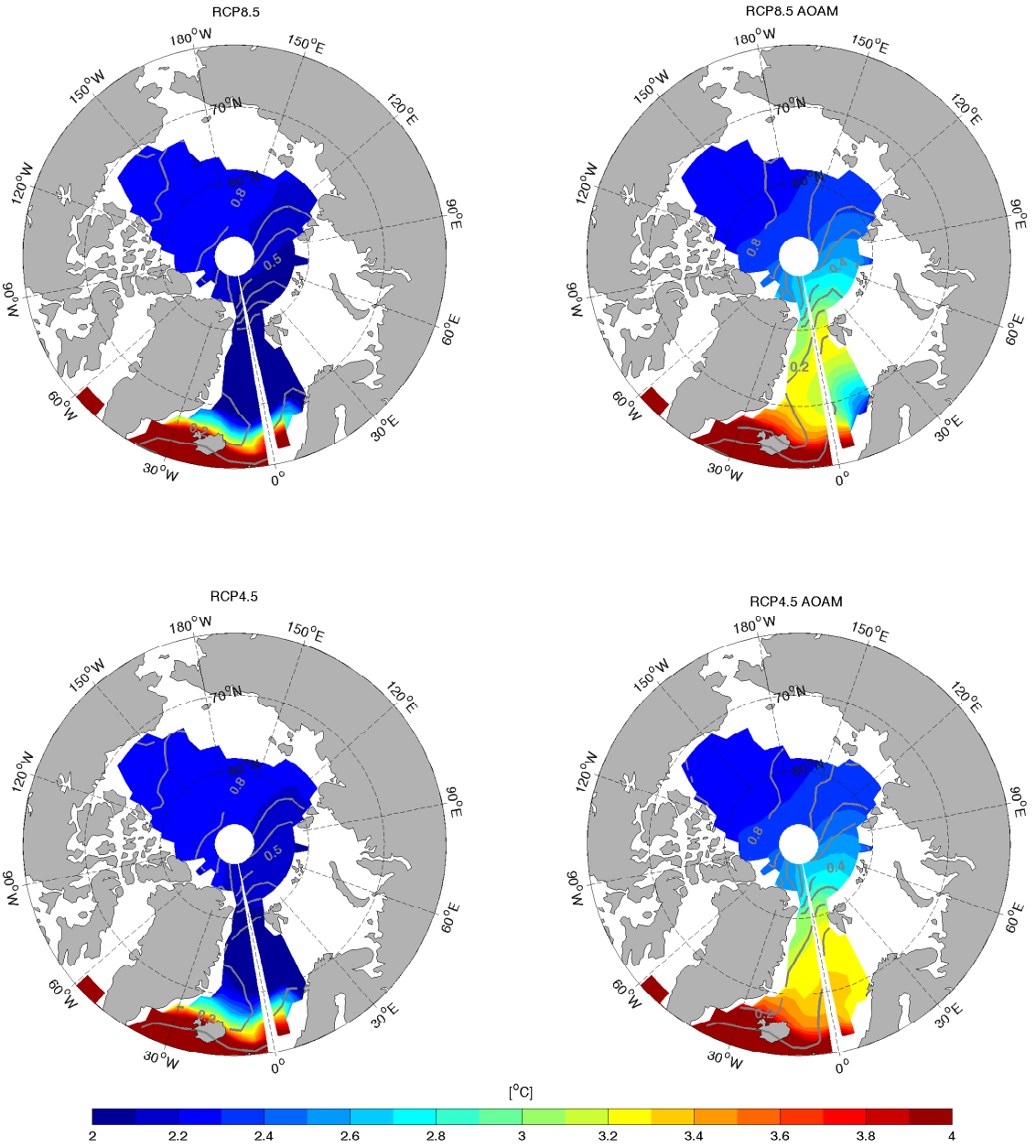

Fig. A.7.: *Arctic ocean temperatures in 2070 at about 850m depth for four experiments. The grey contours show the tracer concentration after 50 years of integration.*

B. Supporting Information for 'Uncertainty in the response of transpiration to CO_2 and implications for climate change'

B.1. Calculation of Water-Use Efficiency for Figure 3.4a

The UVic ESCM's (University of Victoria Earth System Climate Model) spatial resolution does not allow to calculate the water-use efficiency of a single plant or ecosystem. Hence the 'inherent' water-use efficiency (WUE_i) is calculated, which is used to compare water-use efficiencies between species and meteorological conditions [Beer et al., 2009]. For WUE_i the following equation is taken as a reference [Keenan et al., 2012]:

$$WUE_i = (GEP * D)/E_e. \tag{B.1}$$

Here GEP is the gross ecosystem photosynthesis, representing the carboxylation rate minus photorespiration. D is the evaporative demand, and E_e is the ecosystem evapotranspiration. In order to derive the given equation, several assumptions were made [Keenan et al., 2012]: '(1) vapour pressure difference between the leaf and the atmosphere can be approximated by measured atmospheric evaporative demand (D), assuming equal temperatures of leaves and atmosphere, (2) aerodynamic resistance between the canopy and the reference-height for the flux can be neglected, (3) under dry conditions, with no recent precipitation events, measured water vapour fluxes are equivalent to transpiration,[...] that is, evaporation contributes minimally'.
To transfer the measured variables [Keenan et al., 2012] into corresponding model variables, further assumptions had to be made and calculations had to be performed. For the observational-based derived variable GEP, the UVic ESCM variable describing the gross primary productivity of carbon was taken, $GPP_{UVic}(m)$.
In order to derive the model's evaporative demand, D_{UVic}, the saturated vapor pressure, SVP, was calculated with the following equation [Murray, 1967]:

$$SVP = 6.107 * 10^{7.5 * T_{UVic}/(T_{UVic}+237.3)}. \tag{B.2}$$

Here T_{UVic} is the models' atmospheric surface temperature in °C. D_{UVic} then is defined as the difference between the saturation vapor pressure and the specific humidity, h_s, which is given as a model output variable.

$$D_{UVic} = (1 - h_s) * SVP. \tag{B.3}$$

In order to full fill assumption (3), in the observational dataset rain events were excluded [Keenan et al., 2012] i.e. the day of rain and the day thereafter, assuming that in these dry days cases soil and leaf evaporation contributes minimally [Keenan et al., 2012]. The UVic ESCM however does not simulate weather fluctuations, hence this distinction can not be achieved. To fulfil this assumption the terrestrial evapotranspiration from the UVic ESCM would have to be partitioned into its components. The applied scaling however would alter the partitioning of Evapotranspiration, since we increase the amount of vegetational transpiration. Therefore assuming the same partitioning for all runs would introduce an error in the calculations. To avoid these errors, we calculate the UVic ESCM's WUE using simply the model output variable of evapotranspiration E_{UVic}. We thereby do not fulfil the condition to exclude evaporation from soil and leafs, and possibly underestimate the WUE.

$$WUE_{i,UVic} = (GPP_{UVic} * D_{UVic})/E_{UVic}. \tag{B.4}$$

This calculation was performed on a local scale and thereafter globally averaged, in order to produce Figure 3.4a.

Tab. B.1.: *CMIP5 models and modelling groups [Ahlström et al., 2012].*

Modelling centre (or group)	Institute ID	Model name
Canadian Centre for Climate Modelling and Analysis	CCCMA	CanESM2
National Center for Atmospheric Research	NCAR	CCSM4
Centre National de Recherches Meteorologiques/ Centre Europeen de Recherche et Formation Avancees en Calcul Scientifique	CNRM-CERFACS	CNRM-CM5
LASG, Institute of Atmospheric Physics, Chinese Academy of Sciences	LASG-IAP	FGOALS-s2
NOAA Geophysical Fluid Dynamics Laboratory	NOAA GFDL	GFDL-CM3
		GFDL-ESM2M
NASA Goddard Institute for Space Studies	NASA GISS	GISS-E2-R
Met Office Hadley Centre	MOHC	HadGEM2-CC
		HadGEM2-ES
Institute for Numerical Mathematics	INM	INM-CM4
Institut Pierre-Simon Laplace	IPSL	IPSL-CM5A-LR
		IPSL-CM5A-MR
Japan Agency for Marine-Earth Science and Technology, Atmosphere and Ocean Research Institute (The University of Tokyo), and National Institute for Environmental Studies	MIROC	MIROC-ESM
		MIROC-ESM-CHEM
Atmosphere and Ocean Research Institute (The University of Tokyo), National Institute for Environmental Studies, and Japan Agency for Marine-Earth Science and Technology	MIROC	MIROC5
Max Planck Institute for Meteorology	MPI-M	MPI-ESM-LR
Meteorological Research Institute	MRI	MRI-CGCM3
Norwegian Climate Centre	NCC	NorESM1-M

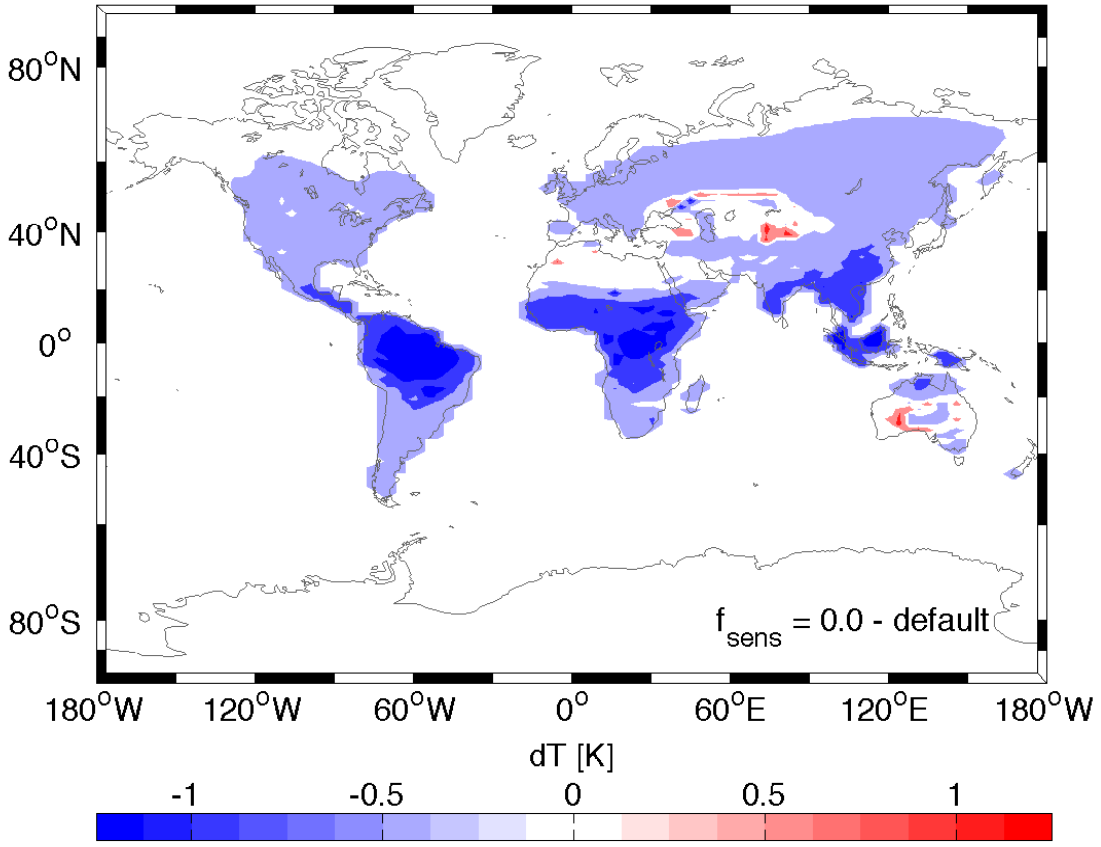

Fig. B.1.: *Map of soil temperature differences in the year 2100 between the sensitivity simulations $f_{sens} = 0.0$ and the default simulation ($f_{sens} = 1.0$) for the CO_2 forced simulations.*

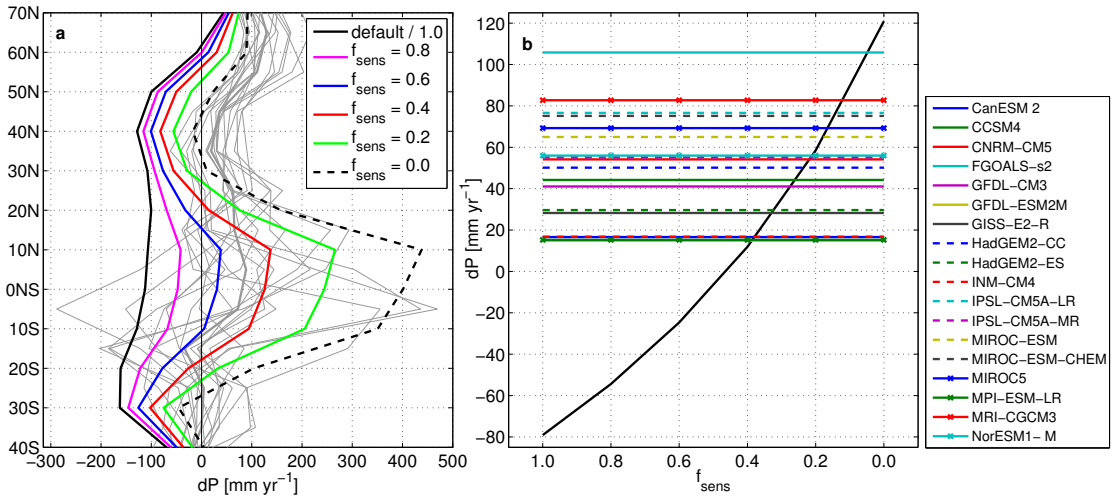

Fig. B.2.: *Same as Figure 3.3 but for the six simulations with an unperturbed terrestrial biosphere.*

C. Supporting Information for 'Systematic Correlation Matrix Evaluation (SCoMaE) - A methodological approach to find Indicators from Earth System variables'

C.1. How sensitive are the correlation matrices to the single parameter perturbations?

For a thorough discussion of this method, we assessed the sensitivities of the correlation matrices towards single parameter perturbations, i.e. how strongly a single sensitivity simulation influences the correlation pattern. Therefore we calculated the respective correlation when leaving out one of the parameter perturbations one at the time. If the standard deviation of the correlations is large, we know that the correlation calculation is very sensitive towards single parameter perturbations. In addition we tested the significance of the correlations, marking the cases where more than two thirds of the correlations are significant, even if we leave out one of them at a time.
From this exercise we learn, that some model output variables are very sensitive to the chosen parameter perturbations. The carbon fluxes in the RCP4.5 scenario, for example show a higher sensitivity to to the terrestrial perturbed parameters (CO_2 fertilisation, q10 variations, transpiration sensitivity to CO_2) than in the other scenarios, since in this forcing scenario natural vegetation is more abundant than in the others. This also explains the high sensitivity of the other land related model output variables, such as L_vegnpp, L_veglai, L_soilresp and L_vegcarb, in the RCP4.5 scenario.
Naturally, this sensitivity analysis would look different if we had chosen different model parameter for our experiment. The high standard deviations in the historical scenarios for O_po4sur and O_motmax for example are mainly due to the variations in the vertical diffusivity and the temperature sensitivity in marine productivity.

C.2. Are global aggregates enough?

To understand how representative the global aggregate of a model output variables is in respect to regional variations, we consider maps of correlations, exemplarily for the headline indicators found for the correlation matrix of the historical scenario. The correlation maps indicate where the regionally resolved model output can be explained by the global aggregate and in which regions the global aggregate is insufficient to explain the regional variability or even show a different trend.
To calculate the correlations we again regarded the differences during the two scenarios

and correlated each grid point of the regionally resolve output variable with the corresponding globally aggregated model output variable. As before a two sided significance test on a 5% significance level, with N = 16 based on a student t distribution was performed. Note that the variable O_motmax is not regionally resolved in the model output and hence misses for this analysis.

For the first headline indicator of the historical scenario, F_precipO, a strong positive correlation between global mean precipitation over ocean and the precipitation over land areas is evident (Figure C.7). This indicates that precipitation over land areas reacts similar to the parameter perturbations as the global mean precipitation over ocean. Over some ocean areas there are negative correlations evident, which indicates that the global mean precipitation over the ocean has an opposite reaction to the parameter perturbations compared to what is happening in these regions. In general the headline indicator F_precipO explains a large fraction of the regionally resolved variability from parameter perturbations.

For the second headline indicator, A_albsurL, the majority of the northern hemisphere land areas show a significant positive correlation to the global mean albedo over land. Nevertheless there are areas especially in the high northern and southern latitudes and the tropics that are either not significantly correlated or show negative correlations. This indicates that the global mean land albedo explains mostly variability due to parameter perturbations of the northern hemisphere land areas, which also take up a large fraction of the global land area.

Both for O_alksur and O_temp almost all correlation is significant and positive, which indicated a large fraction of the surface signal is explained by the global surface mean variable. This looks different for O_phyt where we correlate the global mean ocean phytoplankton with its regionally resolved surface signal. There are still large areas with significant positive correlations, however especially in the upwelling regions and in the high northern latitudes the correlation decreases and changes sign. This indicated that signals other than the parameter perturbations are influencing the surface phytoplankton concentration in these areas. Nevertheless, the positive correlation for phytoplankton is highest at the surface and decreases or even changes sign in deeper levels (not shown).

Tab. C.1.: *List of globally aggregated model output variables considered in this study.*

model output name	description	unit
A_albsurL	land surface albedo	[1]
A_albsurO	sea surface albedo	[1]
A_co2	atmospheric CO_2	[ppm]
A_sat	air surface temperature	[°C]
A_satL	land air surface temperature	[°C]
A_satO	ocean air surface temperature	[°C]
A_shum	surface specific humidity	[1]
A_totcarb	total atmospheric carbon	[Pg C]
F_carba2l	air to land carbon flux	[Pg C yr^{-1}]
F_carba2o	air to sea carbon flux	[Pg C yr^{-1}]
F_dnswr	net surface downward shortwave radiation	[W m^{-2}]
F_evap	global evaporation	[kg H_2O m^{-2} s^{-1}]
F_evapL	evaporation over land	[kg H_2O m^{-2} s^{-1}]
F_evapO	evaporation over ocean	[kg H_2O m^{-2} s^{-1}]
F_heat	ocean heat flux	[W m^{-2}]
F_netrad	net top of atmosphere radiation	[W m^{-2}]
F_outlwr	top of atmosphere outgoing longwave radiation	[W m^{-2}]
F_precip	global precipitation	[kg H_2O m^{-2} s^{-1}]
F_precipL	precipitation over land	[kg H_2O m^{-2} s^{-1}]
F_precipO	precipitation over ocean	[kg H_2O m^{-2} s^{-1}]
F_uplwr	surface net upward longwave radiation	[W m^{-2}]
F_upsens	surface upward sensible heat flux	[W m^{-2}]
L_soilcarb	soil carbon	[Pg C]
L_soilresp	soil respiration	[Pg C yr^{-1}]
L_totcarb	total land carbon	[Pg C]
L_vegcarb	vegetation carbon	[Pg C]
L_veglai	leaf area index	[1]
L_vegnpp	vegetation net primary productivity	[Pg C yr^{-1}]
O_alksur	sea surface alkalinity	[mol m^{-3}]
O_dicsur	sea surface dissolved inorganic carbon	[mol m^{-3}]
O_dsealev	change in sea level	[m]
O_iceareaN	northern hemisphere sea ice area	[m^2]
O_iceareaS	southern hemisphere sea ice area	[m^2]
O_motmax	maximum meridional overturning stream function	[m^3 s^{-1}]
O_no3sur	ocean surface nitrate	[mol m^{-3}]
O_o2	ocean oxygen	[mol m^{-3}]
O_oaragsur	sea surface omega aragonite	[1]
O_ocalcsur	sea surface omega calcite	[1]
O_pco2sur	sea surface partial CO_2 pressure	[ppmv]
O_phsur	sea surface pH	[1]
O_phyt	ocean phytoplankton	[mol N m^{-3}]
O_po4sur	sea surface phosphate	[mol m^{-3}]
O_salsur	sea surface salinity	[1]
O_temp	mean ocean temperature	[°C]
O_tempsur	sea surface temperature	[°C]
O_totcarb	total ocean carbon	[Pg C]

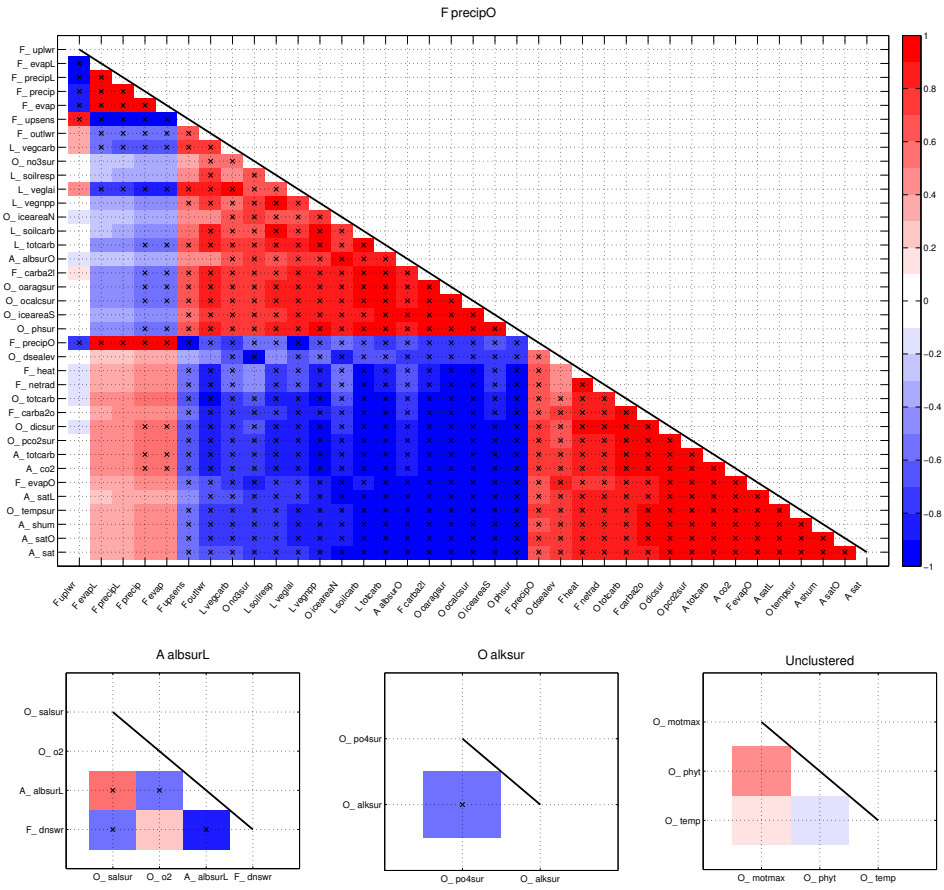

Fig. C.1.: *Correlations of the model output variables as clustered under the different headline indicators found for the historical scenario.*

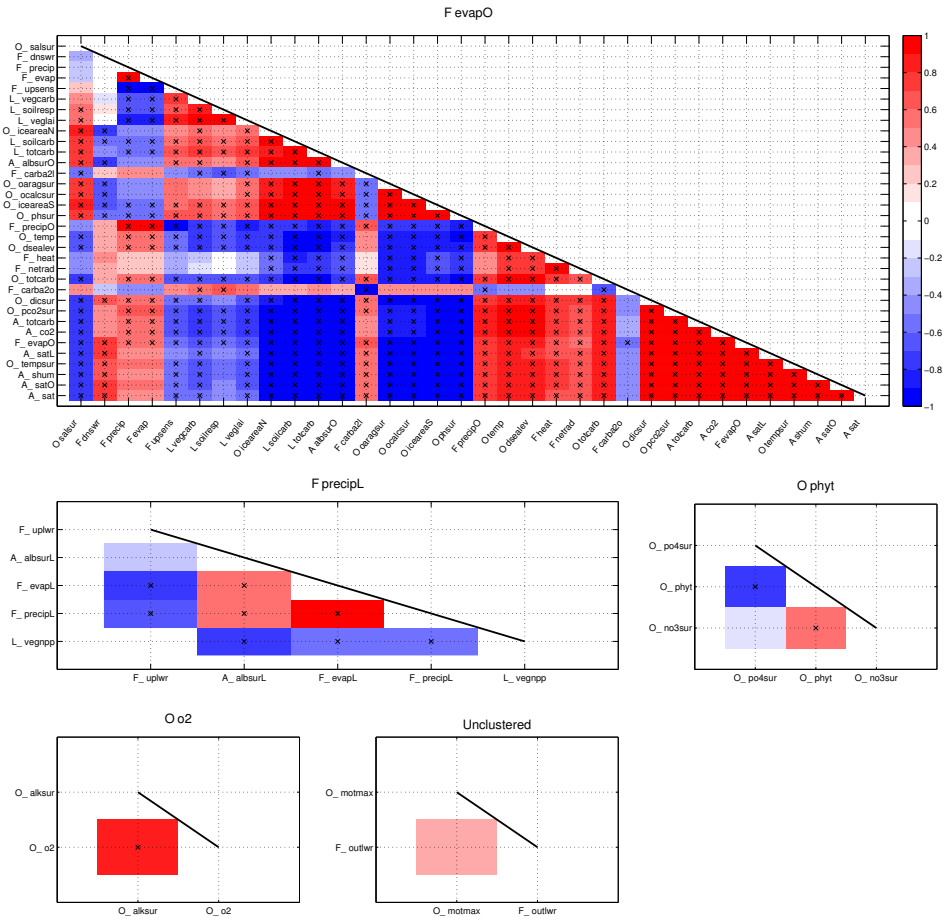

Fig. C.2.: *Correlations of the model output variables as clustered under the different headline indicators found for the RCP4.5 scenario.*

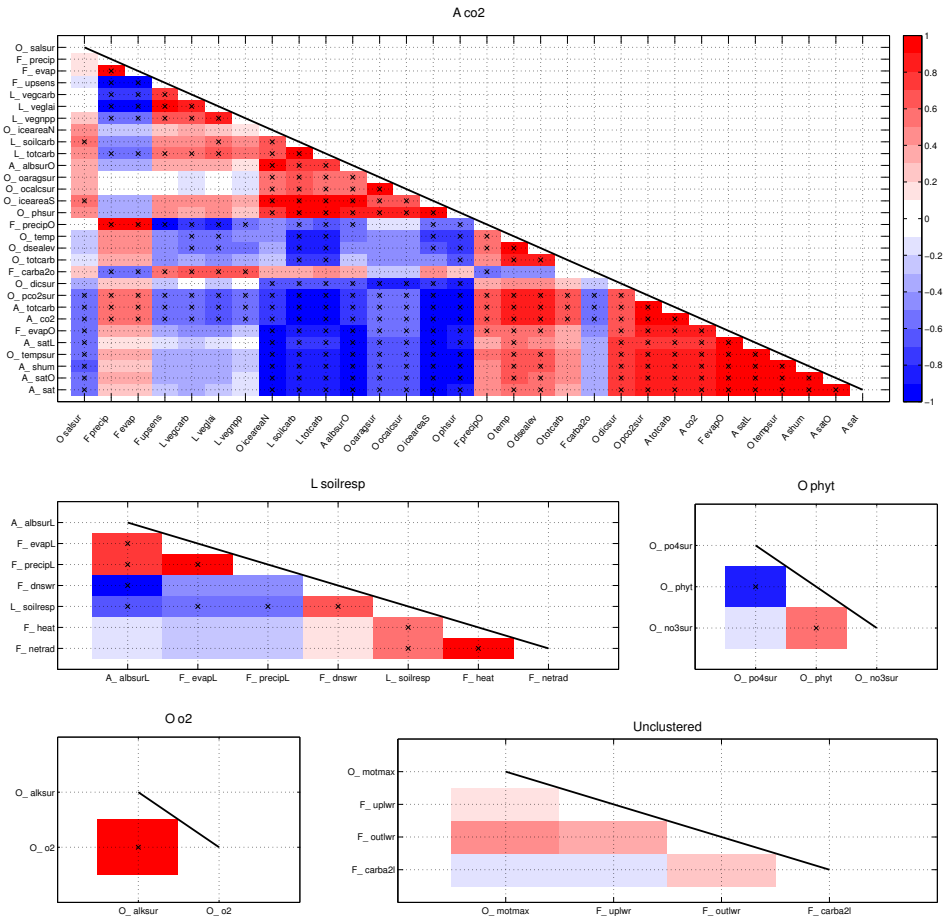

Fig. C.3.: *Correlations of the model output variables as clustered under the different headline indicators found for the RCP8.5 scenario.*

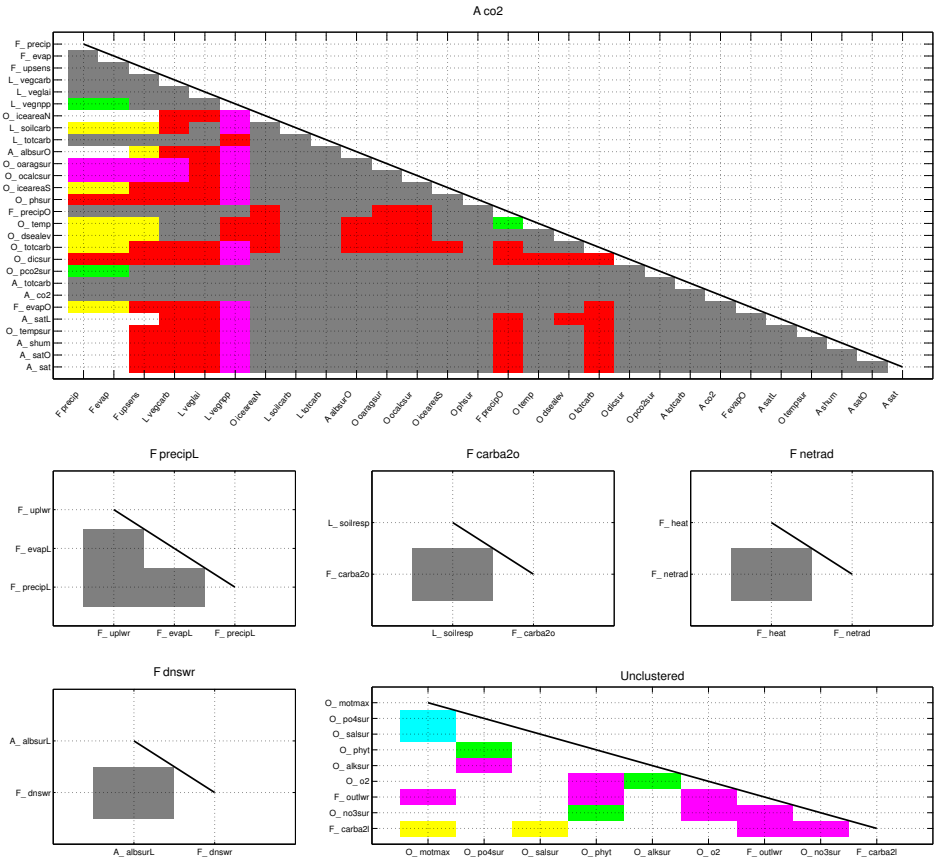

Fig. C.4.: *Correlations of the model output variables as clustered under the different headline indicators found for the common indicator.*

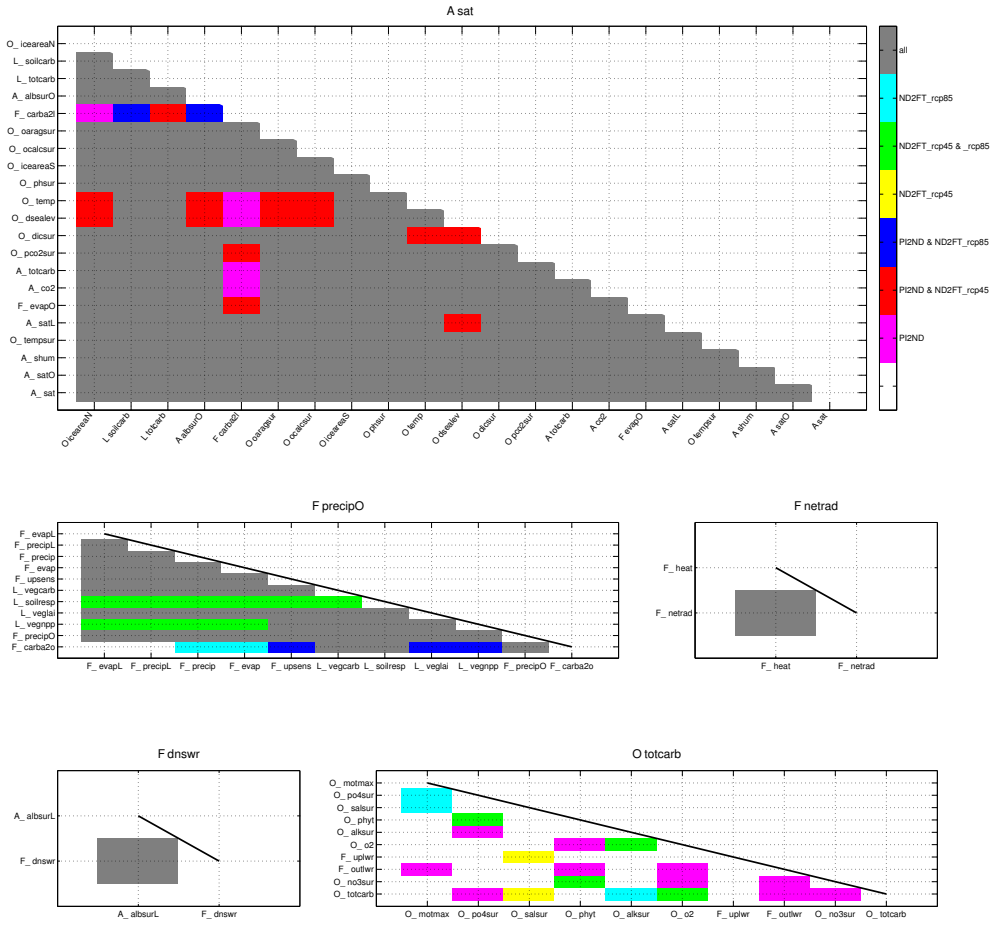

Fig. C.5.: *Correlations of the model output variables as clustered under the different headline indicators found for the common indicator, if A_sat is prescribed to be the first headline indicator.*

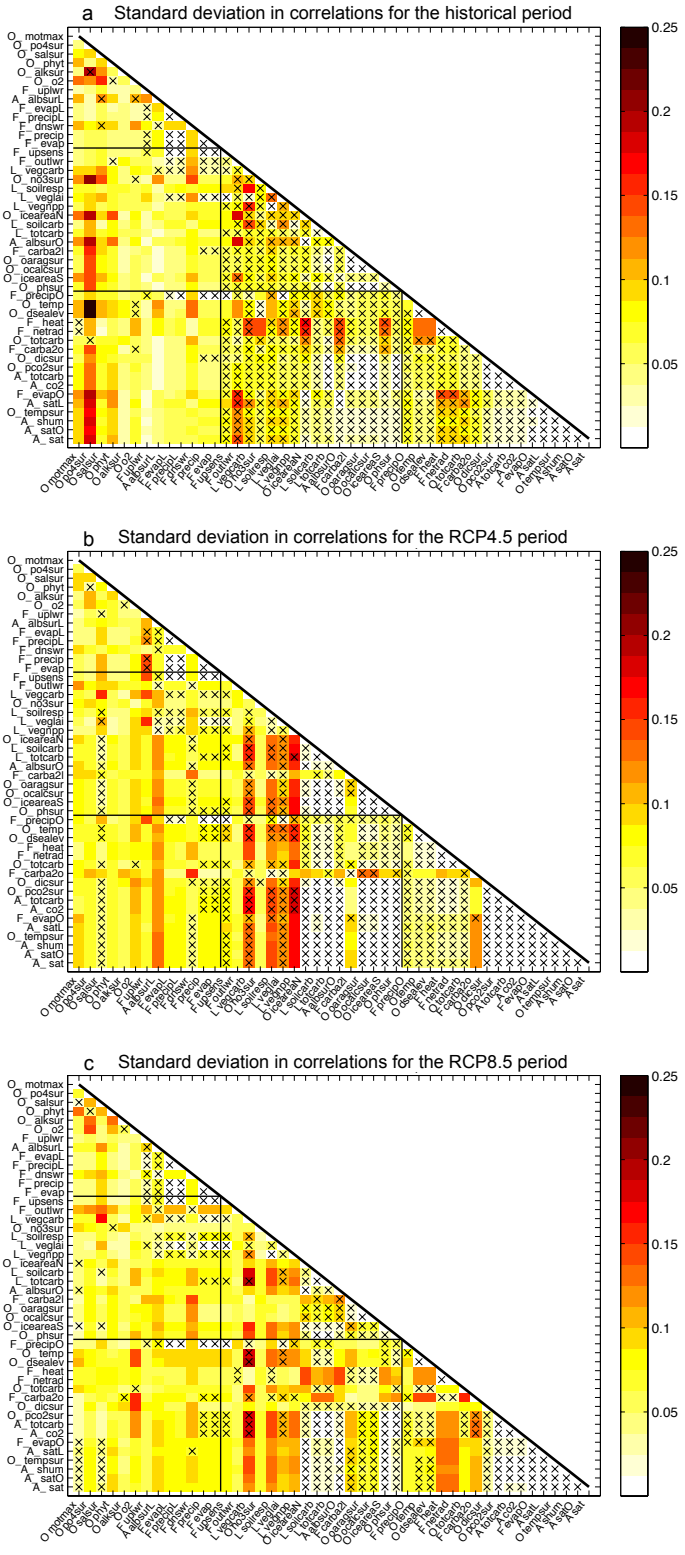

Fig. C.6.: *Standard deviations of the correlations in the respective matrix, if one perturbed parameter at a time is left out and the correlation is calculated from the remaining simulations, a) for the historical scenario, b) for the RCP4.5 scenario and c) for the RCP8.5 scenario.*

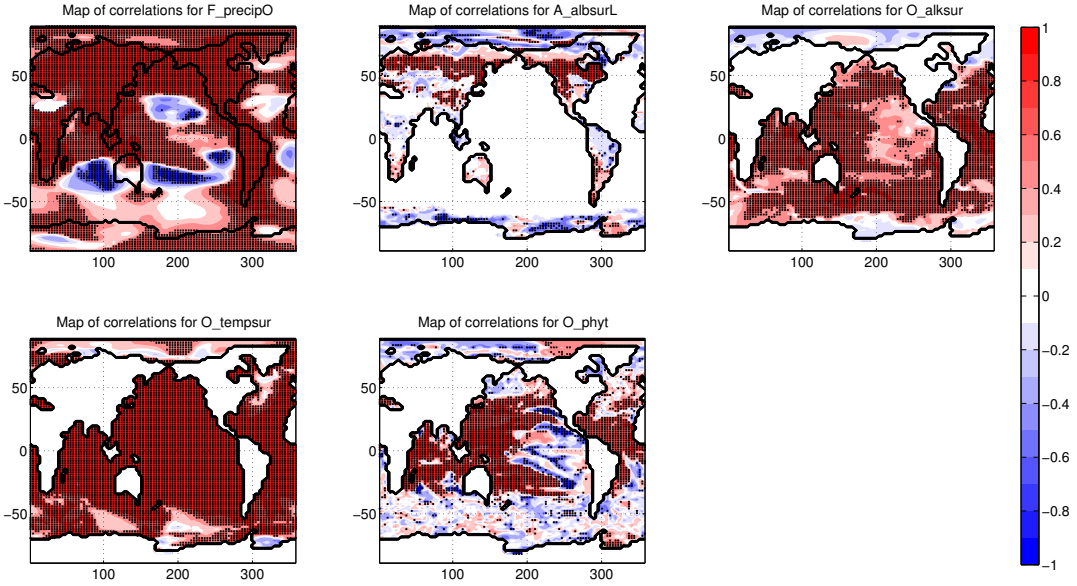

Fig. C.7.: *Maps of correlations from regionally resolved model output variables, with respect to their corresponding globally averaged model output variable. Exemplarily the five regionally resolved indicators found for the historical scenario are shown.The crosses indicate significant correlation.*

D. Supporting Information for 'Selecting Indicators from Earth system variables to assess Climate Engineering'

Climate Engineering Indicators - A Literature Review

Scales on which the indicators are assessed:
Spatial scale: A = global mean, B = global map, C = regional map, D = regional mean, E = other (includes zonal average and hemispheric scales)
Temporal scale: A = annual, B = monthly, C = daily, D = seasonal, E = other

Indicator	Reference										
	Spatial Scale					Time Scale					List
	A	B	C	D	E	A	B	C	D	E	
Surface air temperature	1–41	1,3,4,8,10,13–16,19,22,25,27,28,30–32,34,35,37,39–43	23,44,45	8,9,13,23,28,31,34,38,44–47	2,3,5,9,13,17,27,28,30–33,41,46,48–51	1–45	31,41,46–49	51	4,8,13,23,27,28,32–34,38–41,45	50	1–51
Air temp. at high altitudes	3,5,33,48				7,28,30,32,36,48	3,5,7,28,30,32,33,36	48		33	30	3,5,7,28,30,32,33,36,48
Effectiveness†	2,21,28,31,33,38,40,52–55	53,54		20,38	6,20,27,28,33,38,40,54–65	2,21,28,31,33,38,40,54,55,64	28,40			6,20,27,33,38,54–63,65	2,6,20,21,27,28,31,33,38,40,52–65
Ocean temperature	66,67	42,66			22	22,42,66,67				42	22,42,66,67
Precipitation (rain, snow, etc.)	3–5,8–10,13,14,16,17,19,25,27–32,34,38,40–42,68	4,8,13,14,16,17,19,25,27,30,31,34,36,37,40,42,43		8,13,31,38,45,47,49	5,9,13,17,27,30–32,41,49–51	3–5,8–10,13,14,16,17,19,25,27–32,34,36–38,40–43,45,49,51,68	31,47,49		4,8,17,27,40,45	38,41,50	3–5,8–10,13,14,16,17,19,25,27–32,34,36–38,40–43,45,47,49–51,68
Net water flux	32				32	32					32
Precipitable water	30,32	30			30	30,32					30,32
Evaporation / evapotranspiration	11–14,17,30–32,68,69	13,14,30,42		31	9,13,17,30–32,50,69	9,11–14,17,30–32,42,68,69	31			50	9,11–14,17,30–32,42,68,69
Time / rate of method‡	6,16,18,53,70	6			33,62,70	6,16,18,53,70				33,62,70	6,16,18,33,53,62,70

Cloud properties / cover	27,48	27,30,42			17,33,48, 51	17,27,30, 42,51	33,48				17,27,30, 33,42,48, 51
El Niño Southern Oscillation (ENSO)	34					34					34
Surface heat fluxes	3,11,12,2 7	27		46	3,27	3,11,12,2 7,46	46				3,9,11,12 ,27,46
Surface humidity / H_2O vapor	3,7					3,7					3,7
Moist Static Stability					13	13					13
Polar vortex					41		41				41
Atm. circ. or pressure.	5,12,14,4 2,48	8,14,17,2 7,42			30,33,42	5,12,14,2 7,30	48		8,17,33	42	5,8,12,14 ,17,27,30 ,33,42,48
Atmospheri c water vapor transport				31		31					31
Atmospheri c heat transport				31	34	31				34	31,34
Near surface winds		8,42				42			8	42	8,42
Atmospheri c CO2 or seawater pCO2	1,2,4,6,1 0,16,20– 22,35,55, 70–76	22		20	6,56,57,7 7–79	1,2,4,6,1 0,16,20– 22,35,55, 70–76				6,56,57,7 7–79	1,2,4,6,1 0,16,20– 22,35,55, 57,70– 79
Seawater salinity	67	10				10,67					10,67
Sea level	10					10					10
Atmospheri c GHG concentratio ns other than CO_2	21			21,80	80	21,80					21,80
Energy balance (TOA), surface energy budget, or individual energy fluxes	3,7,10,11 ,13– 15,17,19, 22,24,27, 28,30– 34,40,48, 64,68,81	13,14,17, 24,27,30, 81		31,44,45, 47,80	7,28,30,3 4,40,46,5 1,64,77	3,7,10,11 ,13– 15,17,19, 22,24,27, 30– 34,40,44 – 46,48,51, 64,68,80,	28,47		40,45	77	3,7,10,11 ,13– 15,17,19, 22,24,27, 28,30– 34,40,44 – 48,51,64, 68,77,80,

						81					81
Albedo (surface, TOA, or other)	10,13,27,82	30,81,82		31,44,82	51,77	10,13,27,30,31,44,81	82			51,77	10,13,27,30,31,44,51,77,81,82
Seawater pH	4,6,10,21,35,53,72,76	35,72,76		21,72	21,76,78,79	4,6,10,21,35,53,72,76				78,79	4,6,10,21,35,53,72,76,78,79
Air pollution metrics											
Aerosol related (may be method related for SRM)	17,33,48,64	45			33,36,64	17,33,45,48,64			36		17,33,36,45,48,64
Aerosol deposition	33	33				33	33				33
Atm. chem. inc. ozone	33,83				7,33,41,83	33,41			41	7,41,83	7,33,41,83
Saturation state of aragonite or calcite	10,35,66,72,76	35,66,72,76		21	21,78,79	10,21,35,66,72,76				78,79	10,21,35,66,72,76,78,79
Saturation horizon of aragonite or calcite	76					76					76
Other ocean carbonate chemistry (DIC, ALK, etc.)	20,67,72,76	72			6,67,78,79	20,67,72,76				6,78	6,20,67,72,76,78,79
Carbon budget (complete or indiv. reservoirs)	10,16,20,22,35,76,81,84	10,81			84	10,16,20,22,76,81,84				35,84	10,16,20,22,35,76,81,84
Ocean nutrients	21,67	20,74		21,75	21,75	20,21,67,75				74	20,21,67,74,75
Ocean oxygen	10,21,75	75		21,75,80	21,75,80	10,21,75,80					10,21,75,80
Nitrogen fixation	22					22					22
Land-ocean energy flux	14					14					14
Meridional Overturning Circulation	19				34,46	19				34,46	19,34,46

(MOC or AMOC)											
Ocean physics	22,67	10				10,22,67					10,22,67
Sea ice related	10,30–32	32,34	8,25,31,36,37,40	13,19,23,25,31,32,37,40,41,44,46,49		8,10,13,19,25,30–32,34,37,46			36,46	13,23,31,37,40,41,44,46,49	8,10,13,19,23,25,30–32,34,37,40,41,44,46,49
Snow cover or depth			40	23,31		31	23			40	23,31,40
Crop production or yield*	43		47	47	43,47	43,47				47	43,47
Land C uptake or loss flux	2,10,21					2,10				21	2,10,21
Ocean C uptake or outgassing flux	10,14,20,21,53,55,67,73,75,76,84	73		20,21,73,80	80,84	14,20,21,53,55,67,73,75,76,80,84				21	10,14,20,21,53,55,67,73,75,76,80,84
GPP or NPP on land or ocean**	10,13,25,29,42,53,67,69,74,75	13,25,42,53,69,74,75	45	45,75	9,13,29,69,75	9,10,13,25,29,42,45,53,67,69,74,75	69		45		9,10,13,25,29,42,45,53,67,69,74,75
Ocean biological pump (export production, etc.)	20–22,67,76		21	20,21	21	20–22,67,76				21	20–22,67,76
Other veg. metrics*	29,69					29,69					29,69
Terrestrial respiration	10,29					10,29					10,29
Soil moisture		39				39					39
Habitat area	66	66				66					66
Soil quality (inc. C content)	69					69					69
Physiological response++					79					79	79
Implementation cost+	33,52,63,85				42,59–61,85,86	33,63,85				33,42,59–61,85,86	33,42,52,59–61,63,85,86

Nutrient requirements	84					84					84
Land requirements		1				1					1

† May be a new metric created specifically for the study or the effectiveness of method implementation (e.g., how effectively does a SRM aerosol injection change shortwave radiation fluxes)
‡ This could for example be the rate at which the method works or related to the functioning of the method (e.g., a substance dissolution rate for ocean alkalinization and how it relates to the rate a which ocean alkalinity changes)
+ not necessarily in monetary units
*biomass, leaf area index, etc.
**may also be “new production” for some ocean studies
++the physiological responses that are measured depend on the type of organisms and are not listed in detail here, see references for details

References:

1. Akbari, H., Damon Matthews, H. & Seto, D. The long-term effect of increasing the albedo of urban areas. *Environ. Res. Lett.* **7,** 024004 (2012).

2. Arora, V. K. & Montenegro, A. Small temperature benefits provided by realistic afforestation efforts. *Nat. Geosci.* **4,** 514–518 (2011).

3. Bala, G., Duffy, P. B. & Taylor, K. E. Impact of geoengineering schemes on the global hydrological cycle. *Proc. Natl Acad. Sci.* **105,** 7664–7669 (2008).

4. Brovkin, V. *et al.* Geoengineering climate by stratospheric sulfur injections: Earth system vulnerability to technological failure. *Clim. Change* **92,** 243–259 (2009).

5. Ferraro, A. J., Highwood, E. J. & Charlton-Perez, A. J. Weakened tropical circulation and reduced precipitation in response to geoengineering. *Environ. Res. Lett.* **9,** 014001 (2014).

6. Harvey, L. D. D. Mitigating the atmospheric CO2 increase and ocean acidification by adding limestone powder to upwelling regions. *J. Geophys. Res. Ocean.* **113,** n/a–n/a (2008).

7. Heckendorn, P. *et al.* The impact of geoengineering aerosols on stratospheric temperature and ozone. *Environ. Res. Lett.* **4,** 45108 (2009).

8. Irvine, P. J., Ridgwell, A. & Lunt, D. J. Climatic effects of surface albedo geoengineering. *J. Geophys. Res. Atmos.* **116,** n/a–n/a (2011).

9. Irvine, P. J. *et al.* Key factors governing uncertainty in the response to sunshade geoengineering from a comparison of the GeoMIP ensemble and a perturbed parameter ensemble. *J. Geophys. Res.* **119,** 1–17 (2014).

10. Keller, D. P., Feng, E. Y. & Oschlies, A. Potential climate engineering effectiveness and side effects during a high carbon dioxide-emission scenario. *Nat. Commun.* **5,** 1–11 (2014).

11. Kleidon, A., Kravitz, B. & Renner, M. The hydrological sensitivity to global warming and solar geoengineering derived from thermodynamic constraints. *Geophys. Res. Lett.* **42,** 1–7 (2015).

12. Kleidon, a. & Renner, M. A simple explanation for the sensitivity of the hydrologic cycle to surface temperature and solar radiation and its implications for global climate change. *Earth Syst. Dyn.* **4,** 455–465 (2013).

13. Kravitz, B. *et al.* Climate model response from the Geoengineering Model Intercomparison Project (GeoMIP). *J. Geophys. Res. Atmos.* **118,** 8320–8332 (2013).

14. Kwiatkowski, L., Ricke, K. L. & Caldeira, K. Atmospheric consequences of disruption of the ocean thermocline. *Environ. Res. Lett.* **10,** 34016

15. MacMartin, D. G., Caldeira, K. & Keith, D. W. Solar geoengineering to limit the rate of temperature change. *Philos. Trans. A. Math. Phys. Eng. Sci.* **372,** (2014).

16. Matthews, H. D. & Caldeira, K. Transient climate-carbon simulations of planetary geoengineering. *Proc. Natl. Acad. Sci.* **104,** 9949–9954 (2007).

17. Niemeier, U., Schmidt, H., Alterskjaer, K. & Kristjánsson, J. E. Solar irradiance reduction via climate engineering: Impact of different techniques on the energy balance and the hydrological cycle. *J. Geophys. Res. Atmos.* **118,** n/a–n/a (2013).

18. Ross, A. & Matthews, H. D. Climate engineering and the risk of rapid climate change. *Environ. Res. Lett.* **4,** (2009).

19. Schaller, N., Sedláček, J. & Knutti, R. The asymmetry of the climate system's response to solar forcing changes and its implications for geoengineering scenarios. *J. Geophys. Res. Atmos.* **119,** 5171–5184 (2014).

20. Oschlies, A. Impact of atmospheric and terrestrial CO2 feedbacks on fertilization-induced marine carbon uptake. *Biogeosciences* **6,** 1603–1613 (2009).

21. Oschlies, A., Koeve, W., Rickels, W. & Rehdanz, K. Side effects and accounting aspects of hypothetical large-scale Southern Ocean iron fertilization. *Biogeosciences* **7,** 4017–4035 (2010).

22. Oschlies, A., Pahlow, M., Yool, A. & Matear, R. J. Climate engineering by artificial ocean upwelling - channelling the sorcerer's apprentice. *Geophys. Res. Lett.* **37,** (2010).

23. Berdahl, M. *et al.* Arctic cryosphere response in the Geoengineering Model Intercomparison Project G3 and G4 scenarios. *J. Geophys. Res. Atmos.* **119,** 1308–1321 (2014).

24. Huneeus, N. *et al.* Journal of Geophysical Research : Atmospheres. 1–14 (2014). doi:10.1002/2013JD021110.Received

25. Jones, A. *et al.* The impact of abrupt suspension of solar radiation management (termination effect) in experiment G2 of the Geoengineering Model Intercomparison Project (GeoMIP). *J. Geophys. Res. Atmos.* n/a–n/a (2013). doi:10.1002/jgrd.50762

26. Kravitz, B., MacMartin, D. G., Leedal, D. T., Rasch, P. J. & Jarvis, A. J. Explicit feedback and the management of uncertainty in meeting climate objectives with solar geoengineering. *Environ. Res. Lett.* **9,** 044006 (2014).

27. Schmidt, H. *et al.* Solar irradiance reduction to counteract radiative forcing from a quadrupling of CO2: climate responses simulated by four earth system models. *Earth Syst. Dynam.* **3,** 63–78 (2012).

28. Govindasamy, B & Caldeira, K. Geoengineering Earth's radiation balance to mitigate CO2 induced climate change. *Geophys. Res. Lett.* **27,** 2141–2144 (2000).

29. Govindasamy, B., Thompson, S., Duff, P. B., Caldeira, K. & Delire, C. Impact of geoengineering schemes on the terrestrial biosphere. *Geophysical Research Letters* **29,** 3–6 (2002).

30. Bala, G. *et al.* Albedo enhancement of marine clouds to counteract global warming: Impacts on the hydrological cycle. *Clim. Dyn.* **37,** 915–931 (2011).

31. Caldeira, K. & Wood, L. Global and Arctic climate engineering: numerical model studies. *Philos. Trans. A. Math. Phys. Eng. Sci.* **366,** 4039–4056 (2008).

32. Govindasamy, B., Caldeira, K. & Duffy, P. B. Geoengineering Earth's radiation balance to mitigate climate change from a quadrupling of CO2. *Glob. Planet. Change* **37,** 157–168 (2003).

33. Kravitz, B., Robock, A., Shindell, D. T. & Miller, M. a. Sensitivity of stratospheric geoengineering with black carbon to aerosol size and altitude of injection. *J. Geophys. Res.* **117,** 1–22 (2012).

34. Lunt, D. J., Ridgwell, a., Valdes, P. J. & Seale, a. 'Sunshade World': A fully coupled GCM evaluation of the climatic impacts of geoengineering. *Geophys. Res. Lett.* **35,** 2–6 (2008).

35. Matthews, H. D., Cao, L. & Caldeira, K. Sensitivity of ocean acidification to geoengineered climate stabilization. *Geophys. Res. Lett.* **36,** 1–5 (2009).

36. Rasch, P. J., Crutzen, P. J. & Coleman, D. B. Exploring the geoengineering of climate using stratospheric sulfate aerosols: The role of particle size. *Geophys. Res. Lett.* **35,** 1–6 (2008).

37. Rasch, P. J., Latham, J. & Chen, C.-C. (Jack). Geoengineering by cloud seeding: influence on sea ice and climate system. *Environ. Res. Lett.* **4,** 045112 (2009).

38. Ricke, K. L., Morgan, M. G. & Allen, M. R. Regional climate response to solar-radiation management. *Nat. Geosci.* **3,** 537–541 (2010).

39. Ridgwell, A., Singarayer, J. S., Hetherington, A. M. & Valdes, P. J. Tackling Regional Climate Change By Leaf Albedo Bio-geoengineering. *Curr. Biol.* **19,** 146–150 (2009).

40. Robock, A., Oman, L. & Stenchikov, G. L. Regional climate responses to geoengineering with tropical and Arctic SO2 injections. *J. Geophys. Res. Atmos.* **113,** 1–15 (2008).

41. Tilmes, S., Garcia, R. R., Kinnison, D. E., Gettelman, A. & Rasch, P. J. Impact of geoengineered aerosols on the troposphere and stratosphere. *J. Geophys. Res. Atmos.* **114,** 1–22 (2009).

42. Ornstein, L., Aleinov, I. & Rind, D. Irrigated afforestation of the Sahara and Australian Outback to end global warming. *Clim. Change* **97,** 409–437 (2009).

43. Pongratz, J., Lobell, D. B., Cao, L. & Caldeira, K. Crop yields in a geoengineered climate. *Nat. Clim. Chang.* **2,** 101–105 (2012).

44. Cvijanovic, I., Caldeira, K. & MacMartin, D. G. Impacts of ocean albedo alteration on Arctic sea ice restoration and Northern Hemisphere climate. *Environ. Res. Lett.* **10,** 044020 (2015).

45. Muri, H., Niemeier, U. & Kristjánsson, J. E. Tropical rainforest response to marine sky brightening climate engineering. 1–10 (2015). doi:10.1002/2015GL063363.Received

46. Tilmes, S., Jahn, A., Kay, J. E., Holland, M. & Lamarque, J. Can regional climate engineering save the summer Arctic sea ice ? 1–6 (2014). doi:10.1002/2013GL058731.1.

47. Xia, L. *et al.* Solar Radiation Management Impacts on Agriculture in China: A Case Study in the Geoengineering Model Intercomparison Project (GeoMIP). *J. Geophys. Res. Atmos.* n/a–n/a (2014). doi:10.1002/2013JD020630

48. Kuebbeler, M., Lohmann, U. & Feichter, J. Effects of stratospheric sulfate aerosol geo-engineering on cirrus clouds. *Geophys. Res. Lett.* **39,** (2012).

49. MacMartin, D. G., Keith, D. W., Kravitz, B. & Caldeira, K. Management of trade-offs in geoengineering through optimal choice of non-uniform radiative forcing. *Nat. Clim. Chang.* **in press,** (2012).

50. Ban-Weiss, G. a & Caldeira, K. Geoengineering as an optimization problem. *Environ. Res. Lett.* **5,** 034009 (2010).

51. Doughty, C. E., Field, C. B. & McMillan, A. M. S. Can crop albedo be increased through the modification of leaf trichomes, and could this cool regional climate? *Clim. Change* **104,** 379–387 (2011).

52. Kheshgi, H. S. Sequestering atmospheric carbon dioxide by increasing ocean alkalinity. *Energy* **20,** 915–922 (1995).

53. Köhler, P., Abrams, J. F., Völker, C., Hauck, J. & Wolf-Gladrow, D. a. Geoengineering impact of open ocean dissolution of olivine on atmospheric CO 2 , surface ocean pH and marine biology. *Environ. Res. Lett.* **8,** 014009 (2013).

54. Robinson, J. *et al.* How deep is deep enough ? Ocean iron fertilization and carbon sequestration in the Southern Ocean. 1–7 (2014). doi:10.1002/2013GL058799.Received

55. Zeebe, R. E. & Archer, D. Feasibility of ocean fertilization and its impact on future atmospheric CO2 levels. *Geophys. Res. Lett.* **32,** 1–5 (2005).

56. Hartmann, J. *et al.* Enhanced Chemical Weathering as a Geoengineering Strategy to Reduce Atmospheric Carbon Dioxide, a Nutrient Source and to Mitigate Ocean Acidification. *Rev. Geophys.* **in press,** (2013).

57. Moosdorf, N., Renforth, P. & Hartmann, J. Carbon dioxide efficiency of terrestrial enhanced weathering. *Environ. Sci. Technol.* **48,** 4809–16 (2014).

58. White, A. *et al.* An Open Ocean Trial of Controlled Upwelling Using Wave Pump Technology. *J. Atmos. Ocean. Technol.* **27,** 385–396 (2010).

59. Rau, G. H. Electrochemical splitting of calcium carbonate to increase solution alkalinity: Implications for mitigation of carbon dioxide and ocean acidity. *Environ. Sci. Technol.* **42,** 8935–8940 (2008).

60. Rau, G. H. *et al.* Direct electrolytic dissolution of silicate minerals for air CO2 mitigation and carbon-negative H2 production. *Proc. Natl. Acad. Sci. U. S. A.* **110,** 10095–100 (2013).

61. Strand, S. E. & Benford, G. Ocean sequestration of crop residue carbon: recycling fossil fuel carbon back to deep sediments. *Environ. Sci. Technol.* **43,** 1000–1007 (2009).

62. Vaughan, N. E. & Lenton, T. M. A review of climate geoengineering proposals. *Clim. Change* **109,** 745–790 (2011).

63. Crutzen, P. Albedo Enhancement by Stratospheric Sulfur Injections: A Contribution to Resolve a Policy Dilemma? *Clim. Change* **77,** 211–220 (2006).

64. Niemeier, U., Schmidt, H. & Timmreck, C. The dependency of geoengineered sulfate aerosol on the emission strategy. *Atmos. Sci. Lett.* **12,** 189–194 (2011).

65. Schuiling, R. D. & Krijgsman, P. Enhanced weathering: An effective and cheap tool to sequester CO 2. *Clim. Change* **74,** 349–354 (2006).

66. Couce, E., Irvine, P. J., Gregorie, L. J., Ridgwell, A. & Hendy, E. J. Tropical coral reef habitat in a geoengineered, high-CO2 world. *Geophys. Res. Lett.* n/a–n/a (2013). doi:10.1002/grl.50340

67. Yool, A., Shepherd, J. G., Bryden, H. L. & Oschlies, A. Low efficiency of nutrient translocation for enhancing oceanic uptake of carbon dioxide. *J. Geophys. Res.* **114,** C08009 (2009).

68. Fyfe, J. C., Cole, J. N. S., Arora, V. K. & Scinocca, J. F. Biogeochemical carbon coupling influences global precipitation in geoengineering experiments. *Geophys. Res. Lett.* **40,** 651–655 (2013).

69. Naik, V., Wuebbles, D. J., Delucia, E. H. & Foley, J. A. Influence of Geoengineered Climate on the Terrestrial Biosphere. *Environ. Manage.* **32,** 373–381 (2003).

70. Hangx, S. J. T. & Spiers, C. J. Coastal spreading of olivine to control atmospheric CO2 concentrations: A critical analysis of viability. *Int. J. Greenh. Gas Control* **3,** 757–767 (2009).

71. Heimann, M. Comment on 'Carbon farming in hot, dry coastal areas: an option for climate change mitigation' by Becker et al. (2013). *Earth Syst. Dyn.* **5,** 41–42 (2014).

72. Ilyina, T., Wolf-Gladrow, D., Munhoven, G. & Heinze, C. Assessing the potential of calcium-based artificial ocean alkalinization to mitigate rising atmospheric CO 2 and ocean acidification. *Geophys. Res. Lett.* n/a–n/a (2013). doi:10.1002/2013GL057981

73. Vichi, M., Navarra, A. & Fogli, P. G. Adjustment of the natural ocean carbon cycle to negative emission rates. *Clim. Change* 1–14 (2013). doi:10.1007/s10584-012-0677-0

74. Aumont, O. & Bopp, L. Globalizing results from ocean in situ iron fertilization studies. *Glob. Biogeochem. Cycles* **20,** GB2017 (2006).

75. Sarmiento, J. L. & Orr, J. C. Three-dimensional simulations of the impact of Southern Ocean nutrient depletion on atmospheric CO2 and ocean chemistry. *Limnol. Oceanogr.* **36,** 1928–1950 (1991).

76. Cao, L. & Caldeira, K. Can ocean iron fertilization mitigate ocean acidification? *Clim. Change* **99,** 303–311 (2010).

77. Lenton, T. M. & Vaughan, N. E. The radiative forcing potential of different climate geoengineering options. *Atmos. Chem. Phys. Discuss.* **9,** 2559–2608 (2009).

78. Caldeira, K. & Rau, G. H. Accelerating carbonate dissolution to sequester carbon dioxide in the ocean: Geochemical implications. *Geophys. Res. Lett.* **27,** 225–228 (2000).

79. Cripps, G., Widdicombe, S., Spicer, J. I. & Findlay, H. S. Biological impacts of enhanced alkalinity in Carcinus maenas. *Mar. Pollut. Bull.* **71,** 190–198 (2013).

80. Jin, X. & Gruber, N. Offsetting the radiative benefit of ocean iron fertilization by enhancing N2O emissions. *Geophys. Res. Lett.* **30,** 2249 (2003).

81. Betts, R. A. Offset of the potential carbon sink from boreal forestation by decreases in surface albedo. *Nature* **409,** 187–190 (2000).

82. Seidel, D. J., Feingold, G., Jacobson, A. R. & Loeb, N. Detection limits of albedo changes induced by climate engineering. *Nat. Clim. Chang.* **4,** 228–228 (2014).

83. Tilmes, S., Müller, R. & Salawitch, R. The sensitivity of polar ozone depletion to proposed geoengineering schemes. *Science* **320,** 1201–1204 (2008).

84. Gnanadesikan, A., Sarmiento, J. L. & Slater, R. D. Effects of patchy ocean fertilization on atmospheric carbon dioxide and biological production. *Glob. Biogeochem. Cycles* **17,** 1050 (2003).

85. Robock, A., Marquardt, A., Kravitz, B. & Stenchikov, G. Benefits, risks, and costs of stratospheric geoengineering. *Geophys. Res. Lett.* **36,** 1–9 (2009).

86. Renforth, P., Jenkins, B. G. & Kruger, T. Engineering challenges of ocean liming. *Energy* (2013). doi:10.1016/j.energy.2013.08.006

Bibliography

Ahlström, A., Schurgers, G., Arneth, A., and Smith, B. (2012). Robustness and uncertainty in terrestrial ecosystem carbon response to CMIP5 climate change projections. *Environmental Research Letters*, 7(4):044008.

Allan, R. P., Liu, C., Zahn, M., Lavers, D. A., Koukouvagias, E., and Bodas-Salcedo, A. (2013). Physically Consistent Responses of the Global Atmospheric Hydrological Cycle in Models and Observations. *Surveys in Geophysics*.

Alterskjaer, K., Kristjánsson, J. E., Boucher, O., Muri, H., Niemeier, U., Schmidt, H., Schulz, M., and Timmreck, C. (2013). Sea-salt injections into the low-latitude marine boundary layer: The transient response in three earth system models. *Journal of Geophysical Research: Atmospheres*, 118(21).

Anderson, K. (2015). Duality in climate science. *Nature Geoscience*, 8(12):898–900.

Archer, D., Eby, M., Brovkin, V., Ridgwell, A., Cao, L., Mikolajewicz, U., Caldeira, K., Matsumoto, K., Munhoven, G., Montenegro, A., et al. (2009). Atmospheric lifetime of fossil fuel carbon dioxide. *Annual Review of Earth and Planetary Sciences*, 37(1):117.

Argyris, C. (1976). Single-loop and double-loop models in research on decision making. *Administrative science quarterly*, pages 363–375.

Arora, V. K., Boer, G. J., Friedlingstein, P., Eby, M., Jones, C. D., Christian, J. R., Bonan, G. B., Bopp, L., Brovkin, V., Cadule, P., Hajima, T., Ilyina, T., Lindsay, K., Tjiputra, J. F., and Wu, T. (2013). Carbon–Concentration and Carbon–Climate Feedbacks in CMIP5 Earth System Models. *Journal of Climate*, 26(15):5289–5314.

Arora, V. K. and Montenegro, A. (2011). Small temperature benefits provided by realistic afforestation efforts. *Nature Geoscience*, 4(8):514–518.

Arrhenius, S. (1896). On the influence of carbonic acid in the air upon the temperature of the ground. *The London, Edinburgh, and Dublin Philosophical Magazine and Journal of Science*, 41(251):237–276.

Arrow, K. J., Chenery, H. B., Minhas, B. S., and Solow, R. M. (1961). Capital-labor substitution and economic efficiency. *The Review of Economics and Statistics*, 43(3):225–250.

Aswathy, V. N., Boucher, O., Quaas, M., Niemeier, U., Muri, H., Mülmenstädt, J., and Quaas, J. (2015). Climate extremes in multi-model simulations of stratospheric

aerosol and marine cloud brightening climate engineering. *Atmospheric Chemistry and Physics*, 15(16):9593–9610.

Avis, C. A., Weaver, A. J., and Meissner, K. J. (2011). Reduction in areal extent of high-latitude wetlands in response to permafrost thaw. *Nature Geosci*, 4(7):444–448.

Azar, C., Johansson, D. J. A., and Mattsson, N. (2013). Meeting global temperature targets - the role of bioenergy with carbon capture and storage. *Enviromental Research Letters*, 8:1–8.

Ball, J. T., Woodrow, I. E., and Berry, J. A. (1987). A model predicting stomatal conductance and its contribution to the control of photosynthesis under different environmental conditions. In *Progress in Photosynthesis Research*, volume 4, pages 221–224. Springer.

Beer, C., Ciais, P., Reichstein, M., Baldocchi, D., Law, B., Papale, D., Soussana, J.-F., Ammann, C., Buchmann, N., Frank, D., et al. (2009). Temporal and among-site variability of inherent water use efficiency at the ecosystem level. *Global biogeochemical cycles*, 23(2).

Berdahl, M., Robock, A., Ji, D., Moore, J. C., Jones, A., Kravitz, B., and Watanabe, S. (2014). Arctic cryosphere response in the geoengineering model intercomparison project g3 and g4 scenarios. *Journal of Geophysical Research: Atmospheres*, 119(3):1308–1321.

Betz, G. and Cacean, S. (2012). *Ethical aspects of climate engineering*. KIT Scientific Publishing.

Biastoch, A., Treude, T., Rüpke, L. H., Riebesell, U., Roth, C., Burwicz, E. B., Park, W., Latif, M., Böning, C. W., Madec, G., and Wallmann, K. (2011). Rising Arctic Ocean temperatures cause gas hydrate destabilization and ocean acidification. *Geophysical Research Letters*, 38(8):n/a–n/a.

Bitz, C. M., Holland, M. M., Weaver, A. J., and Eby, M. (2001). Simulating the ice-thickness distribution in a coupled climate model. *Journal of Geophysical Research*, 106(C2):2441–2463.

Bitz, C. M. and Lipscomb, W. H. (1999). An energy-conserving thermodynamic model of sea ice. *Journal of Geophysical Research*, 104(C7):669–677.

Blackstock, J. J., Battisti, D. S., Caldeira, K., Eardley, D. M., Katz, J. I., Keith, D. W., Patrinos, A. A., Schrag, D. P., Socolow, R. H., and Koonin, S. E. (2009). Climate engineering responses to climate emergencies. *arXiv preprint arXiv:0907.5140*.

Böhringer, C. and Jochem, P. E. (2007). Measuring the immeasurable — a survey of sustainability indices. *Ecological economics*, 63(1):1–8.

Burns, W. and Nicholson, S. (2016). 14 governing climate engineering. *New Earth Politics: Essays from the Anthropocene*, page 343.

Caldeira, K. and Wood, L. (2008). Global and Arctic climate engineering: numerical model studies. *Philosophical transactions. Series A, Mathematical, physical, and engineering sciences*, 366(1882):4039–56.

Callendar, G. S. (1938). The artificial production of carbon dioxide and its influence on temperature. *Quarterly Journal of the Royal Meteorological Society*, 64(275):223–240.

Cao, L., Bala, G., Caldeira, K., Nemani, R., and Ban-Weiss, G. (2010). Importance of carbon dioxide physiological forcing to future climate change. *Proceedings of the National Academy of Sciences of the United States of America*, 107(21):9513–8.

Cox, P. M. (2001). Description of the 'TRIFFID' Dynamic Global Vegetation Model. Technical report, Technical Note 24, Hadley Centre, United Kingdom Meteorological Office, Bracknell, UK.

Cox, P. M., Betts, R. A., Bunton, C. B., Essery, R. L. H., Rowntree, P. R., and Smith, J. (1999). The impact of new land surface physics on the GCM simulation of climate and climate sensitivity. *Climate Dynamics*, 15(3):183–203.

Cox, P. M., Huntingford, C., and Harding, R. J. (1998). A canopy conductance and photosynthesis model for use in a GCM land surface scheme. *Journal of Hydrology*, 212-213:79–94.

Crook, J. A., Jackson, L. S., and Forster, P. M. (2016). Can increasing albedo of existing ship wakes reduce climate change? *Journal of Geophysical Research: Atmospheres*.

Crutzen, P. J. (2006). Albedo enhancement by stratospheric sulfur injections: A contribution to resolve a policy dilemma? *Climatic Change*, 77(3):211–220.

Cvijanovic, I., Caldeira, K., and MacMartin, D. G. (2015). Impacts of ocean albedo alteration on Arctic sea ice restoration and Northern Hemisphere climate. *Environmental Research Letters*, 10(4):44020.

Dalby, S. (2015). Geoengineering: the next era of geopolitics? *Geography Compass*, 9(4):190–201.

Damour, G., Simonneau, T., Cochard, H., and Urban, L. (2010). An overview of models of stomatal conductance at the leaf level. *Plant, cell & environment*, 33(9):1419–38.

Dirmeyer, P. a., Gao, X., Zhao, M., Guo, Z., Oki, T., and Hanasaki, N. (2006). GSWP-2: Multimodel Analysis and Implications for Our Perception of the Land Surface. *Bulletin of the American Meteorological Society*, 87(10):1381–1397.

Duteil, O. and Oschlies, a. (2011). Sensitivity of simulated extent and future evolution of marine suboxia to mixing intensity. *Geophysical Research Letters*, 38(January):1–5.

Ebert, U. and Welsch, H. (2004). Meaningful environmental indices: a social choice approach. *Journal of Environmental Economics and Management*, 47:270–283.

Eby, M., Weaver, A. J., Alexander, K., Zickfeld, K., Abe-Ouchi, A., Cimatoribus, A. A., Crespin, E., Drijfhout, S. S., Edwards, N. R., Eliseev, A. V., Feulner, G., Fichefet, T., Forest, C. E., Goosse, H., Holden, P. B., Joos, F., Kawamiya, M., Kicklighter, D., Kienert, H., Matsumoto, K., Mokhov, I. I., Monier, E., Olsen, S. M., Pedersen, J. O. P., Perrette, M., Philippon-Berthier, G., Ridgwell, A., Schlosser, A., Schneider Von Deimling, T., Shaffer, G., Smith, R. S., Spahni, R., Sokolov, A. P., Steinacher, M., Tachiiri, K., Tokos, K. S., Yoshimori, M., Zeng, N., and Zhao, F. (2013). Historical and idealized climate model experiments: an intercomparison of Earth system models of intermediate complexity. *Climate of the Past*, 9(3):1111–1140.

Evans, J. R. G., Stride, E. P. J., Edirisinghe, M. J., Andrews, D. J., and Simons, R. R. (2010). Can oceanic foams limit global warming? *Climate Research*, 42(2):155–160.

Fanning, A. F. and Weaver, A. J. (1996). An atmospheric energy-moisture balance model : climatology , interpentadal climate change , and coupling to an ocean general circulation model. *Journal of Geophysical Research*, 101(D10):111–115.

Feichter, J. and Leisner, T. (2009). Climate engineering: A critical review of approaches to modify the global energy balance. *The European Physical Journal Special Topics*, 176(1):81–92.

Friedlingstein, P., Cox, P. M., Betts, R. A., Bopp, L., Von Bloh, W., Brovkin, V., Cadule, P., Doney, S. C., Eby, M., Fung, I., Bala, G., John, J., Jones, C. D., Joos, F., Kato, T., Kawamiya, M., Knorr, W., Lindsay, K., Matthews, H. D., Raddatz, T., Rayner, P., Reick, C. H., Roeckner, E., Schnitzler, K.-G., Schnur, R., Strassmann, K., Weaver, A. J., Yoshikawa, C., and Zeng, N. (2006). Climate – Carbon Cycle Feedback Analysis : Results from the C4MIP Model Intercomparison. *Journal of Climate*, 19.

Fuss, S., Canadell, J. G., Peters, G. P., Tavoni, M., Andrew, R. M., Ciais, P., Jackson, R. B., Jones, C. D., Kraxner, F., Nakicenovic, N., Le Quéré, C., Raupach, M. R., Sharifi, A., Smith, P., and Yamagata, Y. (2014). Betting on negative emissions. *Nature Climate Change*, 4(10):850–853.

Fyke, J., Eby, M., Mackintosh, A., and Weaver, A. (2014). Impact of climate sensitivity and polar amplification on projections of greenland ice sheet loss. *Climate Dynamics*, 43:2249–2260.

Fyke, J. and Matthews, H. D. (2015). A probabilistic analysis of cumulative carbon emissions and long-term planetary warming. *Environmental Research Letters*, 10(11):115007.

Gallopín, G. C. (1996). Environmental and sustainability indicators and the concept of situational indicators. A systems approach. *Environmental Modeling & Assessment*, 1(3):101–117.

Gordon, A. and Walter, N. (2011). Controlling the Earth's albedo using reflective hollow glass spheres. *International Journal of Global Enviromental Issues*, 11(2):91–108.

Graversen, R. G., Mauritsen, T., Tjernstroem, M., Kaellen, E., and Svensson, G. (2008). Vertical structure of recent Arctic warming. *Nature*, 541(January).

Grosvenor, D. and Wood, R. (2014). The effect of solar zenith angle on modis cloud optical and microphysical retrievals. *Atmos. Chem. Phys. Discuss*, 14:303–375.

Haywood, J. M., Jones, A., Dunstone, N., Milton, S., Vellinga, M., Bodas-Salcedo, A., Hawcroft, M., Kravitz, B., Cole, J., Watanabe, S., et al. (2016). The impact of equilibrating hemispheric albedos on tropical performance in the hadgem2-es coupled climate model. *Geophysical Research Letters*.

Heinze, C., Meyer, S., Goris, N., Anderson, L., Steinfeldt, R., Chang, N., Le Quéré, C., and Bakker, D. C. E. (2015). The ocean carbon sink â€“ impacts, vulnerabilities and challenges. *Earth System Dynamics*, 6(1):327–358.

Held, H., Kriegler, E., Lessmann, K., and Edenhofer, O. (2009). Efficient climate policies under technology and climate uncertainty. *Energy Economics*, 31:S50–S61.

Heutel, G., Moreno-Cruz, J., and Ricke, K. (2015). Climate engineering economics. Technical report, National Bureau of Economic Research.

Holland, M. M. and Bitz, C. M. (2003). Polar amplification of climate change in coupled models. *Climate Dynamics*, 21(3-4):221–232.

House, J. I., Colin Prentice, I., and Le Quere, C. (2002). Maximum impacts of future reforestation or deforestation on atmospheric co2. *Global Change Biology*, 8(11):1047–1052.

Hulme, M. (2014). *Can science fix climate change: A case against climate engineering*. John Wiley & Sons.

Hunke, E. and Dukowicz, J. (1997). An elastic-viscous-plastic model for sea ice dynamics. *Journal of Physical Oceanography*, 27(9):1849–1867.

Ilyina, T., Six, K. D., Segschneider, J., Maier-Reimer, E., Li, H., and Nunez-Riboni, I. (2013). Global ocean biogeochemistry model HAMOCC : Model architecture and performance as component of the MPI-Earth system model in different CMIP5 experimental realizations. *Journal of Advances in Modeling Earth Systems*, 5:287–315.

Irvine, P. J., Sriver, R. L., and Keller, K. (2012). Tension between reducing sea-level rise and global warming through solar-radiation management. *Nature Climate Change*, 2(2):97–100.

Jin, Z. (2004). A parameterization of ocean surface albedo. *Geophysical Research Letters*, 31(22):L22301.

Jones, A., Haywood, J. M., Alterskjær, K., Boucher, O., Cole, J. N., Curry, C. L., Irvine, P. J., Ji, D., Kravitz, B., Egill Kristjánsson, J., et al. (2013). The impact of abrupt suspension of solar radiation management (termination effect) in experiment g2 of the geoengineering model intercomparison project (geomip). *Journal of Geophysical Research: Atmospheres*, 118(17):9743–9752.

Jones, P. D. (1994). Hemispheric surface air temperature variations: a reanalysis and an update to 1993. *Journal of Climate*, 7(11):1794–1802.

Keenan, T. F., Davidson, E., Moffat, A. M., Munger, J. W., and Richardson, A. D. (2012). Using model-data fusion to interpret past trends, and quantify uncertainties in future projections, of terrestrial ecosystem carbon cycling. *Global Change Biology*, 18(8):2555–2569.

Keenan, T. F., Hollinger, D. Y., Bohrer, G., Dragoni, D., Munger, J. W., Schmid, H. P., and Richardson, A. D. (2013). Increase in forest water-use efficiency as atmospheric carbon dioxide concentrations rise. *Nature*, 499(7458):324–7.

Keith, D. W. (2000). Geoengineering the climate: History and Prospect. *Annual Reviews in Energy Environment*, 25:245–84.

Keller, D. P., Feng, E. Y., and Oschlies, A. (2014). Potential climate engineering effectiveness and side effects during a high carbon dioxide-emission scenario. *Nature communications*, 5:3304.

Keller, D. P., Lenton, A., Scott, V., and Vaughan, N. E. (2016). Carbon dioxide removal–model intercomparison project (cdr–mip).

Keller, D. P., Oschlies, A., and Eby, M. (2012). A new marine ecosystem model for the University of Victoria Earth system climate model. *Geoscientific Model Development Discussions*, 5(2):1135–1201.

Kirchofer, A., Brandt, A., Krevor, S., Prigiobbe, V., and Wilcox, J. (2012). Impact of alkalinity sources on the life-cycle energy efficiency of mineral carbonation technologies. *Energy & Environmental Science*, 5(9):8631–8641.

Klepper, G. and Rickels, W. (2014). Climate engineering: Economic considerations and research challenges. *Review of Environmental Economics and Policy*, 8(2):270–289.

Köhler, P., Abrams, J. F., Völker, C., Hauck, J., and Wolf-Gladrow, D. A. (2013). Geoengineering impact of open ocean dissolution of olivine on atmospheric co2, surface ocean ph and marine biology. *Environmental Research Letters*, 8(1):014009.

Kopfmüller, J., Barton, J. R., and Salas, A. (2012). How sustainable is santiago? In *Risk Habitat Megacity*, pages 305–326. Springer.

Koven, C. D., Riley, W. J., and Stern, A. (2013). Analysis of permafrost thermal dynamics and response to climate change in the cmip5 earth system models. *Journal of Climate*, 26(6):1877–1900.

Kravitz, B. (2014). Idealized ocean albedo modification simulations in the geoengineering model intercomparison project (geomip). In *AGU Fall Meeting Abstracts*, volume 1, page 0775.

Kravitz, B., Caldeira, K., Boucher, O., Robock, A., Rasch, P. J., Alterskjaer, K., Karam, D. B., Cole, J. N. S., Curry, C. L., Haywood, J. M., Irvine, P. J., Ji, D., Jones, A., Kristjánsson, J. E., Lunt, D. J., Moore, J. C., Niemeier, U., Schmidt, H., Schulz, M., Singh, B., Tilmes, S., Watanabe, S., Yang, S., and Yoon, J.-H. (2013a). Climate model response from the Geoengineering Model Intercomparison Project (GeoMIP). *Journal of Geophysical Research: Atmospheres*, 118(15):8320–8332.

Kravitz, B., Forster, P. M., Jones, A., Robock, A., Alterskjaer, K., Boucher, O., Jenkins, A. K. L., Korhonen, H., Kristjánsson, J. E., Muri, H., Niemeier, U., Partanen, A.-I., Rasch, P. J., Wang, H., and Watanabe, S. (2013b). Sea spray geoengineering experiments in the geoengineering model intercomparison project (GeoMIP): Experimental design and preliminary results. *Journal of Geophysical Research: Atmospheres*, 118(19):11,175–11,186.

Kravitz, B., Robock, A., Boucher, O., Schmidt, H., Taylor, K. E., Stenchikov, G., and Schulz, M. (2011). The geoengineering model intercomparison project (geomip). *Atmospheric Science Letters*, 12(2):162–167.

Kravitz, B., Robock, A., Tilmes, S., Boucher, O., English, J. M., Irvine, P. J., Jones, A., Lawrence, M. G., MacCracken, M., Muri, H., Moore, J. C., Niemeier, U., Phipps, S. J., Sillmann, J., Storelvmo, T., Wang, H., and Watanabe, S. (2015). The geoengineering model intercomparison project phase 6 (geomip6): simulation design and preliminary results. *Geoscientific Model Development*, 8(10):3379–3392.

Krellenberg, K., Kopfmüller, J., and Barton, J. (2010). How sustainable is santiago de chile? current performance, future trends, potential measures. synthesis report of the risk habitat megacity research initiative (2007-2011). Technical report, UFZ-Bericht, Helmholtz-Zentrum für Umweltforschung.

Kristjánsson, J. E., Muri, H., and Schmidt, H. (2015). The hydrological cycle response to cirrus cloud thinning. *Geophysical Research Letters*.

Kruijt, B., Witte, J.-P. M., Jacobs, C. M., and Kroon, T. (2008). Effects of rising atmospheric CO2 on evapotranspiration and soil moisture: A practical approach for the Netherlands. *Journal of Hydrology*, 349(3-4):257–267.

Kumar, S., Merwade, V., Kinter, J. L., and Niyogi, D. (2013). Evaluation of Temperature and Precipitation Trends and Long-Term Persistence in CMIP5 Twentieth-Century Climate Simulations. *Journal of Climate*, 26(12):4168–4185.

Kuo, K. A., Watson, I., and Hunt, H. E. (2012). The spice project: an example of geoengineering research. In *Water and Climate: Policy Implementation Challenges; Proceedings of the 2nd Practical Responses to Climate Change Conference*, page 479. Engineers Australia.

Kvenvolden, K. A., Ginsburg, G. D., and Soloviev, V. A. (1993). Worldwide distribution of subaquatic gas hydrates. *Geo-marine Letters*, 13(1993):32–40.

Lackner, K. S. (2002). Carbonate chemistry for sequestering fossil carbon. *Annual review of energy and the environment*, 27(1):193–232.

Latham, J. (1990). Control of global warming? *Nature*, 347:339–340.

Latham, J., Bower, K., Choularton, T., Coe, H., Connolly, P., Cooper, G., Craft, T., Foster, J., Gadian, A., Galbraith, L., et al. (2012). Marine cloud brightening. *Philosophical Transactions of the Royal Society of London A: Mathematical, Physical and Engineering Sciences*, 370(1974):4217–4262.

Lawrence, D. M., Thornton, P. E., Oleson, K. W., and Bonan, G. B. (2007). The Partitioning of Evapotranspiration into Transpiration, Soil Evaporation, and Canopy Evaporation in a GCM: Impacts on Land–Atmosphere Interaction. *Journal of Hydrometeorology*, 8(4):862–880.

Leisner, T. and Müller-Kliesner, S. (2010). Aerosolbasierte methoden des climate engineering. eine bewertung. *Technikfolgenabschätzung—Theorie und Praxis*, 19(2):25–32.

Lenton, T. M. (2012). Arctic Climate Tipping Points. *AMBIO*, 41:10–22.

Lenton, T. M., Held, H., Kriegler, E., Hall, J. W., Lucht, W., Rahmstorf, S., and Schellnhuber, H. J. (2008). Tipping elements in the Earth's climate system. *PNAS*, 105(6):1786–1793.

Leuning, R., Cleugh, H. a., Zegelin, S. J., and Hughes, D. (2005). Carbon and water fluxes over a temperate Eucalyptus forest and a tropical wet/dry savanna in Australia: measurements and comparison with MODIS remote sensing estimates. *Agricultural and Forest Meteorology*, 129(3-4):151–173.

Lindsay, R. and Schweiger, A. (2015). Arctic sea ice thickness loss determined using subsurface, aircraft, and satellite observations. *The Cryosphere*, 9(1):269–283.

Lloyd, J. and Taylor, J. (1994). On the temperature dependence of soil respiration. *Functional ecology*, pages 315–323.

MacCracken, M. C., Shin, H.-J., Caldeira, K., and Ban-Weiss, G. (2013). Climate response to imposed solar radiation reductions in high latitudes. *Earth System Dynamics*, 4(2):301–315.

MacDougall, A. H., Avis, C. A., and Weaver, A. J. (2012). Significant contribution to climate warming from the permafrost carbon feedback. *Nature Geoscience*, 5(10):719–721.

Matthews, H. D. (2007). Implications of CO 2 fertilization for future climate change in a coupled climate – carbon model. *Global Change Biology*, 13:1068–1078.

Matthews, H. D. and Caldeira, K. (2007). Transient climate–carbon simulations of planetary geoengineering. *Proceedings of the National Academy of Sciences*, 104(24):9949–9954.

Meier, W., Fetterer, F., Savoie, M., Mallory, S., Duerr, R., and Stroeve, J. (2013). Noaa/nsidc climate data record of passive microwave sea ice concentration. *Boulder, Colorado USA: National Snow and Ice Data Center. doi*, 10(7265):N55M63M1.

Meinshausen, M., Smith, S. J., Calvin, K., Daniel, J. S., Kainuma, M. L. T., Lamarque, J.-F., Matsumoto, K., Montzka, S. A., Raper, S. C. B., Riahi, K., Thomson, A., Velders, G. J. M., and Vuuren, D. P. (2011). The RCP greenhouse gas concentrations and their extensions from 1765 to 2300. *Climatic Change*, 109(1-2):213–241.

Meissner, K. J., Weaver, A. J., Matthews, H. D., and Cox, P. M. (2003). The role of land surface dynamics in glacial inception: a study with the UVic Earth System Model. *Climate Dynamics*, 21(7-8):515–537.

Mengis, N., Keller, D. P., Eby, M., and Oschlies, A. (2015). Uncertainty in the response of transpiration to CO 2 and implications for climate change. *Environmental Research Letters*, 10(9):094001.

Mengis, N., Martin, T., Keller, D., and Oschlies, A. (2016). Assessing climate impacts and risks of ocean albedo modification in the arctic. *Journal of Geophysical Research: Oceans*.

Migliavacca, M., Sonnentag, O., Keenan, T. F., Cescatti, A., O'Keefe, J., and Richardson, a. D. (2012). On the uncertainty of phenological responses to climate change, and implications for a terrestrial biosphere model. *Biogeosciences*, 9(6):2063–2083.

Mitchell, D. L. and Finnegan, W. (2009). Modification of cirrus clouds to reduce global warming. *Environmental Research Letters*, 4(4):045102.

Monteith, J. L. (1981). Evaporation and surface temperature. *Quarterly Journal of the Royal Meteorological Society*, 107(451):1–27.

Muri, H., Kristjánsson, J., Storelvmo, T., and Pfeffer, M. (2014). The climatic effects of modifying cirrus clouds in a climate engineering framework. *Journal of Geophysical Research: Atmospheres*, 119(7):4174–4191.

Murray, F. W. (1967). On the Computation of Saturation Vapor Pressure. *Notes and Correspondance*, pages 203–204.

National Academy of Sciences, T. (2015a). *Climate Intervention:: Carbon Dioxide Removal and Reliable Sequestration*. National Academies Press.

National Academy of Sciences, T. (2015b). *Climate Intervention:: Reflecting Sunlight to Cool Earth*. National Academies Press.

New, M., Todd, M., Hulme, M., and Jones, P. (2001). Precipitation measurements and trends in the twentieth century. *International Journal of Climatology*, 21(15):1889–1922.

Niemeier, U. and Timmreck, C. (2015). What is the limit of climate engineering by stratospheric injection of so 2? *Atmospheric Chemistry and Physics*, 15(16):9129–9141.

Nilsson, S. and Schopfhauser, W. (1995). The carbon-sequestration potential of a global afforestation program. *Climatic Change*, 30(3):267–293.

Niyogi, D., Alapaty, K., Raman, S., and Chen, F. (2009). Development and evaluation of a coupled photosynthesis-based gas exchange evapotranspiration model (gem) for mesoscale weather forecasting applications. *Journal of Applied Meteorology and Climatology*, 48(2):349–368.

Oschlies, A., Schulz, K. G., Riebesell, U., and Schmittner, A. (2008). Simulated 21st century's increase in oceanic suboxia by CO 2 -enhanced biotic carbon export. *Global Biogeochemical Cycles*, 22(4):n/a–n/a.

Ott, K., Klepper, G., Lingner, S., Schäfer, A., Scheffran, J., Sprinz, D., and Schröder, M. (2004). Reasoning goals of climate protection. specification of article 2 unfccc. *Berlin: Umweltbundesamt*.

Pacanowski, R. (1995). Mom 2 documentation, users guide and reference manual, gfdl ocean group technical report 3, geophys. *Fluid Dyn. Lab., Princeton University, Princeton, NJ*.

Perovich, D., Grenfell, T., Light, B., and Hobbs, P. (2002). Seasonal evolution of the albedo of multiyear arctic sea ice. *Journal of Geophysical Research: Oceans*, 107(C10).

Pintér, L., Hardi, P., and Bartelmus, P. (2005). Indicators of sustainable development: proposals for a way forward. In *Expert Group Meeting on Indicators of Sustainable Development. New York*, pages 13–15.

Pollard, R. T., Salter, I., Sanders, R. J., Lucas, M. I., Moore, C. M., Mills, R. A., Statham, P. J., Allen, J. T., Baker, A. R., Bakker, D. C., et al. (2009). Southern ocean deep-water carbon export enhanced by natural iron fertilization. *Nature*, 457(7229):577–580.

Pongratz, J., Lobell, D. B., Cao, L., and Caldeira, K. (2012). Crop yields in a geoengineered climate. *Nature Climate Change*, 2(2):101–105.

Pongratz, J., Reick, C. H., Raddatz, T., Caldeira, K., and Claussen, M. (2011). Past land use decisions have increased mitigation potential of reforestation. *Geophysical Research Letters*, 38(15):n/a–n/a.

Radermacher, W. (2005). The reduction of complexity by means of indicators–case studies in the environmental domain. *Statistics, Knowledge and Policy*, page 163.

Ricciuto, D. M., Davis, K. J., and Keller, K. (2008). A bayesian calibration of a simple carbon cycle model: The role of observations in estimating and reducing uncertainty. *Global Biogeochemical Cycles*, 22(2). GB2030.

Rickels, W., Rehdanz, K., and Oschlies, A. (2010). Methods for greenhouse gas offset accounting: A case study of ocean iron fertilization. *Ecological Economics*, 69(12):2495–2509.

Ridgwell, A., Singarayer, J. S., Hetherington, A. M., and Valdes, P. J. (2009). Tackling regional climate change by leaf albedo bio-geoengineering. *Current biology*, 19(2):146–150.

Riebesell, U., Schulz, K. G., Bellerby, R., Botros, M., Fritsche, P., Meyerhöfer, M., Neill, C., Nondal, G., Oschlies, A., Wohlers, J., et al. (2007). Enhanced biological carbon consumption in a high co2 ocean. *Nature*, 450(7169):545–548.

Robock, A. (2008). 20 Reasons Why Geoengineering May Be a Bad Idea. *Bulletin of the Atomic Scientists*, 64(2):14–18.

Robock, A. (2011). Bubble, bubble, toil and trouble - An editorial comment. *Climate*, (105):383–385.

Robock, A., Jerch, K., and Bunzl, M. (2008a). 20 reasons why geoengineering may be a bad idea. *Bulletin of the Atomic Scientists*, 64(2):14–59.

Robock, A., Oman, L., and Stenchikov, G. L. (2008b). Regional climate responses to geoengineering with tropical and Arctic SO 2 injections. *Journal of Geophysical Research*, 113(D16):D16101.

Romanovsky, V., Smith, S., Christiansen, H., Shiklomanov, N., Drozdov, D., Oberman, N., Kholodov, A., and Marchenko, S. (2011). Permafrost [in arctic report card 2011].

Russell, L. M., Sorooshian, A., Seinfeld, J. H., Albrecht, B. A., Nenes, A., Ahlm, L., Chen, Y.-C., Coggon, M., Craven, J. S., Flagan, R. C., et al. (2013). Eastern pacific emitted aerosol cloud experiment. *Bulletin of the American Meteorological Society*, 94(5):709–729.

Schäfer, S., Lawrence, M., Stelzer, H., Born, W., Low, S., Aaheim, A., Adriázola, P., Betz, G., Boucher, O., Carius, A., et al. (2015). The european transdisciplinary assessment of climate engineering (eutrace): Removing greenhouse gases from the atmosphere and reflecting sunlight away from earth. *Institute for Advanced Sustainability Studies, Potsdam*.

Screen, J. A. and Simmonds, I. (2010). The central role of diminishing sea ice in recent arctic temperature amplification. *Nature*, 464(7293):1334–1337.

Seitz, R. (2011). Bright water: hydrosols, water conservation and climate change. *Climatic Change*, 105(3-4):365–381.

Sellers, W. D. (1969). A Global Climatic Model Based on the Energy Balance of the Earth-Atmosphere System. *Journal of Applied Meteorology*, 8:392–400.

Serreze, M. C. and Barry, R. G. (2011). Processes and impacts of Arctic amplification: A research synthesis. *Global and Planetary Change*, 77(1-2):85–96.

Serreze, M. C. and Francis, J. A. (2006). The arctic amplification debate. *Climatic change*, 76(3-4):241–264.

Skvortsov, A., Eby, M., and Weaver, A. J. (2009). Snow cover validation and sensitivity to CO2 in the UVic ESCM. *Atmosphere-Ocean*, 47(3):224–237.

Sleen, P. V. D., Groenendijk, P., Vlam, M., Anten, N. P. R., Boom, A., Bongers, F., Pons, T. L., Terburg, G., and Zuidema, P. A. (2014). No growth stimulation of tropical trees by 150 years of CO 2 fertilization but water-use efficiency increased. *Nature Geoscience*, (December):1–5.

Solomon, S., Qin, D., Manning, M., Chen, Z., Marquis, M., Averyt, K., Tignor, M., and Miller, H. (2007). The physical science basis. *Contribution of working group I to the fourth assessment report of the intergovernmental panel on climate change*, pages 235–337.

Solow, R. M. (1956). A contribution to the theory of economic growth. *The quarterly journal of economics*, pages 65–94.

Stavi, I. and Lal, R. (2012). Agroforestry and biochar to offset climate change: a review. *Agronomy for Sustainable Development*, 33(1):81–96.

Sterner, T. and Persson, U. M. (2008). An even sterner review: Introducing relative prices into the discounting debate. *Review of Environmental Economics and Policy*, 2(1):61–76.

Stocker, T. F., Qin, D., Plattner, G.-K., Tignor, M., Allen, S. K., Boschung, J., Nauels, A., Xia, Y., Bex, V., and Midgley, P. M. (2013). *IPCC, 2013: Climate Change 2013: The Physical Science Basis. Contribution of Working Group I to the Fifth Assessment Report of the Intergovernmental Panel on Climate Change*. Cambridge University Press.

Storelvmo, T. and Herger, N. (2014). Cirrus cloud susceptibility to the injection of ice nuclei in the upper troposphere. *Journal of Geophysical Research: Atmospheres*, 119(5):2375–2389.

Stroeve, J. C., Kattsov, V., Barrett, A., Serreze, M., Pavlova, T., Holland, M., and Meier, W. N. (2012). Trends in Arctic sea ice extent from CMIP5, CMIP3 and observations. *Geophysical Research Letters*, 39(16):1–7.

Tang, X., Li, H., Desai, A. R., Nagy, Z., Luo, J., Kolb, T. E., Olioso, A., Xu, X., Yao, L., Kutsch, W., Pilegaard, K., Köstner, B., and Ammann, C. (2014). How is water-use efficiency of terrestrial ecosystems distributed and changing on Earth? *Scientific Reports*, 4:7483.

Tarnocai, C., Canadell, J. G., Schuur, E. a. G., Kuhry, P., Mazhitova, G., and Zimov, S. (2009). Soil organic carbon pools in the northern circumpolar permafrost region. *Global Biogeochemical Cycles*, 23(2):n/a–n/a.

Taucher, J. and Oschlies, A. (2011). Can we predict the direction of marine primary production change under global warming? *Geophysical Research Letters*, 38(2):n/a–n/a.

Taylor, K. E., Stouffer, R. J., and Meehl, G. A. (2012). An Overview of CMIP5 and the Experiment Design. *Bulletin of the American Meteorological Society*, 93(4):485–498.

Tietsche, S., Notz, D., Jungclaus, J., and Marotzke, J. (2011). Recovery mechanisms of arctic summer sea ice. *Geophysical Research Letters*, 38(2).

Tilmes, S., Fasullo, J., Lamarque, J.-F., Marsh, D. R., Mills, M., Alterskjaer, K., Muri, H., Kristjánsson, J. E., Boucher, O., Schulz, M., Cole, J. N. S., Curry, C. L., Jones, A., Haywood, J., Irvine, P. J., Ji, D., Moore, J. C., Karam, D. B., Kravitz, B., Rasch, P. J., Singh, B., Yoon, J.-H., Niemeier, U., Schmidt, H., Robock, A., Yang, S., and Watanabe, S. (2013). The hydrological impact of geoengineering in the Geoengineering Model Intercomparison Project (GeoMIP). *Journal of Geophysical Research: Atmospheres*, 118(19):11,036–11,058.

Tilmes, S., Jahn, A., Kay, J. E., Holland, M., and Lamarque, J.-f. (2014). Can regional climate engineering save the summer Arctic sea ice ? *Geophysical Research Letters*, 41:880–885.

Trenberth, K. E. and Dai, A. (2007). Effects of mount pinatubo volcanic eruption on the hydrological cycle as an analog of geoengineering. *Geophysical Research Letters*, 34(15).

Twomey, S. (1974). Pollution and the planetary albedo. *Atmospheric Environment (1967)*, 8(12):1251–1256.

UNFCCC (2015). *Conference of the Parties: Adoption of the Paris Agreement. Proposal by the president. FCCC/CP/2015/L.9/Rev.1*. UNFCCC, retrieved 12 December 2015.

Wadhams, P. (2012). Arctic Ice Cover, Ice Thickness and Tipping Points. *AMBIO*, 41(January):23–33.

Wang, K. and Dickinson, R. E. (2012). A review of global terrestrial evapotranspiration: Observation, modeling, climatology, and climatic variability. *Reviews of Geophysics*, 50(RG2005):1–54.

Weaver, A. J., Eby, M., Wiebe, E. C., Bitz, C. M., Duffy, P. B., Ewen, T. L., Fanning, A. F., Holland, M. M., MacFadyen, A., Matthews, H. D., Meissner, K. J., Saenko, O., Schmittner, A., Wang, H., and Yoshimori, M. (2001). The UVic earth system climate model: Model description, climatology, and applications to past, present and future climates. *Atmosphere-Ocean*, 39(4):361–428.

Wentz, F. J., Ricciardulli, L., Hilburn, K., and Mears, C. (2007). How much more rain will global warming bring? *Science (New York, N.Y.)*, 317(5835):233–5.

Ylhäisi, J. S., Garrè, L., Daron, J., and Räisänen, J. (2015). Quantifying sources of climate uncertainty to inform risk analysis for climate change decision-making. *Local Environment*, 20(7):811–835.

List of Figures

List of Tables

Acknowledgements - Danksagung

First of all I want to thank Andreas Oschlies for giving me the opportunity to work on this topic, for the support and supervision, the discussions, for giving me the many opportunities to visit conferences, workshops and summer schools and for always being friendly and supportive. By giving me the freedom to explore my one research ideas, he enabled me to trust in myself, which might be the most important thing I learned during my time as PhD student.

A special thanks goes to my second supervisor David Keller, for his initial help with the UVic model, for always taking time to read paper/chapter drafts, for his interesting discussions and his friendly reminders to have a social life. Thank you, without you, this thesis would not have been possible.

I want to thank Andreas Oschlies and Martin Visbeck for taking the time to be my examiners, and Mojib Latif and Martin Quaas for being in my committee. In addition, I would like to thank Andreas Oschlies, David Keller and Martin Quaas, for taking the time to be my ISOS supervisors.

Apart from that I would like to thank the Biogeochemical Modelling department for warmly welcoming me in the group. Especially I would like to thank, Wolfgang Koeve, for his advice in all 'Lebenslagen', Julia Getzlaff for an open ear and the possibility to also once in a while talk about Not-Work, Ulrike Loeptien and Heiner Dietze, for taking the time to give me really helpful advice and Ulrike Bernitt, who always had my back.

I would like to thank the members of the Priority Program for interesting discussions, which much broadened my understanding of the topic, and especially the members of the ComparCE project for giving me great input for my studies. My fellow Phd students, especially Christine, Christian, Vera, Lena, Miriam, Aswathy and Fabian, made all the meetings much more fun!! Many thanks for that!!

I would like to thank my friends in Kiel, most of all Laura, Katha, Ina, Anni, Kerstin, Cathleen, Micha, Anna and Kai, who all supported me in their individual ways in finishing this thesis. A special thanks goes to my peer coaching group, Thekla, Melli, Anika and Anna, who are purposefully listed here as my friends!
And finally, I would like to thank my family, for the moral support and encouragements. To Elisabeth, lets make the next months count!!

Erklärung

Hiermit erkläre ich, dass die vorliegende Arbeit mit dem Titel: 'Towards a comprehensive, comparative assessment of Climate Engineering schemes - Metrics, Indicators and Uncertainties' von mir selbstständig angefertigt wurde. Bis auf zitierte Referenzen und Beratung meiner Betreuer wurden keine weiteren Quellen verwendet. Diese Arbeit ist unter Einhaltung der Regeln guter wissenschaftlicher Praxis der Deutschen Forschungsgemeinschaft entstanden. Sie wurde weder im Rahmen eines Prüfungsverfahrens an anderer Stelle vorgelegt noch veröffentlicht. Ich erkläre mich einverstanden, dass diese Arbeit an die Bibliothek des GEOMAR und die Universitätsbibliothek der CAU weitergeleitet wird.

Kiel, April 2016

_____

(Nadine Mengis)